# In vitro evaluation of the toxicological profile of silica nanoparticles and nanoemulsions

Taghrid Zaiter

**THESE DE DOCTORAT**

**DE L'ETABLISSEMENT UNIVERSITE BOURGOGNE FRANCHE-COMTE**

**PREPAREE A UFR SCIENCE DE LA SANTE**

Ecole doctorale n°554

Environnements-Santé

Doctorat de biochimie et biologie moléculaire

Par

Taghrid Zaiter

# *In vitro* evaluation of the toxicological profile of silica nanoparticles and nanoemulsions

**Soutenance le 13 décembre 2022 à Besançon**

Composition du jury :

| | | |
|---|---|---|
| Mme SAPIN-MINET Anne | Professeur des universités, Université de Lorraine | Président |
| Mme BOLAND Sonja | Ingénieur de Recherche, Université Paris-Diderot | Rapporteur |
| Mme SAPIN-MINET Anne | Professeur des universités, Université de Lorraine | Rapporteur |
| M. DAHER Ahmad | Professeur des Universités, Université Libanaise | Examinateur |
| Mme MARTIN Hélène | Maitre de Conférences, Université de Franche-Comté | Examinatrice |
| M. BEDUNEAU Arnaud | Maitre de Conférences, Université de Franche-Comté | Directeur de thèse |
| Mme DIAB-ASSAF Mona | Professeur des Universités, Université Libanaise | Codirectrice de thèse |
| M. CORNU Raphaël | Ingénieur de Recherche, Université de Franche-Comté | Invité |

# Acknowledgement

This work was achieved in the department of Pharmaceutical Engineering of the PEPITE EA4267, University of Franche-Comté; Besancon; France.

Allow me to thank the members of the jury: Dr. BOLAND Sonja and Pr. SAPIN-MINET Anne for accepting to be part of my thesis jury as reporters, Dr. MARTIN Hélène, and Pr. DAHER Ahmad for agreeing to examine this work.

I would like to thank Dr. Raphael Cornu for his support and for his presence during the period of my thesis. I would also like to express my immense gratitude for your guidance, your scientific and moral help. Thank you for attending as a guest member.

I would like to thank my thesis director Dr. Arnaud Béduneau for all his advices and encouragement throughout my thesis, and to his scientific honesty. His teachings have always been of high quality, they have brought me a lot and will remain an example for me. I also thank him for the long hours of work on this manuscript.

I also express my thanks to my co-director, Pr. Mona Diab-Assaf. Thank you for your guidance and help.

I would like to thank Pr. Céline Demougeot for trusting and welcoming me to the laboratory.

I would also like to thank Dr. Hélène Martin and Dr. Georges Moarbess for agreeing to follow this work during the thesis monitoring committees.

I would also like to thank Pr. Yann Pellequer and Claire Chrétien for their help and advice.

I thank Pr. Nadine Millot and her team for their participation in the physicochemical characterisation of E551 food additive.

I thank my colleagues Wassim El basset and Thomas Antoine for the great moments we shared in the laboratory.

I dedicate this work to my adorable mum Insaf and my dear dad Haidar, to my loving brothers Ali and Mahdi. Without your prayers and blessings, I would never have come this far. I thank my fiancé Mustapha for his presence by my side and for his support. This Thesis is yours.

**Table of contents**

# List of figures

# ABBREVIATIONS AND ACRONYMS

**AL:** aluminum

**Au:** gold

**Ag:** silver

**BET:** specific surface area

**CO:** corn oil

**CO:** cobalt

**Cu:** copper

**$Fe_2O_3$:** iron oxide

**Fe:** iron

**GIT:** gastrointestinal tract

**GT:** glyceryl trioctanoate

**GTOL:** glyceryl trioleate

**IL8:** interleukin 8

**LCT:** long chain triglyceride

**MWNT:** multi-walled nanotubes

**MEs:** microemulsion

**MCT:** medium chain triglyceride

**MUC5AC:** mucin 5AC

**NPs:** nanoparticles

**NMs:** nanomaterials

**NEs:** nanoemulsion

**NOAEL:** no observed adverse effects

**OO:** olive oil

**O/W:** oil in water

**PDI:** polydispersity index

**PLA:** poly- (lactic acid)

**PLGA:** poly-(lactide-co-glycolide)

**PIT:** phase inversion temperature

**QDs:** quantum dots

**ROS:** reactive oxygen species

**SG:** stratum granulosum

**SS:** stratum spinosum

**SC:** stratum corneum

**SGF:** simulated gastric fluid

**SIF:** simulated intestinal fluid

**SOR:** surfactant oil ratio

**SWNTs:** single- walled nanotubes

**SLN:** Solid Lipid Nanoparticles

**$SiO_2$:** silicon dioxide

**TEER:** transepithelial electrical resistance

**TGA:** thermogravimetric analysis

**TJs:** tights junction

**Ti:** titane

**$TiO_2$:** titanium dioxide

**TEM:** transmission electron microscopy

**WOR:** water oil ratio

**W/O:** water in oil

**ZnO:** zinc oxide

**Zn:** zinc

**ZO-1:** zonula occludens

# CHAPTER I: GENERAL INTRODUCTION

## I. Nanomaterials and nanoparticles

### 1. Definition

The definition of nanomaterials (NM) published in 2011 in the Official Journal of the European Commission (2011/696/EU) (1) has been very recently updated (2). NM are defined as natural, incidental, or manufactured materials consisting of solid particles including single, agglomerated, and aggregated particles where at least 50% of particles in the number size distribution have one or more external dimensions comprised between 1 nm and 100 nm. Compared with the previous definition, two other conditions were added to consider the shape:

- Particles with an elongated shape, such as rods, fibers, or tubes, where two external dimensions are smaller than 1 nm and the other one is larger than 100 nm.
- Particles with a plate-like shape, where one external dimension is smaller than 1 nm and the other ones are larger than 100 nm."

The specific surface by volume greater than 60 $m^2/cm^3$ which was another condition in the definition of 2011 but was not considered anymore. High surface area is not always directly correlated to the dimensions of particles but rather to their internal structure.

Nanoparticles (NPs) are a subclass of NM composed of three dimensions less than 100 nm (3).

## 2. Economic market

Due to their physicochemical properties, NM are used in many fields, including electronic, healthcare, aerospace, food, and textile industries. Their use is in constant increase, with an annual growth rate that should reach 13.1 % between 2021 and 2028 (4) **(Figure 1)**.

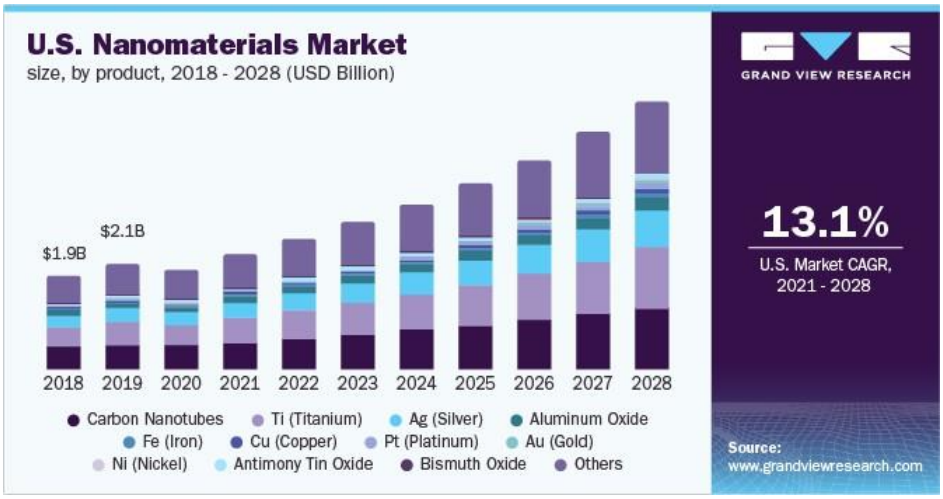


***Figure 1: estimation of various nanomaterials uses over a span of 10 years. According to Market Analysis Report* (4) .**

The medical segment of NM market is the most important with 29.98% of revenues in 2020. Other applications of NPs are also continuously growing such as electronics, paints, and energy. (**Figure 2)**.

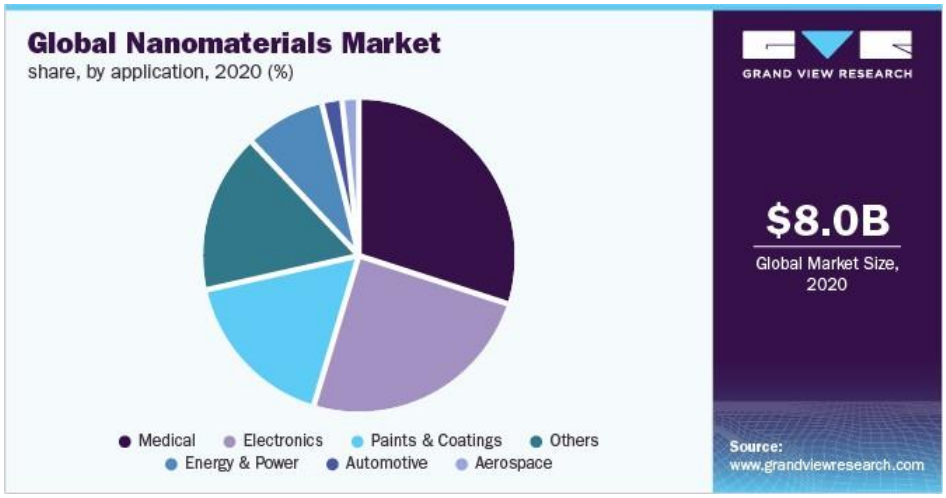


***Figure 2: applications insights of nanomaterials in 2020. According to Market Analysis Report* (4).**

Considering the rapid evolution of nanofoods, the part of food industries in the global market of NM should rapidly increase.

## 3. The different types of nanoparticles

NPs are generally divided into organic, inorganic, and carbon-based NPs. Organic NPs mainly include polymeric nanospheres and nanocapsules, polymeric micelles, liposomes, nanoemulsions (NE), and dendrimers. Inorganic NPs are represented by silica NPs, metal oxide NPs, metal NPs and quantum dots. The carbon-based nanomaterials include fullerenes, graphenes and carbon nanotubes (5) **(Figure 3)**.

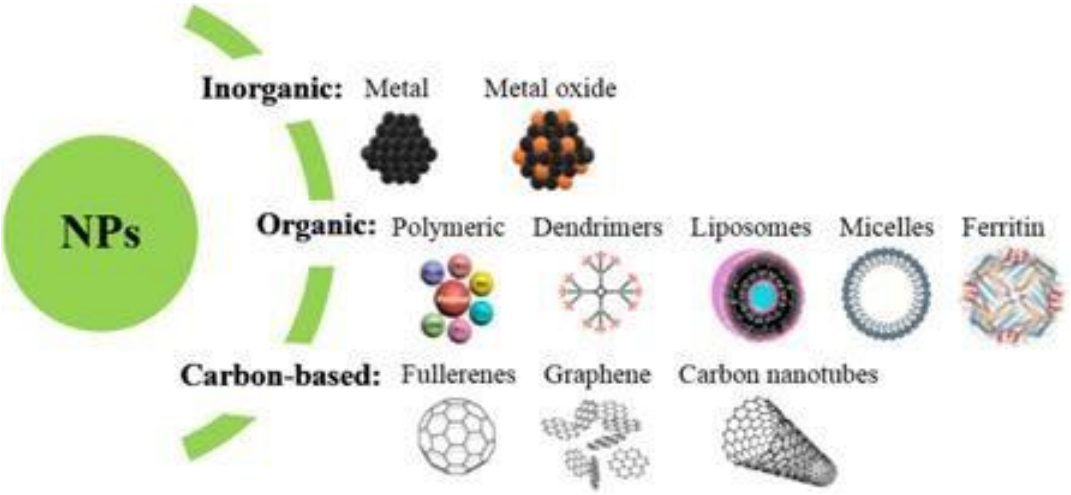


***Figure 3: classification of NPs. According to Shah et al 2020* (5)**.

### 3.1. Organic NPs

#### 3.1.1. Polymeric NPs

In 1979, Couvreur *et al.* developed the first polymeric NPs based on poly-(alkyl-cyanoacrylates) as a drug delivery system for cancer therapy. New polymers have been used such as poly- (lactic acid) (PLA), poly- (glycolic acid) (PGA) and their copolymer poly-(lactide-co-glycolide) (PLGA). These biocompatible and biodegradable polymers are approved as pharmaceutical inactive ingredient. Their degradation does not lead to the formation of toxic metabolites and their high stability gives them essential characteristics for applications in the biomedical field. There are two types of polymeric NPs, nanospheres and nanocapsules. Nanospheres are composed of a polymeric matrix in which drug is entrapped. Nanocapsules are composed of a core containing the drug and surrounded by a polymer shell **(Figure 4)** (6).

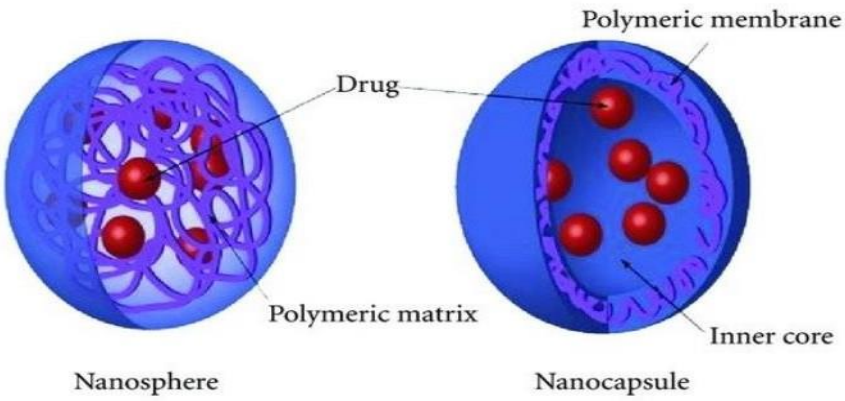


***Figure 4: the types of polymeric nanoparticles used as drug delivery. According to Christoforidis et al 2012* (6).**

### 3.1.2. Polymeric micelles

Used as drug delivery system for cancer therapy, the polymeric micelles are the result of self-assembly of amphiphilic polymers, usually in aqueous solution **(Figure 5)**. The inner core of these micelles includes a hydrophobic region of polymer that contains the drug, while the hydrophilic region provides stability in the aqueous environment. Depending on the route of administration, the stability of the micelles can be affected by the environmental changes such as the pH and the temperature (7).

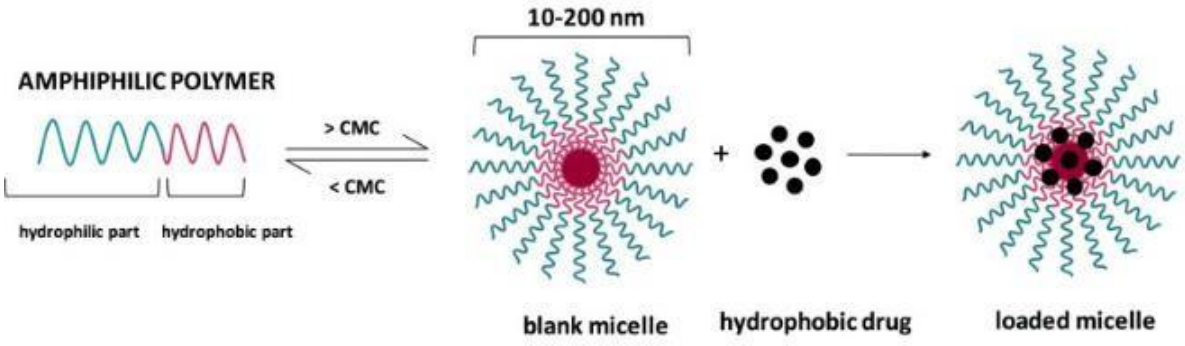


***Figure 5: schematic representation of polymeric micelles. According to Ghezzi et al 2021* (8)**.

### 3.1.3. Liposomes

The use of liposomes is focused on biomedical applications. They can be easily used for a precise active targeting. Liposomes are lipid vesicles composed of aqueous cavities enclosed by one or several lipid bilayers. They can vary in diameter, from nanometers to microns, depending on their chemical composition and the preparation methods. Hydrophilic and lipophilic drugs can be encapsulated within the inner aqueous compartments and the lipid bilayer, respectively **(Figure 6)** (9)**.** Liposomes are also used for the protection and transport of nutrients. The stability of liposomes used as drug delivery system can be affected by the pH and temperature changes, causing a rapid degradation and then, the early release of the active compound (10).

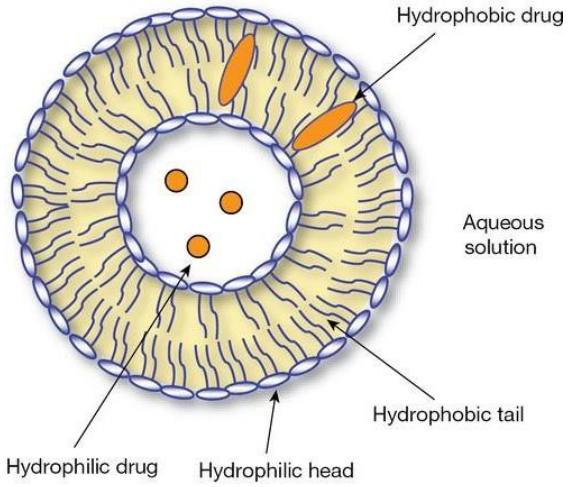


***Figure 6: schematic representation of liposome. According to lembo et al 2010* (9).**

### 3.1.4. Nanoemulsions

NE are lipid drug delivery systems composed of two immiscible liquids such as water and oil and stabilized by an appropriate surfactant. Many surfactants with various characteristics (ionic or nonionic) were used for their preparation. NE are classified in two categories: Oil-in-Water (O/W) and Water-in-Oil (W/O) systems. They have the ability to incorporate lipophilic and hydrophilic drugs and to enhance their oral bioavailability due to their physicochemical characteristics, especially the small droplet size **(Figure 7)** (11).

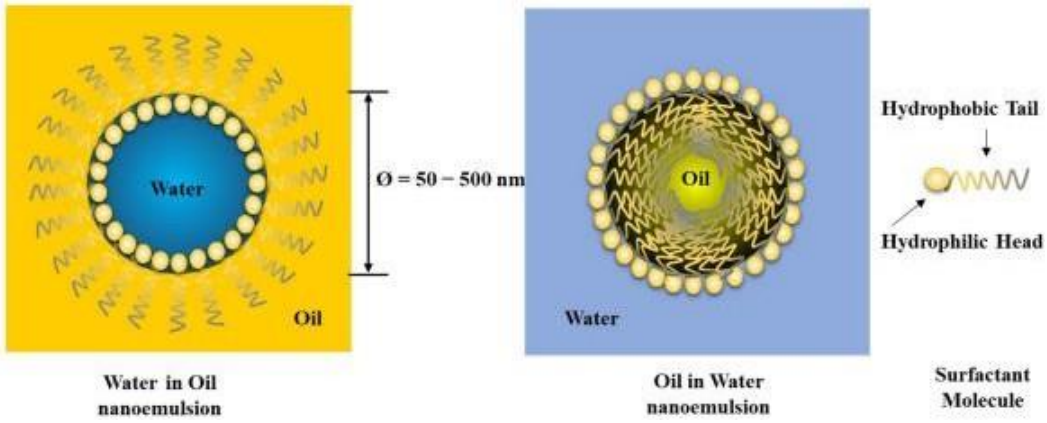


***Figure 7: schematic representation of nanoemulsion types. According to Che Marzuki et al 2019* (12).**

### 3.1.5. Dendrimers

In 1978 the branched molecules were discovered by Fritz Vogtle. Dendrimer structure begins from a central body formed by one or more atoms. From this central structure, branches of other atoms called "dendrons" grow through a variety of chemical reactions **(Figure 8)**. In biomedical field, dendrimers are used as drug delivery system. The active molecules can be covalently bond to the ends of branches or entrapped in the hydrophobic cavities (13).

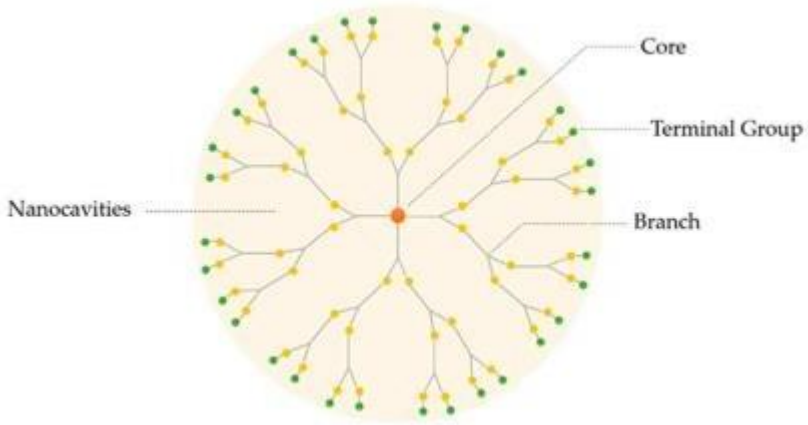


***Figure 8: schematic representation of dendrimers structure. According to Santos et al 2013* (14).**

## 3.2. Inorganic NPs

### 3.2.1. Metallic and metallic oxide NPs

The most common metallic NPs are synthesized from aluminum (Al), cobalt (Co), gold (Au), silver (Ag), zinc (Zn), iron (Fe), copper (Cu) and titanium (Ti). The metallic oxides such as iron oxide ($Fe_2O_3$), ZnO, $TiO_2$ are also widely used. They are prepared by chemical, photochemical, or biological methods. Conjugations with several chemical compounds such as enzymes, ligands and drug were performed for biomedical applications (15,16). Metallic nanoparticles were also developed in other fields, including electronics, cosmetics, and food industries. $TiO_2$ NPs are commonly used as sunscreen, thickening and opacifying agents in food products.

### 3.2.2. Quantum dots

Quantum dots (QDs) are spherical crystals where the size is comprised between 2 and 10 nm. They are composed of semiconductor metals (CdS, CdSe, CdTe, ZnS, PbS). Generally, they consist of a semiconductor core, covered with a shell such as ZnS, and a cap that allows a better solubility in aqueous buffers. QDs are used in biomedical domains, especially in cancer therapy where they have a selective binding to malignant cells and thus sparing normal ones from unwanted side effects (17).

### 3.2.3. Silica NPs

Silicon dioxide appears as the simplest model of tectosilicates. Eight crystallized forms of silica are known today. Their many applications in cosmetics, pharmaceuticals, and food industries require nevertheless a careful evaluation of their toxicity in Human (18). Silica NPs can be synthesized according to three different techniques. Inverse microemulsion, where the spherical micelles are formed by the dissolution of surfactant molecules in the presence of water. This method has been used successfully developed for nanoparticles coating and the attachment of functional groups. The high temperature decomposition of organometallic precursors is also a method used for the synthesis of silica nanoparticles. This method has been widely used in the

commercial synthesis of silica nanoparticles under powder form. Sol-gel method involves the hydrolysis and condensation of tetraethyl orthosilicate (TEOS) or inorganic salts as sodium silicate in presence of mineral acid (19).

## 3.3. Carbon-based nanomaterials

Carbon nanotubes are cylindrical particles with an arrangement of carbon atoms in hybrid shapes. Its internal structure is hollow, and the surface consists of one or more layers of graphene sheets. Based on the presence of layer, carbon nanotubes are divided into two categories such as single-walled carbon nanotubes (SWNTs) and multi-walled carbon nanotubes (MWNTs) **(Figure 9)**.They have a wide range of applications, especially in the biomedical field (20). Unlike carbon nanotubes, C60 fullerene is characterized by a spherical shape.

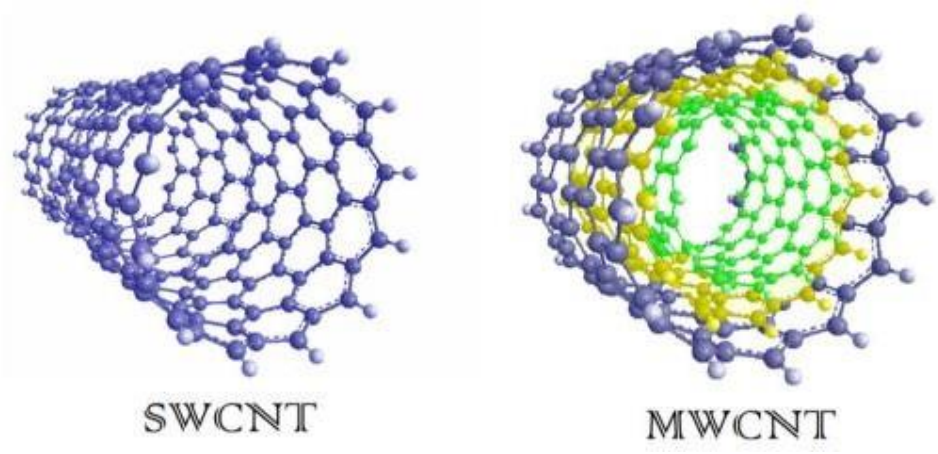


***Figure 9: schematic representation of carbon nanotubes. According to Abazari et al 2020* (21).**

## 4. Applications of nanoparticles

The NPs currently on the market have large-scale applications in cosmetics, food industry, medicine, renewable energies, electronics, and others **(Figure 10)**.

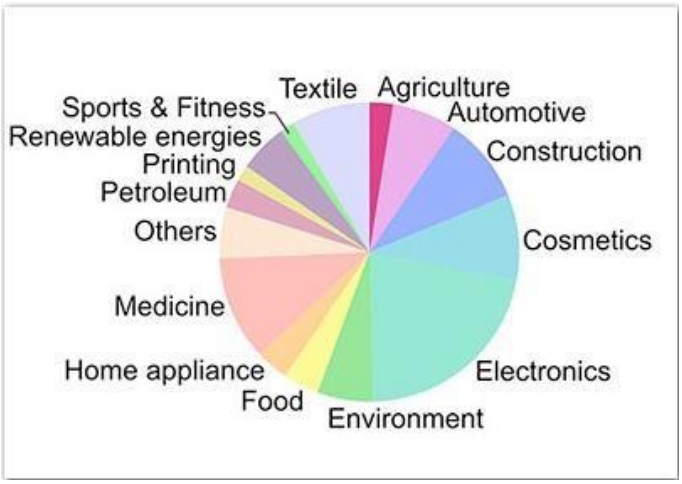


***Figure 10: Global nanotechnology market. According to Talebian et al 2021* (22).**

## 4.1. Cosmetics field

The use of NPs in cosmetic is to increase the stability, the solubility, and the efficiency of active compounds. Cosmetics products should not reach the bloodstream but rather act only on the superficial layers of the skin. $TiO_2$ NPs are used as sunscreen. Their small size increases the surface area, facilitates the spreading, and reduces the whitish appearance compared with microparticles. NPs improve the quality of make-up and hair dyes (23). Cosmetic NE facilitate the skin moisturization and penetration. In addition, they offer a uniform distribution of the product on the skin, and a transparency. Kerastase® Nutritive is a NE developed for moisturizing dry hair (24). Due to their ability to incorporate both hydrophilic and lipophilic substances, liposomes are essential compounds in some anti-aging products, sunscreens, and moisturizers. Some marketed products can be cited, such as liposomes carrying ceramides, tanning agents (25). Solid lipid nanoparticles (SLN) characterized by a solid lipid core unlike NE are used in cosmetics for their stability, their ability to control the active compound release and to protect them from degradations (26). Carbon nanotubes, dendrimers, nanospheres and gold nanoparticles are used also in hair coloring, lotions, creams, hairstyling gel and hair colorant (27). The small size of NPs confers them very interesting properties in cosmetic products but at the same time, it could be considered as a toxicity factor. NPs could be internalized in cutaneous cells or even reach the bloodstream after penetration in the deep cutaneous layers.

## 4.2. Pharmaceutical field

Pharmacokinetic profile and biodistribution of active compounds can be improved by nanomedicines. NP have the ability, depending on their characteristics, to modulate the distribution, metabolism, and elimination of drugs. They allow the transport of lipophilic drugs and can control the release kinetic of active ingredients (28). Due to the small size and then their high surface area, dissolution rate of nanosized drugs can be widely improved (29). NPs protect the encapsulated active compound from enzymatic and chemical degradations (30). Liposomes are used in drug delivery because of their ability to encapsulate hydrophilic molecules in the internal phase, as well as hydrophobic molecules in the phospholipid bilayers. Many liposome-based products are currently on the market (Caelyx®, Daunoxome®, Myocet®…). Their main advantages compared to conventional forms are to modify the pharmacokinetic and the bioavailability of drugs, usually anticancer agents and to reduce side effects. The polymeric NPs are used for the sustained release of active compounds. Metallic nanoparticles can be effectively internalized in organs and cells. The ferumoxytol (Feraheme™) was approved by FDA for the treatment of iron anemia in adult patients. Other forms such as nanoemulsions, dendrimers and inorganic nanoparticles showed a real interest for biomedical applications. Even if the nanoparticles exhibit numerous advantages as drug delivery systems, their toxicity including the empty form (without active compound) must be evaluated using tools adapted to their physicochemical properties. Their biodistribution in the body and the elimination process need also to be fully characterized for safety concerns (31).

## 4.3. Food industry field

Food industry uses nanotechnologies to create functional and preservative ingredients. NM allow increasing the physical stability of food dispersion by reducing the sedimentation/skimming. NE and phospholipid vesicles improve the solubility of active ingredients and flavors (32). Metal oxide nanoparticles, including zinc oxide, titanium dioxide known as E171 in Europe or silica dioxide E551, were added to some pastries as a coloring or opacifying agents. NM are also present in the packaging to increase the shelf life of food. They are usually embedded in plastic matrices to limit bacterial growth or prevent the permeation of gases or UV rays. Silver, zinc oxide and titanium dioxide nanoparticles possess antibacterial

properties (34). Other applications of nanotechnologies were reported in the food sector. Nanoporous materials were developed for water filtration and for removing unwanted flavors or allergens from food products (32). Few studies focused on the consequences of the consumption of NM-containing food in human. Due to their small size, NM could accumulate in the intestinal mucus or in Peyer's patches. A chronic exposure to NPs could alter the integrity of the epithelium and modulate the intestinal permeability (33).

## 5. Routes of human exposure to nanoparticles

The effects of NPs on the human body are related to the route of entry into the organism and to their particulate form. NPs can enter the body by ingestion, inhalation, transdermal penetration, or intravascular injection and then be randomly distributed to organs (**Figure 11**).

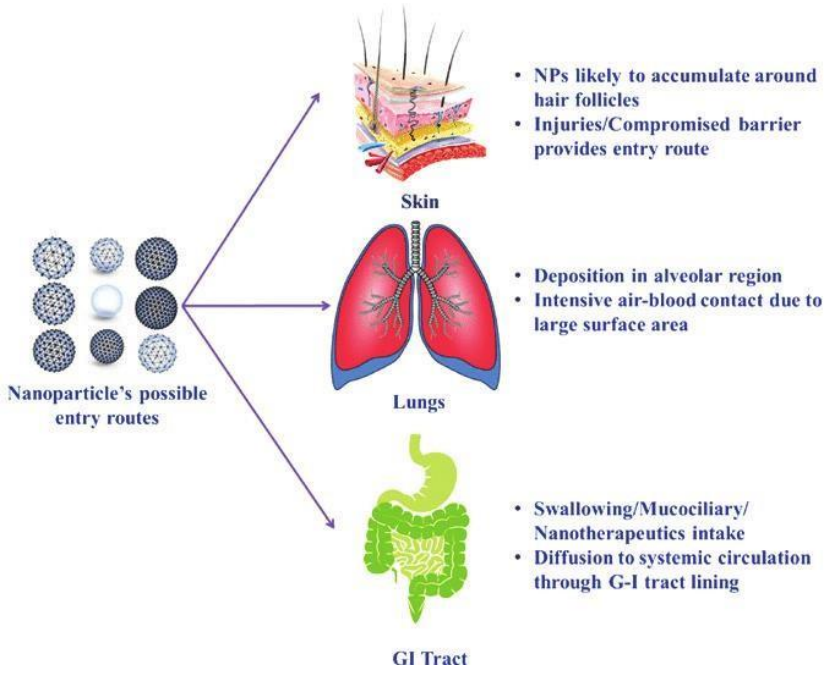


***Figure 11: main exposure routes of human body to nanoparticles. According to Naseer et al 2018* (34).**

## 5.1. Dermal route

Human skin is characterized by a surface area of approximately 2 m². It is composed of three distinct layers, the epidermis which represents the outermost layer, the dermis, and the hypodermis. The skin forms an effective barrier against the invasion of pathogens, chemical and physical attacks, as well as the uncontrolled loss of water and solutes (35). Engineered NPs are used in many skin products as sunscreen, texture agents, colorants, and drug delivery systems. The small size of NPs could promote their interaction with skin cells. NPs could cross the barrier by paracellular pathway, crossing the stratum corneum and passing through the lipid matrix between keratinocytes or along the hair follicles (**Figure 12**) (36). However, most of NPs are usually located in the epidermis which represents a very efficient protective barrier.

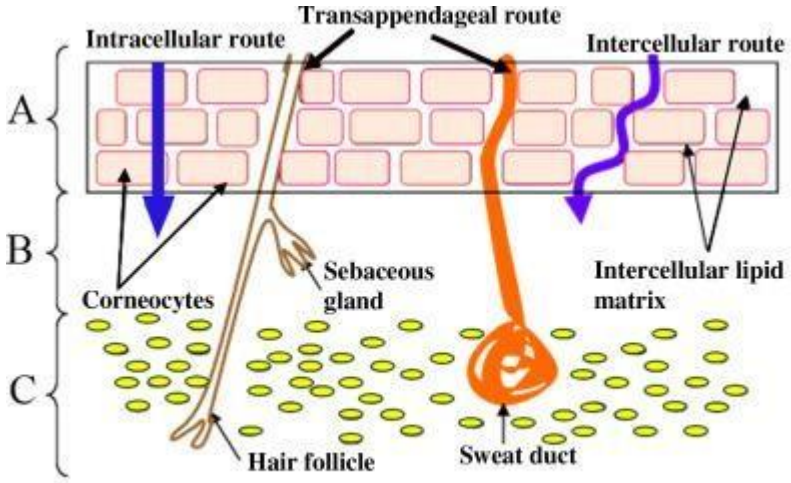


***Figure 12: schematic represent the different NPs penetration pathways through skin barrier. According to Nafisi et al 2018* (37).**

## 5.2. Oral route

A large part of NPs enters in the human body by the oral route. NPs are used as anti-caking agents to obtain a more homogeneous, smoother mixture, but also to improve the assimilation of nutrients. $TiO_2$ nanoparticles are present in most toothpaste (1-10 µg/mg of product). Their use in food products represents a significant part of oral exposure to NPs in Human (38). They are also present in environment, including natural and anthropogenic NPs. Silica nanoparticles are used as an anti-caking agent (food additives E550/551) in most food powders such as the salt. Both *in vitro* and *in vivo* studies reported that some NPs are able to cross the intestinal barrier, depending on their physicochemical characteristics and compositions (39). However, the translocation pathway stays unclear. Immunohistochemically monitoring is faced with the nanometric scale which requires a high-resolution level for imaging instruments. The translocation of ingested NPs can occur by several routes including the paracellular and transcellular routes (**Figure 13**) (40). The paracellular passage is classically an exchange pathway for water and electrolytes. Only small hydrophilic molecules cross the intestinal epithelium by this route in healthy individuals (41). However, NPs can increase the intestinal permeability by acting on the tight junctions and then promote the paracellular transport (42). Transcellular transport occurs by endocytosis and transcytosis through enterocytes and M cells in Peyer's patches for small NPs characterized by diameter below 100 nm. (43).

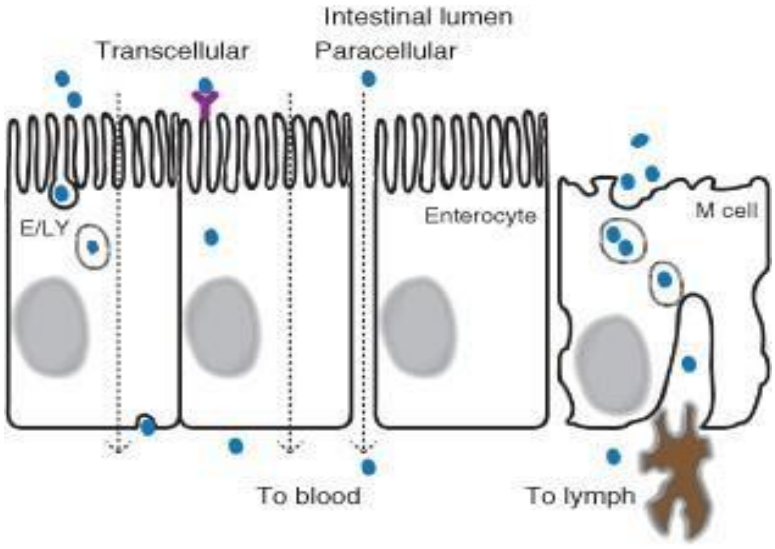


***Figure 13: schematic represent the different NPs penetration pathways through gastro-intestinal tract. According to Bellmann et al 2015* (44).**

## 5.3. Pulmonary route

Inhalation is a very commune route of exposure for NPs. Once inhaled, NM can either be exhaled or be deposited in the different regions of the respiratory tree. The upper airways include nasal cavities, mouth, pharynx, and larynx. The tracheo-bronchial tree is composed of the trachea, bronchi, and bronchioles and the pulmonary alveoli (**Figure 14**). The deposition of NPs depends on the diameter, the aggregation/agglomeration degree, and the density. Particles with a diameter between 10 and 100 nm are mainly deposited in the deep lung, at the level of the pulmonary alveoli. The penetration of NM through the respiratory tract is greater in impaired lung functions due for example, to chronic bronchitis (45).

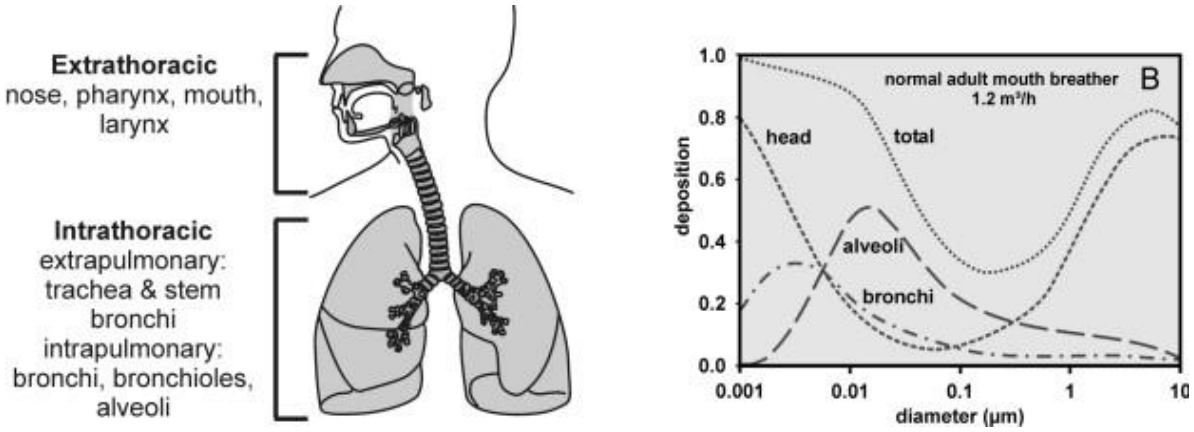


***Figure 14: deposition of nanoparticles in respiratory tract depending on their size. According to Geiser et al 2010* (46)**.

## 5.4. Ocular route

The ocular route concerns fine particles in the air but also NPs for therapeutic purposes **(Figure 15).** They can be administered by periocular, intravitreal injection or corneal absorption (47).

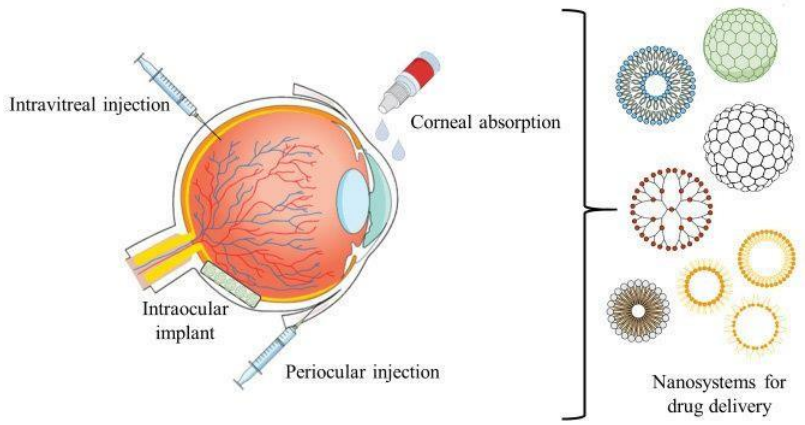


***Figure 15: schematic represent the different NPs penetration route through eye. According to Souto et al 2019* (47).**

## 5.5. Parenteral route

The parenteral route is used for the administration of NPs for biomedical applications. NPs can be intravenously, subcutaneously, intradermally, or intramuscularly injected. The intravenous route provides an instantaneous response. It is also suitable for drugs that cannot be absorbed by the gastrointestinal tract or cannot be injected into muscles or other tissues (48). Intravenously injected NPs improve the pharmacokinetic profile of drugs by extending the plasma half-life and preserve them from chemical degradations. They can also control the biodistribution by targeting specific tissues and cells. Abraxane®, an albumin NP was approved by the FDA in 2006 for paclitaxel-based treatments (49). A better therapeutic response was observed in women with a metastatic breast cancer compared with the standard formulation of paclitaxel (50). Distribution of untargeted NPs after intravenous administration was observed in many organs. 60% of the injected dose of gold NPs was detected in the liver, lungs, spleen, heart, kidneys and brain after intravenous injection (51). Uncoated NPs characterized by a hydrophobic surface are mainly phagocytosed by macrophages in liver, spleen, and lungs, especially when the diameter is higher than 5 nm. Smaller NPs are eliminated from the body by renal excretion. Surface modification is an effective way to reduce clearance and enhance cellular uptake for a maximum drug accumulation in target sites (50).

## 6. Regulations of nanomaterials

The articles L-523-1 to L523-3 of The French environmental Code require an annual declaration system for “substances in nanoparticle state”. From January 1st, 2013, all the manufacturers, importers, and distributors of NM need to fill a declaration in the R-nano register when quantities are greater than 100g per year. It must include the quantity, the physicochemical properties, and the application. The available information regarding the health and environmental hazards must be mentioned (52). From January 1st, 2020, the European Commission requested to identify the size, shape, surface structure as well as dissolution and stability parameters of nanomaterials (53). Regulations are recommended for the use of nanoparticles in various fields, including food industry, cosmetics, and the pharmaceutical applications. Since 2014, the European INCO regulation (Information du Consommateur UE 1169/2011) has required that the mention "nano" should appear on the labels of nanoparticle-containing foods (54). In 2011, the European Food Safety Authority (EFSA) published a guide for the risk assessment of nanoscience and nanotechnology applications in the food chain. This guide details the risk assessment procedure in three steps: identification, exposure assessment and risk characterization (55). Titanium dioxide was authorized as a food additive named E171 by European regulations in foodstuffs, mainly in confectionery, bakery products and sauces. It is also used in other fields like cosmetics, paints, and medicines. In May 2021, EFSA concluded that titanium dioxide could no longer be considered safe as a food additive, due to its genotoxic potential and accumulation in the organism (56). EFSA panel published in 2018 a re-evaluation of the E551 as a food additive. The panel concluded the European specifications of the additive are still insufficient. This requests a better size characterization of silica particles to identify the presence and the ratio of nano silicates. Besides, it was not possible to confirm the current acceptable daily intake not specified due to the limited toxicological data. The Cosmetics Regulation made obligatory, from July 2013, the reporting of the “nanomaterials” presence in the ingredient list of cosmetic products. In February 2022, the European Commission notified the world trade organization a draft amendment to cosmetics regulation. The aim is to prohibit the use of nanomaterials in cosmetic products for which the Scientific Committee on Consumers Safety (SCCS) identified a risk for human health. This is the case for copper NPs. In France, nanoparticles used in cosmetics are subject, like other nanomaterials, to the obligation of declaration in the R-nano register

(57). Concerning the use of nanoparticles in the pharmaceutical field, it was extremely difficult to establish a single regulation given the diversity of nanomedicines, their chemical nature and their many applications (58). In general, there was a lack of studies in the evaluation of nanomedicines. Currently, new nanoparticle-based drugs are evaluated by the Food and Drug Administration (FDA), the European Medicines Agency (EMA) and other agencies using a benefit/risk analysis approach (59).

# References


1. European Commission. Commission recommendation for nanoparticles definition. J Off Union Eur [Internet]. 2022 Jun 10

2. European commission. Commission recommendation for nanoparticles definition. J Off Union Eur. 2011 Oct 18;3.

3. ISO/TC 229 - Nanotechnologies [Internet]. ISO

4. Nanomaterials Market Size & Share Report, 2021-2028 [Internet]. [cited 2022 Mar 8]. Available from: https://www.grandviewresearch.com/industry-analysis/nanotechnology-and-nanomaterials-market

5. Shah KW, Huseien GF. Inorganic nanomaterials for fighting surface and airborne pathogens and viruses. Nano Express. 2020 Nov;1(3):032003.

6. Christoforidis J, Chang S, Jiang A, Wang J, Cebulla C. Intravitreal Devices for the Treatment of Vitreous Inflammation. Mediators Inflamm. 2012 Sep 5;2012:126463.

7. Owen SC, Chan DPY, Shoichet MS. Polymeric micelle stability. Nano Today. 2012 Feb;7(1):53–65.

8. Ghezzi M, Pescina S, Padula C, Santi P, Del Favero E, Cantù L, et al. Polymeric micelles in drug delivery: An insight of the techniques for their characterization and assessment in biorelevant conditions. J Control Release Off J Control Release Soc. 2021 Apr 10;332:312–36.

9. Lembo D, Cavalli R. Nanoparticulate Delivery Systems for Antiviral Drugs. Antivir Chem Chemother. 2010 Dec 1;21:53–70.

10. Sopyan I. A Review: A Novel of Efforts to Enhance Liposome Stability as Drug Delivery Approach. 2020;11(6):8.

11. Gurpreet K, Singh SK. Review of Nanoemulsion Formulation and Characterization Techniques. Indian J Pharm Sci. 2018 Aug 31;80(5):781–9.

12. Che Marzuki NH, Wahab RA, Abdul Hamid M. An overview of nanoemulsion: concepts of development and cosmeceutical applications. Biotechnol Biotechnol Equip. 2019 Jan 1;33(1):779–97.

13. Abbasi E, Aval SF, Akbarzadeh A, Milani M, Nasrabadi HT, Joo SW, et al. Dendrimers: synthesis, applications, and properties. Nanoscale Res Lett. 2014 May 21;9(1):247.

14. Santos A, Veiga F, Figueiras A. Dendrimers as Pharmaceutical Excipients: Synthesis, Properties, Toxicity and Biomedical Applications. Materials. 2019 Dec 21;13(1):65.

15. K HK, Venkatesh N, Bhowmik H, Kuila A. Metallic Nanoparticle: A Review. Biomed J Sci Tech Res. 2018;4(2):3765–75.

16. Mody VV, Siwale R, Singh A, Mody HR. Introduction to metallic nanoparticles. J Pharm Bioallied Sci. 2010;2(4):282–9.

17. Manchandani P, Chandrawanshi HK, Pilaniya U, Pilaniya K. Quantum Dots as multifunctional nanoparticles - A review. :8.

18. Jeelani P, Mulay P, Venkat R, Ramalingam C. Multifaceted Application of Silica Nanoparticles. A Review. undefined. 2019

19. Jeelani PG, Mulay P, Venkat R, Ramalingam C. Multifaceted Application of Silica Nanoparticles. A Review. Silicon. 2020 Jun;12(6):1337–54.

20. Rathinavel S, Priyadharshini K, Panda D. A review on carbon nanotube: An overview of synthesis, properties, functionalization, characterization, and the application. Mater Sci Eng B. 2021 Jun;268:115095.

21. Abazari S, Shamsipur A, Bakhsheshi-Rad HR, Ismail AF, Sharif S, Razzaghi M, et al. Carbon Nanotubes (CNTs)-Reinforced Magnesium-Based Matrix Composites: A Comprehensive Review. Materials. 2020 Oct 4;13(19):4421.

22. Talebian S, Rodrigues T, das Neves J, Sarmento B, Langer R, Conde J. Facts and Figures on Materials Science and Nanotechnology Progress and Investment. ACS Nano. 2021 Oct 26;15(10):15940–52.

23. Chiari-Andréo BG, Almeida-Cincotto MGJ de, Oshiro JA, Taniguchi CYY, Chiavacci LA, Isaac VLB. Nanoparticles for cosmetic use and its application. In: Nanoparticles in Pharmacotherapy. Elsevier; 2019

24. de Melo A, Amadeu M, Lancellotti M, Hollanda L, Machado D. The role of nanomaterials in cosmetics: National and international legislative aspects. Quím Nova. 2015 May 1;38.

25. Daudt RM, Emanuelli J, Külkamp-Guerreiro IC, Pohlmann AR, Guterres SS. A nanotecnologia como estratégia para o desenvolvimento de cosméticos. Ciênc E Cult. 2013 Jul;65(3):28–31.

26. Mihranyan A, Ferraz N, Strømme M. Current status and future prospects of nanotechnology in cosmetics. Prog Mater Sci. 2012 Jun 1;57(5):875–910.

27. Kaul S, Gulati N, Verma D, Mukherjee S, Nagaich U. Role of Nanotechnology in Cosmeceuticals: A Review of Recent Advances. J Pharm. 2018 Mar 27;2018:e3420204.

28. Allen TM, Cullis PR. Drug delivery systems: entering the mainstream. Science. 2004 Mar 19;303(5665):1818–22.

29. Jordanovska S. Les nanoparticules dans l'industrie pharmaceutique: comparaison des méthodes de fabrication. :61.

30. Wang AZ, Langer R, Farokhzad OC. Nanoparticle delivery of cancer drugs. Annu Rev Med. 2012;63:185–98.

31. De Jong WH, Borm PJ. Drug delivery and nanoparticles: Applications and hazards. Int J Nanomedicine. 2008 Jun;3(2):133–49.

32. Chaudhry Q, Castle L. Food applications of nanotechnologies: An overview of opportunities and challenges for developing countries. Trends Food Sci Technol - TRENDS FOOD SCI TECHNOL. 2011 Nov 1;22:595–603.

33. Blanco E, Shen H, Ferrari M. Principles of nanoparticle design for overcoming biological barriers to drug delivery. Nat Biotechnol. 2015 Sep;33(9):941–51.

34. Naseer B, Srivastava G, Qadri O, Faridi S, Islam R, Younis K. Importance and Health Hazards of Nanoparticles Used in the Food Industry. Nanotechnol Rev. 2018 Sep 1;7.

35. Proksch E, Brandner JM, Jensen JM. The skin: an indispensable barrier. Exp Dermatol. 2008 Dec;17(12):1063–72.

36. Valenzuela P, Simon JA. Nanoparticle delivery for transdermal HRT. Nanomedicine Nanotechnol Biol Med. 2012 Sep;8:S83–9.

37. Nafisi S, Maibach HI. Chapter 3 - Skin penetration of nanoparticles. In: Shegokar R, Souto EB, editors. Emerging Nanotechnologies in Immunology. Boston: Elsevier; 2018

38. Mc L, C H, S V, Sm G, A C, Rp T, et al. Dietary sources of inorganic microparticles and their intake in healthy subjects and patients with Crohn's disease The British journal of nutrition. 2004

39. Jani P, Halbert GW, Langridge J, Florence AT. Nanoparticle uptake by the rat gastrointestinal mucosa: quantitation and particle size dependency. J Pharm Pharmacol. 1990 Dec;42(12):821–6.

40. Houdeau E. Nanoparticules et barrière intestinale : comprendre les mécanismes de franchissement. 2012 Jan 1;

41. Turner J. Molecular basis of epithelial barrier regulation: From basic mechanisms to clinical application. Am J Pathol. 2007 Jan 1;169:1901–9.

42. Cornu R, Chrétien C, Pellequer Y, Martin H, Béduneau A. Small silica nanoparticles transiently modulate the intestinal permeability by actin cytoskeleton disruption in both Caco-2 and Caco-2/HT29-MTX models. Arch Toxicol. 2020 Apr;94(4):1191–202.

43. Shakweh M, Ponchel G, Fattal E. Particle uptake by Peyer's patches: a pathway for drug and vaccine delivery. Expert Opin Drug Deliv. 2004 Nov;1(1):141–63.

44. Bellmann S, Carlander D, Fasano A, Momcilovic D, Scimeca JA, Waldman WJ, et al. Mammalian gastrointestinal tract parameters modulating the integrity, surface properties, and absorption of food-relevant nanomaterials. WIREs Nanomedicine Nanobiotechnology. 2015;7(5):609–22.

45. da Silva AL, Cruz FF, Rocco PRM, Morales MM. New perspectives in nanotherapeutics for chronic respiratory diseases. Biophys Rev. 2017 Sep 15;9(5):793–803.

46. Geiser M, Kreyling W. Deposition and biokinetics of inhaled nanoparticles. Part Fibre Toxicol. 2010 Jan 20;7:2.

47. Souto EB, Dias-Ferreira J, Lopez-Machado A, Ettcheto Arriola M, Cano A, Camins A, et al. Advanced Formulation Approaches for Ocular Drug Delivery: State-Of-The-Art and Recent Patents. Pharmaceutics. 2019 Sep 6;11:460.

48. Parker SE, Davey PG. Pharmacoeconomics of intravenous drug administration. PharmacoEconomics. 1992 Feb;1(2):103–15.

49. Kalepu S, Nekkanti V. Insoluble drug delivery strategies: review of recent advances and business prospects. Acta Pharm Sin B. 2015 Sep;5(5):442–53.

50. Chenthamara D, Subramaniam S, Ramakrishnan SG, Krishnaswamy S, Essa MM, Lin FH, et al. Therapeutic efficacy of nanoparticles and routes of administration. Biomater Res. 2019 Nov 21;23:20.

51. Bednarski M, Dudek M, Knutelska J, Nowiński L, Sapa J, Zygmunt M, et al. The influence of the route of administration of gold nanoparticles on their tissue distribution and basic biochemical parameters: In vivo studies. Pharmacol Rep PR. 2015 Jun;67(3):405–9.

52. Nanomatériaux, nanoparticules. Réglementation - Risques - INRS [Internet]. [cited 2022 May 25]. https://www.inrs.fr/risques/nanomateriaux/reglementation.html

53. RÈGLEMENT (UE) 2018/1881 DE LA COMMISSION. J Off Union Eur. 2018 Dec 3;20.

54. Aschberger K, Rauscher H, Crutzen H, Rasmussen K, Christensen FM, Sokull-Klüttgen B, et al. Considerations on information needs for nanomaterials in consumer products. 2014;72.

55. L'Autorité Européenne de Sécurité des Aliments – Les nanoparticules dans l'alimentation. 2011 https://controverses.minesparis.psl.eu/public/promo16/promo16_G14/www.controverses-minesparistech-3.fr/_groupe14/lautorite-europeenne-de-securite-des-aliments/index.html

56. Dioxyde de titane : le E171 n'est plus considéré comme sûr en tant qu'additif alimentaire | EFSA https://www.efsa.europa.eu/fr/news/titanium-dioxide-e171-no-longer-considered-safe-when-used-food-additive

57. European Commission. Directorate General for Health and Food Safety. Scientific advice on the safety of nanomaterials in cosmetics. https://data.europa.eu/doi/10.2875/125512

58. Nanotoxicologie et réglementation des nanomédicaments [Internet]. Techniques de l'Ingénieur. https://www.techniques-ingenieur.fr/base-documentaire/innovation-th10/nanotechnologies-pour-l-energie-l-environnement-et-la-sante-42514210/nanotoxicologie-et-reglementation-des-nanomedicaments-nm4040/

59. Desai N. Challenges in Development of Nanoparticle-Based Therapeutics. AAPS J. 2012 Mar 10;14(2):282–95.

# CHAPTER II: NANOTOXICITY: BIBLIOGRAPHIC PART

## 1. Nanotoxicology

The fundamental aspect for understanding the toxicity of NPs is their physicochemical characterization. Their small size, surface charge and composition are critical factors governing the interactions with the biological environment. These bio–nano interactions are essential for understanding the biodistribution and toxic effects of many nanomaterials in both *in vitro* and *in vivo* models. Nanomaterials can form "aggregates" or "agglomerates" in contact with biological fluids, modulating the toxicity of the original nanomaterial (1). Due to their small size, NPs have the ability to penetrate the human body, cross the various biological barriers and reach the most sensitive organs (2). For particles with the same composition, the size change leads to different levels of cytotoxicity (3). Small NPs can be internalized in cells, causing toxicity issues (4).Changes in the surface charge result also in dramatic differences in cell internalization and biodistribution of NPs. NPs with a positively charged surface are known to have the highest toxicity. The chemical composition also influences the toxicity of NPs. In the literature, the most documented toxic NPs are metallic type NPs(5).

## 2. Toxicological model studies

To study the toxic effects of nanomaterials, cellular and animal models are usually used. The choice of model depends essentially on the study objective and the expected result. From literature, rats and mice are the most common species for *in vivo* toxicity studies. However, the pharmaceuticals regulation requires to include non-rodent species in safety studies. The number of *in vitro* toxicity studies have been multiplied in recent years due to the growing development of alternative methods to the use of animals in experiments (5). Cell types are mainly macrophages, blood cells, hepatocytes, epithelial and endothelial cells (7). An *in vitro* and *in vivo* correlation is necessary to validate the cellular model.

# References


1. Hobson DW, Guy RC. Nanotoxicology. In: Encyclopedia of Toxicology [Internet]. Elsevier; 2014

2. Wahajuddin, Arora S. Superparamagnetic iron oxide nanoparticles: magnetic nanoplatforms as drug carriers. Int J Nanomedicine. 2012;7:3445–71.

3. Gliga AR, Skoglund S, Odnevall Wallinder I, Fadeel B, Karlsson HL. Size-dependent cytotoxicity of silver nanoparticles in human lung cells: the role of cellular uptake, agglomeration and Ag release. Part Fibre Toxicol. 2014 Feb 17;11(1):11.

4. Zhu M, Nie G, Meng H, Xia T, Nel A, Zhao Y. Physicochemical properties determine nanomaterial cellular uptake, transport, and fate. Acc Chem Res. 2013 Mar 19;46(3):622–31.

5. Bahadar H, Maqbool F, Niaz K, Abdollahi M. Toxicity of Nanoparticles and an Overview of Current Experimental Models. Iran Biomed J. 2016;20(1):1–11.

6. Jones CF, Grainger DW. In vitro assessments of nanomaterial toxicity. Adv Drug Deliv Rev. 2009 Jun 21;61(6):438–56.


## 3. Oral toxicity

Ingested nanoparticles mainly come from drug delivery systems and food products. They can be also released from packaging materials. Another origin is their presence in in the air and drinking water, including natural and anthropogenic NPs. After ingestion, they are in contact with the gastrointestinal tract, especially the intestinal barrier which offers a large exposure surface. A review of the literature on the intestinal toxicity of ingested NPs was carried out in this part. Toxicokinetic and toxicological endpoints including cytotoxicity, genotoxicity, oxidative stress, and inflammatory response were considered.

# Interaction and Toxicity of Ingested Nanoparticles on the Intestinal Barrier

Thomas Stalder[a, b], Taghrid Zaiter[a], Wassim El Basset[a], Raphaël Cornu[a], Hélène Martin[a], Mona Diab[c], Arnaud Béduneau[a,*]

a: PEPITE EA4267, Univ. Bourgogne Franche-Comté, F-25000 Besançon, France

b: Department of Pharmacy, University Hospital of Besançon, F-25000 Besançon, France

c: EDST, Pharmacology and Cancerology Laboratory, Faculty of Sciences, Lebanese University, Beirut 1500, Lebanon

*Corresponding author:

arnaud.beduneau@univ-fcomte.fr

**Abstract**

The gastrointestinal tract represents one of primary routes of entry for many nanomaterials. Their size in the nanometer range and their high surface area confer them very interesting properties as food additives. They are used as texturizing, opacifying or anticaking agents. Food packaging contains nanomaterials with antimicrobial properties. Humans are also orally exposed to nanoparticles (NPs) present in the air or drinking water. Ingested NPs can then reach the intestinal lumen and interact with the gastrointestinal fluids, microbiota, mucus layer and the epithelial barrier, allowing a potential translocation. The toxicological profile of ingested NPs is still unclear due to the variety of NPs in terms of composition and physicochemical properties as well as the limited number of investigations. Their unique properties related to their small size could however affect the intestinal ecosystem but also the physical and functional properties of the intestinal barrier. This review focuses on the fate of ingested organic and inorganic NPs in the intestinal lumen and their toxicity on the microbiota and epithelial cells.

**Keywords :** Nanoparticles, Intestinal cells, Microbiota, Intestinal permeability, Cytotoxicity, Genotoxicity

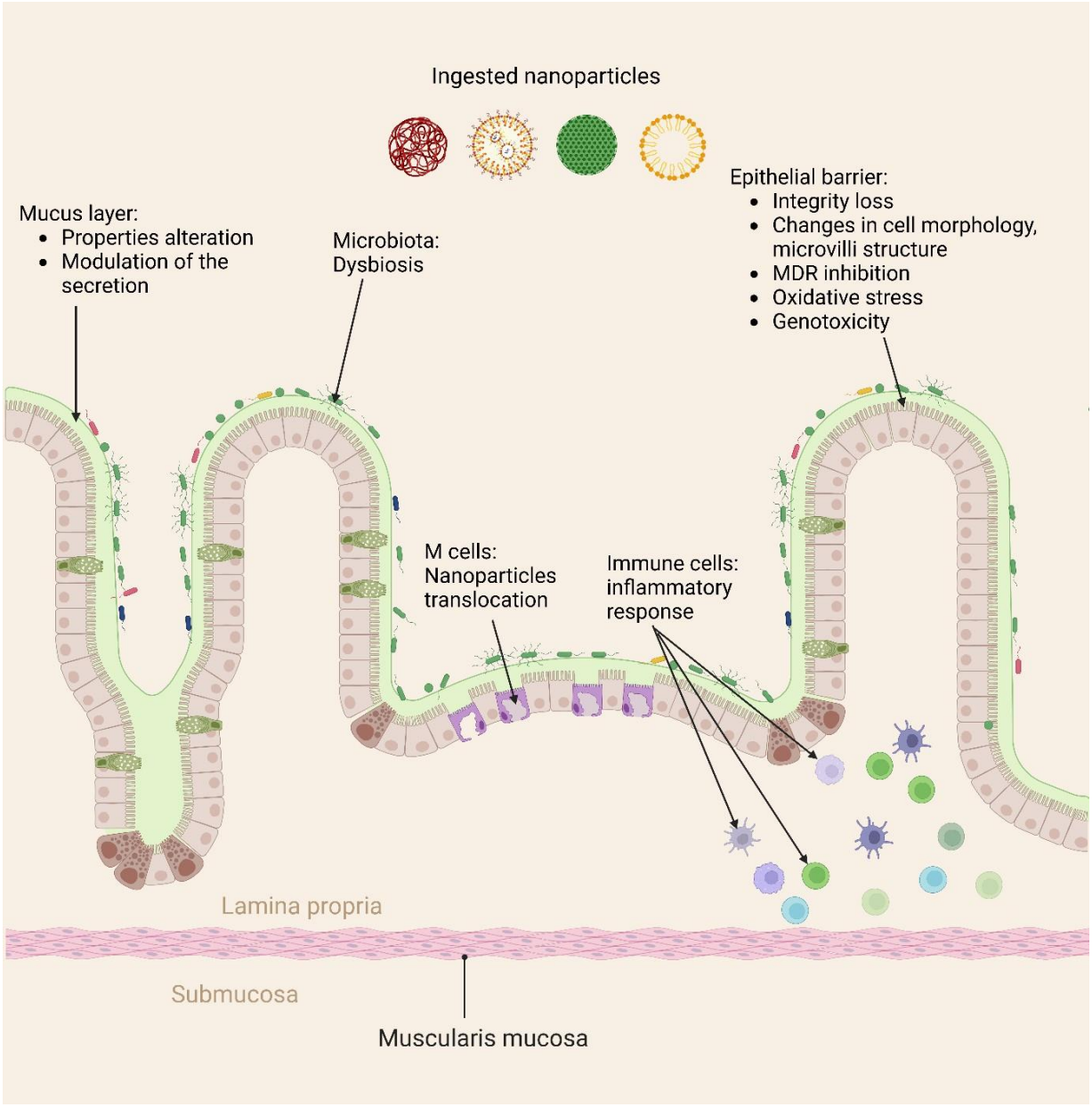


**Graphical abstract**

# I. Introduction

In the first definition issued by the European Commission (EC) in 2011, nanomaterials were described as solid particles including single, agglomerated, and aggregated particles where at least 50 % of particles in the number size distribution have one or more external dimensions between 1 nm and 100 nm (Commission Européenne, 2011). Two other conditions have been added in the new definition published in 2022 by the EC (Commission Européenne, 2022). This includes the elongated particles characterized by two dimensions smaller than 1 nm and another one larger than 100 nm such as the rods, fibers, and tubes. Platelet particle with one dimension below 1 nm and two others above 100 nm are also defined as nanomaterials. According to the ISO/TS 80004-2:2015 guidelines, nanoparticles (NPs) are characterized by three external dimensions in the nanoscale comprised between 1 and 100 nm and approximately in the same range ("ISO/TS 80004-1:2015, Nanotechnologies ). NPs represent a sub-class of nanomaterials. They are composed of organic (lipid and polymeric NPs, dendrimers, micelles) and inorganic (silica, titanium dioxide, metal and metal oxide NPs) materials (Maroof et al., 2016). Some of them, especially inorganic NPs are present in food products due to their coloring or texturing properties. Organic NPs especially lipid and polymeric NPs are mainly used as drug delivery systems to enhance the solubility, stability, and bioavailability of drug molecules (Dilnawaz, 2017). Humans can also ingest natural and incidental anthropogenic NPs present in the environment. Silica and iron NPs are released from volcanic ash clouds while carbon nanotubes were detected during the combustion of pines (Griffin et al., 2018). After oral administration, NPs can reach the Gastrointestinal Tract (GIT), where the intestine, which offers a large exposure surface, is present. Their small dimensions and their high surface area grant those many advantages as food and pharmaceutical ingredients. At the same time, these features promote their interactions with the biological environment, including cells, mucus and bacteria. An alteration of physical and functional properties of the intestine could be reasonably assumed. However, the fate and the toxicity of NPs after oral ingestion has not been yet fully elucidated due to the growing number of nanomaterials and the lack in toxicological studies. Are they able to modulate the intestinal permeability or reach the systemic circulation after translocation? Can they affect the microbiota and the epithelial cells, inducing digestive disorders, inflammatory responses, genotoxicity or oxidative stress? This present work faces the published toxicological data on ingested nanomaterials to identify the critical factors responsible for the intestinal nanotoxicity.

## II- The multilayer intestinal barrier

The intestine is an important body organ which prevents microorganisms and xenobiotics including NPs from reaching the systemic circulation (Lundquist and Artursson, 2016; Segata et al., 2012). The intestine could be considered as a barrier composed of multilayers. The first one is the bacterial microbiota. It is responsible for many functions such as regulating host immunity, protecting against pathogens and preserving gut integrity (Thursby and Juge, 2017). It also plays an important role in the collection of energy from food to synthetize vitamins and amino acids. Disruption of the bacterial microbiota can lead to many diseases as the Inflammatory Bowel Disease (IBD) and metabolic syndrome (Barko et al., 2018). The mucus represents the second layer which protects the epithelium from mechanical damages. Mucus acts as a physical barrier, hindering pathogens from reaching epithelial (Pelaseyed et al., 2014). This hydrogel is composed of large glycoproteins, mainly mucins. Mucins are organized in two adjacent layers. The inner one is thin and strongly adherent in contrast to the outer one. The main mucins secreted in the small intestine by goblet cells are the MUC2 and MUC5AC. In the jejunum, each MUC2 binds to three other mucins to form a hexagonal mesh. The synthesis of these mucins is influenced by the intestinal microbiota as well as the luminal substances including bioactive compounds present in functional food (Damiano et al., 2018; Walsh et al., 2013). The intestinal epithelium represents the third layer. It is formed of a continuous polarized monolayer of cells interconnected and bound to a basement membrane by proteins, mainly integrins (Pompili et al., 2021). It regulates solute transport and selective transporters for amino acids, electrolytes, short chain fatty acids and sugars (Groschwitz and Hogan, 2009). The epithelium is mainly composed of absorptive enterocytes, covering a large surface, and making up to 80-90 % of the epithelium and goblet cells (8 %). The apical membrane of the enterocytes is covered by microvilli that increase the intestine's surface area (Faust et al., 2014b; Lundquist and Artursson, 2016). Paneth cells, enteroendocrine cells, Microfold cell (M cells) and stem cells are also present in the intestinal epithelium but at a smaller proportion (Gehart and Clevers, 2019). M cells located in the Peyer's patches are responsible for the transport of antigens from the lumen of the small intestine to the lymphoid follicles. They are involved in the mucosal immunity response (Corr et al., 2008).

Intestinal permeability is governed by two major pathways: paracellular and transcellular routes. The intercellular space is regulated by proteins (Salvo Romero et al., 2015). They are involved in different types of junctions such as Tight Junctions (TJs), anchoring and

communicating junctions. TJs (as occludins, claudins), Junction Adhesion Molecules and tricellulin regulate the paracellular trafficking of molecules. They are arranged as multiprotein complexes that form a selective permeable seal between adjacent epithelial cells (Lee, 2015). The expression of claudins 1, 4 and 5 consolidates the permeability of TJs while claudin-2 depletion enhances the barrier function of the intestine (Suzuki et al., 2011; Weber, 2012). TJs are associated with Zonula Occludens (ZO-1 ZO-2 and ZO-3) which are bound to F actin (Rodgers and Fanning, 2011). Thus, ZO proteins allow the anchorage of TJs to the actin cytoskeleton. The interaction loss between TJs and cytoskeleton by actin depolymerisation can lead to a drastic increase in the intestinal paracellular permeability (Shen and Turner, 2005). Occludin phosphorylation by protein kinase C (PKC) can also weaken the interaction with actin, leading to a dissociation from the junctional complex (Lee, 2015). The inflammatory response involving the activation of the subepithelial immune system with dendritic cells, neutrophils, and macrophages can affect the TJ integrity. Interleukin 8 (IL-8) which is a major neutrophil recruiting chemokines induces actin rearrangement, thus increasing TJ permeability (Gerloff et al., 2013; Talavera et al., 2004). Other cytokines like TNF-α, IL-1β, IL-6, IL-13 and IL-17 can affect the actin arrangement and increase claudin-2 expression through the MEK/ERK and PI3K pathways (Mankertz et al., 2009; Nighot et al., 2015; Shen et al., 2011; Suzuki et al., 2011; Talavera et al., 2004). On the contrary, anti-inflammatory cytokines secreted by regulatory T cells (T4) such as the IL-10 and TGF-β increase TJs' expression through MEK/ERK signalling and therefore reduce the intestinal permeability (Sun et al., 2008). The anchoring junctions connect the cytoskeleton of each cell to that of neighbouring cells or to the extracellular matrix. They include adherent junction and desmosomes and play an important role in various cell processes such as differentiation, proliferation, and morphogenesis. The communicating junctions link the cytoplasm of adjacent cells by forming a channel of connexins through their membranes. They also play a crucial role in the growth and development of epithelial cells as well as in the barrier function maintenance (Salvo Romero et al., 2015). The transcellular pathway consists of transporting molecules across the enterocytes using different mechanisms. This can include energy-dependent selective transporters (active transport), passive or facilitated diffusion, and receptor or absorptive-mediated endocytosis. The type of mechanism involved depends on the size and physicochemical properties of the molecules (Turner, 2009). Passive transport enables the diffusion of small lipophilic molecules through the enterocyte membrane. The solute carriers, termed SLC, carry drugs according to their concentration gradient without adenosine triphosphate (ATP) molecules (Liu and Liu, 2013; Oostendorp et al., 2009). Transporters of the ATP-binding cassette family such as the P-

glycoprotein (P-gp) are involved in the efflux mechanisms. They prevent the systemic distribution of toxins and some xenobiotics located in the intestinal lumen (Fu, 2013). Endocytosis is a vesicle-mediated transcellular transport. Various endocytic processes were reported such as pinocytosis, clathrin-mediated endocytosis, caveolae-mediated endocytosis, and clathrin-caveolae independent endocytosis (Panariti et al., 2012; Talkar et al., 2018; Zhang et al., 2014).

## III- Ingested nanoparticles

### 1. Nanoparticle description

NPs administered by the oral route are used as drug delivery systems, imaging agents and food additive. Many research works focused on innovative biomedical applications of NPs, especially for the diagnosis and the treatment of colorectal cancer and IBD (Pridgen et al., 2015; Tyagi, 2016; Abbas and Alqahtani, 2021). Moreover, the oral route for drug administration offers many advantages such as convenience and medication compliance, especially in the treatment of chronic or long-term diseases that require frequent administration (Pridgen et al., 2015). Active pharmaceutical ingredients and imaging agents entrapped in NPs are protected from chemical and enzymatic degradations (Araújo et al., 2015; Ojer et al., 2015). Insulin and calcitonin were protected against proteases after encapsulation in polymeric NPs (Lowe and Temple, 1994). The encapsulation improves the solubility and the systemic absorption of drugs (Tan and Billa, 2021). A 7.3-fold increase of the curcumin bioavailability was observed with nanoemulsions of ethyl oleate (Wan et al., 2016). E551 food additive composed of amorphous silica NPs is commonly used as anti-caking or thickening agents (Fruijtier-Pölloth, 2016). Titanium dioxide ($TiO_2$) NPs contained in E171 additive are widely present in food products due to their colouring and opacifying properties (Younes et al., 2021). Inorganic NPs were also used in packaging materials to protect food products. Containers were designed with antimicrobial Titanium, Zinc (Zn) or other inorganic NPs to prevent the proliferation of bacteria (Carrillo-Inungaray et al., 2018). However, their release in food products was reported (Huang et al., 2018). Humans are also exposed to natural nanomaterials. Volcanic activity, rock weathering and forest fires produce inorganic NPs such as silica, iron and carbon NPs (Barhoum

et al., 2022). Anthropogenic NPs are incidentally released in the environment during the industrial processes and the combustion of fuels such as carbonaceous NPs (D'Anna, 2009).

## 2. Fate of ingested NPs

After ingestion, NP diffuses into the GIT. The GIT has a pH gradient varying from highly acidic in the stomach to basic with a pH of 7.5 in the colon (Kararli, 1995). During the digestion process, NPs undergo numerous chemical modifications as oxidation, deamidation and hydrolysis (Sood and Panchagnula, 2001). In addition, gut enzymes as proteases, nucleases and lipases present in the GIT are also involved in the degradation of NPs (Ganapathy et al., 2006). The feeding status and meal content also need to be considered (Lundquist and Artursson, 2016). Therefore, potential exposure of NPs to proteins, carbohydrates and lipids present in food products in gastrointestinal fluid can also modify their physicochemical properties. Changes in the surface properties due to adsorption at the surface of NPs as well aggregation/agglomeration or dissolution processes were reported (Wang et al., 2019; Shi et al., 2020; Mbanga et al., 2022). The aggregation state, surface charge and morphology of polyvinylpyrrolidone-coated silver (Ag-PVP) NPs were modified in contact with simulated gastrointestinal fluids. The acidic pH of human gastric intestinal fluids in a fasted state termed FaSSGF, induced the release of silver (Ag) ions, subsequently forming an AgCl precipitate (Jiang et al., 2018). Agglomerates of $TiO_2$ NPs were observed in simulated gastric fluid compared to water (Jones et al., 2015). Gastric digestion induced the clustering of silica (SiO2) NPs due to the acidic pH and high electrolytes concentrations. However, NPs were reformed in the intestinal fluid, suggesting a pH-dependent agglomeration state (Peters et al., 2012).

The interaction of NPs with the mucus layer is mainly modulated by their physicochemical properties; especially size, surface charge and chemistry (Figure 1) (Lamprecht et al., 2001). The mucus mesh size of approximately 100 nm allows only the diffusion of small particles (Fröhlich and Roblegg, 2012; Olmsted et al., 2001). For example, Ag particles characterized by a size of 200 nm were entrapped to a great extent in the mucus layer of a TC7/Caco-2 co-culture model unlike 20 nm NPs (Georgantzopoulou et al., 2016a). Similarly, SiO2 NPs with hydrodynamic diameters of 20 and 30 nm were able to reach the HT29-MTX goblet cells while NPs of 70 and 200 nm were mainly stuck to the mucus layer (Zaiter et al., 2022). Mucins facilitate the mucoadhesion by electrostatic interactions of positively charged NPs (Fröhlich

and Roblegg, 2012). Moreover, interactions with mucins can occur by hydrogen binding, Van der Waals interactions, hydrophobic forces or polymer chain interpenetration (Ojer et al., 2015; Pridgen et al., 2015; Talkar et al., 2018; Woodley, 2001). Some NPs as polyethylene glycol (PEG)-coated NPs were characterized by mucus-penetrating properties (Fröhlich and Roblegg, 2012; Lai et al., 2007; Pridgen et al., 2015). PEG confers hydrophilic properties and a neutral charge to NPs, reducing the interactions with mucins. However, long PEG chains limit the mucus penetration due to steric hindrance (Lundquist and Artursson, 2016).

Mucus-penetrating NPs reach the epithelial cell surface. Different basic internalization mechanisms of particles in cells were reported. Macro-pinocytosis is non-specific and induces the formation of vesicles with about 1 µm in diameter. It allows the internalization of large NPs or agglomerates in cells (Sahay et al., 2010). Clathrin-mediated and caveolae-mediated endocytosis form vesicle at specific regions of the membrane with a diameter of less than 0.1 µm. They are the main cellular internalization pathways of nanomaterials such as PEG-polylactic acid (PLA), polylactic-co-glycolyc acid (PLGA), $SiO_2$, chitosan and gold (Au) NPs (Sahay et al., 2010). Clathrin-independent and caveolae-independent endocytosis induce the formation of small vesicles and occur continuously in the cell. They are also involved in the cell uptake of polymeric NPs such as PLGA NPs (Palocci et al., 2017). The caveolae/lipid raft is the main internalization pathway of nanoemulsions (Fan et al., 2017). The physicochemical properties of NPs, in particular their size and surface charge, are the most important factors involved in the cell uptake (Sahin et al., 2017). The size range comprised between 10 and 60 nm was considered as an optimum diameter. As for the charge, it was reported that positively charged NPs electrostatically bind to the negative cytoplasmic membrane and are then endocytosed (Sabourian et al., 2020). However, they are not able to cross the mucus layer in a significant manner. The interaction of negatively charged NPs with the cell membrane should be low compared with cationic and neutral particles. However, a significant internalization of carboxymethyl dextran-coated NPs with a surface charge of -50 mV was observed in Caco-2 cells (Ayala et al., 2013).

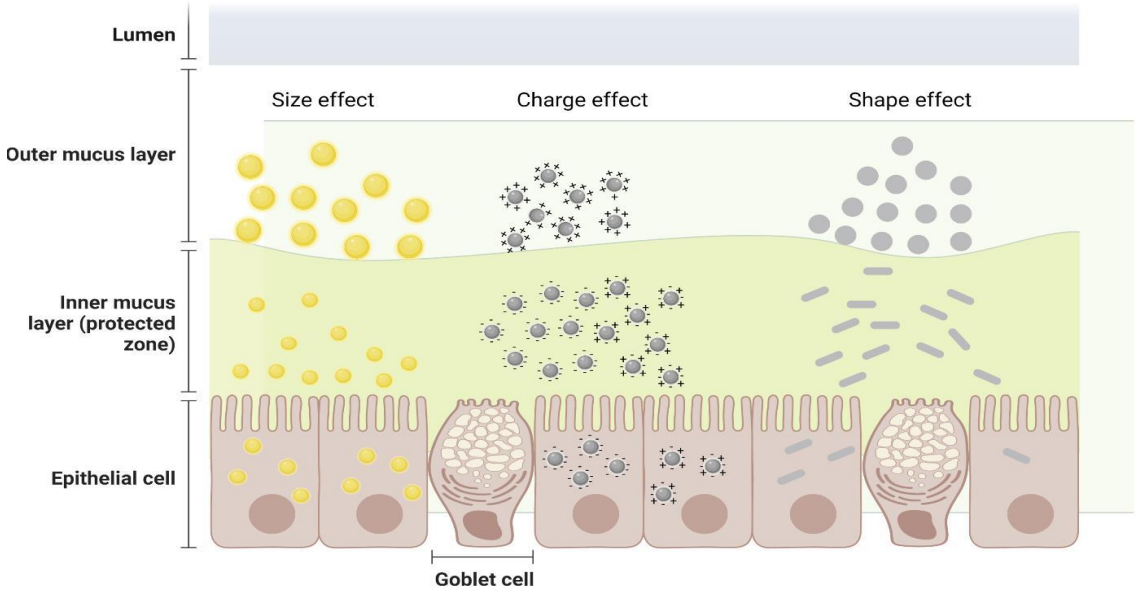


***Figure 1: Schematic representation of the main factors affecting the intestinal distribution of NPs***

Very few studies investigated the transport of NPs across the intestinal barrier. After oral administration, $SiO_2$ NPs were found in kidneys and liver, suggesting their ability to cross the intestinal barrier (Lee et al., 2014). A translocation of $TiO_2$ NPs through the ileum and Peyer's patches was reported (Brun et al., 2014). Oral administration of 75 nm $TiO_2$ NPs in young rats for 30 days also caused hepatic damages (Wang et al., 2013). This is in accordance with the elimination pathway of circulating NPs which involves Kupffer cells (Moghimi et al., 2005). However, the mechanism involved in the transepithelial transport of NPs remains unclear even if the transcytosis across the Peyer's patches seems the potential route (Jani et al., 1992).

## IV. Nanotoxicology

The main toxicity endpoints reported in literature include cytotoxicity, genotoxicity, and inflammatory response on intestinal cells using both *in vitro* and *in vivo* models. Inorganic NPs were mainly responsible for intestinal damages (Table 1) while very few studies clearly demonstrated a toxicity of organic NPs (Table 2). Their influence on the microbiota and the mucus protective barrier was slightly investigated despite their critical role in the intestinal homeostasis.

**Table 1: Intestinal toxicity of inorganic NPs**

| NPs | Size (nm)<br>Surface charge (mV) | Concentration of NPs | Exposure Time | models | Observations | References |
|---|---|---|---|---|---|---|
| | | | ***In vitro* models** | | | |
| Ag | 20 and 200 nm<br>-12.8 and -13.9 mV | 0.1 - 100 mg/mL | Short time exposure: 24 h | Coculture of Human colon colorectal adenocarcinoma Caco-2/TC7 and HT29-MTX cells | Increase in IL-8 in a dose- and size-dependent manner with a lack of cytotoxicity and oxidative stress. | (Georgantzopoulou et al., 2016b) |
| Bare-Ag (Ag-B) | 23 nm<br>-7.7 mV | 0.1 - 2.0 µg/mL | Short time exposure: 24 h<br>Long time exposure: 21 days | Human colon colorectal adenocarcinoma Caco-2 cell | Decrease in cellular viability in a dose and coating dependent manner Increase in IL-8 release in a dose and time dependent manner. | (Chen et al., 2016) |
| Citrate-coated Ag (Ag-CIT) | 24 nm<br>-9.6 mV | | | | | |
| poly (*N*-vinyl-2-pyrrolidone)-coated Ag NP (Ag-PVP) | 30 nm<br>-8.4 mV | | | | | |
| $TiO_2$<br><br>Pure anastase crystal-structure nanospheres of $TiO_2$ | 265 nm<br>-14.1 mv | 62.5, 250 and 1000 µM<br><br>12.5 and 350 µg/mL | 12 h and 24 h<br><br>24 and 48 h | Human intestinal carcinoma epithelial cell lines, SW480 / Normal human intestinal mucosa epithelial cell line NCM460 and coculture of Human colon colorectal adenocarcinoma Caco-2 and HT29-MTX cells | Change of cells morphology<br><br>Decrease in cellular viability in a dose and time dependent manner Increase in DNA damage. | (Setyawati et al., 2015; García-Rodríguez et al., 2018c) |
| | 70 - 80 nm | | | | | |
| Pure rutile crystal-structure nanorods of $TiO_2$ | 40 - 70 nm | | | | | |

| | | | | | | |
|---|---|---|---|---|---|---|
| Nanowires of $TiO_2$ | 8 - 14 nm | | | | | |
| $SiO_2$ | 271.1 nm<br>-13.2 mV | 62.5, 250 and 1000 µM | 12 h and 24 h | Human intestinal carcinoma epithelial cell lines, SW480 / Normal human intestinal mucosa epithelial cell line NCM460 | No cytotoxicity was detected<br>Increase in DNA damage | (Setyawati et al., 2015) |
| CuO | 55.8 nm<br>-27 mV | 2 and 10 µg/mL | 24 h | Human colon colorectal adenocarcinoma | No cytotoxicity was detected | (Schneider et al., 2017a) |
| Au | 31.99 nm<br>-33.93 mV | 2 and 10 µg/mL | 24 h | Human colon colorectal adenocarcinoma | No cytotoxicity was detected | (Schneider et al., 2017a) |
| ZnO | 58.4 nm<br>-13.7 mV | 2 and 10 µg/mL | 24 h | Human colon colorectal adenocarcinoma | No cytotoxicity was detected | (Schneider et al., 2017a) |
| | 148.2 nm<br>-15.1 mV | 62.5, 250 and 1000 µM | 12 h and 24 h | Human intestinal carcinoma epithelial cell lines / Normal human intestinal mucosa epithelial cell line NCM460. | Decrease in cellular viability in a dose dependent manner | (Setyawati et al., 2015) |
| | 50 - 70 nm | 2 - 92 µg/mL | 24 - 72 h | Human colon carcinoma cells | Increase in ROS and IL-8 release<br><br>Decrease in cellular viability in a dose dependent manner. | (De Berardis et al., 2010) |
| ***In vivo* models** | | | | | | |
| Ag | 10 and 110 nm | 9, 18, and 36 mg/kg/day<br>100,480 µg/day | 90 days | Sprague–Dawley rats | Increase in intestinal permeability | (Orr et al., 2019; Munger et al., 2014 ) |
| | 5 - 10 nm<br>25 - 40 nm | | 14 days | Healthy volunteers | No significant toxicity markers | |

| | | | | | | |
|---|---|---|---|---|---|---|
| PVP-Ag | 55.17 nm | 46 - 4600 µg/kg/day | 28 days | C57BL/6 female mice | No toxicity was detected | |
| citrate-Ag | 20 and 110 nm | 0.1, 1 and 10 mg/kg/day | 3 or 9 days | Male C57BL/6NCrl mice | No significant toxicity and accumulation in tissues | |
| $TiO_2$ | 21 nm | 180 - 4200 µg/day | 5 or 10 days | C57Bl/6J*pun*/*p*un mice | Increase in DNA double strands breaks | (Trouiller et al., 2009; Ruiz et al., 2017) |
| | 30 and 50 nm | 50 and 500 mg/day/kg | 8 days | Wild-type and NLRP3-deficient mice | Enhance of the intestinal inflammation | |
| $TiO_2$ anastase<br>$TiO_2$ rutile | In simulated gastric fluid: 134.45 nm -32.56 mV In simulated intestinal fluid: 419.99 nm -13.67 mV In simulated gastric fluid: 148.1 nm -19.85 mV In simulated intestinal fluid: 360.92 nm -6.33 mV | 100 mg/kg/day | 28 days | Male C57BL/6 mice | Rutile NPs cause irregular villus epithelium cell arrangement Rutile NPs influence the gut microbiota | |
| $SiO_2$ | 21 nm -38.3 mV | 500, 1000 and 2000 mg/kg/day | 90 days | Sprague-Dawley rats | No toxic effect was detected | (Kim et al., 2014) |
| | 91.6 nm -45.2 mV | | | | | |
| Au | 23 nm | 10 mg/kg/day | 30 days | Adult male ICR outbred mice | Sequestration of NPs in the lumen of these tissues | (Hinkley et al., 2015) |
| ZnO | 26.6 nm | 350 mg/kg/day | 4 weeks | Male Wistar albino rats | Increase of proinflammatory cytokines; IL-1β, TNF-α | (Abass et al., 2017; Srivastav et al., 2017) |
| | 100 nm Positively and negatively charged | 31.25, 125 and 500 mg/kg/day | 90 days | Sprague Dawley rats | A statistically significant changes in feed and water consumption. | |

| | | | | | | |
|---|---|---|---|---|---|---|
| | 39.45 nm<br>-32.1 mv | 300<br>and 2000 mg/kg | 2 days | Swiss mice | Genotoxic response in a dose-dependent manner. | |

**Table 2: Intestinal toxicity of organic NPs.**

| NPs | Size (nm)<br>Surface charge (mV) | Concentration of NPs | Exposure Time | Intestinal models | Observations | Reference |
|---|---|---|---|---|---|---|
| ***In vitro* models** | | | | | | |
| Chitosan (CS) loaded with a model antigen ovalbumin (OVA) | 290 nm<br>43.3 mV | 1 mg/mL | 1 h | Human colon colorectal adenocarcinoma Caco-2 cells | No significant cytotoxicity of CS NPs was observed | (Slütter et al., 2009) |
| Chitosan conjugated with a goblet cell-target peptide, (CSK) peptide. | 135.2 nm<br>6.3 mV | 0.125, 0.25, 0.375 and 0.5 mg/mL | 3 h | | No cytotoxicity was observed | |
| Poly (amidoamine) PA MAM Generation number:<br>G0, G1, G2<br>G3, G4 | / | 0.1 1 and 10 mM | 210 min | Human colon colorectal adenocarcinoma Caco-2 cells | G2, G3, G4 induced a significant leakage of Lactate Dehydrogenase in a dose dependent manner. | (El-Sayed et al., 2002) |
| PLGA | 175 nm | 12.5 - 200 µg/mL | 8 h | Human colon colorectal adenocarcinoma Caco-2 cells | No cytotoxicity was observed. | (Chaves et al., 2018) |
| | 211 nm | 15.63 - 250 µg/mL | | Human colon colorectal adenocarcinoma Caco-2 cells and HT29 MTX | | |
| ***In vivo* models** | | | | | | |
| Chitosan | 253.2 nm<br>28.2 mV | 5 mg/kg/day | 7 days | Male Wistar rats | No cytotoxicity was observed | (Sonaje et al., 2011; Liu et al., 2013) |

| | | | | | | |
|---|---|---|---|---|---|---|
| Oleoyl-carboxymethyl-chitosan | 171.34 nm<br>19.26 mV | | | Pregnant Kunming mouse | | |
| PAMAM<br>G3.5<br>G4 | G3.5: 1.3 nm<br>G4: 1.7 nm | 100 and 300 mg/kg | 0.5 - 8 h | Female CD-1 mice | No cytotoxicity was observed<br>No histologic changes to the epithelial layer of the gastrointestinal tract | (Sadekar et al., 2013) |
| PLGA | 112 nm<br>2.1 mV | 12 mg/kg/day | 7 - 21 days | Male F344 rats | Minimal toxicity in intestine, without significant impact on other organs | (Navarro et al., 2016) |

## 1. Microbiota and mucus interactions

The influence of NPs on the GIT bacteria is mainly controlled by electrostatic interactions which depends on the pH and the composition of the gastrointestinal fluids (Gangadoo et al., 2021). Their effect is mediated through various mechanisms, such as Reactive Oxygen Species (ROS) production, release of cationic ions and disruption of cell membrane (Figure 2). Cationic Au NPs were more toxic on both Gram-positive and Gram-negative bacteria compared with anionic NPs (Vivian Feng et al., 2015). The toxicity was explained by an accumulation at the surface of bacteria, likely causing membrane destabilization. Modifications of microbiota after oral exposure to $TiO_2$ NPs were also reported. A significant increase in *Lactobacillus reuteri* was observed after 90-day oral administration (Chen et al., 2019). This bacteria is beneficial for human health due to its ability to produce metabolic molecules and prevent the migration and expansion of opportunistic pathogens (Mu et al., 2018). In contrast, chronic ingestion of rutile $TiO_2$ NPs-containing foods reduced the proliferation of *Bifidobacterium* and facilitated the invasion of opportunistic pathogens such as *Escherichia-Shigella* (Li et al., 2018). Toxicity of Ag NPs on commensal bacteria in human GIT was also identified due to their antibacterial properties (Mercier-Bonin et al., 2018). Two mechanisms were hypothesized: an accumulation of Ag NPs in the bacterial cell membrane or the Ag cations release, inducing ROS production (Ladaycia et al., 2021). $SiO_2$ NPs in the GIT increased the abundance of *Lactobacillus genus* after oral ingestion. A complexation of $SiO_2$ NPs with bacteria was reported, reducing their cytotoxicity on human epithelial cells (Siemer et al., 2018). The interactions of inorganic NPs with the microbiota seems to depend on the bacteria type, especially the composition of the cell membrane and on the features of NPs (Vivian Feng et al., 2015). Metallic NPs are well-known for their antibacterial activity while $SiO_2$ and $TiO_2$ inhibit or induce the proliferation of commensal bacteria, depending on the strain (Slavin et al., 2017). Gut microbiota dysbiosis was also observed in mice after oral exposure to polystyrene (PS) NPs having a size of 500 nm for 5 weeks. The population of *Firmicutes* and α- *Proteobacteria* was significantly affected at a concentration in NPs of 1mg/L (Lu et al., 2018). Multi-walled carbon nanotubes (MWCNTs) administered by intratracheal instillation in doxorubicin-treated mice affected the gut microbiota through the proliferation of *Helicobacteraceae* and *Coriobacteriaceae* (Liu et al., 2020).

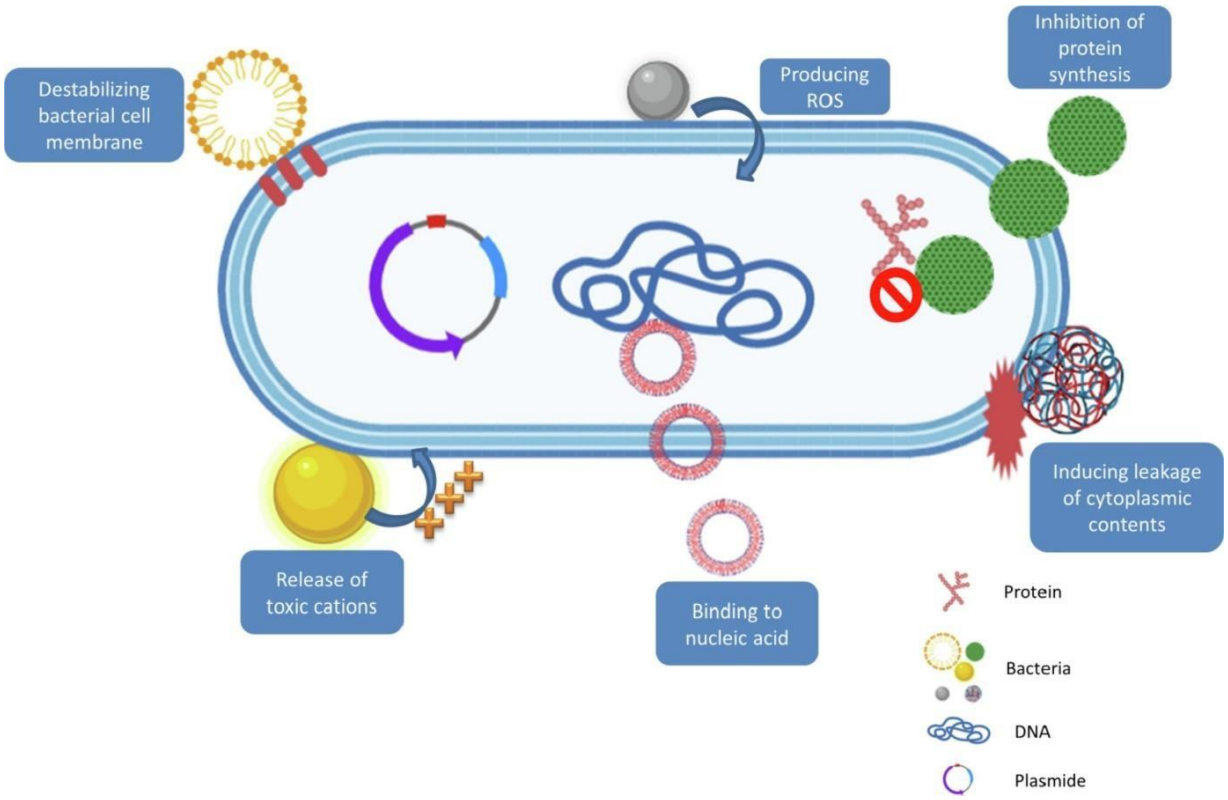


***Figure 2: Schematic representation of interactions between nanomaterials and bacteria. Figure is reproduced with permission from reference*** (Ladaycia et al., 2021)

NPs easily penetrate the mucus layer due to their small size. The biochemical composition of the mucus produced by a co-culture of enterocytes and goblet cells changed after exposure to $TiO_2$, $SiO_2$, Zinc oxide (ZnO) or Iron (III) oxide ($Fe_2O_3$) NPs for 4 h. The concentration in neutral mucins was significantly reduced. Ag NPs exerted a mucosecretagogue effect in the ileum and rectum through the hypersecretion of mucus in the intestinal lumen. An increase of the mucus secretion in Zebrafish intestines was observed after exposure to 100 nm PS NPs (Gu et al., 2020). Changes in the composition of neutral and acidic mucins were also observed (Mercier-Bonin et al., 2016).

Despite the limited number of studies, the NPs tested induced a modification of the biochemical composition of mucus. This could weaken the mucus' protective effect. Further investigations could confirm this hypothesis.

## 2. Intestinal cell damages

NPs in contact with intestinal epithelial cells can damage the brush border of enterocytes and then their absorptive properties. Scanning Electron Microscopy (SEM) revealed an affectation of the microvilli structure of Caco-2 after exposure to $TiO_2$ NPs at a concentration of 10 µg/ml (Koeneman et al., 2010). This finding was supported by other studies that showed a 42 % loss of microvilli (Faust et al., 2014a) and brush border disruption by $TiO_2$ NPs (Faust et al., 2014b). Disruption of epithelial cell microvilli was also observed in mice exposed to Ag NPs for 21 days at a dose of 20 mg/kg (van der Zande et al., 2012). An alteration of actin filaments reported for $TiO_2$ and Ag NPs (Déciga-Alcaraz et al., 2020; Xu et al., 2013) could be hypothesized, considering that brush border is supported by a bundle of cytoskeleton compounds (Costa de Beauregard et al., 1995).

Cytotoxicity of NPs in food products on intestinal cells was widely reported (Fröhlich and Fröhlich, 2016; Cornu et al., 2022). After 24 and 48 h exposure to ZnO NPs, a decrease in the cell viability of human colon cells was observed. The viability loss was concomitant with a ROS content increase, suggesting an oxidative stress-related mechanism. Direct interaction of ZnO NPs with the cell surface could trigger the intracellular signal activation, altering mitochondrial and/or endoplasmic reticulum functionalities (De Berardis et al., 2010). Similarly, $TiO_2$ NPs injected in the abdominal cavity of mice for 14 days significantly increased lipid peroxidation, decreased glutathione (GSH) level and altered antioxidant enzyme activity in a dose-dependent manner (Ma et al., 2010). A viability drop was also seen after 24 h exposure of metallic and metallic oxide NPs to human colorectal adenocarcinoma HT29 (Schneider et al., 2017a). Morphological changes of cells and granular inclusions suggests an apoptotic process. Early and late apoptotic cells were observed by flow cytometry after contact with most of NPs except for Au and cerium oxide NPs (Schneider et al., 2017a). The digestion process of NPs involving enzymes and acidic conditions was considered in viability assays. Cytotoxicity of copper oxide NPs increased by 30 % compared to native NPs when pre-treated with simulated gastrointestinal fluids. This was explained by a diameter decrease of NPs after incubation with pepsin (Henson et al., 2018). The same effect was observed with digested $TiO_2$ NPs after exposure to mucin-producing cells termed HT29-MTX-E12. A cytotoxicity increase was observed compared to undigested $TiO_2$ NPs due to a reduction of the agglomeration state

(Bettencourt et al., 2020). Unlike inorganic NPs, neutral or negatively charged polymeric NPs including PLGA NPs did not show any damages on epithelial cells in use conditions. Their biodegradable feature could reduce the exposure time to cellular compounds and then limit their toxicity. Only cytotoxicity was observed with cationic polymeric NPs in Caco-2 cell models. Chitosan NPs characterized by a size of 25 nm reduced the mitochondrial dehydrogenase activity at pH 6 while no effect was observed at pH 7.4 (Loh et al., 2012). This was explained by the positive charge of chitosan at acidic pH. Toxicity of poly(amidoamine) dendrimers termed PAMAM on Caco-2 cells was dependent on the number of generations. While lactate dehydrogenase release was observed with generations (G) 3 and 4, no toxic effect was reported with G0-G2 (El-Sayed et al., 2002). This result suggests a synergistic effect of both size and positive surface on the cytotoxicity of dendrimers. However, the lack of a mucus layer in the Caco-2 model does not allow an extrapolation of results to *in vivo* conditions, especially in the case of positively charged NPs.

## 3. Genotoxicity

Nanomaterials can lead to DNA damage and mutagenic events (García-Rodríguez et al., 2018a; AshaRani et al., 2009). Guidelines for genotoxicity evaluation of manufactured nanomaterials were established by OECD (OECD, 2014). Ames test was excluded for nanogenotoxicity investigation while the *in vitro* micronucleus assay was adopted by requiring an exposure time without cyto B. Another recommendation is the need to conduct a toxicokinetic investigation prior to the genotoxicity study. The aim is to ensure that nanomaterials will reach the target cell/tissue. Ag NPs led to a DNA double-strand break in Caco-2 cells. An increase in the percentage of γH2AX-positive cells was observed in a dose and time dependent manner (Gillois et al., 2021). Caco-2/HT29 co-culture were exposed to $TiO_2$ nanospheres (NS), nanorods (NR) and nanowires (NW) for 48 h (García-Rodríguez et al., 2018b). NS, NR and NW were characterised using electron microscopy by sizes of 70-80, 40-70 and 8-14 nm, respectively. $TiO_2$ NS did not modulate the gene expression of ZO-1 while it was downregulated in presence of $TiO_2$ NR at 50 µg/ml and upregulated with NW at 150 µg/ml. Only NR induced a genotoxic damage evaluated by comet assay after 48 h exposure while no oxidative DNA damage was reported. After oral gavage of E171 food-grade $TiO_2$ in rat, titanium accumulation was detected in the nucleus of cells located in the Peyer's Patches. However, no DNA damage including DNA strand breaks formation and oxidative DNA damages was reported after treatment for 7

days (Bettini et al., 2017). Preneoplastic lesions were nevertheless detected in the colon after a long-term oral exposure of 100 days in rat.

## 4. Intestinal permeability modulation

NPs can modulate the intestinal permeability, especially the paracellular transport due to their toxicity on epithelial cells or by interacting with TJ network. Intestinal integrity can be assessed by measurements of the TransEpithelial Electrical Resistance (TEER) in intestinal barrier models and the paracellular flux of molecular markers such as lucifer yellow, fluorescein isothiocyanate-dextran and mannitol (Graziani et al., 2019). An increase in the intestinal paracellular permeability could facilitate the transport in the blood compartment of pathogenic substances or modify the bioavailability of drugs and nutrients. A disruption of the intestinal barrier would facilitate the bacterial translocation, causing drastic sequelae as sepsis. Ag NPs increase the permeability of a monolayer of T84 human colorectal carcinoma cell lines in a dose and size dependent manner. A downregulation of the cytoplasmatic actin which plays a major role in the epithelial integrity maintenance and the regulation of TJs, was observed (Baranwal et al., 2012; Ku et al., 1999; Georgantzopoulou et al., 2016a). $SiO_2$ NPs smaller than 200 nm caused reversible relaxation of TJs in Caco-2 monolayer due to the activation of Myosin Light Chain Kinase (MLCK) enzymes. Activated MLCK enables the phosphorylation of the myosin part of the cytoskeleton, inducing TJs contraction (Lamson et al., 2020). A reversible TEER drop and a paracellular permeability increase were also observed in a Caco-2/HT29-MTX intestinal barrier models after exposure to amorphous 20 and 30 nm $SiO_2$ NPs (Cornu et al., 2020). In the same study, no significant modulation of the permeability was observed with 200 nm $SiO_2$ NPs due to the lack of cell internalization. In addition, no downregulation of TJs as claudin 2 and ZO-1 was observed, suggesting a TJ rearrangement after cytoskeleton disruption. The opposite effect was observed with ZnO NPs in a Caco-2/HT29-MTX coculture model. After 24 h incubation, a significant TEER increase was observed (Mittag et al., 2022). Zn increased the expression of ZO-1 in a Caco-2 model due the activation of PI3K/AKT/mTOR signaling pathway (Shao et al., 2017). Oral exposure to Single-Walled Carbon Nanotubes (SWCNTs) increased the intestinal permeability in mice at a daily dose of 2.5mg/kg for 7 days (Chen et al., 2018). Intestinal permeability modulation of organic nanomaterials is usually attributed to the additives contained in the formulation rather than the nanoparticle structure. The manufacturing of lipid-drug delivery systems such as nanoemulsions and solid lipid NPs

requires surfactants to decrease the interfacial tension between the immiscible phases and to guarantee their long-term storage (Chen, 2008). Due to their amphiphilic properties, they insert into the membrane of epithelial cells, increasing their fluidity (Danielsen and Hansen, 2017; Dimitrijevic et al., 2010). Direct interaction of surfactants with TJs was reported. Structural separation of TJs was observed in a Caco-2 model in the presence of sucrose monoester fatty acids (Mine and Zhang, 2003). Modulation of the efflux pump was also observed in presence of surfactants (Nieto Montesinos et al., 2012). Nanoemulsions increased the apical-to-basolateral flux of paeonol across a Caco-2 monolayer by a factor of 1.7 compared with the solution and decreased the efflux ratio in the same range. This effect was attributed to the P-gp inhibition by the Cremophor EL35 surfactant (S. Chen et al., 2018). Amphiphilic polymers used in the preparation of micelles and NPs such as Pluronic block copolymers were also able to inhibit the multidrug resistance mechanism in the intestinal epithelium (Fang et al., 2016; Kabanov et al., 2002). Mixed micelles of Pluronic P85 and F68 reversed the efflux activity of the intestinal multidrug resistance protein 2 by affecting the structure and the function of mitochondria (Chen et al., 2017). Pluronic 85 was able able to inhibit the Pgp drug efflux due to an ATP depletion associated to a membrane fluidization (Batrakova et al., 2001).

## 5. Inflammatory response

Inflammatory reactions after oral administration of NPs were widely reported in literature (Martirosyan et al., 2012). Ag NPs having a size of 20 nm exposed to Caco-2/TC7 cells at a concentration of 30 mg/L increased the expression of IL-8 proinflammatory cytokines while no effect was observed with 200 nm NPs (Georgantzopoulou et al., 2016a ;Őrfi and Szebeni, 2016), suggesting a size effect. This finding was confirmed by an *in vivo* study on female rats that showed a pro-inflammatory response in the intestinal mucosa after oral gavage of Ag NPs for 13 days (Orr et al., 2019). However, no size-effect was observed with $TiO_2$ NPs after 10-day gavage in mice. Both 66 nm NPs and 260 nm microparticles induced in the same manner, the secretion of pro-inflammatory cytokines such as TNF-α and IFN-γ (Carolina Maciel Nogueira et al., 2012). The differences observed between nanomaterials could be explained by their composition. The small size of Ag NPs increases their surface area, facilitating the release of Ag ions responsible for the inflammatory response. By contrast, $TiO_2$ NPs directly interact with the immune cells, especially macrophages which are able to phagocytose both small and large NPs (Becker et al., 2012;Huang et al., 2017). Crystal structure of $TiO_2$ NPs also needs to

be considered. Unlike rutile NPs, anatase $TiO_2$ NPs at a concentration of 50 µg/ml increased the expression of IL-8 and IL-1β in Caco-2 and THP-1-derived macrophages, respectively (Tada-Oikawa et al., 2016). Concomitant production of IL-8, $H_2O_2$/OH•, and intracellular GSH by LoVo human colon cells was observed after 24 h exposure to ZnO NPs (De Berardis et al., 2010). Inflammatory response in this case was correlated to oxidative stress. Another indirect mechanism involving the microbiota was reported. Oral administration of single wall carbon nanotubes at 2.5 mg/kg per day for 1 week induced the proliferation of proinflammatory bacteria named *Alistipes uncultured bacterium* and *Lachnospiraceae bacterium A4*. They were responsible for the inflammatory cell infiltrations and the production of IL-1β, IL-6 and TNF-α in the duodenum and colon (H. Chen et al., 2018). General population of lymphocytes was characterized by flow cytometry after oral ingestion of $SiO_2$ NPs in rats for 3 months. Reductions by 33 % and 13 % in the number of leukocyte and T helper cells were observed. A 27 % decrease of the CD4/CD8 ratio was observed. This change in the immune cell populations is characteristic of an immunosuppression mechanism (Shumakova et al., 2015). The immune response in the gut was affected by Ag NPs after 13-day exposure. A decrease in the expression of immunomodulatory genes such as FOXP3, GPR43, TLR 2 and 4 was identified (Williams et al., 2015). E171 $TiO_2$ additive reduced Treg cells activity after 100 day-oral exposure in rat while $TiO_2$ nanotubes affected the immune response by inhibiting MAPK and NF-κB inflammatory signalling pathways (Bettini et al., 2017; Neacsu et al., 2015). 0.5 µm PS NPs exposed to Zebrafish for 14 days increased both the mRNA and the protein levels of IL1α, IL1β and interferons in the gut (Jin et al., 2018). An Inflammatory response was also reported in mice after oral administration of SWCNTs at a dose of 2.5mg/kg for one week. An increase of the expression of IL-1β, IL6 and TNF-α was observed in duodenum and colon (Chen et al., 2018). Intratracheal instillation in mice of MWCNTs increased the M1-like polarization of macrophages in colon. This effect associated to a gut microbiota dysbiosis exacerbated the cardiotoxicity of doxorubicin (Liu et al., 2020). This combined toxicity of the loaded active ingredient and the MWCNTs emphasizes the importance to consider the intrinsic toxicity of nanomaterials, especially when they are used as drug delivery systems.

## IV- Conclusion

Physicochemical properties of nanomaterials are critical factors mediating the distribution of nanomaterials in the intestine. A small size usually below 100 nm, neutral or negatively charged NPs facilitate the penetration across the mucus layer, acting as a protective barrier for the intestinal epithelium. The positive NPs, potentially more toxic for cells are stuck to the mucus layer and are unable to reach the epithelial cells in healthy models. Physical and chemical modifications of nanomaterials after contact with gastrointestinal fluids also need to be considered in toxicity studies. Changes in the surface charge and agglomeration state were reported, impacting their toxicological profile. Some nanomaterials are able to interact with the different layers of the intestinal barrier including microbiota, mucus layer and epithelial monolayer. Gut microbiota dysbiosis and changes in the secretion and the composition of mucus were observed. Intestinal permeability modulation can be directly correlated to epithelial cell damages. Another mechanism is attributed to the destabilization of the actin cytoskeleton of epithelial cells and the rearrangement of TJs. Besides the physicochemical properties of nanomaterials, the composition is another critical factor in the intestinal nanotoxicity. Inorganic materials are usually more toxic than polymeric and lipid-based NPs. Mainly surfactants used as additives for the preparation of organic particles were responsible for the cytotoxicity and the intestinal permeability modulation. Two toxicity pathways are suggested for the inorganic nanomaterials. The high surface area of metallic NPs such as Ag particles facilitates the release of ions, affecting the biological functions of cells. The second could be attributed to the lower biodegradation rate of inorganic NPs such as $SiO_2$ and $TiO_2$ NPs compared with organic materials. The contact time with the cellular compounds is then prolonged and a chronic exposure would result in their accumulation in the cells. Microbiota was affected by some NPs through the proliferation of pathogenic and pro-inflammatory bacteria. The antibacterial features of some metallic properties reduced the population of commensal microorganisms. Unlike to epithelium damages, the inflammation response triggered by nanomaterials was less dependent on their physicochemical properties. Despite the numerous investigations, consistency issues were usually observed in the toxicological data reported in literature. Harmonized guidelines should be established for a better prediction of the intestinal nanotoxicity. For example, the presence of a mucus layer in *in vitro* models would prevent an overestimation of the nanotoxicity. Toxicokinetic investigations and consideration of digestion process would guarantee the relevancy of toxicological endpoints.

## Conflicts of interest

There are no conflicts to declare.


## Acknowledgement

T. Zaiter is supported by a fellowship from the “Centre Islamique d’Orientation et de l’Enseignement Supérieur (CIOES)”. Some figures were designed using BioRender.com.

# References


Abass, M.A., Selim, S.A., Selim, A.O., El-Shal, A.S., Gouda, Z.A., 2017. Effect of orally administered zinc oxide nanoparticles on albino rat thymus and spleen. IUBMB Life 69, 528–539. https://doi.org/10.1002/iub.1638

Abbas, M., Alqahtani, M.S., 2021. The Potential Role of Nanoparticles as an Anticancer Therapy in the Treatment of Rectal Cancer. Processes 9, 2172. https://doi.org/10.3390/pr9122172

Araújo, F., Shrestha, N., Granja, P.L., Hirvonen, J., Santos, H.A., Sarmento, B., 2015. Safety and toxicity concerns of orally delivered nanoparticles as drug carriers. Expert Opin. Drug Metab. Toxicol. 11, 381–393. https://doi.org/10.1517/17425255.2015.992781

AshaRani, P.V., Low Kah Mun, G., Hande, M.P., Valiyaveettil, S., 2009. Cytotoxicity and genotoxicity of silver nanoparticles in human cells. ACS Nano 3, 279–290. https://doi.org/10.1021/nn800596w

Ayala, V., Herrera, A.P., Latorre-Esteves, M., Torres-Lugo, M., Rinaldi, C., 2013. Effect of surface charge on the colloidal stability and in vitro uptake of carboxymethyl dextran-coated iron oxide nanoparticles. J. Nanoparticle Res. Interdiscip. Forum Nanoscale Sci. Technol. 15, 1874. https://doi.org/10.1007/s11051-013-1874-0

Baranwal, S., Naydenov, N.G., Harris, G., Dugina, V., Morgan, K.G., Chaponnier, C., Ivanov, A.I., 2012. Nonredundant roles of cytoplasmic β- and γ-actin isoforms in regulation of epithelial apical junctions. Mol. Biol. Cell 23, 3542–3553. https://doi.org/10.1091/mbc.E12-02-0162

Barhoum, A., García-Betancourt, M.L., Jeevanandam, J., Hussien, E.A., Mekkawy, S.A., Mostafa, M., Omran, M.M., S. Abdalla, M., Bechelany, M., 2022. Review on Natural, Incidental, Bioinspired, and Engineered Nanomaterials: History, Definitions, Classifications, Synthesis, Properties, Market, Toxicities, Risks, and Regulations. Nanomaterials 12, 177. https://doi.org/10.3390/nano12020177

Barko, P.C., McMichael, M.A., Swanson, K.S., Williams, D.A., 2018. The Gastrointestinal Microbiome: A Review. J. Vet. Intern. Med. 32, 9–25. https://doi.org/10.1111/jvim.14875

Batrakova, E.V., Li, S., Vinogradov, S.V., Alakhov, V.Y., Miller, D.W., Kabanov, A.V., 2001. Mechanism of pluronic effect on P-glycoprotein efflux system in blood-brain barrier: contributions of energy depletion and membrane fluidization. J Pharmacol Exp Ther 299, 483–493.

Becker, H.M., Bertschinger, M.M., Rogler, G., 2012. Microparticles and their impact on intestinal immunity. Dig. Dis. Basel Switz. 30 Suppl 3, 47–54. https://doi.org/10.1159/000342602

Bettencourt, A., Gonçalves, L.M., Gramacho, A.C., Vieira, A., Rolo, D., Martins, C., Assunção, R., Alvito, P., Silva, M.J., Louro, H., 2020. Analysis of the Characteristics and Cytotoxicity of Titanium Dioxide Nanomaterials Following Simulated In Vitro Digestion. Nanomaterials 10, 1516. https://doi.org/10.3390/nano10081516

Bettini, S., Boutet-Robinet, E., Cartier, C., Coméra, C., Gaultier, E., Dupuy, J., Naud, N., Taché, S., Grysan, P., Reguer, S., Thieriet, N., Réfrégiers, M., Thiaudière, D., Cravedi, J.-P., Carrière, M., Audinot, J.-N., Pierre, F.H., Guzylack-Piriou, L., Houdeau, E., 2017. Food-grade TiO2 impairs intestinal and systemic immune homeostasis, initiates preneoplastic lesions and promotes aberrant crypt development in the rat colon. Sci. Rep. 7, 40373. https://doi.org/10.1038/srep40373

Brun, E., Barreau, F., Veronesi, G., Fayard, B., Sorieul, S., Chanéac, C., Carapito, C., Rabilloud, T., Mabondzo, A., Herlin-Boime, N., Carrière, M., 2014. Titanium dioxide nanoparticle impact and translocation through ex vivo, in vivo and in vitro gut epithelia. Part. Fibre Toxicol. 11, 13. https://doi.org/10.1186/1743-8977-11-13

Carolina Maciel Nogueira, W.M. de A., rgio Hiroshi Toma, A., Zonetti de Arruda Leite, M.L.L., cia Ortiz-Agostinho, M.I.S.D., 2012. Titanium dioxide induced inflammation in the small intestine. World J. Gastroenterol. 18, 4729–4735. https://doi.org/10.3748/wjg.v18.i34.4729

Carrillo-Inungaray, M.L., Trejo-Ramirez, J.A., Reyes-Munguia, A., Carranza-Alvarez, C., 2018. Chapter 15 - Use of Nanoparticles in the Food Industry: Advances and Perspectives, in: Grumezescu, A.M., Holban, A.M. (Eds.), Impact of Nanoscience in the Food Industry, Handbook of Food Bioengineering. Academic Press, pp. 419–444. https://doi.org/10.1016/B978-0-12-811441-4.00015-7

Chaves, L.L., Costa Lima, S.A., Vieira, A.C.C., Barreiros, L., Segundo, M.A., Ferreira, D., Sarmento, B., Reis, S., 2018. Nanosystems as modulators of intestinal dapsone and clofazimine delivery. Biomed. Pharmacother. Biomedecine Pharmacother. 103, 1392–1396. https://doi.org/10.1016/j.biopha.2018.04.195

Chen, H., Zhao, R., Wang, B., Zheng, L., Ouyang, H., Wang, H., Zhou, X., Zhang, D., Chai, Z., Zhao, Y., Feng, W., 2018. Acute Oral Administration of Single-Walled Carbon Nanotubes Increases Intestinal Permeability and Inflammatory Responses: Association with the Changes in Gut Microbiota in Mice. Adv. Healthc. Mater. 7, 1701313. https://doi.org/10.1002/adhm.201701313

Chen, M.-L., 2008. Lipid excipients and delivery systems for pharmaceutical development: a regulatory perspective. Adv. Drug Deliv. Rev. 60, 768–777. https://doi.org/10.1016/j.addr.2007.09.010

Chen, N., Song, Z.-M., Tang, H., Xi, W.-S., Cao, A., Liu, Y., Wang, H., 2016. Toxicological Effects of Caco-2 Cells Following Short-Term and Long-Term Exposure to Ag Nanoparticles. Int. J. Mol. Sci. 17. https://doi.org/10.3390/ijms17060974

Chen, T., Li, Y., Li, C., Yi, X., Wang, R., Lee, S.M.-Y., Zheng, Y., 2017. Pluronic P85/F68 Micelles of Baicalein Could Interfere with Mitochondria to Overcome MRP2-Mediated Efflux and Offer Improved Anti-Parkinsonian Activity. Mol. Pharmaceutics 14, 3331–3342. https://doi.org/10.1021/acs.molpharmaceut.7b00374

Chen, S., Zhang, J., Wu, L., Wu, H., Dai, M., 2018. Paeonol nanoemulsion for enhanced oral bioavailability: optimization and mechanism. Nanomed. 13, 269–282. https://doi.org/10.2217/nnm-2017-0277

Chen, Z., Zhou, D., Han, S., Zhou, S., Jia, G., 2019. Hepatotoxicity and the role of the gut-liver axis in rats after oral administration of titanium dioxide nanoparticles. Part. Fibre Toxicol. 16, 48. https://doi.org/10.1186/s12989-019-0332-2

Commission Européenne, 2022. Recommandation de la Commission du 10 juin 2022 relative à la définition des nanomatériaux (Texte présentant de l'intérêt pour l'EEE) 2022/C 229/01.

Commission Européenne, 2011. Recommandation de la Commission du 18 octobre 2011 relative à la définition des nanomatériauxTexte présentant de l'intérêt pour l'EEE. J. Off. Union Eur. 3.

Cornu, R., Béduneau, A., Martin, H. , 2022. Ingestion of titanium dioxide nanoparticles: a definite health risk for consumers and their progeny. Arch. Toxicol. 96, 2655-2686. https://doi.org/10.1007/s00204-022-03334-x.

Cornu, R., Chrétien, C., Pellequer, Y., Martin, H., Béduneau, A., 2020. Small silica nanoparticles transiently modulate the intestinal permeability by actin cytoskeleton disruption in both Caco-2 and Caco-2/HT29-MTX models. Arch. Toxicol. 94, 1191–1202. https://doi.org/10.1007/s00204-020-02694-6

Corr, S.C., Gahan, C.C.G.M., Hill, C., 2008. M-cells: origin, morphology and role in mucosal immunity and microbial pathogenesis. FEMS Immunol. Med. Microbiol. 52, 2–12. https://doi.org/10.1111/j.1574-695X.2007.00359.x

Costa de Beauregard, M.A., Pringault, E., Robine, S., Louvard, D., 1995. Suppression of villin expression by antisense RNA impairs brush border assembly in polarized epithelial intestinal cells. EMBO J. 14, 409–421. https://doi.org/10.1002/j.1460-2075.1995.tb07017.x

Damiano, S., Sasso, A., De Felice, B., Di Gregorio, I., La Rosa, G., Lupoli, G.A., Belfiore, A., Mondola, P., Santillo, M., 2018. Quercetin Increases MUC2 and MUC5AC Gene Expression and Secretion in Intestinal Goblet Cell-Like LS174T via PLC/PKCα/ERK1-2 Pathway. Front. Physiol. 9.

Danielsen, E.M., Hansen, G.H., 2017. Intestinal surfactant permeation enhancers and their interaction with enterocyte cell membranes in a mucosal explant system. Tissue Barriers 5, e1361900. https://doi.org/10.1080/21688370.2017.1361900

D'Anna, A., 2009. Combustion-formed nanoparticles. Proc. Combust. Inst. 32, 593–613. https://doi.org/10.1016/j.proci.2008.09.005

De Berardis, B., Civitelli, G., Condello, M., Lista, P., Pozzi, R., Arancia, G., Meschini, S., 2010. Exposure to ZnO nanoparticles induces oxidative stress and cytotoxicity in human colon carcinoma cells. Toxicol. Appl. Pharmacol. 246, 116–127. https://doi.org/10.1016/j.taap.2010.04.012

Déciga-Alcaraz, A., Delgado-Buenrostro, N.L., Ispanixtlahuatl-Meráz, O., Freyre-Fonseca, V., Flores-Flores, J.O., Ganem-Rondero, A., Vaca-Paniagua, F., Pilar Ramos-Godinez, M. del, Morales-Barcenas, R., Sánchez-Pérez, Y., García-Cuéllar, C.M., Chirino, Y.I., 2020. Irreversible disruption of the cytoskeleton as induced by non-cytotoxic exposure to titanium dioxide nanoparticles in lung epithelial cells. Chem. Biol. Interact. 323, 109063. https://doi.org/10.1016/j.cbi.2020.109063

Dilnawaz, F., 2017. Polymeric Biomaterial and Lipid Based Nanoparticles for Oral Drug Delivery. Curr. Med. Chem. 24, 2423–2438. https://doi.org/10.2174/0929867323666161028160004

Dimitrijevic, D., Shaw, A.J., Florence, A.T., 2010. Effects of Some Non-ionic Surfactants on Transepithelial Permeability in Caco-2 Cells. J. Pharm. Pharmacol. 52, 157–162. https://doi.org/10.1211/0022357001773805

Effect of surface charge on the colloidal stability and in vitro uptake of carboxymethyl dextran-coated iron oxide nanoparticles | SpringerLink [WWW Document], n.d. URL https://link.springer.com/article/10.1007/s11051-013-1874-0 (accessed 8.24.22).

Effects of Some Non-ionic Surfactants on Transepithelial Permeability in Caco-2 Cells | Journal of Pharmacy and Pharmacology | Oxford Academic [WWW Document], n.d. URL https://academic.oup.com/jpp/article/52/2/157/6157565 (accessed 8.24.22).

El-Sayed, M., Ginski, M., Rhodes, C., Ghandehari, H., 2002. Transepithelial transport of poly(amidoamine) dendrimers across Caco-2 cell monolayers. J. Control. Release Off. J. Control. Release Soc. 81, 355–365. https://doi.org/10.1016/s0168-3659(02)00087-1

Fan, Y., Zhang, Y., Yokoyama, W., Yi, J., 2017. Endocytosis of Corn Oil-Caseinate Emulsions In Vitro: Impacts of Droplet Sizes. Nanomaterials 7, 349. https://doi.org/10.3390/nano7110349

Fang, Z., Chen, S., Qin, J., Chen, B., Ni, G., Chen, Z., Zhou, J., Li, Z., Ning, Y., Wu, C., Zhou, L., 2016. Pluronic P85-coated poly(butylcyanoacrylate) nanoparticles overcome phenytoin resistance in P-glycoprotein overexpressing rats with lithium-pilocarpine-induced chronic temporal lobe epilepsy. Biomaterials 97, 110–121. https://doi.org/10.1016/j.biomaterials.2016.04.021

Faust, J.J., Doudrick, K., Yang, Y., Westerhoff, P., Capco, D.G., 2014a. Food grade titanium dioxide disrupts intestinal brush border microvilli in vitro independent of sedimentation. Cell Biol. Toxicol. 30, 169–188. https://doi.org/10.1007/s10565-014-9278-1

Faust, J.J., Masserano, B.M., Mielke, A.H., Abraham, A., Capco, D.G., 2014b. Engineered nanoparticles induced brush border disruption in a human model of the intestinal epithelium. Adv. Exp. Med. Biol. 811, 55–72. https://doi.org/10.1007/978-94-017-8739-0_4

Fröhlich, E., Roblegg, E., 2012. Models for oral uptake of nanoparticles in consumer products. Toxicology 291, 10–17. https://doi.org/10.1016/j.tox.2011.11.004

Fröhlich, E.E., Fröhlich, E., 2016. Cytotoxicity of Nanoparticles Contained in Food on Intestinal Cells and the Gut Microbiota. Int. J. Mol. Sci. 17, 509. https://doi.org/10.3390/ijms17040509

Fruijtier-Pölloth, C., 2016. The safety of nanostructured synthetic amorphous silica (SAS) as a food additive (E 551). Arch. Toxicol. 90, 2885–2916. https://doi.org/10.1007/s00204-016-1850-4

Fu, D., 2013. Where is it and How Does it Get There – Intracellular Localization and Traffic of P-glycoprotein. Front. Oncol. 3.

Ganapathy, V., Gupta, N., Martindale, R., 2006. Protein Digestion and Absorption, in: Physiology of the Gastrointestinal Tract. pp. 1667–1692. https://doi.org/10.1016/B978-012088394-3/50068-4

Gangadoo, S., Nguyen, H., Rajapaksha, P., Zreiqat, H., Latham, K., Cozzolino, D., Chapman, J., Truong, V.K., 2021. Inorganic nanoparticles as food additives and their influence on the human gut microbiota. Environ. Sci. Nano 8, 1500–1518. https://doi.org/10.1039/D1EN00025J

García-Rodríguez, A., Vila, L., Cortés, C., Hernández, A., Marcos, R., 2018a. Exploring the usefulness of the complex in vitro intestinal epithelial model Caco-2/HT29/Raji-B in nanotoxicology. Food Chem. Toxicol. Int. J. Publ. Br. Ind. Biol. Res. Assoc. 113, 162–170. https://doi.org/10.1016/j.fct.2018.01.042

García-Rodríguez, A., Vila, L., Cortés, C., Hernández, A., Marcos, R., 2018b. Effects of differently shaped TiO2NPs (nanospheres, nanorods and nanowires) on the in vitro model (Caco-2/HT29) of the intestinal barrier. Part. Fibre Toxicol. 15, 33. https://doi.org/10.1186/s12989-018-0269-x

Gehart, H., Clevers, H., 2019. Tales from the crypt: new insights into intestinal stem cells. Nat. Rev. Gastroenterol. Hepatol. 16, 19–34. https://doi.org/10.1038/s41575-018-0081-y

Georgantzopoulou, A., Serchi, T., Cambier, S., Leclercq, C.C., Renaut, J., Shao, J., Kruszewski, M., Lentzen, E., Grysan, P., Eswara, S., Audinot, J.-N., Contal, S., Ziebel, J., Guignard, C., Hoffmann, L., Murk, A.J.,

Gutleb, A.C., 2016b. Effects of silver nanoparticles and ions on a co-culture model for the gastrointestinal epithelium. Part. Fibre Toxicol. 13, 9. https://doi.org/10.1186/s12989-016-0117-9

Gerloff, K., Pereira, D.I.A., Faria, N., Boots, A.W., Kolling, J., Förster, I., Albrecht, C., Powell, J.J., Schins, R.P.F., 2013. Influence of simulated gastrointestinal conditions on particle-induced cytotoxicity and interleukin-8 regulation in differentiated and undifferentiated Caco-2 cells. Nanotoxicology 7, 353–366. https://doi.org/10.3109/17435390.2012.662249

Gillois, K., Stoffels, C., Leveque, M., Fourquaux, I., Blesson, J., Mils, V., Cambier, S., Vignard, J., Terrisse, H., Mirey, G., Audinot, J.-N., Theodorou, V., Ropers, M.-H., Robert, H., Mercier-Bonin, M., 2021. Repeated exposure of Caco-2 versus Caco-2/HT29-MTX intestinal cell models to (nano)silver in vitro: Comparison of two commercially available colloidal silver products. Sci. Total Environ. 754, 142324. https://doi.org/10.1016/j.scitotenv.2020.142324

Graziani, C., Talocco, C., De Sire, R., Petito, V., Lopetuso, L.R., Gervasoni, J., Persichilli, S., Franceschi, F., Ojetti, V., Gasbarrini, A., Scaldaferri, F., 2019. Intestinal permeability in physiological and pathological conditions: major determinants and assessment modalities. Eur. Rev. Med. Pharmacol. Sci. 23, 795–810. https://doi.org/10.26355/eurrev_201901_16894

Griffin, S., Masood, M.I., Nasim, M.J., Sarfraz, M., Ebokaiwe, A.P., Schäfer, K.-H., Keck, C.M., Jacob, C., 2018. Natural Nanoparticles: A Particular Matter Inspired by Nature. Antioxidants 7, 3. https://doi.org/10.3390/antiox7010003

Groschwitz, K.R., Hogan, S.P., 2009. Intestinal barrier function: molecular regulation and disease pathogenesis. J. Allergy Clin. Immunol. 124, 3–20; quiz 21–22. https://doi.org/10.1016/j.jaci.2009.05.038

Gu, W., Liu, S., Chen, L., Liu, Y., Gu, C., Ren, H., Wu, B., 2020. Single-Cell RNA Sequencing Reveals Size-Dependent Effects of Polystyrene Microplastics on Immune and Secretory Cell Populations from Zebrafish Intestines. Environ. Sci. Technol. 54, 3417–3427. https://doi.org/10.1021/acs.est.9b06386

Henson, T., Navratilova, J., Bradham, K., Rogers, K., Hughes, M., 2018. Cytotoxicity of copper (II) oxide nanoparticles in rat intestinal cells: effect of simulated gastrointestinal fluids and generation of oxidative stress. Soc. Toxicol.

Hinkley, G.K., Carpinone, P., Munson, J.W., Powers, K.W., Roberts, S.M., 2015. Oral absorption of PEG-coated versus uncoated gold nanospheres: does agglomeration matter? Part. Fibre Toxicol. 12, 9. https://doi.org/10.1186/s12989-015-0085-5

Huang, C., Sun, M., Yang, Y., Wang, F., Ma, X., Li, J., Wang, Y., Ding, Q., Ying, H., Song, H., Wu, Y., Jiang, Y., Jia, X., Ba, Q., Wang, H., 2017. Titanium dioxide nanoparticles prime a specific activation state of macrophages. Nanotoxicology 11, 737–750. https://doi.org/10.1080/17435390.2017.1349202

Huang, Y., Mei, L., Chen, X., Wang, Q., 2018. Recent Developments in Food Packaging Based on Nanomaterials. Nanomaterials 8, 830. https://doi.org/10.3390/nano8100830

ISO/TS 80004-1:2015(en), Nanotechnologies — Vocabulary — Part 1: Core terms [WWW Document], n.d. URL https://www.iso.org/obp/ui/#iso:std:iso:ts:80004:-1:ed-2:v1:en (accessed 8.24.22).

Jani, P.U., McCarthy, D.E., Florence, A.T., 1992. Nanosphere and microsphere uptake via Peyer's patches: observation of the rate of uptake in the rat after a single oral dose. Int. J. Pharm. 86, 239–246. https://doi.org/10.1016/0378-5173(92)90202-D

Jansman, F.G.A., Postma, M.J., van Hartskamp, D., Willemse, P.H.B., Brouwers, J.R.B.J., 2004. Cost-benefit analysis of capecitabine versus 5-fluorouracil/leucovorin in the treatment of colorectal cancer in the Netherlands. Clin. Ther. 26, 579–589. https://doi.org/10.1016/s0149-2918(04)90060-4

Jiang, X., Wu, Y., Gray, P., Zheng, J., Cao, G., Zhang, H., Zhang, X., Boudreau, M., Croley, T.R., Chen, C., Yin, J.-J., 2018. Influence of gastrointestinal environment on free radical generation of silver nanoparticles and implications for their cytotoxicity. NanoImpact 10, 144–152. https://doi.org/10.1016/j.impact.2018.04.001

Jin, Y., Xia, J., Pan, Z., Yang, J., Wang, W., Fu, Z., 2018. Polystyrene microplastics induce microbiota dysbiosis and inflammation in the gut of adult zebrafish. Environmental Pollution 235, 322–329. https://doi.org/10.1016/j.envpol.2017.12.088

Jones, K., Morton, J., Smith, I., Jurkschat, K., Harding, A.-H., Evans, G., 2015. Human in vivo and in vitro studies on gastrointestinal absorption of titanium dioxide nanoparticles. Toxicol. Lett. 233, 95–101. https://doi.org/10.1016/j.toxlet.2014.12.005

Kabanov, A.V., Batrakova, E.V., Alakhov, V.Y., 2002. Pluronic® block copolymers as novel polymer therapeutics for drug and gene delivery. Journal of Controlled Release 82, 189–212. https://doi.org/10.1016/S0168-3659(02)00009-3

Kararli, T.T., 1995. Comparison of the gastrointestinal anatomy, physiology, and biochemistry of humans and commonly used laboratory animals. Biopharm. Drug Dispos. 16, 351–380. https://doi.org/10.1002/bdd.2510160502

Kim, Y.-R., Lee, S.-Y., Lee, E.J., Park, S.H., Seong, N., Seo, H.-S., Shin, S.-S., Kim, S.-J., Meang, E.-H., Park, M.-K., Kim, M.-S., Kim, C.-S., Kim, S.-K., Son, S.W., Seo, Y.R., Kang, B.H., Han, B.S., An, S.S.A., Lee, B.-J., Kim, M.-K., 2014. Toxicity of colloidal silica nanoparticles administered orally for 90 days in rats. Int. J. Nanomedicine 9 Suppl 2, 67–78. https://doi.org/10.2147/IJN.S57925

Koeneman, B.A., Zhang, Y., Westerhoff, P., Chen, Y., Crittenden, J.C., Capco, D.G., 2010. Toxicity and cellular responses of intestinal cells exposed to titanium dioxide. Cell Biol. Toxicol. 26, 225–238. https://doi.org/10.1007/s10565-009-9132-z

Ku, N.O., Zhou, X., Toivola, D.M., Omary, M.B., 1999. The cytoskeleton of digestive epithelia in health and disease. Am. J. Physiol. 277, G1108-1137. https://doi.org/10.1152/ajpgi.1999.277.6.G1108

Ladaycia, A., Passirani, C., Lepeltier, E., 2021. Microbiota and nanoparticles: Description and interactions. Eur. J. Pharm. Biopharm. 169, 220–240. https://doi.org/10.1016/j.ejpb.2021.10.015

Lai, S.K., O'Hanlon, D.E., Harrold, S., Man, S.T., Wang, Y.-Y., Cone, R., Hanes, J., 2007. Rapid transport of large polymeric nanoparticles in fresh undiluted human mucus. Proc. Natl. Acad. Sci. U. S. A. 104, 1482–1487. https://doi.org/10.1073/pnas.0608611104

Lamprecht, A., Schäfer, U., Lehr, C.M., 2001. Size-dependent bioadhesion of micro- and nanoparticulate carriers to the inflamed colonic mucosa. Pharm. Res. 18, 788–793. https://doi.org/10.1023/a:1011032328064

Lamson, N.G., Berger, A., Fein, K.C., Whitehead, K.A., 2020. Anionic nanoparticles enable the oral delivery of proteins by enhancing intestinal permeability. Nat. Biomed. Eng. 4, 84–96. https://doi.org/10.1038/s41551-019-0465-5

Lee, J.-A., Kim, Mi-Kyung, Paek, H.-J., Kim, Y.-R., Kim, Meyoung-Kon, Lee, J.-K., Jeong, J., Choi, S.-J., 2014. Tissue distribution and excretion kinetics of orally administered silica nanoparticles in rats. Int. J. Nanomedicine 9, 251–260. https://doi.org/10.2147/IJN.S57939

Lee, S.H., 2015. Intestinal permeability regulation by tight junction: implication on inflammatory bowel diseases. Intest. Res. 13, 11–18. https://doi.org/10.5217/ir.2015.13.1.11

Li, J., Yang, S., Lei, R., Gu, W., Qin, Y., Ma, S., Chen, K., Chang, Y., Bai, X., Xia, S., Wu, C., Xing, G., 2018. Oral administration of rutile and anatase TiO2 nanoparticles shifts mouse gut microbiota structure. Nanoscale 10, 7736–7745. https://doi.org/10.1039/C8NR00386F

Liu, Y., Kong, M., Feng, C., Yang, K.K., Li, Y., Su, J., Cheng, X.J., Park, H.J., Chen, X.G., 2013. Biocompatibility, cellular uptake and biodistribution of the polymeric amphiphilic nanoparticles as oral drug carriers. Colloids Surf. B Biointerfaces 103, 345–353. https://doi.org/10.1016/j.colsurfb.2012.11.012

Liu, Z., Liu, K., 2013. The transporters of intestinal tract and techniques applied to evaluate interactions between drugs and transporters. Asian J. Pharm. Sci. 8, 151–158. https://doi.org/10.1016/j.ajps.2013.07.020

Loh, J.W., Saunders, M., Lim, L.-Y., 2012. Cytotoxicity of monodispersed chitosan nanoparticles against the Caco-2 cells. Toxicol. Appl. Pharmacol. 262, 273–282. https://doi.org/10.1016/j.taap.2012.04.037

Lowe, P.J., Temple, C.S., 1994. Calcitonin and Insulin in Isobutylcyanoacrylate Nanocapsules: Protection Against Proteases and Effect on Intestinal Absorption in Rats. J. Pharm. Pharmacol. 46, 547–552. https://doi.org/10.1111/j.2042-7158.1994.tb03854.x

Liu, X., Liu, Y., Chen, Xuewei, Wang, C., Chen, Xuehan, Liu, W., Huang, K., Chen, H., Yang, J., 2020. Multi-walled carbon nanotubes exacerbate doxorubicin-induced cardiotoxicity by altering gut microbiota and pulmonary and colonic macrophage phenotype in mice. Toxicology 435, 152410. https://doi.org/10.1016/j.tox.2020.152410

Lu, L., Wan, Z., Luo, T., Fu, Z., Jin, Y., 2018. Polystyrene microplastics induce gut microbiota dysbiosis and hepatic lipid metabolism disorder in mice. Science of The Total Environment 631–632, 449–458. https://doi.org/10.1016/j.scitotenv.2018.03.051

Lundquist, P., Artursson, P., 2016. Oral absorption of peptides and nanoparticles across the human intestine: Opportunities, limitations and studies in human tissues. Adv. Drug Deliv. Rev. 106, 256–276. https://doi.org/10.1016/j.addr.2016.07.007

Ma, L., Liu, J., Li, N., Wang, J., Duan, Y., Yan, J., Liu, H., Wang, H., Hong, F., 2010. Oxidative stress in the brain of mice caused by translocated nanoparticulate TiO2 delivered to the abdominal cavity. Biomaterials 31, 99–105. https://doi.org/10.1016/j.biomaterials.2009.09.028

Mankertz, J., Amasheh, M., Krug, S.M., Fromm, A., Amasheh, S., Hillenbrand, B., Tavalali, S., Fromm, M., Schulzke, J.D., 2009. TNFalpha up-regulates claudin-2 expression in epithelial HT-29/B6 cells via phosphatidylinositol-3-kinase signaling. Cell Tissue Res. 336, 67–77. https://doi.org/10.1007/s00441-009-0751-8

Maroof, K., Zafar, F., Ali, H., Naveed, S., Tanwir, S., 2016. Scope of Nanotechnology in Drug Delivery. J. Bioequivalence Bioavailab. 8, 1–5. https://doi.org/10.4172/jbb.1000257

Martirosyan, A., Polet, M., Bazes, A., Sergent, T., Schneider, Y.-J., 2012. Food Nanoparticles and Intestinal Inflammation: A Real Risk?, in: Szabo, I. (Ed.), Inflammatory Bowel Disease. InTech. https://doi.org/10.5772/52887

Mbanga, O., Cukrowska, E., Gulumian, M., 2022. Dissolution kinetics of silver nanoparticles: Behaviour in simulated biological fluids and synthetic environmental media. Toxicol. Rep. 9, 788–796. https://doi.org/10.1016/j.toxrep.2022.03.044

Mercier-Bonin, M., Despax, B., Raynaud, P., Houdeau, E., Thomas, M., 2018. Mucus and microbiota as emerging players in gut nanotoxicology: The example of dietary silver and titanium dioxide nanoparticles. Crit. Rev. Food Sci. Nutr. 58, 1023–1032. https://doi.org/10.1080/10408398.2016.1243088

Mercier-Bonin, M., Despax, B., Raynaud, P., Houdeau, E., Thomas, M., 2016. Exposition orale et devenir dans l'intestin des nanoparticules alimentaires : exemple de l'argent et du dioxyde de titane. Cah. Nutr. Diététique 51, 195–203. https://doi.org/10.1016/j.cnd.2016.03.001

Mine, Y., Zhang, J.W., 2003. Surfactants enhance the tight-junction permeability of food allergens in human intestinal epithelial Caco-2 cells. Int. Arch. Allergy Immunol. 130, 135–142. https://doi.org/10.1159/000069009

Mittag, A., Owesny, P., Hoera, C., Kämpfe, A., Glei, M., 2022. Effects of Zinc Oxide Nanoparticles on Model Systems of the Intestinal Barrier. Toxics 10, 49. https://doi.org/10.3390/toxics10020049

Moghimi, S.M., Hunter, A.C., Murray, J.C., 2005. Nanomedicine: current status and future prospects. FASEB J. Off. Publ. Fed. Am. Soc. Exp. Biol. 19, 311–330. https://doi.org/10.1096/fj.04-2747rev

Mu, Q., Tavella, V.J., Luo, X.M., 2018. Role of Lactobacillus reuteri in Human Health and Diseases. Front. Microbiol. 9, 757. https://doi.org/10.3389/fmicb.2018.00757

Munger, M.A., Radwanski, P., Hadlock, G.C., Stoddard, G., Shaaban, A., Falconer, J., Grainger, D.W., Deering-Rice, C.E., 2014. In vivo human time-exposure study of orally dosed commercial silver nanoparticles. Nanomedicine Nanotechnol. Biol. Med. 10, 1–9. https://doi.org/10.1016/j.nano.2013.06.010

nanoparticle - Nanoparticle applications in materials | Britannica [WWW Document], n.d. URL https://www.britannica.com/science/nanoparticle (accessed 5.10.22).

Navarro, S.M., Morgan, T.W., Astete, C.E., Stout, R.W., Coulon, D., Mottram, P., Sabliov, C.M., 2016. Biodistribution and toxicity of orally administered poly (lactic-co-glycolic) acid nanoparticles to F344 rats for 21 days. Nanomed. 11, 1653–1669. https://doi.org/10.2217/nnm-2016-0022

Neacsu, P., Mazare, A., Schmuki, P., Cimpean, A., 2015. Attenuation of the macrophage inflammatory activity by $TiO_2$ nanotubes via inhibition of MAPK and NF-κB pathways. Int. J. Nanomedicine 10, 6455–6467. https://doi.org/10.2147/IJN.S92019

Nieto Montesinos, R., Béduneau, A., Pellequer, Y., Lamprecht, A., 2012. Delivery of P-glycoprotein substrates using chemosensitizers and nanotechnology for selective and efficient therapeutic outcomes. J. Control. Release Off. J. Control. Release Soc. 161, 50–61. https://doi.org/10.1016/j.jconrel.2012.04.034

Nighot, P.K., Hu, C.-A.A., Ma, T.Y., 2015. Autophagy enhances intestinal epithelial tight junction barrier function by targeting claudin-2 protein degradation. J. Biol. Chem. 290, 7234–7246. https://doi.org/10.1074/jbc.M114.597492

OECD, 2014. Genotoxicity of manufactured nanomaterials: report of the OECD expert meeting. Series on the Safety of Manufactured Nanomaterials No 43

Ojer, P., Iglesias, T., Azqueta, A., Irache, J.M., López de Cerain, A., 2015. Toxicity evaluation of nanocarriers for the oral delivery of macromolecular drugs. Eur. J. Pharm. Biopharm. Off. J. Arbeitsgemeinschaft Pharm. Verfahrenstechnik EV 97, 206–217. https://doi.org/10.1016/j.ejpb.2015.10.005

Olmsted, S.S., Padgett, J.L., Yudin, A.I., Whaley, K.J., Moench, T.R., Cone, R.A., 2001. Diffusion of macromolecules and virus-like particles in human cervical mucus. Biophys. J. 81, 1930–1937. https://doi.org/10.1016/S0006-3495(01)75844-4

Oostendorp, R.L., Beijnen, J.H., Schellens, J.H.M., 2009. The biological and clinical role of drug transporters at the intestinal barrier. Cancer Treat. Rev. 35, 137–147. https://doi.org/10.1016/j.ctrv.2008.09.004

Őrfi, E., Szebeni, J., 2016. The immune system of the gut and potential adverse effects of oral nanocarriers on its function. Adv. Drug Deliv. Rev., Oral delivery of peptides 106, 402–409. https://doi.org/10.1016/j.addr.2016.09.009

Orr, S.E., Gokulan, K., Boudreau, M., Cerniglia, C.E., Khare, S., 2019. Alteration in the mRNA expression of genes associated with gastrointestinal permeability and ileal TNF-α secretion due to the exposure of silver nanoparticles in Sprague-Dawley rats. J. Nanobiotechnology 17, 63. https://doi.org/10.1186/s12951-019-0499-6

Palocci, C., Valletta, A., Chronopoulou, L., Donati, L., Bramosanti, M., Brasili, E., Baldan, B., Pasqua, G., 2017. Endocytic pathways involved in PLGA nanoparticle uptake by grapevine cells and role of cell wall and membrane in size selection. Plant Cell Rep. 36, 1917–1928. https://doi.org/10.1007/s00299-017-2206-0

Panariti, A., Miserocchi, G., Rivolta, I., 2012. The effect of nanoparticle uptake on cellular behavior: disrupting or enabling functions? Nanotechnol. Sci. Appl. 5, 87–100. https://doi.org/10.2147/NSA.S25515

Pelaseyed, T., Bergström, J.H., Gustafsson, J.K., Ermund, A., Birchenough, G.M.H., Schütte, A., van der Post, S., Svensson, F., Rodríguez-Piñeiro, A.M., Nyström, E.E.L., Wising, C., Johansson, M.E.V., Hansson, G.C., 2014. The mucus and mucins of the goblet cells and enterocytes provide the first defense line of the gastrointestinal tract and interact with the immune system. Immunol. Rev. 260, 8–20. https://doi.org/10.1111/imr.12182

Peters, R., Kramer, E., Oomen, A.G., Herrera Rivera, Z.E., Oegema, G., Tromp, P.C., Fokkink, R., Rietveld, A., Marvin, H.J.P., Weigel, S., Peijnenburg, A.A.C.M., Bouwmeester, H., 2012. Presence of Nano-Sized Silica during In Vitro Digestion of Foods Containing Silica as a Food Additive. ACS Nano 6, 2441–2451. https://doi.org/10.1021/nn204728k

Pompili, S., Latella, G., Gaudio, E., Sferra, R., Vetuschi, A., 2021. The Charming World of the Extracellular Matrix: A Dynamic and Protective Network of the Intestinal Wall. Front. Med. 8.

Pridgen, E.M., Alexis, F., Farokhzad, O.C., 2015. Polymeric nanoparticle drug delivery technologies for oral delivery applications. Expert Opin. Drug Deliv. 12, 1459–1473. https://doi.org/10.1517/17425247.2015.1018175

Rodgers, L.S., Fanning, A.S., 2011. Regulation of epithelial permeability by the actin cytoskeleton. Cytoskelet. Hoboken NJ 68, 653–660. https://doi.org/10.1002/cm.20547

Ruiz, P.A., Morón, B., Becker, H.M., Lang, S., Atrott, K., Spalinger, M.R., Scharl, M., Wojtal, K.A., Fischbeck-Terhalle, A., Frey-Wagner, I., Hausmann, M., Kraemer, T., Rogler, G., 2017. Titanium dioxide nanoparticles exacerbate DSS-induced colitis: role of the NLRP3 inflammasome. Gut 66, 1216–1224. https://doi.org/10.1136/gutjnl-2015-310297

Sabourian, P., Yazdani, G., Ashraf, S.S., Frounchi, M., Mashayekhan, S., Kiani, S., Kakkar, A., 2020. Effect of Physico-Chemical Properties of Nanoparticles on Their Intracellular Uptake. Int. J. Mol. Sci. 21, 8019. https://doi.org/10.3390/ijms21218019

Sadekar, S., Thiagarajan, G., Bartlett, K., Hubbard, D., Ray, A., McGill, L.D., Ghandehari, H., 2013. Poly(amido amine) dendrimers as absorption enhancers for oral delivery of camptothecin. Int. J. Pharm. 456, 175–185. https://doi.org/10.1016/j.ijpharm.2013.07.071

Sahay, G., Alakhova, D.Y., Kabanov, A.V., 2010a. Endocytosis of nanomedicines. J. Control. Release Off. J. Control. Release Soc. 145, 182–195. https://doi.org/10.1016/j.jconrel.2010.01.036

Sahin, A., Esendagli, G., Yerlikaya, F., Caban-Toktas, S., Yoyen-Ermis, D., Horzum, U., Aktas, Y., Khan, M., Couvreur, P., Capan, Y., 2017. A small variation in average particle size of PLGA nanoparticles prepared by nanoprecipitation leads to considerable change in nanoparticles' characteristics and efficacy of intracellular delivery. Artif. Cells Nanomedicine Biotechnol. 45, 1657–1664. https://doi.org/10.1080/21691401.2016.1276924

Salvo Romero, E., Alonso Cotoner, C., Pardo Camacho, C., Casado Bedmar, M., Vicario, M., 2015. The intestinal barrier function and its involvement in digestive disease. Rev. Espanola Enfermedades Dig. Organo Of. Soc. Espanola Patol. Dig. 107, 686–696. https://doi.org/10.17235/reed.2015.3846/2015

Schneider, T., Westermann, M., Glei, M., 2017a. In vitro uptake and toxicity studies of metal nanoparticles and metal oxide nanoparticles in human HT29 cells. Arch. Toxicol. 91, 3517–3527. https://doi.org/10.1007/s00204-017-1976-z

Segata, N., Haake, S.K., Mannon, P., Lemon, K.P., Waldron, L., Gevers, D., Huttenhower, C., Izard, J., 2012. Composition of the adult digestive tract bacterial microbiome based on seven mouth surfaces, tonsils, throat and stool samples. Genome Biol. 13, R42. https://doi.org/10.1186/gb-2012-13-6-r42

Setyawati, M.I., Tay, C.Y., Leong, D.T., 2015. Mechanistic Investigation of the Biological Effects of $SiO_2$, $TiO_2$, and ZnO Nanoparticles on Intestinal Cells. Small Weinh. Bergstr. Ger. 11, 3458–3468. https://doi.org/10.1002/smll.201403232

Shao, Y., Wolf, P.G., Guo, S., Guo, Y., Gaskins, H.R., Zhang, B., 2017. Zinc enhances intestinal epithelial barrier function through the PI3K/AKT/mTOR signaling pathway in Caco-2 cells. J. Nutr. Biochem. 43, 18–26. https://doi.org/10.1016/j.jnutbio.2017.01.013

Shen, L., Turner, J.R., 2005. Actin depolymerization disrupts tight junctions via caveolae-mediated endocytosis. Mol. Biol. Cell 16, 3919–3936. https://doi.org/10.1091/mbc.e04-12-1089

Shen, L., Weber, C.R., Raleigh, D.R., Yu, D., Turner, J.R., 2011. Tight junction pore and leak pathways: a dynamic duo. Annu. Rev. Physiol. 73, 283–309. https://doi.org/10.1146/annurev-physiol-012110-142150

Shi, J.H., Axson, J.L., Bergin, I.L., Ault, A.P., 2020. Nanoparticle Digestion Simulator Reveals pH-Dependent Aggregation in the Gastrointestinal Tract. Anal. Chem. 92, 12257–12264. https://doi.org/10.1021/acs.analchem.0c01844

Shumakova, A.A., Efimochkina, N.R., Minaeva, L.P., Bykova, I.B., Batishchava, S.Y., Markova, Y.M., Trushina, E.N., Mustafina, O.K., Sharanova, N.E., Gmoshinsky, I.V., Khanferyan, R.A., Khotimchenko, S.A., Sheveleva, S.A., Tutelyan, V.A., 2015. [Toxicological assessment of nanostructured silica. III. Microecological, hematological indices, state of cellular immunity]. Vopr. Pitan. 84, 55–65.

Siemer, S., Hahlbrock, A., Vallet, C., McClements, D.J., Balszuweit, J., Voskuhl, J., Docter, D., Wessler, S., Knauer, S.K., Westmeier, D., Stauber, R.H., 2018. Nanosized food additives impact beneficial and pathogenic bacteria in the human gut: a simulated gastrointestinal study. Npj Sci. Food 2, 22. https://doi.org/10.1038/s41538-018-0030-8

Slavin, Y.N., Asnis, J., Häfeli, U.O., Bach, H., 2017. Metal nanoparticles: understanding the mechanisms behind antibacterial activity. J. Nanobiotechnology 15, 65. https://doi.org/10.1186/s12951-017-0308-z

Slütter, B., Plapied, L., Fievez, V., Sande, M.A., des Rieux, A., Schneider, Y.-J., Van Riet, E., Jiskoot, W., Préat, V., 2009. Mechanistic study of the adjuvant effect of biodegradable nanoparticles in mucosal vaccination. J. Control. Release Off. J. Control. Release Soc. 138, 113–121. https://doi.org/10.1016/j.jconrel.2009.05.011

Sonaje, K., Lin, K.-J., Tseng, M.T., Wey, S.-P., Su, F.-Y., Chuang, E.-Y., Hsu, C.-W., Chen, C.-T., Sung, H.-W., 2011. Effects of chitosan-nanoparticle-mediated tight junction opening on the oral absorption of endotoxins. Biomaterials 32, 8712–8721. https://doi.org/10.1016/j.biomaterials.2011.07.086

Sood, A., Panchagnula, R., 2001. Peroral route: an opportunity for protein and peptide drug delivery. Chem. Rev. 101, 3275–3303. https://doi.org/10.1021/cr000700m

Srivastav, A.K., Kumar, A., Prakash, J., Singh, D., Jagdale, P., Shankar, J., Kumar, M., 2017. Genotoxicity evaluation of zinc oxide nanoparticles in Swiss mice after oral administration using chromosomal aberration, micronuclei, semen analysis, and RAPD profile. Toxicol. Ind. Health 33, 821–834. https://doi.org/10.1177/0748233717717842

Sun, X., Yang, H., Nose, K., Nose, S., Haxhija, E.Q., Koga, H., Feng, Y., Teitelbaum, D.H., 2008. Decline in intestinal mucosal IL-10 expression and decreased intestinal barrier function in a mouse model of total parenteral nutrition. Am. J. Physiol. Gastrointest. Liver Physiol. 294, G139-147. https://doi.org/10.1152/ajpgi.00386.2007

Suzuki, T., Yoshinaga, N., Tanabe, S., 2011. Interleukin-6 (IL-6) regulates claudin-2 expression and tight junction permeability in intestinal epithelium. J. Biol. Chem. 286, 31263–31271. https://doi.org/10.1074/jbc.M111.238147

Tada-Oikawa, S., Ichihara, G., Fukatsu, H., Shimanuki, Y., Tanaka, N., Watanabe, E., Suzuki, Y., Murakami, M., Izuoka, K., Chang, J., Wu, W., Yamada, Y., Ichihara, S., 2016. Titanium Dioxide Particle Type and Concentration Influence the Inflammatory Response in Caco-2 Cells. Int. J. Mol. Sci. 17, 576. https://doi.org/10.3390/ijms17040576

Talavera, D., Castillo, A.M., Dominguez, M.C., Gutierrez, A.E., Meza, I., 2004. IL8 release, tight junction and cytoskeleton dynamic reorganization conducive to permeability increase are induced by dengue virus infection of microvascular endothelial monolayers. J. Gen. Virol. 85, 1801–1813. https://doi.org/10.1099/vir.0.19652-0

Talkar, S., Dhoble, S., Majumdar, A., Patravale, V., 2018. Transmucosal Nanoparticles: Toxicological Overview. Adv. Exp. Med. Biol. 1048, 37–57. https://doi.org/10.1007/978-3-319-72041-8_3

Tan, S.L.J., Billa, N., 2021. Improved Bioavailability of Poorly Soluble Drugs through Gastrointestinal Muco-Adhesion of Lipid Nanoparticles. Pharmaceutics 13, 1817. https://doi.org/10.3390/pharmaceutics13111817

Thursby, E., Juge, N., 2017. Introduction to the human gut microbiota. Biochem. J. 474, 1823–1836. https://doi.org/10.1042/BCJ20160510

Trouiller, B., Reliene, R., Westbrook, A., Solaimani, P., Schiestl, R.H., 2009. Titanium dioxide nanoparticles induce DNA damage and genetic instability in vivo in mice. Cancer Res. 69, 8784–8789. https://doi.org/10.1158/0008-5472.CAN-09-2496

Turner, J.R., 2009. Intestinal mucosal barrier function in health and disease. Nat. Rev. Immunol. 9, 799–809. https://doi.org/10.1038/nri2653

Tyagi, S., 2016. Nanoparticles – An Overview of Classification and Applications.

van der Zande, M., Vandebriel, R.J., Van Doren, E., Kramer, E., Herrera Rivera, Z., Serrano-Rojero, C.S., Gremmer, E.R., Mast, J., Peters, R.J.B., Hollman, P.C.H., Hendriksen, P.J.M., Marvin, H.J.P., Peijnenburg, A.A.C.M., Bouwmeester, H., 2012. Distribution, elimination, and toxicity of silver nanoparticles and silver ions in rats after 28-day oral exposure. ACS Nano 6, 7427–7442. https://doi.org/10.1021/nn302649p

Vivian Feng, Z., L. Gunsolus, I., A. Qiu, T., R. Hurley, K., H. Nyberg, L., Frew, H., P. Johnson, K., M. Vartanian, A., M. Jacob, L., E. Lohse, S., D. Torelli, M., J. Hamers, R., J. Murphy, C., L. Haynes, C., 2015. Impacts of gold nanoparticle charge and ligand type on surface binding and toxicity to Gram-negative and Gram-positive bacteria. Chem. Sci. 6, 5186–5196. https://doi.org/10.1039/C5SC00792E

Walsh, M.D., Clendenning, M., Williamson, E., Pearson, S.-A., Walters, R.J., Nagler, B., Packenas, D., Win, A.K., Hopper, J.L., Jenkins, M.A., Haydon, A.M., Rosty, C., English, D.R., Giles, G.G., McGuckin, M.A., Young, J.P., Buchanan, D.D., 2013. Expression of MUC2, MUC5AC, MUC5B, and MUC6 mucins in colorectal cancers and their association with the CpG island methylator phenotype. Mod. Pathol. 26, 1642–1656. https://doi.org/10.1038/modpathol.2013.101

Wan, K., Sun, L., Hu, X., Yan, Z., Zhang, Y., Zhang, X., Zhang, J., 2016. Novel nanoemulsion based lipid nanosystems for favorable in vitro and in vivo characteristics of curcumin. Int. J. Pharm. 504, 80–88. https://doi.org/10.1016/j.ijpharm.2016.03.055

Wang, Y., Chen, Z., Ba, T., Pu, J., Chen, T., Song, Y., Gu, Y., Qian, Q., Xu, Y., Xiang, K., Wang, H., Jia, G., 2013. Susceptibility of young and adult rats to the oral toxicity of titanium dioxide nanoparticles. Small Weinh. Bergstr. Ger. 9, 1742–1752. https://doi.org/10.1002/smll.201201185

Wang, Y., Li, M., Xu, X., Tang, W., Xiong, L., Sun, Q., 2019. Formation of Protein Corona on Nanoparticles with Digestive Enzymes in Simulated Gastrointestinal Fluids. J. Agric. Food Chem. 67, 2296–2306. https://doi.org/10.1021/acs.jafc.8b05702

Weber, C.R., 2012. Dynamic properties of the tight junction barrier. Ann. N. Y. Acad. Sci. 1257, 77–84. https://doi.org/10.1111/j.1749-6632.2012.06528.x

Williams, K., Milner, J., Boudreau, M.D., Gokulan, K., Cerniglia, C.E., Khare, S., 2015. Effects of subchronic exposure of silver nanoparticles on intestinal microbiota and gut-associated immune responses in the ileum of Sprague-Dawley rats. Nanotoxicology 9, 279–289. https://doi.org/10.3109/17435390.2014.921346

Woodley, J., 2001. Bioadhesion: new possibilities for drug administration? Clin. Pharmacokinet. 40, 77–84. https://doi.org/10.2165/00003088-200140020-00001

Xu, F., Piett, C., Farkas, S., Qazzaz, M., Syed, N.I., 2013. Silver nanoparticles (AgNPs) cause degeneration of cytoskeleton and disrupt synaptic machinery of cultured cortical neurons. Mol. Brain 6, 29. https://doi.org/10.1186/1756-6606-6-29

Younes, M., Aquilina, G., Castle, L., Engel, K., Fowler, P., Frutos, M., Fürst, P., Gundert-Remy, U., Gürtler, R., Husøy, T., Manco, M., Mennes, W., Moldeus, P., Passamonti, S., Shah, R., waalkens-Berendsen, I., Wölfle, D., Corsini, E., Cubadda, F., Wright, M., 2021. Safety assessment of titanium dioxide (E171) as a food additive. EFSA J. 19. https://doi.org/10.2903/j.efsa.2021.6585

Zaiter, T., Cornu, R., Millot, N., Herbst, M., Pellequer, Y., Moarbess, G., Martin, H., Diab-Assaf, M., Béduneau, A., 2022. Size effect and mucus role on the intestinal toxicity of the E551 food additive and engineered silica nanoparticles. Nanotoxicology 16, 165–182. https://doi.org/10.1080/17435390.2022.2063084

Zhang, J., Zhu, X., Jin, Y., Shan, W., Huang, Y., 2014. Mechanism study of cellular uptake and tight junction opening mediated by goblet cell-specific trimethyl chitosan nanoparticles. Mol. Pharm. 11, 1520–1532. https://doi.org/10.1021/mp400685v

## 4. Dermal toxicity

Nanoparticles are used in cosmetic and dermatology products. The environment is also a source of human exposure to nanoparticles. Their toxicity after contact with the skin is still questioned mainly due to the lack of relevant *in vitro* models mimicking accurately the skin barrier. While the nanotoxicity by direct exposure to cutaneous cells was widely demonstrated, their ability to reach the viable epidermis stays unclear. The present review focused on the *in vitro* models and the toxicological effects of nanoparticles in contact with the skin barrier.

J Nanopart Res (2022) 24: 149
https://doi.org/10.1007/s11051-022-05523-2

REVIEW

# Toxicity assessment of nanoparticles in contact with the skin

**Taghrid Zaiter · Raphaël Cornu · Wassim El Basset · Hélène Martin · Mona Diab · Arnaud Béduneau**

Received: 11 February 2022 / Accepted: 27 June 2022 / Published online: 11 July 2022


**Abstract** Due to their unique physicochemical properties, engineered nanoparticles (NPs) are used in numerous skin products as sunscreen, texture agents, colorant, and drug delivery systems. While the skin is considered the first line of defense against xenobiotic entrance, the small size of NPs could promote the interaction with cutaneous cells. This review investigates the fate and the toxicological effects of organic and inorganic NPs used in cosmetic and dermatology. After direct exposure to skin cells, cytotoxicity, oxidative stress, inflammatory response, and genotoxicity were reported in a dose and time-dependent manner, especially for inorganic NPs. Despite these findings, the toxicity of nanoparticles applied to a healthy skin could be questioned due to their inability, for most of them, to reach the viable epidermis. Advanced skin models and toxicity tests validated for nanomaterials should be required for a better prediction of the dermal nanotoxicity.

**Keywords** Skin barrier · Nanoparticles · Cytotoxicity · Genotoxicity · Inflammation · 3D skin models

## Introduction

Nanomaterials in cosmetic products are defined in Europe by the cosmetic regulation no 1123/2009 [1]. They are considered insoluble or biopersistent and intentionally manufactured materials with at least one external dimension between 1 and 100 nm. Contrary to the European Commission (EC), the Food and Drug Administration (FDA) did not clearly establish a regulatory definition of nanomaterials, but issued guidance for products involved in the application of nanotechnology [2]. The latter needs to be applied if a material or the end product has an external dimension between 1 and 100 nm or dimension-dependent properties. According to the FDA, particles having dimensions outside the nanoscale range may influence physical, chemical, and biological properties of some materials. Organic and inorganic nanomaterials, especially nanoparticles (NPs), are contained in cosmetic products. NPs are characterized by 3 external dimensions in the size range from 1 to 100 nm according to ISO/TS 27,687 [3]. They are used in skin care products as active or inactive ingredients

**Supplementary Information** The online version contains supplementary material available at https://doi.org/10.1007/s11051-022-05523-2.

T. Zaiter · R. Cornu · W. El Basset · H. Martin (✉) · A. Béduneau (✉)
PEPITE EA4267, Univ. Bourgogne Franche-Comté, 25000 Besançon, France
e-mail: helene.martin@univ-fcomte.fr

A. Béduneau
e-mail: arnaud.beduneau@univ-fcomte.fr

M. Diab
EDST, Pharmacology and Cancerology Laboratory, Faculty of Sciences, Lebanese University, Beirut 1500, Lebanon

[4]. Titanium ($TiO_2$) and zinc (ZnO) oxide NPs are used in conventional sunscreens as a physical barrier against UV radiations [5]. Lipid NPs including liposomes and nanoemulsions were designed for the topical skin lipid supplementation or to promote the dermal delivery of active ingredients.

The present review investigates the fate and the toxicity of NPs applied to the skin. The penetration pathways and trafficking will be described and discussed. The toxicological endpoints, the most documented in literature including cytotoxicity, inflammation, and genotoxicity, were reported and related to their composition and physicochemical properties.

## Structure and composition of the human skin

The human skin is considered one of the body's largest organs due to its estimated surface area of 2 $m^2$ [6]. It is composed of 3 overlapping layers which include the epidermis, the dermis, and the hypodermis. The epidermis is the outermost layer of the skin and is by itself subdivided into four distinct superimposed layers. The stratum basal (SB) is the deepest layer that makes the epidermis, followed by stratum spinosum (SS), stratum granulosum (SG), and finally the most superficial being stratum corneum (SC). The longevity and continuity of the epithelium are ensured by the cellular proliferation within SB yielding keratinocytes. The process continues after debarking from the SB, and keratinocytes undergo a multistep process of differentiation that continues outward through the different layers of the epidermis. It is worth mentioning that SB houses other skin cell types with versatile actions such as melanocytes (involved in the UV protection), Langerhans cells (LCs; involved in the skin's immune system as an inducer of skin allergy), and Merkel cells (mechanoreceptors) [7]. The second layer of the skin is the dermis, which contains collagen, elastic fibers, and an extra fibrillary matrix which together participate to the skin elasticity. The cellular composition of the dermis mainly includes fibroblasts and immune cells such as macrophages, mast cells, and lymphocytes T and B. The dermis and the epidermis are separated by a basement membrane [8]. The hypodermis located under the dermis is the deepest skin layer. It is considered a connective tissue with adipocytes. Due to its composition, the hypodermis protects the body from physical shocks and temperature variations and serves as a fat reserve. Only the dermis and hypodermis are vascularized. Skin appendages include nails, sweat glands involved in the human thermoregulation, pilosebaceous, and sebaceous glands associated with hair follicles [9].

The skin acts a polyvalent barrier having the following properties:

– Antimicrobial

Due to the constant daily exposure of the skin to the external environment, the risk of being in contact with pathological agents is evident and thus requires a modulation to prevent a potential contamination. This modulation is assured by the skin via many mechanisms among which stands the microbiome and the sebum. The former can be defined as a constellation of commensal bacteria present at the surface of the skin, in the epidermis and also in deeper layers such as the dermis [10]. It acts as a shield to protect the host against colonization of pathogens by secreting bacteriocins [11]. For example, commensal *Staphylococcus epidermidis* blocks the proliferation of pathogenic *Staphylococcus aureus*, by secreting a specific protease. In addition, antimicrobial peptides (AMPs) such as human β-defensins and cationic amphiphilic molecules which are produced by different skin cells specifically keratinocytes, sebocytes, and neutrophils are strongly involved in the protection against microbial infections due to their deleterious effects on viruses, bacteria, fungi, and parasites [12]. The latter (sebum), which is produced by sebaceous glands, is also involved in the antimicrobial barrier due to its antifungal and antibacterial properties [13].

– Immunological

The immune barrier comprises several resident cell populations in the cutaneous epidermis and dermis in addition to keratinocytes (which represent 95% of the epidermal cells) producing immunological substances such as thymic stromal lymphopoietin (TSLP), tumor necrosis factor (TNF), and interleukins (IL) 33 and 1. These cytokines are involved in the recruitment of immune cells in the skin barrier [14]. Tissue-resident memory T cells previously recruited during an infection or inflammation reside in the healthy epidermis. They provide a specific response against pathogens

reinfecting the skin tissue [15]. LC also plays an important role in the immune system of the skin barrier. They constitute a subset of dendritic cells and are located at the base of the epidermis. They express Langerin, a protein involved in the presentation of non-peptide antigen to T cells. Typically, when they are confronted to a pathogen, LC migrate from the epidermis to the lymph nodes and present the antigen to T cells, leading to the induction of an adaptive immune response [16].

– Physical barrier

SC is the first skin layer in contact with xenobiotics. It is composed of mature, denucleated, and flattened keratinocytes called corneocytes. The keratinocytes present in the SG produce free fatty acids, ceramides, and cholesterols [7]. The deeper layers of the epiderma (SG, SS, and SB) are also involved in the physical barrier function of the skin. They are composed of viable epithelial cells linked by cell–cell junctions which play a major role in the paracellular permeability. They are involved in the cell proliferation, differentiation, and signal transduction processes [17]. Junction proteins are composed of transmembrane proteins (claudins), tight junction (TJ)-associated marvel proteins (occludins), and junctional adhesion molecules (JAMs), as well as TJ plaque proteins (zonula occludens, proteins 1–3, multi-PDZ containing protein-1, and cingulin). Adherent junctions and desmosomes are also present in SB, SS, and SG while gap junctions are located particularly in the SS. TJ, adherent junctions, and desmosomes guarantee the mechanical cohesion of cells and gap junctions facilitate the intercellular exchange of ions and small molecules through channels [17].

The barrier function of the skin can be affected by the pH, hydration level, cutaneous diseases, and environmental factors such as temperature, UV exposure, chemical compounds, and NPs [18].

## Localization and trafficking of NPs in skin layers

To understand the mechanism(s) governing NP toxicity, their localization in the skin and its subsequent layers needs to be characterized. Many studies shed light on that using different NPs to elucidate a potential mechanistic approach behind their toxicity. ZnO and $TiO_2$ NPs were extensively evaluated in the literature. For example, Filipe et al. showed that these NPs were only located at the skin surface and in the top layer of the SC after 2-h exposure [19]. In fact, analysis of biopsies of living porcine and human skins revealed the localization of $TiO_2$ NPs having a diameter of 20 nm in the first 3 to 5 corneocyte layers [20]. However, other studies showed a difference in the skin penetration of $TiO_2$ NPs between in vitro and in vivo models. As such, one study performed on an isolated porcine skin model showed that $TiO_2$ NPs having diameters of 4 nm and 60 nm did not penetrate the viable dermis after 24-h exposure. In contrast, only $TiO_2$ NPs having a diameter of 4 nm were observed in the deep layers of the epidermis of pig's ear after 30 days of exposure [21]. As for ZnO NPs, those having a size between 20 and 30 nm were found in the SC, skin folds, and hair follicle roots, and no penetration into the viable epidermis was detected [22]. After 6 h of human exposure to ZnO NPs, confocal laser scanning microscopy revealed the presence of liquid-state liposomes characterized by a flexible bilayer into the viable epidermis and dermis in rat. Conversely, gel-state liposomes and micelles were located in the SC layer [23]. Au NPs with various sizes were also investigated on an excised abdominal skin model. In this experiment, exposure time was 24 h and results showed an immediate maximal penetration of Au NPs having a size of 15 nm. Au NPs with sizes of 102 and 198 nm showed a permeation delay with a lag time of 3 and 6 h respectively [24]. In addition, silver (Ag) NPs were detected by electron microscopy in the SC and the outermost layers of the human abdominal epidermis. In general, the physical state of the skin can also influence the propensity and the magnitude of NP penetration. Thus, enhanced permeation of NPs is detected when skin is damaged [25]. For example, Larese Filon et al. showed that only small NPs with diameter less than 4 nm can penetrate the intact skin; however, large NPs with a size higher than 45 nm are able to permeate damaged skin [26]. In addition to size, the surface properties of NPs, especially the charge, can affect their penetration into the negatively charged skin under physiological condition. Kohli and Alpar demonstrated that negatively charged latex NPs can pass through the SC to reach the viable epidermis in contrast to neutral and positive NPs [27].

To illustrate the penetration of NPs into the skin, different pathways across the skin barrier were suggested. Three main pathways to date are described: the intercellular, the follicular, and the intracellular pathways (Fig. 1). The intercellular penetration is favored by many parameters such as the presence of lipid in the intracellular space and surface hydrophobicity of NPs. On one hand, transmission electron microscope (TEM) demonstrated the favorability of the first condition where NPs were present in the intercellular lipids of the SC layer. The second condition was validated with Au NPs. In fact, one study compared hydrophilic Au NPs to hydrophobized ones and showed that the further did not penetrate the deep layer of the skin unlike the latter that were distributed in deeper layers [28]. Other portals for NP entry include the follicular orifices. These structures are characterized by their size which fall in the micrometer range and allow the entrance of NPs into the hair follicle [29]. These orifices represent 0.1% of the total skin surface and are present in the hair. They play a mediator role between NPs and the dermis. Upon NP contact with hair orifices, the hair follicles reach the dermis. However, the tight junctions in the lower part of the follicle prevent and control the liberal diffusion of nanoparticles to the living cells. It is thus reasonable to consider the hair as a storage site for local release of drugs instead of a route for NP penetration into the viable epidermis

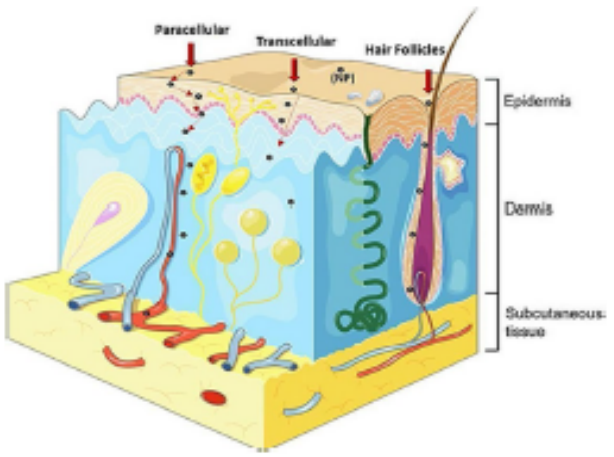


**Fig. 1** Schematic representation of the different pathways of nanoparticle penetration: the paracellular (between cells), follicular (transport by hair follicles), and transcellular (inside the cells) pathways. Figure is reproduced with permission from reference [35]

[30]. A total of 20 and 200 nm polystyrene (PS) NPs coated with multiple carboxylic acids were not able to diffuse across the SC to reach deeper skin layers. Only the smallest PS NP (20 nm) was shown to accumulate in hair follicles (20 nm) [31]. A permeation study across pig skin explants showed that 50 and 500 nm latex NPs characterized by a negative zeta potential reached the hair follicles [27]. Baroli et al. demonstrated the penetration of very small metallic maghemite and iron NPs into hair follicles and the SC, while no NP was detected into the viable dermis [32]. Poly-lactic-co-glycolic acid (PLGA) NPs with sizes comprised between 122 and 860 nm and silica ($SiO_2$) NPs from 300 to 1000 nm were applied on the ear porcine skin. The penetration depth in the hair follicles was obtained with an intermediary size close to 640 nm for both $SiO_2$ and PLGA NPs [33]. The transcellular route requires that the permeant traverse the alternating layers of cells and extracellular matrix. This involves a sequence of partitioning and diffusion into alternating hydrophilic and lipophilic domains [34]. Finally, NP penetration in non-follicular skin structures is limited by the presence of the SC which represents a very efficient protective barrier. Very few studies observed NPs in deeper layers of the epidermis. Only lipophilic nanocarriers such as liposomes with a flexible bilayer or very small metallic NPs could reach viable cells of the epithelium [4].

## Skin models for nanotoxicity studies

Numerous skin models were designed to predict interactions of chemical compounds and NPs with the cutaneous barrier by mimicking the physiological one (Table 1). These models can be classified into the following:

– Cellular models

This is the most basic and oldest model in all scientific aspects. In skin-related toxicity studies, keratinocytes and fibroblasts are the commonly used cell types. For example, HaCaT cells are immortalized human keratinocytes expressing all the major surface markers and functional activities of isolated keratinocyte cells. These cells are extensively used in this field due to their low cost, ease of use, rapid cell proliferation, and high reproducibility compared

**Table 1** Potential skin models to predict nanotoxicity

| Skin models | | Description | Applications | References |
|---|---|---|---|---|
| In vitro models | 2D monoculture | HaCaT | Cytotoxicity and skin penetration of $TiO_2$ NPs | [36, 58] |
| | | HDFs | Evaluation of DNA damage and oxidative stress caused by cerium oxide ($CeO_2$) NPs | [58] |
| | | HEK | Cytotoxicity of chemical compound carbon nanotubes | [39, 59] |
| | | A431 | Evaluation of Ni NP toxicity | [59] |
| | | MNT1 | Effect of platinum NPs on melanogenesis | [41] |
| | 3D monoculture | Keratinocytes derived from human foreskin | Cytotoxicity of Ag NPs | [60] |
| | | Normal human keratinocytes | Evaluation of metallic NP effects and penetration of Au NPs | [32, 46] |
| | 3D co-culture | HaCaT and HDFs | Exposure to cytotoxic agents | [61] |
| | | Primary human keratinocytes and fibroblasts | Cytotoxicity and skin penetration of NPs | [46] |
| Ex vivo models | | Skin pieces of healthy human donor | Skin penetration of metallic NPs | [32] |
| | | Pig ear skin | Drug permeation with liposomes | [62] |
| | | Male rat dorsal skin | Drug permeation with $SiO_2$ NPs | [63] |
| | | Pig back skin | Toxicity of Ag NPs | [49] |
| | | Nc/Nga mice | Toxicity of $SiO_2$ NPs | [64] |
| | | Isolated perfused human skin flap | Penetration of liposomes | [47] |
| In vivo models of dermatitis | | Right flank of male SKH1 mice | Penetration and distribution of $SiO_2$ NPs | [65] |
| | | Back skin of Nc/Nga mice | Allergic and inflammation response to allergens and NPs | [54] |

with more complex models. Many scholars used this model to investigate the toxicity of Ag NPs like Carrola et al. in their study on Ag NPs and their consequent role in oxidative stress generation after a 24-h exposure to HaCaT cells [36] or Wu et al. who studied the impact of their shape on skin toxicity. Other scholars used this cell line in their investigation on ZnO NP chronic toxicity [37]. Alternatively, primary cell culture can also be employed such as human epidermal keratinocyte (HEK) cell lines and human dermal fibroblasts (HDFs). These cell lines offer an incontestable advantage as they express almost all functional markers of the origin tissue and are therefore the closest to mimic skin physiology compared with cancer cell lines which may carry mutations. Notwithstanding their apparent advantages, they also present numerous inconveniences. Firstly, they exhibit a shorter lifespan compared to immortalized cell lines (which are cancerous) and are consequently unable to be used in the evaluation of long-term toxicity of NPs. Another limitation is their heterogeneity and this is due to variabilities among donors and this needs to be accounted for in the analysis of data. HEKs are of a particular advantage as they accurately mimic the epidermal barrier and the skin's biological response making them an excellent candidate for nanotoxicity analysis [38]. In the literature, they were used in the evaluation of the cytotoxicity and the inflammatory response of functionalized single-wall carbon nanotubes after 24-h exposure [39]. The other primary cell line (HDFs) is made up of cells directly obtained from human skin biopsies and is used for the same purpose as its congers. It was used by Auffan et al. for the investigation of $CeO_2$ NP genotoxicity after 2, 6, and 24-h exposure [40].

In the literature, the immune and cytotoxicity responses of metallic nanoparticles were evaluated in cell-based in vitro models mainly performed on 2D single culture consisting of keratinocyte or fibroblast monolayer growth on a plastic or glass surface [28]. Single culture of immortalized human melanocytes (MNT-1) or in primary culture was also designed to

investigate the effects of platinum NPs on the melanogenesis [41]. Few studies focused on the 2D co-culture of different types of cutaneous cells. HaCaT cells and primary human skin fibroblasts were co-cultivated to evaluate the cell adhesion and the proliferation on nanostructured titanium surfaces and the cell–cell interactions [42]. More complex cell-based models were designed to consider the three-dimensional (3D) skin structure at the liquid–air interface. 3D models of epidermis were developed to mimic the morphological, biochemical, and physiological properties of the human epidermis [43]. They are composed of several layers of keratinocytes. Many models are currently marketed. Among them, EpiSkin™ and EpiDerm™ were approved by the European Center for the Validation of Alternative Methods [35]. EpiSkin™, a 3D culture of normal human keratinocytes at the air–liquid interface, was used to evaluate the skin irritation caused by metallic NPs such as aluminum oxide NPs, $TiO_2$, and Ag NPs after short and long-term incubations [44] and the epidermal penetration of Au NPs [45]. The most advanced 3D skin models are full-thickness skin equivalents. This approach requires the superposition of different layers of human cells in an artificial matrix. It can be composed of collagens, fibrin fibers, alginate, or synthetic polymers. Epiderm-FT™ and Advanced Skin Test 2000® models mimic the epidermis and the dermis using a co-culture of keratinocytes and fibroblasts. They were developed to predict the cutaneous permeation and the toxicity of active molecules used in pharmaceutical and cosmetic products [46].

– Human ex vivo models

Human ex vivo models were established from skin biopsies or from skin samples obtained after plastic surgery. They were mainly used to evaluate the penetration of NPs. This is for example the case in the study of Baroli et al. in which maghemite and iron NPs having a size inferior to 10 nm were applied to excised human skin samples using vertical diffusion cells, before a TEM analysis of the NP penetration [32]. An alternative model named isolated perfused human skin flap was designed to characterize the penetration of liposomes and solid lipid NPs [47]. Perfusion allowed maintaining the metabolic activity of tissue during 6 h.

– Animal skin ex vivo models

Animal skin ex vivo models especially pig skin exhibit numerous similar properties with human, such as the thickness and the composition of the SC as well as the densities in hair follicle and blood vessels [48]. The porcine ear skin is the body part with the highest degree of similarities. These models were especially used for the transdermal drug delivery.

– In vivo animal skin models

Studies focusing on the nanotoxicity and the NP penetration were also performed in different healthy animals. Influence of size and coating of Ag NPs on toxicity and inflammatory response has been tested on porcine [49]. Guinea pigs can be also used. The subchronic toxicity of Ag NPs for example was determined by Korani et al. with this model [50].

– In vivo rodent skin models

In vivo skin models on rodents like mice and rats exhibit major differences with human. This includes high permeability, low thickness, and high density of hair follicles [51]. Nevertheless, they remain an attractive model due to their low price, availability, small size, and reproducibility. In addition, hairless rodent strains can be also used. These in vivo models have for example been used to evaluate the long-term toxicity of $TiO_2$ NPs and the penetration deep in the skin [52].

– "Skin disease" in vivo models

"Skin disease" in vivo models were also developed to evaluate both the drug distribution and the therapeutic efficiency of new treatments. These models offer an advantage as they are useful for an initial screening and estimation of nanotoxicity and the NP penetration. An in vivo study demonstrated a preferential accumulation of small PLGA NPs in inflamed skin [53] In vivo mouse models of atopic dermatitis (AD) were developed using different approaches including the epicutaneous sensitization with allergens such as ovalbumin, transgenic mice, and Nc/Nga mice that spontaneously develop cutaneous lesions in conventional housing conditions [54].

– "Skin disease" in vitro models

"Skin disease" in vitro models were also designed. For example, a 3D co-culture at the air–liquid interface was established using human foreskin fibroblast, HaCaT cells, and activated memory effector T cells (CD45RO+) to mimic eczematous dermatitis [55].

## Cytotoxicity

Due to their small size, NPs can infiltrate through the different skin strata, intercalate with various skin structures, and induce toxic effects (Table 2). Various NPs were investigated in the literature to unravel their cytotoxicity potential and the mechanisms behind such effect. For example, HaCaT cells were exposed to CuO NPs (having a size of 50 nm) at different concentration ranges from 5 to 30 µg/mL. Exposure time was 24 or 48 h and results showed that CuO

**Table 2** Cytotoxicity evaluation of nanoparticles in skin models

| NPs | Size (nm) | Skin models | Applications | Cytotoxic effects | References |
|---|---|---|---|---|---|
| Au | 20<br>16.7 | HaCaT | Photothermal therapy, biological application | Cell viability decrease, ROS production | [75] |
| | 21.8 | HDFs | Therapeutic medicine value | Cell cycle perturbation, reduced ATP level, ROS production | [76] |
| Ni | 52.10 | A431 | Jewelry, handle coins | Cytotoxicity leading to skin cancer, apoptosis through ROS-triggered mitochondrial pathway | [59] |
| CuO | 50 | HaCaT | Cosmetics | Cell viability decrease, ROS production | [66] |
| ZnO | Uncoated 65.5<br>Coated 74.3 | Human epidermal membrane prepared from freshly excised abdominal skin<br>Ex vivo | Ultraviolet filter, sunscreens | No toxicity | [77] |
| | 23.47 | HDF | Cosmetics, sunscreen | Cell viability decrease, apoptosis throughp53 and p38 pathways | [67] |
| | 165 | A431 | Sunscreen | Cell viability decrease | [78] |
| Ag | 25 | HaCaT | Treatment of burns, prevention of infection, antimicrobial agent | Cell viability decrease, antiproliferative effect | [49] |
| | 37 | HaCaT | Disinfectants, deodorants, room spray | Anti-proliferative, ROS production | [70] |
| $TiO_2$ | 124.9 | A431 | Cosmetics | ROS production, mitochondrial dysfunction leading to apoptosis | [79] |
| | 414.9 | HaCaT | Cosmetics, sunscreen | No significant toxic effect | [80] |
| | 38 | HaCaT | Treatment of acne, cosmetics | Very low cytotoxic effect | [56] |
| | 20 | HaCaT | Cosmetics | Cell viability decrease | [71] |
| | 180–500 | Primary human skin fibroblast | Sunscreen, self-cleaning, water purification | No toxicity | [81] |
| $SiO_2$ | 15–30 | HaCaT | Cosmetics | Cell viability decrease, cell cycle stop in S phase leading to apoptosis | [69] |
| | 50 | HaCaT | Cosmetics | Cell viability decrease | [68] |
| | 20 | Rat's skin | Cosmetics, sunscreen | No toxicity | [82] |

NPs induced a dose and time-dependent decrease of the cell viability. Molecular studies showed that this was due to a decrease in the glutathione (GSH) level, an increase in intracellular reactive oxygen species (ROS) represented as an increase in superoxide dismutase, lipid peroxidase, and catalase activity level. In addition, CuO NPs induced apoptosis in HaCaT cells through increased caspase-3 activity and formation of apoptotic bodies [66]. ZnO NPs' cytotoxic effect was also evaluated on HDF cells. These particles having a size of 23.5 nm were placed in contact with the aforementioned cell line for 24 h. Results showed that ZnO NPs did not penetrate into the viable epidermis, but instead were only located in the SC. In addition, cytotoxicity was seen and apoptotic signs were noticed when these NPs were used at a concentration of 50 µg/mL. This was due to the phosphorylation of p53 tumor suppressor protein and activation of p38 MAP kinase [67]. Similar to CuO, $SiO_2$ NPs' cytotoxic effect was evaluated on HaCaT cell line. A dose-dependent decrease in cell viability was seen and a similar mechanism to that of CuO was detected as $SiO_2$ caused a GSH level decrease leading to ROS generation [68]. Nevertheless, other mechanisms were also observed. For example, Yang et al. showed that $SiO_2$ NPs with sizes of 15 and 30 nm caused significant morphological changes and decrease of HaCaT cell viability (Fig. 2), as they were able to arrest the cell cycle in the S phase and induce apoptosis. In addition, $SiO_2$ NPs can also cause an alteration of many proteins involved in oxidative stress production [69]. Other NPs as Ag were also investigated. They were shown, when used in a size of 37 nm, to affect the viability of HaCaT cells after 24-h exposure as detected by with sulforhodamine B assay that revealed their anti-proliferative effect. In addition, TEM analysis showed that only few Ag NPs were found remaining in the cells. Mechanisms behind Ag-induced cell death were evaluated and shown to be oxidative stress independent. This was proven when cells were treated with apocynin and N (G)-monomethyl-L-arginine, inhibitors of NADPH-oxidase and nitric-oxide synthase, respectively. The decrease in cell viability despite the presence of the aforementioned inhibitors clearly shows the lack of relationship with oxidative stress with Ag NP anti-proliferative effect [70]. The same cell line, HaCaT, was also used to evaluate the toxicity of $TiO_2$ NPs having a size of 38 nm. These cells were placed in contact with $TiO_2$ NPs for 7 days. The NPs in question induced a decrease in cell viability marked by plasma membrane damage seen as early as the first

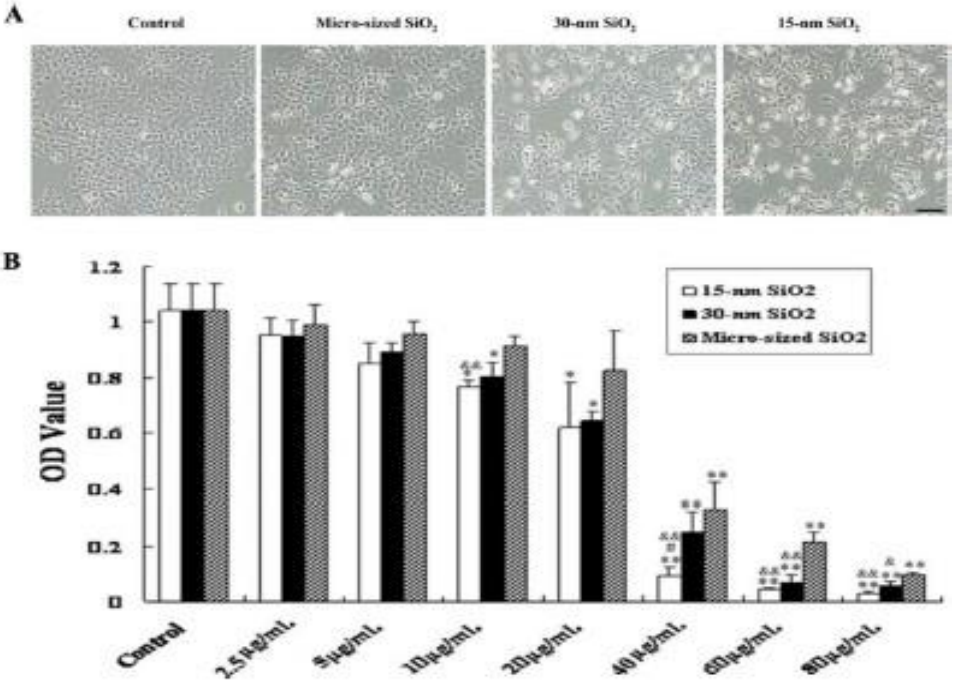


**Fig. 2** **A** Morphological changes induced by $SiO_2$ exposure. HaCaT cells were exposed to 15-nm, 30-nm, and micro-sized $SiO_2$ particles at 10 µg/mL for 24 h. Scale bar = 30 µm. **B** Viability of HaCaT cells after 24-h exposure to 15-nm, 30-nm, or micro-sized $SiO_2$ particles. Values were mean ± SD from three independent experiments. $*p < 0.05$, $**p < 0.01$ vs. control cells; $\#p < 0.05$ vs. cells exposed to 30-nm $SiO_2$ particles; $\&p < 0.05$, $\&\&p < 0.01$ vs. cells exposed to micro-sized $SiO_2$ particles. Figure is reproduced with permission from reference [69]

incubation day [56]. This is in agreement with Gandamalla et al. who also showed a high cytotoxicity of $TiO_2$ NPs having a size of 20 nm after 48-h exposure to HaCaT cells at concentrations of 100 and 300 µg/mL [71]. Other NPs as nickel (Ni) having a size of 68 nm were also investigated. These NPs were incubated with A431 human squamous carcinoma cells at 2, 4, 8, and 20 µg/mL. After 48-h exposure, A431 cells were spherical and detached from the surface, suggesting a dose and time-dependent viability decrease confirmed by MTT and lactate deshydrogenase assays. In addition, Ni NPs caused an increase in ROS secretion—which could be halted when N-acetylcystein is added and thus partly preventing apoptosis—and a caspase-3 activity increase [59]. But, not all NPs decrease cell viability. Some NPs were shown to favor viability as Au NPs. Flow cytometry assays showed that Au NPs caused an increase in cell number in Go/G1 and a decrease in the S phase in studies on HaCaT exposed to 23 nm Au NPs at 10 µg/mL [72]. Thus, except for Au NPs, most of inorganic NPs affect the viability of epidermal cells in a dose and time-dependent manner after direct exposure to 2D skin models. These models provide precious information about the intrinsic toxicity of NPs and the risk factors such as the size or the composition. However, this model has its limitations as previously described and no conclusion regarding their potential skin toxicity can be drawn without considering their ability to reach the viable epidermis. This point is taken into account in the OECD guidelines for testing chemicals [73]. Three-dimensional (3D) models were thus designed for a more realistic prediction of nanotoxicity. For example, in 3D EpiDerm™, the toxicity of polystyrene and $TiO_2$ NPs was evaluated. Results showed neither cytotoxicity, nor irritation after treatments with 1000 µg/mL of polystyrene and 100 µg/mL of $TiO_2$. Similarly, in vivo studies revealed the lack of nanotoxicity. In contrast, the treatment of human immortalized HaCaT cells with polystyrene NPs induced a cytotoxicity increase in a dose-dependent manner. This confirms that 3D cultures are more relevant models to predict the dermal nanotoxicity compared with 2D skin cell monolayers [74]. The same findings were observed by comparing an epidermal model EpiKutis® and a keratinocyte monolayer exposed to Ag NPs for 24 h. No cytotoxicity was observed with the 3D model in contrast to the 2D culture [60]. The skin irritation in vitro test requires reconstructed human epidermis models including EpiDerm™ and EpiSkin™ for viability assays. Both the barrier function and the morphology of 3D model especially the lipid composition and the multilayer structure must be considered to evaluate the toxicity of NPs.

## Inflammatory response

Upon contact with the skin, NPs can stimulate the immune system (Table 3). This result in an inflammatory response manifested as activation of immune cells, secretion of cytokines, and pro-inflammatory biomarkers. Molecular data from in vivo studies showed the involvement of cyclooxygenase-2 as an important key player in this immune response induced by NPs. For example, Pal et al. exposed the dorsal surface of female SKH-1 hairless mice to ZnO NPs (used in sunscreens) followed by UVB irradiations and showed a significant increase in COX-2 expression measured at different time intervals (6, 24, and 48 h) [83]. This is in contrast with other studies that showed ZnO NPs acting as anti-inflammatory molecule with repeated exposure on mice model for atopic dermatitis. This discrepancy in ZnO effects can be explained by the fact that in the latter, ZnO NPs were located in the deeper layers of the dermis. However, a production of IgE was also observed, which could cause allergy aggravation [84].

Other NPs like $SiO_2$ showed the same inflammatory behavior on the transcriptional level. For example, Kundu et al. showed an increase in the expression of COX-2 mRNA after exposure to $SiO_2$ NPs having a size of 20 nm on a HaCaT model. In addition, $SiO_2$ NPs also caused an increase in the phosphorylation of signal transducer and activator of transcription 3 (STAT3) by the virtue of Janus kinase 2, Src, and Akt (upstream kinase) phosphorylation [85]. Moreover, these NPs can also aggravate AD-like skin disease where an increase in the IgE levels was seen in NC/Nga mice after an intradermal injection of $SiO_2$ NPs followed by an exposure to Dermatophagoides pteronyssinu allergen (Dp) [64]. On the same spectrum, $TiO_2$ NPs were also evaluated in NC/Nga mice and resulted in an increase of IL-4 and IgE expressions [86]. Other NPs like PS were shown to cause like its congers an increased release of pro-inflammatory cytokines

**Table 3** Inflammatory evaluation of nanoparticles in skin models

| NPs | Size (nm) | Skin models | Applications | Immune responses | References |
|---|---|---|---|---|---|
| Ag | 200 to 800 | 2D and 3D cultures of keratinocytes derived from human foreskin | Antimicrobial properties, food packaging, water disinfectant | In 3D model: no toxicity<br>In 2D model: increase of pro-inflammatory cytokine levels (IL-1α, IL-6, and IL-8) | [60] |
| | 10.4 | NHDFs, NHEKs, normal primary cell culture from skin of healthy donors | Antimicrobial activity | IL-6 production | [88] |
| | 30.8<br>47.7<br>75.5 | HEK (in vitro), porcine skin (in vivo) | Cosmetics, acne creams, baby wipes | In HEK cell: increase of IL-1β, IL-6, IL-8, and TNF-α concentrations<br>In porcine skin: focal inflammation observed by microscopy | [51, 89] |
| PS | 25<br>50<br>100 | Nc/Nga mice (AD model disease) | Cosmetics | Aggravation of AD by TH2 immune response | [87] |
| ZnO | < 100 | Female SKH-1 hairless mice | Sunscreen | Increase of COX-2 level in a size-dependent manner | [83] |
| $TiO_2$ | 15, 40, and 100 | Nc/Nga mice | cosmetics | IL-4 and IgE secretions after co-exposure with Dp allergen, IL-13 production with NPs alone | [86] |
| $SiO_2$ | 1136<br>264<br>106<br>76<br>39 | Nc/Nga mice | Cosmetics | IL-18 release, TSLP secretion leading to Th2 response, aggravation of AD-like skin lesions | [64] |
| | 20 | HaCaT | Cosmetics | Increase of COX-2 level | [85] |

(IL-4, histamine, CCL2 (monocyte chemotactic protein-I), CCL3 (macrophage inflammatory protein-1α), and CCL4 (macrophage inflammatory protein-1β)) when applied on an AD model. However, they were also shown to aggravate AD by the virtue of TH2 immune response similarly to TiO2 NPs [87]. Finally, Ag NPs induced a secretion of IL-1β, IL-6, IL-8, and IL-10 in HEK cells [49]. These findings were consistent with a study carried out on epidermal keratinocytes which showed an inflammatory response due to Ag NP. However, the same Ag NP treatment did not modulate the secretion of pro-inflammatory cytokine in a 3D Epikutis model showing an overt discrepancy in the two models [60]. The same findings were observed after exposure of Ag NPs to EpiDerm™ model. No pro-inflammatory markers (as IL-1α) were secreted [44].

## Genotoxicity response

Studies showed that NPs can interact directly or indirectly with DNA after cell uptake, causing genotoxicity such as mutations, epigenetic modifications, chromosome aberrations, and chromatin condensation [72] (Table 4). One study showed ROS generation after 6 h of incubation with 20 µg/mL ZnO NPs probably associated with DNA damage. Another study showed that ZnO NPs caused an increase in the levels of γ-H2AX, the phosphorylated form of H2AX, a marker of DNA damage after 24-h exposure to HEKs [89]. Other NPs as $TiO_2$ used at concentrations of 1 and 3 µg/mL increased the levels of 3 markers of DNA strand breaks γ-H2AX, ataxia-telangiectasia mutated (ATM) and cell cycle checkpoint kinase 2 (chk2) in HDFs after 24-h exposure [90]. In addition; $SiO_2$ NPs' toxic effects were investigated on HaCaT

**Table 4** Genotoxicity evaluation of nanoparticles in skin models

| NPs | Size (nm) | Skin models | Applications | Genotoxic effects | References |
|---|---|---|---|---|---|
| CuO | 55.8 | HaCaT | Biocide properties, antimicrobial textiles, paints, plastics | ROS production, DNA damage | [66] |
| $CeO_2$ | 30 | HDFs | Industrial purposes applied as oxygen sensor, fuel additive | ROS production, chromosomal breakage | [58] |
| ZnO | 205.9 | Primary mouse keratinocytes | Cosmetics, care products, sunscreen | Nuclear translocation, DNA damages, cell cycle arrest at G0/G1 phase | [92] |
| | 32.55 | HaCaT | Sunscreen, facial cream | Epigenetic change | [89] |
| $SiO_2$ | 15 | HaCaT | Food packaging, drug delivery | Chromosomal aberration | [94] |
| | 70<br>300<br>1000 | HaCaT | Cosmetics, foundation creams, sunscreen | Oxidative DNA damages with 70 nm NP | [95] |
| | 15<br>30<br>100 | HaCaT | Manufacturing of ceramics and plastic biomedical | DNA damages for NP< 100 nm | [69] |
| | 15 | HaCaT | Biomedicine, pharmaceuticals | Decrease of genomic DNA methylation, epigenetic dysregulation | [91] |
| Ni | 52.10 | A431 | Jewelry, handle coins | DNA fragmentation | [59] |
| $TiO_2$ | 124.9 | A431 | Cosmetics | ROS production, DNA damages | [79] |
| | 15 | HDF | Cosmetics, sunscreen | Increase of γ-H2AX, ATM, and Chk2 | [90] |

cell line. This resulted in a decrease in the methylation level of DNA and formation of 7′8 ′-dihydro-8-oxo-deoxyguanosine (8-OH-dG), a marker of mutagenesis and carcinogenesis [91, 92]. Other NPs as ZnO (having a size of 50 nm) were investigated on primary mouse keratinocytes. This resulted in a translocation of ZnO NPs into the keratinocyte nucleus generating a cascade of events from ROS generation to DNA damage detected by immunocytochemical staining of γ-H2AX [92]. Furthermore; Ni NPs having a size of 68 nm were investigated on A341 and were shown to induce DNA damage when used at a concentration of 8 µg/mL [59]. The same cell line was used by other scholars. For example, Shukla et al. showed a link between ROS production and DNA damage with $TiO_2$ NPs used at a concentration of 0.8 µg/mL and having a size of 124.9 nm after an incubation time of 6 h. This was detected by Comet assay [79] (Fig. 3). On the same spectrum of damage, CuO NPs were also investigated on HaCaT cells. A dose-dependent harm manifested as ROS generation and DNA damage was seen after 48-h exposure [66]. Guidelines for the in vitro genotoxicity tests including gene mutation (471, 476, 490) and chromosomal aberration assays (473, 487) were issued by the OECD. However, interferences with some nanomaterials were reported in in vitro genotoxicity tests due to their optical properties, chemical composition, and surface properties [93]. For this reason, the Scientific Committee on Consumer Safety (SCCS) recommended validating the in vitro genotoxicity tests for nanomaterials by including additional controls. Guidelines of mammalian cell-based tests are currently being amended by the OECD for a better adaptation to nanomaterials. In addition, the SCCS requires associating cellular and nuclear cell uptake studies to genotoxicity tests. This will help in evaluating the direct exposure of nanomaterials to DNA and then investigating the involved mechanism in the genotoxicity.

## Conclusion

Toxicological effects of NPs on cutaneous cells include cytotoxicity, inflammatory response, and genotoxicity. Such effects can be explained by their composition, with a higher toxicity of inorganic NPs as well as their physicochemical properties (size and surface charge). The mechanism involving these actions is not fully elucidated but it is noted that cell

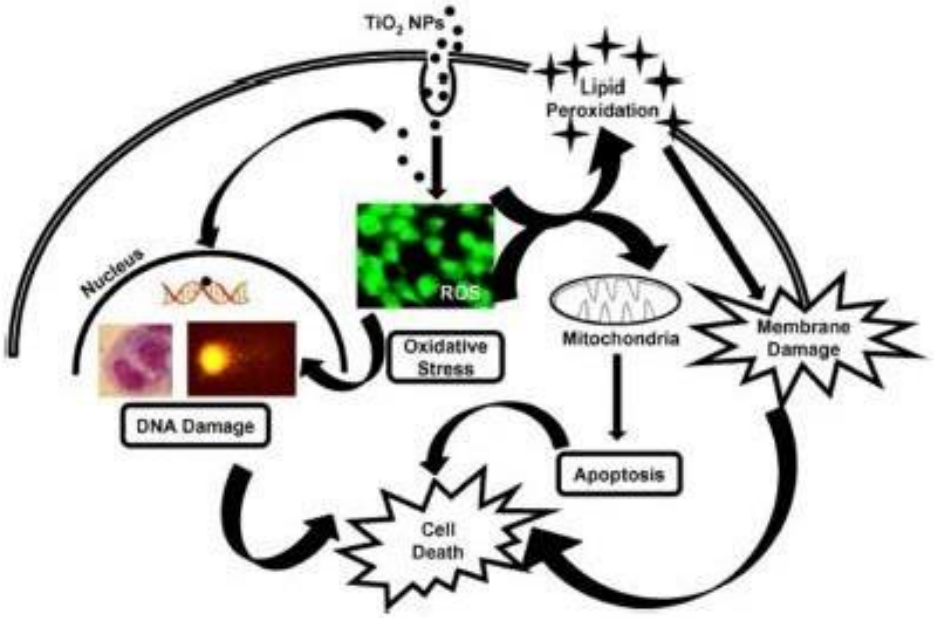


**Fig. 3** Possible mechanism of $TiO_2$ NPs induced genotoxicity in human epidermal cells. Figure is reproduced with permission from reference [79]

death, oxidative stress, and release of pro-inflammatory cytokines are inanimately seen with numerous NPs incubated with cutaneous cells. Moreover, genotoxicity was the result of either a direct penetration of small NPs into the nucleus or an indirect process often correlated with ROS production (Fig. 4). It is worth mentioning that numerous toxicological studies were performed on 2D models without considering the NP diffusion across the skin layers. Trafficking studies revealed that most of NPs, even the smallest ones, were unable to reach the viable epidermis. They usually stay in the stratum corneum or are located into hair follicles and consequently they seldom are in direct contact with viable cutaneous cells. This observation suggests an overestimation of their local toxicity of NPs in 2D cell-based models and a limited systemic distribution of NPs after topical application. Three dimension cultures or skin explants that consider the NP diffusion represent more predictive models for the nanotoxicity assessment. This was consistent with the in vitro skin corrosion test in OECD 431 which recommends validated reconstructed human epidermis. Skin's disease models should be also included in the toxicity tests due to the high permeability of the damaged skin. Besides the models, the guidelines of in vitro toxicity tests need to be adapted

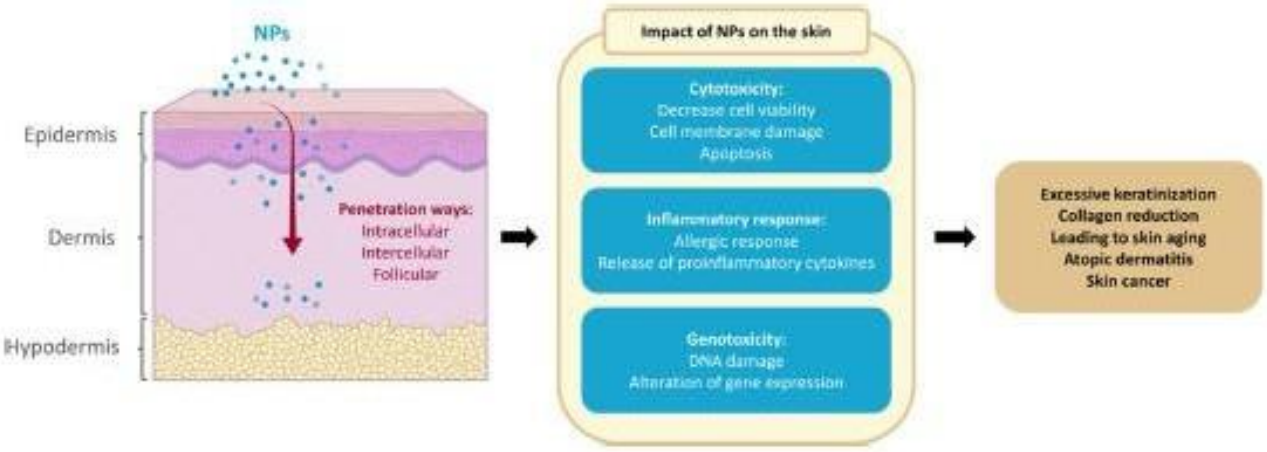


**Fig. 4** Schematic representation of NP penetration and their impact on the skin

and validated for nanomaterials. Interferences in various assays including cytotoxicity and genotoxicity were reported and then could induce a misinterpretation of data. A harmonized methodology using tests validated for nanomaterials and advanced skin models would allow a better prediction of the dermal toxicity of nanomaterials in use conditions.

**Author contribution** The literature search and data analysis were performed by Taghrid Zaiter. The initial draft of the manuscript was written by Taghrid Zaiter, reviewed and revised by Wassim El Basset and critically revised by Raphaël Cornu, Hélène Martin, Mona Diab, and Arnaud Béduneau. All authors read and approved the final manuscript.

**Funding** T. Zaiter is supported by a fellowship from the "Centre Islamique d'Orientation et de l'Enseignement Supérieur (CIOES)".

**Declarations**

**Conflict of interest** The authors declare no competing interests.

## References

1. (2009) Regulation (EC) No 1223/2009 of the European Parliament and of the Council of 30 November 2009 on cosmetic products. 151
2. (2011) Guidance for industry considering whether an FDA-regulated product involves the application of nanotechnology. Biotechnology Law Report 30:613–616. https://doi.org/10.1089/blr.2011.9814
3. ISO/TC 229, Nanotechnologies (2017) ISO/TR 18401:2017 nanotechnologies — language explanation of selected terms from the ISO/IEC 80004 series
4. Liang X, Xu Z, Grice J, et al (2013) Penetration of nanoparticles into human skin. Current pharmaceutical design 19:. https://doi.org/10.2174/1381612811319350011
5. Lu P-J, Huang S-C, Chen Y-P et al (2015) Analysis of titanium dioxide and zinc oxide nanoparticles in cosmetics. J Food Drug Anal 23:587–594. https://doi.org/10.1016/j.jfda.2015.02.009
6. Hameed A, Akhtar N (2019) The skin melanin: an inhibitor of vitamin-D3 biosynthesis: with special emphasis with structure of skin. A mini review. Dermatol Case Rep 04: https://doi.org/10.35248/2684-124X.19.4.149
7. Proksch E, Brandner JM, Jensen J-M (2008) The skin: an indispensable barrier. Exp Dermatol 17:1063–1072. https://doi.org/10.1111/j.1600-0625.2008.00786.x
8. Brown TM, Krishnamurthy K (2021) Histology, dermis. In: StatPearls. StatPearls Publishing, Treasure Island (FL)
9. OpenStaxCollege (2013) Layers of the skin. In: Anatomy & Physiology
10. Coates M, Lee MJ, Norton D, MacLeod AS (2019) The skin and intestinal microbiota and their specific innate immune systems. Front Immunol 10:. https://doi.org/10.3389/fimmu.2019.02950
11. Harder J, Schröder J-M, Gläser R (2013) The skin surface as antimicrobial barrier: present concepts and future outlooks. Exp Dermatol 22:1–5. https://doi.org/10.1111/exd.12046
12. Herman A, Herman AP (2019) Antimicrobial peptides activity in the skin. Skin Res Technol 25:111–117. https://doi.org/10.1111/srt.12626
13. Baker LB (2019) Physiology of sweat gland function: the roles of sweating and sweat composition in human health. Temperature 6:211–259. https://doi.org/10.1080/23328940.2019.1632145
14. Kabashima K, Honda T, Ginhoux F, Egawa G (2019) The immunological anatomy of the skin. Nat Rev Immunol 19:19–30. https://doi.org/10.1038/s41577-018-0084-5
15. Clark RA (2015) Resident memory T cells in human health and disease. Sci Transl Med 7:269rv1. https://doi.org/10.1126/scitranslmed.3010641
16. Yan B, Liu N, Li J et al (2020) The role of Langerhans cells in epidermal homeostasis and pathogenesis of psoriasis. J Cell Mol Med 24:11646–11655. https://doi.org/10.1111/jcmm.15834
17. Bäsler K, Bergmann S, Heisig M et al (2016) The role of tight junctions in skin barrier function and dermal absorption. J Control Release 242:105–118. https://doi.org/10.1016/j.jconrel.2016.08.007
18. Schmid-Wendtner M-H, Korting HC (2006) The pH of the skin surface and its impact on the barrier function. Skin Pharmacol Physiol 19:296–302. https://doi.org/10.1159/000094670
19. Filipe P, Silva JN, Silva R et al (2009) Stratum corneum is an effective barrier to TiO2 and ZnO nanoparticle percutaneous absorption. Skin Pharmacol Physiol. https://doi.org/10.1159/000235554
20. Smijs TGM, Bouwstra JA (2010) Focus on skin as a possible port of entry for solid nanoparticles and the toxicological impact. J Biomed Nanotechnol 6:469–484. https://doi.org/10.1166/jbn.2010.1146
21. Wu J, Liu W, Xue C et al (2009) Toxicity and penetration of TiO2 nanoparticles in hairless mice and porcine skin after subchronic dermal exposure. Toxicol Lett 191:1–8. https://doi.org/10.1016/j.toxlet.2009.05.020
22. Zvyagin AV, Zhao X, Gierden A et al (2008) Imaging of zinc oxide nanoparticle penetration in human skin in vitro and in vivo. J Biomed Opt 13:064031. https://doi.org/10.1117/1.3041492
23. van Kuijk-Meuwissen MEMJ, Mougin L, Junginger HE, Bouwstra JA (1998) Application of vesicles to rat skin in vivo: a confocal laser scanning microscopy study. J Control Release 56:189–196. https://doi.org/10.1016/S0168-3659(98)00087-X
24. Sonavane G, Tomoda K, Sano A et al (2008) In vitro permeation of gold nanoparticles through rat skin and rat intestine: effect of particle size. Colloids Surf, B 65:1–10. https://doi.org/10.1016/j.colsurfb.2008.02.013
25. Larese FF, D'Agostin F, Crosera M et al (2009) Human skin penetration of silver nanoparticles through intact and damaged skin. chen. Toxicology 255:33–37. https://doi.org/10.1016/j.tox.2008.09.025

26. Larese Filon F, Mauro M, Adami G et al (2015) Nanoparticles skin absorption: new aspects for a safety profile evaluation. Regul Toxicol Pharmacol 72:310–322. https://doi.org/10.1016/j.yrtph.2015.05.005
27. Kohli AK, Alpar HO (2004) Potential use of nanoparticles for transcutaneous vaccine delivery: effect of particle size and charge. Int J Pharm 275:13–17. https://doi.org/10.1016/j.ijpharm.2003.10.038
28. Wang M, Lai X, Shao L, Li L (2018) Evaluation of immunoresponses and cytotoxicity from skin exposure to metallic nanoparticles. Int J Nanomedicine 13:4445–4459. https://doi.org/10.2147/IJN.S170745
29. Fang C-L, Aljuffali IA, Li Y-C, Fang J-Y (2014) Delivery and targeting of nanoparticles into hair follicles. Ther Deliv 5:991–1006. https://doi.org/10.4155/tde.14.61
30. Nanoparticles and their interactions with the dermal barrier. https://www.ncbi.nlm.nih.gov/pmc/articles/PMC2835875/. Accessed 8 Feb 2022
31. Alvarez-Román R, Naik A, Kalia YN et al (2004) Skin penetration and distribution of polymeric nanoparticles. J Control Release 99:53–62. https://doi.org/10.1016/j.jconrel.2004.06.015
32. Baroli B, Ennas MG, Loffredo F et al (2007) Penetration of metallic nanoparticles in human full-thickness skin. J Invest Dermatol 127:1701–1712. https://doi.org/10.1038/sj.jid.5700733
33. Patzelt A, Richter H, Knorr F et al (2011) Selective follicular targeting by modification of the particle sizes. J Control Release 150:45–48. https://doi.org/10.1016/j.jconrel.2010.11.015
34. Ng KW, Lau WM (2015) Skin deep: the basics of human skin structure and drug penetration. In: Dragicevic N, Maibach HI (eds) Percutaneous penetration enhancers chemical methods in penetration enhancement: drug manipulation strategies and vehicle effects. Springer, Berlin, Heidelberg, pp 3–11
35. Sanches PL, Geaquinto LR de O, Cruz R, et al (2020) Toxicity evaluation of TiO2 nanoparticles on the 3D skin model: a systematic review. Front Bioeng Biotechnol 8:.https://doi.org/10.3389/fbioe.2020.00575
36. Carrola J, Bastos V, Jarak I et al (2016) Metabolomics of silver nanoparticles toxicity in HaCaT cells: structure–activity relationships and role of ionic silver and oxidative stress. Nanotoxicology 10:1105–1117. https://doi.org/10.1080/17435390.2016.1177744
37. Wu Z, Yang H, Archana G et al (2018) Human keratinocytes adapt to ZnO nanoparticles induced toxicity via complex paracrine crosstalk and Nrf2-proteasomal signal transduction. Nanotoxicology 12:1215–1229. https://doi.org/10.1080/17435390.2018.1537409
38. O'Neill AT, Monteiro-Riviere NA, Walker GM (2008) Characterization of microfluidic human epidermal keratinocyte culture. Cytotechnology 56:197–207. https://doi.org/10.1007/s10616-008-9149-9
39. Zhang LW, Zeng L, Barron AR, Monteiro-Riviere NA (2007) Biological interactions of functionalized single-wall carbon nanotubes in human epidermal keratinocytes. Int J Toxicol 26:103–113. https://doi.org/10.1080/10915810701225133
40. Auffan M, Rose J, Orsiere T et al (2009) CeO2 nanoparticles induce DNA damage towards human dermal fibroblasts in vitro. Nanotoxicology 3:161–171. https://doi.org/10.1080/17435390902788086
41. Goenka S, Toussaint J (2020) Citrate-coated platinum nanoparticles exhibit a primary particle-size dependent effect on stimulating melanogenesis in human melanocytes. Cosmetics 7:88. https://doi.org/10.3390/cosmetics7040088
42. Tan J, Zhao C, Zhou J et al (2017) Co-culturing epidermal keratinocytes and dermal fibroblasts on nano-structured titanium surfaces. Mater Sci Eng C Mater Biol Appl 78:288–295. https://doi.org/10.1016/j.msec.2017.04.036
43. Sarkiri M, Fox SC, Fratila-Apachitei LE, Zadpoor AA (2019) Bioengineered skin intended for skin disease modeling. Int J Mol Sci 20:. https://doi.org/10.3390/ijms20061407
44. Kim H, Choi J, Lee H et al (2016) Skin corrosion and irritation test of nanoparticles using reconstructed three-dimensional human skin model, EpiDerm™. Toxicol Res 32:311–316. https://doi.org/10.5487/TR.2016.32.4.311
45. Hao F, Jin X, Liu QS et al (2017) Epidermal penetration of gold nanoparticles and its underlying mechanism based on human reconstructed 3D Episkin model. ACS Appl Mater Interfaces 9:42577–42588. https://doi.org/10.1021/acsami.7b13700
46. Suhail S, Sardashti N, Jaiswal D et al (2019) Engineered skin tissue equivalents for product evaluation and therapeutic applications. Biotechnol J 14:1900022. https://doi.org/10.1002/biot.201900022
47. Ternullo S, de Weerd L, Holsæter AM et al (2017) Going skin deep: a direct comparison of penetration potential of lipid-based nanovesicles on the isolated perfused human skin flap model. Eur J Pharm Biopharm 121:14–23. https://doi.org/10.1016/j.ejpb.2017.09.006
48. Abd E, Yousuf SA, Pastore MN et al (2016) Skin models for the testing of transdermal drugs. CPAA 8:163–176. https://doi.org/10.2147/CPAA.S64788
49. Samberg ME, Oldenburg SJ, Monteiro-Riviere NA (2010) Evaluation of silver nanoparticle toxicity in skin in vivo and keratinocytes in vitro. Environ Health Perspect 118:407–413. https://doi.org/10.1289/ehp.0901398
50. Korani M, Rezayat SM, Arbabi Bidgoli S (2013) Subchronic dermal toxicity of silver nanoparticles in Guinea pig: special emphasis to heart, bone and kidney toxicities. Iran J Pharm Res 12:511–519
51. Moniz T, Costa Lima SA, Reis S (2020) Human skin models: from healthy to disease-mimetic systems; characteristics and applications. Br J Pharmacol 177:4314–4329. https://doi.org/10.1111/bph.15184
52. Adachi K, Yamada N, Yamamoto K et al (2010) In vivo effect of industrial titanium dioxide nanoparticles experimentally exposed to hairless rat skin. Nanotoxicology 4:296–306. https://doi.org/10.3109/17435391003793095
53. Abdel-Mottaleb MMA, Moulari B, Beduneau A et al (2012) Nanoparticles enhance therapeutic outcome in inflamed skin therapy. Eur J Pharm Biopharm 82:151–157. https://doi.org/10.1016/j.ejpb.2012.06.006
54. Jin H, He R, Oyoshi M, Geha RS (2009) Animal models of atopic dermatitis. J Invest Dermatol 129:31–40. https://doi.org/10.1038/jid.2008.106
55. Engelhart K, El Hindi T, Biesalski H-K, Pfitzner I (2005) In vitro reproduction of clinical hallmarks of eczematous

dermatitis in organotypic skin models. Arch Dermatol Res 297:1–9. https://doi.org/10.1007/s00403-005-0575-7
56. Crosera M, Prodi A, Mauro M et al (2015) Titanium dioxide nanoparticle penetration into the skin and effects on HaCaT cells. Int J Environ Res Public Health 12:9282–9297. https://doi.org/10.3390/ijerph120809282
57. Colombo I, Sangiovanni E, Maggio R, et al (2017) HaCaT cells as a reliable in vitro differentiation model to dissect the inflammatory/repair response of human keratinocytes. Mediators Inflamm 2017:. https://doi.org/10.1155/2017/7435621
58. Benameur L, Auffan M, Cassien M et al (2015) DNA damage and oxidative stress induced by CeO2 nanoparticles in human dermal fibroblasts: evidence of a clastogenic effect as a mechanism of genotoxicity. Nanotoxicology 9:696–705. https://doi.org/10.3109/17435390.2014.968889
59. Alarifi S, Ali D, Alakhtani S et al (2014) Reactive oxygen species-mediated DNA damage and apoptosis in human skin epidermal cells after exposure to nickel nanoparticles. Biol Trace Elem Res 157:84–93. https://doi.org/10.1007/s12011-013-9871-9
60. Chen L, Wu M, Jiang S et al (2019) Skin toxicity assessment of silver nanoparticles in a 3D epidermal model compared to 2D keratinocytes. Int J Nanomedicine 14:9707–9719. https://doi.org/10.2147/IJN.S225451
61. Sun T, Jackson S, Haycock JW, MacNeil S (2006) Culture of skin cells in 3D rather than 2D improves their ability to survive exposure to cytotoxic agents. J Biotechnol 122:372–381. https://doi.org/10.1016/j.jbiotec.2005.12.021
62. Knudsen NØ, Rønholt S, Salte RD et al (2012) Calcipotriol delivery into the skin with PEGylated liposomes. Eur J Pharm Biopharm 81:532–539. https://doi.org/10.1016/j.ejpb.2012.04.005
63. Mohamed AL, Elmotasem H, Salama AAA (2020) Colchicine mesoporous silica nanoparticles/hydrogel composite loaded cotton patches as a new encapsulator system for transdermal osteoarthritis management. Int J Biol Macromol 164:1149–1163. https://doi.org/10.1016/j.ijbiomac.2020.07.133
64. Hirai T, Yoshikawa T, Nabeshi H et al (2012) Amorphous silica nanoparticles size-dependently aggravate atopic dermatitis-like skin lesions following an intradermal injection. Part Fibre Toxicol 9:3. https://doi.org/10.1186/1743-8977-9-3
65. Ostrowski A, Nordmeyer D, Boreham A et al (2014) Skin barrier disruptions in tape stripped and allergic dermatitis models have no effect on dermal penetration and systemic distribution of AHAPS-functionalized silica nanoparticles. Nanomedicine: Nanotechnology. Biology and Medicine 10:1571–1581. https://doi.org/10.1016/j.nano.2014.04.004
66. Alarifi S, Ali D, Verma A et al (2013) Cytotoxicity and genotoxicity of copper oxide nanoparticles in human skin keratinocytes cells. Int J Toxicol 32:296–307. https://doi.org/10.1177/1091581813487563
67. Meyer K, Rajanahalli P, Ahamed M et al (2011) ZnO nanoparticles induce apoptosis in human dermal fibroblasts via p53 and p38 pathways. Toxicol In Vitro 25:1721–1726. https://doi.org/10.1016/j.tiv.2011.08.011
68. Liang H, Jin C, Tang Y et al (2014) Cytotoxicity of silica nanoparticles on HaCaT cells. J Appl Toxicol 34:367–372. https://doi.org/10.1002/jat.2953
69. Yang X, Liu J, He H et al (2010) SiO2 nanoparticles induce cytotoxicity and protein expression alteration in HaCaT cells. Part Fibre Toxicol 7:1. https://doi.org/10.1186/1743-8977-7-1
70. Zanette C, Pelin M, Crosera M et al (2011) Silver nanoparticles exert a long-lasting antiproliferative effect on human keratinocyte HaCaT cell line. Toxicol In Vitro 25:1053–1060. https://doi.org/10.1016/j.tiv.2011.04.005
71. Gandamalla D, Lingabathula H, Reddy Y (2017) Cytotoxicity evaluation of titanium and zinc oxide nanoparticles on human cell lines. International Journal of Pharmacy and Pharmaceutical Sciences 9:240. https://doi.org/10.22159/ijpps.2017v9i11.21924
72. Sooklert K, Nilyai S, Rojanathanes R et al (2019) N-acetylcysteine reverses the decrease of DNA methylation status caused by engineered gold, silicon, and chitosan nanoparticles. Int J Nanomedicine 14:4573–4587. https://doi.org/10.2147/IJN.S204372
73. OCDE (2015) Test No. 431: in vitro skin corrosion: reconstructed human epidermis (RHE) test method
74. Park Y-H, Jeong SH, Yi SM et al (2011) Assessment of phototoxicity, skin irritation, and sensitization potential of polystyrene and TiO2nanoparticles. J Phys: Conf Ser 304:012050. https://doi.org/10.1088/1742-6596/304/1/012050
75. Schaeublin NM, Braydich-Stolle LK, Maurer EI et al (2012) Does shape matter? Bioeffects of gold nanomaterials in a human skin cell model. Langmuir 28:3248–3258. https://doi.org/10.1021/la204081m
76. Huang Y, Lu X, Qu Y et al (2015) MicroRNA sequencing and molecular mechanisms analysis of the effects of gold nanoparticles on human dermal fibroblasts. Biomaterials 37:13–24. https://doi.org/10.1016/j.biomaterials.2014.10.042
77. Leite-Silva VR, Sanchez WY, Studier H et al (2016) Human skin penetration and local effects of topical nano zinc oxide after occlusion and barrier impairment. Eur J Pharm Biopharm 104:140–147. https://doi.org/10.1016/j.ejpb.2016.04.022
78. Sharma V, Shukla RK, Saxena N et al (2009) DNA damaging potential of zinc oxide nanoparticles in human epidermal cells. Toxicol Lett 185:211–218. https://doi.org/10.1016/j.toxlet.2009.01.008
79. Shukla RK, Sharma V, Pandey AK et al (2011) ROS-mediated genotoxicity induced by titanium dioxide nanoparticles in human epidermal cells. Toxicol In Vitro 25:231–241. https://doi.org/10.1016/j.tiv.2010.11.008
80. Kocbek P, Teskac K, Kreft ME, Kristl J (2010) Toxicological aspects of long-term treatment of keratinocytes with ZnO and TiO2 nanoparticles. Small 6:1908–1917. https://doi.org/10.1002/smll.201000032
81. Browning CL, The T, Mason MD, Wise JP (2014) Titanium dioxide nanoparticles are not cytotoxic or clastogenic in human skin cells. J Environ Anal Toxicol 4:. https://doi.org/10.4172/2161-0525.1000239
82. Ryu HJ, Seong N, So BJ et al (2014) Evaluation of silica nanoparticle toxicity after topical exposure for 90 days. IJN 9:127–136. https://doi.org/10.2147/IJN.S57929

83. Pal A, Alam S, Chauhan L, et al (2016) UVB exposure enhanced the dermal penetration of zinc oxide nanoparticles and induced inflammatory responses through oxidative stress mediated of MAPKs and NF-κB signaling in SKH-1 hairless mouse skin. Toxicol Res 5:. https://doi.org/10.1039/C6TX00026F
84. Ilves M, Palomäki J, Vippola M et al (2014) Topically applied ZnO nanoparticles suppress allergen induced skin inflammation but induce vigorous IgE production in the atopic dermatitis mouse model. Part Fibre Toxicol 11:38. https://doi.org/10.1186/s12989-014-0038-4
85. Kundu J, Kim D-H, Chae IG et al (2018) Silicon dioxide nanoparticles induce COX-2 expression through activation of STAT3 signaling pathway in HaCaT cells. Toxicol In Vitro 52:235–242. https://doi.org/10.1016/j.tiv.2018.06.008
86. Yanagisawa R, Takano H, Inoue K-I et al (2009) Titanium dioxide nanoparticles aggravate atopic dermatitis-like skin lesions in NC/Nga mice. Exp Biol Med (Maywood) 234:314–322. https://doi.org/10.3181/0810-RM-304
87. Yanagisawa R, Takano H, Ki I et al (2010) Size effects of polystyrene nanoparticles on atopic dermatitis-like skin lesions in NC/NGA mice. Int J Immunopathol Pharmacol 23:131–141. https://doi.org/10.1177/039463201002300112
88. Galandáková A, Franková J, Ambrožová N et al (2016) Effects of silver nanoparticles on human dermal fibroblasts and epidermal keratinocytes. Hum Exp Toxicol 35:946–957. https://doi.org/10.1177/0960327115611969
89. Gao F, Ma N, Zhou H et al (2016) Zinc oxide nanoparticles-induced epigenetic change and G2/M arrest are associated with apoptosis in human epidermal keratinocytes. Int J Nanomedicine 11:3859–3874. https://doi.org/10.2147/IJN.S107021
90. Prasad RY, Chastain PD, Nikolaishvili-Feinberg N et al (2013) Titanium dioxide nanoparticles activate the ATM-Chk2 DNA damage response in human dermal fibroblasts. Nanotoxicology 7:1111–1119. https://doi.org/10.3109/17435390.2012.710659
91. Gong C, Tao G, Yang L et al (2010) SiO2 nanoparticles induce global genomic hypomethylation in HaCaT cells. Biochem Biophys Res Commun 397:397–400. https://doi.org/10.1016/j.bbrc.2010.05.076
92. Pal A, Alam S, Mittal S et al (2016) UVB irradiation-enhanced zinc oxide nanoparticles-induced DNA damage and cell death in mouse skin. Mutat Res Genet Toxicol Environ Mutagen 807:15–24. https://doi.org/10.1016/j.mrgentox.2016.06.005
93. Magdolenova Z, Lorenzo Y, Collins A, Dusinska M (2012) Can standard genotoxicity tests be applied to nanoparticles? J Toxicol Environ Health A 75:800–806. https://doi.org/10.1080/15287394.2012.690326
94. Gong C, Yang L, Zhou J et al (2017) Possible role of PAPR-1 in protecting human HaCaT cells against cytotoxicity of SiO2 nanoparticles. Toxicol Lett 280:213–221. https://doi.org/10.1016/j.toxlet.2017.07.213
95. Nabeshi H, Yoshikawa T, Matsuyama K et al (2011) Amorphous nanosilica induce endocytosis-dependent ROS generation and DNA damage in human keratinocytes. Part Fibre Toxicol 8:1. https://doi.org/10.1186/1743-8977-8-1

# CHAPTER III: Nanotoxicity: Experimental Part

## 1. SILICATES NANOPARTICLES

### 1.1. Contexts and objectives

Silica particles are widely used in food products to prevent the powder agglomeration. Despite their presence in the market for a long time, doubts regarding their oral toxicity remain as mentioned by the EFSA in its report on the re-evaluation of the food additive E551. This could be explained by the insufficient toxicological data but also the variability in the size distribution of additives between manufacturers. No specifications have been yet established, allowing the presence of nano silica. Due to their small size, they could interact with the intestinal cells and then alter the intestinal barrier. Thus, an investigation on the intestinal toxicity of silica particles was performed using *in vitro* models of the intestinal barrier. The influence of the mucus, digestion process and the size was evaluated using E551 additive and engineered silica NPs.

### 1.2. Methodology

The effects of silica NPs, native and digested E551 additives on the intestinal barrier were evaluated *in vitro* on Caco-2 and HT29-MTX cell lines in mono and coculture cultivated in Transwell®. This support mimics the *in vivo* configuration of the intestine. It is composed of an apical compartment that represents the intestinal lumen and a basolateral compartment corresponding to the blood vessels. These two compartments are separated by a membrane on which the cells forming the intestinal barrier are seeded. The Transwell® is used to study the intestinal permeability of drugs or the passage of toxins (**Figure 16**). E551 additive was incubated in gastric and intestinal simulated fluids to accurately mimic gastrointestinal digestion before exposure. The engineered silica NPs, native and digested E551 were then incubated with the cells for 7 days. Cytotoxicity, ROS production, cytokine expression and transepithelial electrical resistance modulation were investigated.

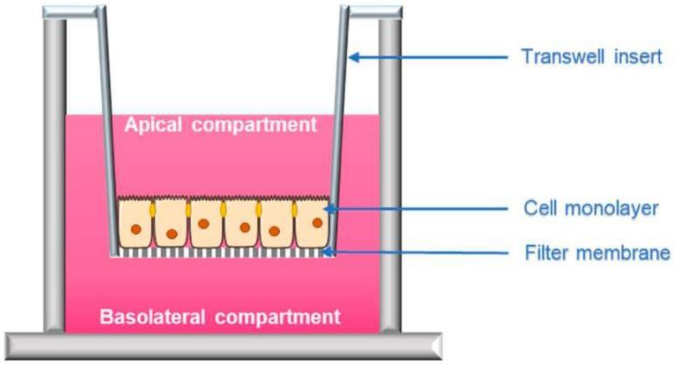


***Figure16: schematic representation of a Transwell®.***

## 1.3. Main Finding/Conclusions

This study showed that:

- Digestion did not affect the physicochemical properties of the E551 additive
- The mucus layer produced by a single culture of HT29-MTX acted as an effective protective barrier against both small and large silica particles.
- Small nanoparticles affected the transepithelial electrical resistance of the Caco-2/HT29-MTX co-culture despite the presence of a mucus layer.
- 70 nm was considered as a threshold diameter above which silica particles do not cause intestinal toxicity

## 1.4. Scientific article

NANOTOXICOLOGY
https://doi.org/10.1080/17435390.2022.2063084

Taylor & Francis
Taylor & Francis Group

RESEARCH ARTICLE



# Size effect and mucus role on the intestinal toxicity of the E551 food additive and engineered silica nanoparticles

Taghrid Zaiter[a], Raphaël Cornu[a], Nadine Millot[b], Michaële Herbst[b], Yann Pellequer[a], Georges Moarbess[c], Hélène Martin[a], Mona Diab-Assaf[c] and Arnaud Béduneau[a]

[a]PEPITE EA4267, Univ. Bourgogne Franche-Comté, Besançon, France; [b]Laboratoire Interdisciplinaire Carnot de Bourgogne, UMR 6303, CNRS/Université Bourgogne Franche-Comté, Dijon, France; [c]EDST, Pharmacology and Cancerology Laboratory, Faculty of Sciences, Lebanese University, Beirut, Lebanon

**ABSTRACT**

The E551 food additive is composed of synthetic amorphous silica particles. The current regulation does not mention any specifications regarding their size and granulometric distribution, thus allowing the presence of silica nanoparticles despite their potential toxicity. The digestion process could modify their physicochemical properties and then influence their toxicological profile. After physicochemical characterization, subacute toxicity of engineered silica nanoparticles from 20 to 200 nm, native and digested E551 additives were evaluated from *in vitro* models of the intestinal barrier. Single cultures and a co-culture of enterocytes and mucus-secreting cells were established to investigate the mucus role. Toxicological endpoints including cytotoxicity, ROS production, intestinal permeability increase, and actin filament disruption were addressed after a 7-day exposure. The results showed a size-dependent effect of silica nanoparticles on cytotoxicity and intestinal permeability. A time-dependent disruption of actin filaments was observed in Caco-2 cells. The mucus layer spread on the HT29-MTX single culture acted as an efficient protective barrier while in the co-culture, small nanoparticles were able to cross it to reach the cells. From a hydrodynamic diameter of 70 nm, nanoparticles were not internalized in the intestinal cells, even in mucus-free models. Digestion did not affect the physicochemical properties of the additive. Due to a mean hydrodynamic diameter close to 200 nm, both native and digested E551 additives did not induce any toxic effect in intestinal barrier models. This study emphasized a cutoff size of 70 nm from which the interactions of the E551 additive with intestinal cells would be limited.

**ARTICLE HISTORY**
Received 4 January 2022
Revised 29 March 2022
Accepted 4 April 2022

**KEYWORDS**
Silica nanoparticles; E551; mucus; intestinal barrier; toxicity

## Introduction

E551 additive is commonly used as an anti-caking agent or thickener in numerous food products. It is composed of amorphous silica synthesized by thermal (fumed) and wet processes (precipitated). Particles in E551 are usually characterized by a mean diameter in the micrometer range (Fruijtier-Pölloth 2016). However, no size limit was mentioned in the specifications, while the dimensions of particles are often reported as a toxicity factor (Dong et al. 2020). A study showed the presence of silica nanoparticles (NPs) in food products with a diameter comprised between 10 and 50 nm (Athinarayanan et al. 2014). The European Food Safety Authority (EFSA) recommended including in oral toxicity studies, nano silicon dioxide considering they can be contained in E551 additives complying with the current specifications (Younes et al. 2018). In addition, size could be reduced during the digestion process. A modification of the aggregation state was reported after contact with biological fluids including gastric and intestinal fluids (Yoo et al. 2021). Silica NPs in foods prepared with E551 additive were also present after intestinal digestion (Peters et al. 2012).

Many *in vitro* studies on the intestinal toxicity of silica particles, including E551 additive, were reported in the literature. Unfortunately, they exhibit major limitations. They were usually performed by incubations of NPs with intestinal cell lines, especially Caco-2 without considering the mucus layer (Hempt et al. 2020). Mucus secreting

CONTACT Arnaud Béduneau amaud.beduneau@univ-fcomte.fr PEPITE EA4267, Univ. Bourgogne Franche-Comté, Besançon, France
Supplemental data for this article can be accessed online at https://doi.org/10.1080/17435390.2022.2063084.

intestinal models were developed for other types of nanomaterials such as copper oxide and silver NPs (Georgantzopoulou et al. 2016; Gillois et al. 2021; Ude et al. 2019b). A reduced number of toxicological endpoints were addressed including DNA damages, immune response and cytotoxicity, while the impact on intestinal permeability was seldom investigated. (Gerloff et al. 2009; Mu et al. 2012; Tarantini et al. 2015). The alteration of the intestinal barrier could induce numerous adverse effects due to bacterial translocation or absorption modifications. We have recently reported that 20 and 30 nm silica NPs increased the intestinal permeability of co-culture after acute exposure (Cornu et al. 2020). Besides, short-term exposures no longer than 24 h were usually carried out despite the presence of the additive E551 in daily food products (Ude et al. 2019a).

The present study investigates the size-dependent intestinal toxicity of silica particles contained in E551 additive by considering the mucus layer. Single cultures of intestinal cell lines including Caco-2 and HT29-MTX as well as a co-culture of both cell types were exposed to E551 additive and engineered silica NPs for 7 days. Caco-2 was extensively used in *in vitro* models mimicking intestinal permeability (Le Ferrec et al. 2001). After differentiation, they exhibit functional and structural characteristics of human enterocytes, including microvilli, tight junction proteins and P-glycoproteins (Hendriks et al. 1991). HT29-MTX are human carcinoma cell lines differentiated into mucus-secreting cells after methotrexate exposure (Lesuffleur et al. 1993). Co-culture of Caco-2 and HT29-MTX were characterized by a continuous mucus layer on the apical side (Béduneau et al. 2014). This model close to the human small intestine physiology represents an alternative method to animal testing for oral toxicity prediction. Besides marketed food-grade additives, engineered silica NPs with diameters ranging from 20 nm to 200 nm were included in the study to cover the full-size range of particles in E551 additives. Their dimensions were in line with the study of Dekkers *et al.* that showed the presence of nano-silica in food products with sizes between 50 and 200 nm (Dekkers et al. 2011). NPs below 100 nm were also detected for ten of eleven samples of E511 food additive (Barahona et al. 2016). This methodological approach consisting of the use of engineered NPs is a recommendation of the EFSA panel in charge of the reevaluation of silicon dioxide as a food additive (Younes et al. 2018). Prior to the exposure, additives were incubated in gastric and intestinal simulated fluids to accurately mimic gastrointestinal digestion. Their physicochemical properties were characterized using transmission electron microscopy (TEM), dynamic light scattering (DLS), Brunauer–Emmett–Teller (BET) and thermogravimetry analysis (TGA). The influence of the size and the mucus layer on toxicological endpoints including cytotoxicity, ROS production, inflammatory response, transepithelial electrical resistance and actin filament disruption was evaluated. The cell uptake in intestinal cell lines was investigated using fluorescent engineered silica NPs.

## Materials and methods

### *Chemicals and reagents*

Silica NPs (plain Sicastar®) and fluorescent silica NPs (Sicastar®-redF) with different sizes from 20 nm to 200 nm were purchased from Micromod Partikeltechnologie GmbH (Rostock, Germany) and E551 (EMPROVE® ESSENTIAL) from Merck (Germany). Caco-2 cells were provided from the American Type Culture Collection (ATCC) and HT29-MTX cell line was kindly provided by Dr. Thécla Lesuffleur from INSERM UMR S 938 (Paris, France). The cell culture reagents were purchased from Gibco. Other chemicals used in our experiments were from Sigma Aldrich (Steinheim, Germany) unless stated otherwise.

### *Physicochemical characterization of silica particles*

*Physicochemical characterization of silica particles*

***Dynamic light scattering/laser doppler electrophoresis.*** The size and zeta potential of silica NPs and E551 additive were measured using a ZetaSizer Nano-ZS90 (Malvern). Average hydrodynamic diameters and the polydispersity index (PDI) were determined by dynamic light scattering at 25 °C after suspension in a free-serum cell culture medium. Zeta potential measurements were determined by laser Doppler electrophoresis at 25 °C at a final concentration of 1 mg.mL$^{-1}$. For the determination of the isoelectric point of additives, 4 mg of powder were resuspended in 10 mL of HCL solution at pH 1.5 followed by the addition of 20 µL of NaCl at

5 M. Measurements were carried out at 25.0 °C, immediately after homogenization by ultrasound bath for 10 min. pH was adjusted between 2 and 11 using 100 mM HCl or NaOH at 100 or 10 mM. Zeta Potential was then measured in triplicate at each pH, using a ZetaSizer NanoZSP (Malvern).

***Transmission electron microscopy (TEM).*** The morphology of silica NPs was observed by Transmission electron microscopy (TEM) using a JEOL JEM 2100 F microscope operating at 200 kV (point-to-point resolution of 0.19 nm). The samples were prepared by evaporating a diluted suspension of NPs in a mixture of deionized (DI) water and ethanol. The mixture then underwent ultrasounds using a tip (few min, 375 W, Sonics Vibra-Cells). Then, a few drops were deposited on a carbon-coated copper grid. About 100 NPs were counted in order to estimate their average size.

***BET specific surface area.*** Specific surface area measurement ($S_{BET}$) was carried out using a Micromeritics Tristar II apparatus. Samples were outgassed *in situ* for 4 hours at 80 °C under the pressure of *ca.*≈30 µbar (≈ 90 mg). The measurements were performed at liquid $N_2$ temperature using $N_2$ as the adsorbing gas. The BET method was used in the calculation of the surface area value from the isotherm of nitrogen adsorption.

***Thermogravimetric analysis (TGA).*** The weight losses of silica NPs were studied by thermogravimetric analyses (TGA) with a TA Instruments Discovery TGA under an airflow rate of 25 mL.min$^{-1}$. The analyses were done using the following thermal program: ramp 1 of 20 °C.min$^{-1}$ from 25 °C to 100 °C; isotherm at 100 °C for 30 min (to remove the remaining moisture) and ramp 2 of 5 °C.min$^{-1}$ from 100 °C to 700 °C. TGA weight losses were considered only from the second ramps.

### *Physical stability study of silica particles*

The stability of silica NPs and E551 was evaluated at 37 °C in a serum-free cell culture medium for 48 h. NP suspensions were prepared at 1 mg.mL$^{-1}$. Hydrodynamic diameters, PDI, and zeta potential were measured before and after 48 h of incubation.

### *Digestion of E551 in simulated gastric fluid (SGF) and intestinal fluid (SIF)*

The gastro-intestinal fluids were prepared according to the protocol of the United States Pharmacopeia (USP). Briefly, to prepare the simulated gastric fluid (SGF), 1.28 g of purified pepsin from porcine stomach mucosa was added to osmosed water containing 0.8 g of NaCl. After 15 min of mixing, 2.8 mL of HCl were added. pH was finally adjusted to 1.5 with 10 N NaOH. Finally, SGF solution was centrifuged for 10 min, at 15 000 *g* under 4 °C, filtered and stored at the same temperature. To prepare the simulated intestinal fluid (SIF), 4 g of pancreatin were added to osmosed water containing 2.72 g of monobasic potassium phosphate and 3.2 g of sodium hydroxide. After 15 min of mixing, pH was adjusted to 6.8 with 0.4 N NaOH. SIF solution was finally centrifuged for 1 h at 20 000 *g* under 4 °C, filtered and then stored at the same temperature.

Simulated digestion of E551 additive was realized. It consists of double digestion in SGF and SIF. Briefly, E551 suspended in water was sonicated for 30 min in the ultrasonic bath, and then mixed with SGF solution at 37 °C. This solution was placed at 37 °C for 2 h under agitation. After incubation, E551 digested with SGF was washed 3 times by centrifugation at 5000 *g* and 4 °C for 10 min. The samples were finally suspended in water and frozen at −80 °C for 1 h before a freeze-drying step. Freeze-dried NPs were then resuspended in SIF and incubated for 2h at 37°C. After 3 washings and centrifugation at 5000 g, double digested NPs were finally frozen and freeze-dried.

### *Cell culture*

***Caco-2/HT29-MTX co-culture in transwell®.*** Two passages after thawing, Caco-2 and HT29-MTX were seeded in Gluta-Max Dulbecco's Modified Eagle Medium containing 15% fetal bovine serum (FBS), 1% non-essential amino acids and 100 µg.mL$^{-1}$ streptomycin/100 UI/mL penicillin in Transwell®-24 well 0.33 cm$^2$ permeable support with a polycarbonate membrane. Caco-2 were seeded at 5000 cells/insert and HT29-MTX at 10 000 cells/insert 5 days later. The Transwell® supports were used after 21 days. TEER values of at least 400 ohm.cm$^2$ were a requirement for the *in vitro* studies. Immunostaining of ZO-1 and Muc5AC was periodically performed to

check the preservation of physiological characteristics of the co-culture.

***Culture in 96-wells plate.*** Caco-2 or HT29-MTX cells were seeded in a 96-wells plate at a final concentration of 17 500 cells/well. Plates were used after 7 days of culture Gluta-Max Dulbecco's Modified Eagle Medium.

### *Preparation of silica particle suspensions for in vitro studies*

Native and digested E551 additives suspensions were prepared by adding dried particles in a serum-free culture medium at a final concentration of 1 mg.mL$^{-1}$. They were then dispersed by a sonication step for 30 min at 4 °C using an ultrasonic bath. The samples of engineered NPs were obtained after dilution of commercial aqueous suspensions in a serum-free culture medium at a final concentration of 1 mg.mL$^{-1}$. Prior to the incubations, the hydrodynamic diameters, and the Zeta potentials of silica particles in suspension were characterized by dynamic light scattering and laser doppler electrophoresis.

### *Cytotoxicity assay*

The cell viability was evaluated using the 3-(4, 5-dimethylthiazol-2-yl)-5-(3-carboxymethoxyphenyl)-2-(4-sulfophenyl)-2H-tetrazolium (MTS) assay. A control medium with 1% water corresponding to the water fraction in the samples of engineered NPs was then added to the study. Cells in a 96-wells plate were incubated with silica NPs and E551 at 1 mg.mL$^{-1}$ for 7 days. The treatment was renewed every 2 days. Cell cultures were washed 3 times with Phosphate-Buffered Saline (PBS) before 2 h of incubation at 37 °C with MTS solution (Promega). Absorbance was measured at 570 nm using the microplate reader (Synergy HT BioTek).

### *ROS quantification*

The extracellular ROS production was evaluated using the ROS-Glo $H_2O_2$ assay kit (Promega). Briefly, after 7 days of incubation of Caco-2 and HT29-MTX with silica NPs and additive E551 at 1 mg.mL$^{-1}$, the supernatant was collected and incubated for 20 min at room temperature with ROS-Glo detection solution. The relative luminescence was then measured.

### *IL-8 Quantification*

The level of interleukin-8 (IL-8) was assessed using a human ELISA kit (Life Technologies-ThermoFisher) according to the labeled instructions. Briefly, the levels of IL-8 were evaluated after exposing Caco-2 and HT29-MTX in the 96 well plates to silica NPs and additive E551 at a concentration of 1 mg.mL$^{-1}$ for 7 days and then the supernatant was collected for analysis.

### *Transepithelial electrical resistance measurement*

The Caco-2/HT29-MTX co-culture in Transwell® supports was incubated with silica NPs and E551 for 7 days. The treatment was renewed every 2 days. The NPs were added in the apical compartment and cell culture medium with FBS in the basolateral compartment. Transepithelial electrical resistance (TEER) measurement was realized before and after incubation with NPs using the Millicell Electrical Resistance System (Millipore).

### *Quantification of silica particles in cell models*

Fluorescent silica NPs at 1 mg.mL$^{-1}$ were incubated for 2 h, 8 h or 24 h with Caco-2 and HT29-MTX single cultures and Caco-2/HT29-MTX co-culture. Regarding the HT29-MTX culture, three different treatments were performed to investigate the mucus role. The soluble mucus layer was removed from HT29-MTX by successive washings with DPBS before and after ("no mucus" condition) the incubation of NPs while for the "mucus removal" condition, only one washout step is carried out after the incubation of NPs. Briefly, the culture medium was discarded and 100 µL of DPBS was added to the apical surface of the cells. After 2 min gentle mixing, the DPBS was removed. The washing was repeated twice. The last treatment termed "mucus" consisted in fixing with 3.7% of paraformaldehyde (PFA) for 15 minutes the HT29-MTX including the mucus layer after incubation and before the washing steps. PFA fixation was also performed in the two first treatments. The cells were finally washed 3 times with DPBS and then lysed with 0.25 N NaOH. Samples were transferred to black 96-well plates. Fluorescence was immediately measured using a microplate reader. $\lambda_{excitation}$ and $\lambda_{emission}$ were 569 nm and 585 nm, respectively. The fluorescence intensity (%) was determined from a standard curve

prepared by successive dilutions of fluorescent NP suspensions in NaOH 0.25 N.

### *Fluorescent staining*

***Immunostaining of Muc5AC.*** HT29-MTX cells seeded in chamber slide support were incubated for 24 h with fluorescent NP30 and NP200 at 1 mg.mL$^{-1}$. After 15 min of fixation with 3.7% of PFA, the cells were washed 3 times with PBS Tween 0.1% and then blocked with FBS for 1 h. Muc5AC protein was labeled with Mucin 5AC Alexa fluor 488 (Santa Cruz biotechnology SC-33667) diluted in PBS Tween 0.1% to reach a final concentration of 2 µg.mL$^{-1}$ overnight at 4 °C. Cells were washed 3 times with PBS Tween 0.1%. This was followed by a 1 min-incubation with DAPI. Cells were washed again 3 times. The chamber slides were sealed using DAKO fluorescent mounting medium. Slides were analyzed with a confocal microscope LSM 800 AiryScan (Zeiss). Some HT29-MTX seeded in chamber slide was labeled with Muc5AC at different times, where a washout of soluble mucus layer was realized at T0, T2 h, T8 h and T24 h.

***Staining of actin.*** HT29-MTX or Caco-2 cells seeded in chamber slide support were incubated with native or digested E551, or NP30, NP200 nm at 1 mg.mL$^{-1}$ for 24 h. Cells were washed twice with PBS and then fixed for 15 min with 3.7% of PFA. Cells were permeabilized for 10 min with 0.5% Triton X100 in PBS. After two steps of washing, actin was labeled with 150 nM Acti-stain 488 phalloidin (Cytoskeleton, Inc. PHDG1-A) for 45 min at room temperature. After a final step of washing, the cells were incubated for 1 min with DAPI. The chamber slides were sealed using DAKO fluorescent mounting medium. Slides were analyzed with a confocal microscope LSM 800 AiryScan (Zeiss).

### *Statistics*

All data are means ± SD and performed on three independent experiments ($n = 3$). Statistical analysis was performed using one-way ANOVA followed by a Holm-Sidak test. Results were considered statistically significant at $p \leq 0.05$.

## Results and discussion

### *Physicochemical characterization of silica nanoparticles*

E551 was digested by successive incubations in simulated gastric (SGF) and intestinal fluids (SIF) for 2 × 2 h at 37 °C. Two batches were prepared. The incubation times were mentioned in the INFOGEST protocol regarding the static *in vitro* gastrointestinal digestion (Brodkorb et al. 2019). The SGF and SIF were prepared according to the recommendations of the USP. Centrifugation and washing steps were performed after each incubation to exchange the simulated fluids and to remove the free compounds such as enzymes. Additives were finally freeze-dried for BET analysis and to assess the particle loss during the centrifugation steps. The SIF was not used for the *in vitro* studies due to the cytotoxicity of the pancreatin (Antoine et al. 2015). Only the E551 additive was treated to evaluate the impact of the digestion on the physicochemical properties, especially the size and the specific surface area. An increase in the concentration of silica NPs after intestinal digestion as reported by Peters *et al.* could cause toxicity (Peters et al. 2012). Silica particles were dispersed in a culture medium without FBS to overcome stability issues (data not shown). Serum was nevertheless added in the basolateral compartment of the Transwell® device for the *in vitro* experiments. Unlike engineered NPs obtained from concentrated aqueous suspensions, 1 h-sonication was requested to redisperse the powders of native and digested additives. Hydrodynamic diameters of native and digested E551 additive were measured by dynamic light scattering in culture medium immediately after sonication (T0) and after 48 h at 37 °C. In Table 1, native E551 and the two batches of digested additives were characterized by hydrodynamic diameters of 232 nm, 166 nm and 215 nm, respectively. Digestion did not modify the Zeta Potential of E551 additives with a similar value of −23 mV. The isoelectric point (IP) of native and digested E551 was in the same range, between 3.2 and 3.5 (Figure S1). The low IP values were consistent with the high negative surface charge of the additives in the culture medium, guaranteeing their electrostatic stability for 48 h in the culture medium. Despite incubation in SGF at a pH 1.5 close the additive IP, no aggregation of

**Table 1.** Physicochemical characterization of natives and digested E551 additives.

| | E551 | E551-d1 | E551-d2 |
|---|---|---|---|
| Dynamic light scattering | | | |
| Hydrodynamic diameter (nm) | | | |
| T0 | 232 ± 39 | 166 ± 17 | 215 ± 22 |
| T48h | 245 ± 13 | 207 ± 16 | 230 ± 18 |
| Polydispersity index | | | |
| T0 | 0.21 ± 0.01 | 0.17 ± 0.03 | 0.14 ± 0.06 |
| T48h | 0.35 ± 0.06 | 0.19 ± 0.01 | 0.11 ± 0.08 |
| Laser doppler electrophoresis | | | |
| Zeta potential (mV) | − 23 ± 1 | −23 ± 1 | −23 ± 1 |
| Isoelectric point | 3.5 | 3.4 | 3.2 |
| TEM | | | |
| Diameter ($n = 100$, nm) | 13.9 ± 2.1 | 13.7 ± 2.1 | 13.5 ± 2.1 |
| BET | | | |
| Surface area ($m^2.g^{-1}$) | 208 | 181 | 182 |
| ATG | | | |
| Weight Loss (%) | 0.32 | 2.96 | 3.06 |
| Peak d(w)/d(T) (°C) | 266 | 280 | 282 |

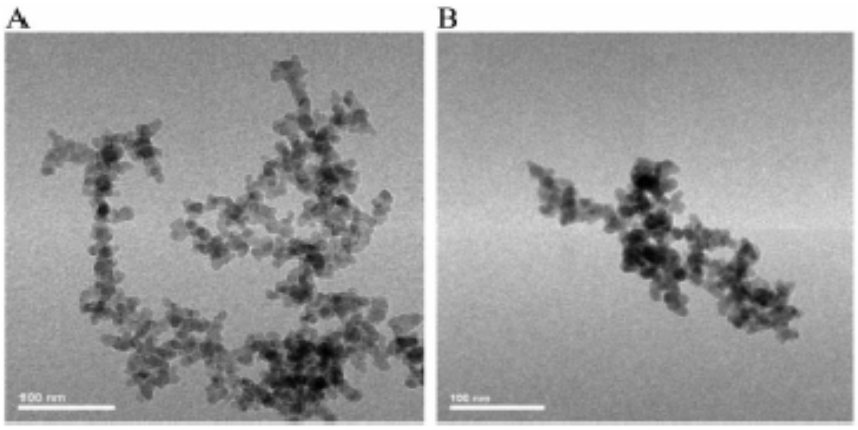


**Figure 1.** Electron microscopy images of native E551 (A) and digested E551 (B) at a 50K magnification.

digested silica particles was observed compared with the native E551. BET analysis showed a specific surface area of 208 and 180–182 $m^2.g^{-1}$ for native and digested additives, respectively. Considering the density of 2.56 $g.cm^{-3}$ specified by the manufacturer, E551 additives could be classified as nanomaterials according to the European Commission (EC) definition due to surface areas greater than 60 $m^2.cm^{-3}$ (533 $m^2.cm^{-3}$ and 461–466 $m^2.cm^{-3}$) for native and digested additives, respectively.

Electron microscopy of E551 powders (native or digested) showed primary particles with a mean size close to 14 nm (Figure 1). This was in agreement with the literature which defines synthetic amorphous silica's as aggregates of small particles strongly bonded between them (van Kesteren et al. 2015). The release of primary particles has never been observed even under high mechanical stress (Fruijtier-Pölloth 2016; Gray and Muranko 2006). Thus, nanosized silica previously observed in E551 additive could be only explained by the presence of small aggregates rather than individual primary particles (Barahona et al. 2016). High-energy technics such as sonication are nevertheless required to separate the agglomerates prior to the DLS measurements. No treatment was performed for surface area analysis by BET and the surface measured are consistent with NPs. Besides electron microscopy images confirmed the classification of the Emprove® E551 additive as nanomaterial. According to the EC, both agglomerates and aggregates are defined as nanomaterials if the dimension of constituent particles is comprised between 1 and 100 nm. Thermogravimetry analysis showed a weight loss from 200 °C, due to a dehydroxylation process and the desorption of chemisorbed water (Zhuravlev 2000). The weight loss was 10-fold higher with digested additives

Table 2. Hydrodynamic diameter and Zeta potential of engineered silica nanoparticles.

| | NP20 | NP30 | NP70 | NP200 |
|---|---|---|---|---|
| Dynamic light scattering | | | | |
| Hydrodynamic diameter (nm) | | | | |
| T0 | 21 ± 1 | 30 ± 2 | 71 ± 3 | 206 ± 3 |
| T48h | 24 ± 4 | 33 ± 1 | 72 ± 2 | 201 ± 19 |
| Polydispersity index | | | | |
| T0 | 0.11 ± 0.07 | 0.07 ± 0.01 | 0.03 ± 0.02 | 0.03 ± 0.03 |
| T48h | 0.25 ± 0.13 | 0.30 ± 0.03 | 0.08 ± 0.06 | 0.06 ± 0.04 |
| Laser doppler electrophoresis | | | | |
| Zeta potential (mV) | −14 ± 2 | −15 ± 0 | −21 ± 2 | −23 ± 1 |

compared with native ones (Figure S2). This suggests significant chemical adsorption of water molecules during the digestion step despite the freeze-drying downstream process. However, both thermogravimetric analysis and Zeta potential measurements were similar for all the additive batches, demonstrating no adsorption of organic compounds such as enzymes during the digestion.

The engineered silica NPs exhibited a hydrodynamic diameter in line with the manufacturer specifications, except for the smallest NPs (Table 2). They were characterized by a hydrodynamic diameter of 20 nm rather than 10 nm (data from manufacturer) and then were finally termed NP20. The size and the polydispersity index of silica NPs were maintained after 48 h incubation in a culture medium. Zeta potential values were close to −14 and −15 mV for NP20 and NP30, respectively. The absolute values were higher for the NP70 and NP200 with potentials of −21 and −23 mV, respectively. Both the surface charge and the hydrodynamic diameter of NP200 were in the same value ranges as the E551 additive.

### *Toxicity of silica nanoparticles in Caco-2 and HT29-MTX single cultures*

For the *in vitro* experiments, the concentration in silica particles including E551 was fixed at 1 mg.mL$^{-1}$. Recent work by *Cornu et al.* showed silica particles do not induce any *in vitro* intestinal toxicity after 2 h-incubation at 1 mg.mL$^{-1}$ unlike 10 mg.mL$^{-1}$ (Cornu et al. 2020). However, long-term exposure needs also to be evaluated due to the presence of silica NPs in daily food products. Besides, the assessment of a potential toxic concentration threshold requires considering high concentration values such as 1 mg.mL$^{-1}$ without any relationship with the dietary daily exposure. This was in line with the EFSA report on the reevaluation of the E551 additive. The scientific committee was not able to confirm the acceptable daily intake (ADI) "not specified" due to numerous limitations in the available toxicological data (Younes et al. 2018). In a first step, only single cultures of Caco-2 and HT29-MTX were exposed to silica particles to correlate the potential nanotoxicity with the intestinal cell type and the mucus layer. Engineered silica NPs, native and digested E551 additives were incubated for 7 days. The particle suspensions were renewed every 2 days to preserve the NPs properties, especially the size. MTS assay was performed after 7-day exposure to assess the viability of cells (Figures 2A and 2B). Native and digested E551 did not affect the viability of Caco-2 with values of 93 ± 8% and 96 ± 8%, respectively. Values for both additives were close to 110% in HT29-MTX culture. The digestion process of the E551 additive did not alter the cellular viability, likely due to similar surface areas and hydrodynamic diameters. By contrast, incubation of the smallest silica NPs on the Caco-2 monolayer induced a significant loss of viability. Values dropped to 66 ± 5% and 69 ± 4% with NP20 and NP30, whereas they were 78 ± 4% and 98 ± 14% with NP70 and NP200 respectively. Surprisingly, silica NPs significantly increased the viability of HT29-MTX. Values ranged from 156 ± 17% to 128 ± 21% between NP20 and NP200. These results revealed a proliferative effect which was also observed with 12 nm and 14 nm silica NPs in contact with HT29 and rat lung epithelial cells (Gehrke et al. 2013; Sydlik et al. 2006). Another study reported the proliferation of osteoblast-like cells in presence of silicon (Shie et al. 2011). A partial release of silicon without affecting the NP size could occur at physiological pH as suggested by

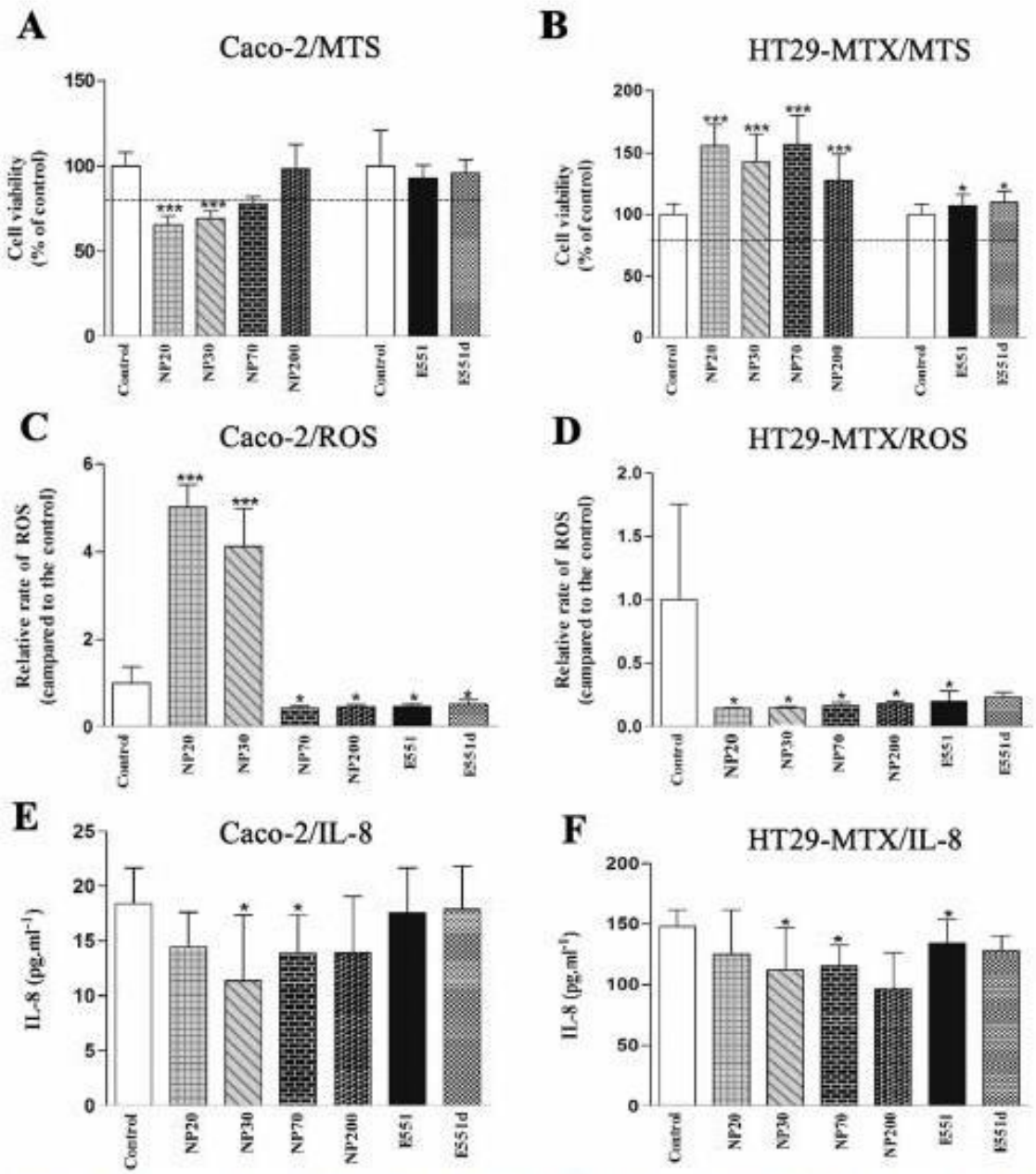


Figure 2. Viability of Caco-2 (A) and HT29-MTX (B) cells after 7 day-incubation with engineered silica NPs as well as digested and native E551 additive at 1 mg.mL-1. Controls were performed in culture medium. One percent water was added for silica NPs. Effect of silica NPs (1 mg.mL-1) after 7 day- exposure on the ROS production in Caco-2 (C) and HT29-MTX (D). Relative ROS rate was expressed from the control. IL-8 secretion was determined by ELISA assay after 7 days exposure of the silica NPs (1 mg.mL-1) in Caco-2 (E) and HT29-MTX (F). Values were reported as mean ± standard deviation from two or three independent experiments performed in triplicate. Statistical analysis was performed using one way ANOVA followed by a Holm-Sidak test. Results were considered as statistically significant at $P < 0.001$ (***), $P < 0.01$ (**) and $P < 0.05$ (*).

Diedrich *et al.* (Diedrich et al. 2012). For both free silicon and silica NPs, interaction with MAPK/ERK signaling pathway was suggested to explain cell proliferation. Rather than a proliferative action, a metabolic activity increase due to a hormetic effect could be also hypothesized (Mytych et al. 2016). ROS was also quantified after 7-day exposure to silica particles (Figures 2C and 2D). While no ROS production was detected in HT29-MTXs single cultures, ROS production increased by at least 4-fold after incubation of NP20 and NP30 with Caco-2 cells. No effect of NP70, NP200 and E551 additive was observed. IL8 pro-inflammatory cytokine was not produced after NP exposure to both single

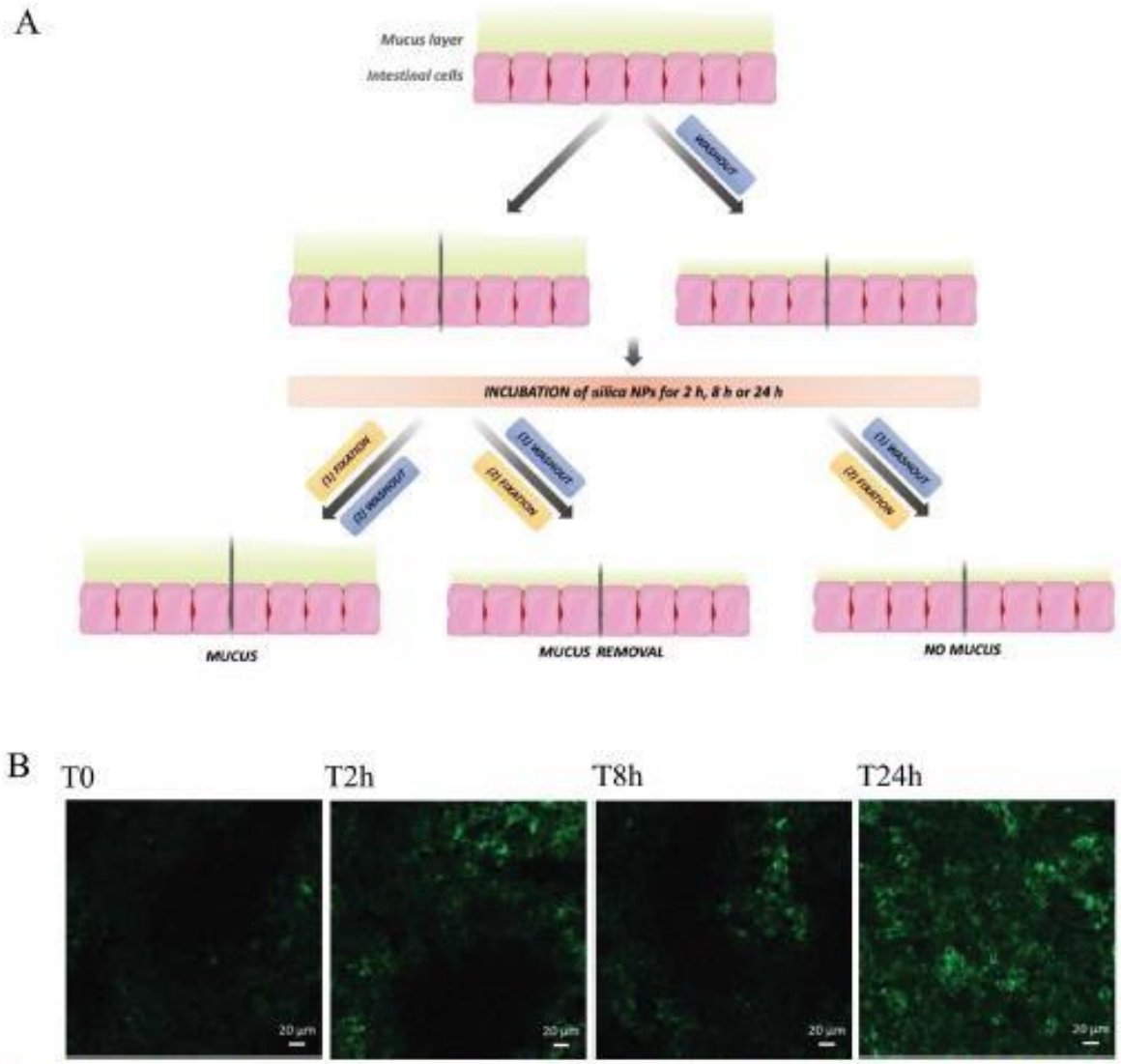


**Figure 3.** (A) Diagram describing the different washing steps of HT29-MTX culture. (B) MucSAC immunostaining in HT29-MTX single culture at different times after DPBS washout.

cultures (Figures 2E and 2F), suggesting the lack of an inflammatory response. Therefore, the toxic effect of silica particles including cytotoxicity and ROS production depends on both their size and the cell type. Mucus layer spread on HT29-MTX could also play a major role in the toxicological profile of engineered silica NPs.

### *Mucus effect on the cell uptake of engineered silica NPs*

Fluorescent silica NPs with sizes ranging from 20 nm to 200 nm were incubated between 2 h and 24 h with Caco-2 and HT29-MTX single cultures. A longer incubation time was not considered to preserve the dye's fluorescent properties. Experiments with HT29-MTX cell single culture were performed under three different conditions (Figure 3A): (i) washout with DPBS to remove the mucus layer prior to the incubation (no mucus); ii) washout with DPBS to remove the mucus layer after incubation (mucus removal); iii) fixation of the mucus layer with paraformaldehyde (PFA) immediately after incubation to retain the soluble layer during the elimination of NPs and the washing steps (mucus). While many experimental protocols use mucolytic agents for removing mucus, confocal microcopy revealed the lack of a mucus layer after washout with DPBS (Figure 3B) (Behrens et al. 2001; Mahler et al. 2009). This observation was in line with the

study of Wikman-Larhed and Artursson (1995). After 2 successive items of washing with Hanks' Balanced Salt Solution (HBSS), the thickness of the mucus secreted by HT29-MTX cells dropped to 38% and the surface coverage was reduced to 70%. The HBSS washing procedure was also used by Hilgendorf *et al.* to remove the mucus layer at the surface of HT29-MTX cells (Hilgendorf et al. 2000). This could be explained by the features of the gastrointestinal mucus. It is mainly composed of a weakly adherent layer that can be easily removed by suction (Atuma et al. 2001). A second layer strongly attached to the mucosa is characterized by a low thickness in the small intestine and is even sometimes absent. Besides, a *de novo* mucus secretion was observed from 2 h after DPBS washout, but the HT29-MTX was not entirely covered. A continuous mucus layer was only obtained at 24 h post washout. These results were consistent with the rapid intestinal mucus turnover (between 47 and 270 min) reported by Lehr et al. (1991).

Accumulation of fluorescent silica NPs in Caco-2 and HT29-MTX single cultures was compared (Figure 4). In Figure 4A, the fluorescence levels after 24 h-incubation with HT29-MTX covered by a mucus layer were similar between NP20 and NP30 as well as between N70 and NP200. The accumulation of both large NPs was greater than 20% of the applied dose while the values were approximately 14% for silica NPs with hydrodynamic diameters of 20 and 30 nm. After DPBS washout leading to the mucus removal, negligible fluorescence intensity was then detected for every silica NPs. This suggests an accumulation in the mucus layer rather than a cell uptake. In the lack of mucus, the trend was inverted with a higher accumulation of two smaller NPs, especially NP20. The fluorescence intensity was 39 ± 6% for NP20 while the values were 11 ± 3% and 9 ± 1% for NP70 and NP200, respectively. The accumulation kinetics of silica NPs in HT29-MTX culture covered by a mucus layer was also observed in Figure 4B. No tremendous increase in the fluorescence intensity between 2 h and 24 h was noticed for NP30, NP70 and NP200, due to a rapid accumulation in the mucus layer. The behavior of NP20 was different with fluorescence intensity of 2 ± 0.5% and 10 ± 1% at 2 h and 8 h finally reaching 14 ± 2% after 24 h. Whereas a rapid mucoadhesion was suggested for NP30, NP70 and NP200, a slower diffusion of NP20 into the mucus layer could be hypothesized. An opposite effect was reported with polystyrene (PS) NPs. A higher flux and permeability coefficient of negatively charged 50 nm PS NPs across a layer of rabbit intestinal mucus was observed compared with 200 nm NPs (Bandi et al. 2020). Yildiz *et al.* also demonstrated the transport of carboxylate-modified PS particles across porcine jejunum mucus decreased with the size of particles (Yildiz et al. 2015). The pore dimensions of the mucus network comprised between 100 and 200 nm could limit the diffusion of large PS NPs (Pearson et al. 2016). However, aggregation of mucins leading to the formation of larger spaces, up to 1000 nm was reported by Cone (2009). In line with this finding, polyethylene-glycol (PEG) coated NPs of 200 and 500 nm were characterized by higher diffusion coefficients through human mucus than 100 nm NPs (Rodgers and Fanning 2011). Thus, the same mucoadhesion mechanism could be suggested with silica particles due to their hydrophilic feature unlike PS NPs (Sakuma et al. 1999). This would also explain the highest accumulation of NP70 and NP200 in the mucus compared with NP20 and NP30. In Figure 4C, an accumulation kinetic was observed over 24 h for both smaller NPs in the lack of a mucus layer. For NP20 and NP30, the fluorescence intensities were of 16 ± 3% and 17 ± 3% at 2 h. They finally reached values of 39 ± 6% and 28 ± 4% after 24 h incubation. Regarding NP70 and NP200, the values were of 13 ± 3% and 11.0 ± 5% at 2 h, then 11 ± 3% and 9 ± 1% at 24 h. The accumulation of NP20 and NP30 over the time is typical of a cell uptake while a cytoadhesion of silica NPs from a hydrodynamic of 70 nm could be suggested. The same behavior was observed with Caco-2. In Figure 4D, the fluorescence intensities of cells exposed to NP20 and NP30 were 7 ± 2% and 2 ± 0.3% at 2 h. A fluorescence increase was observed after 24 h with values of 25 ± 2% and 18 ± 2%. In the same way as "no mucus" HT29-MTX cultures, no accumulation kinetic was reported with NP70 and NP200 with values below 10%. Thus, in the lack of mucus, small NPs were able to be internalized both in enterocytes and HT29-MTX, unlike NP70 and NP200. Despite mesh pores of at least 100 nm (Cone 2009), mucus hindered NP20 and NP30 to reach the HT29-MTX cells. This could be attributed to a strong

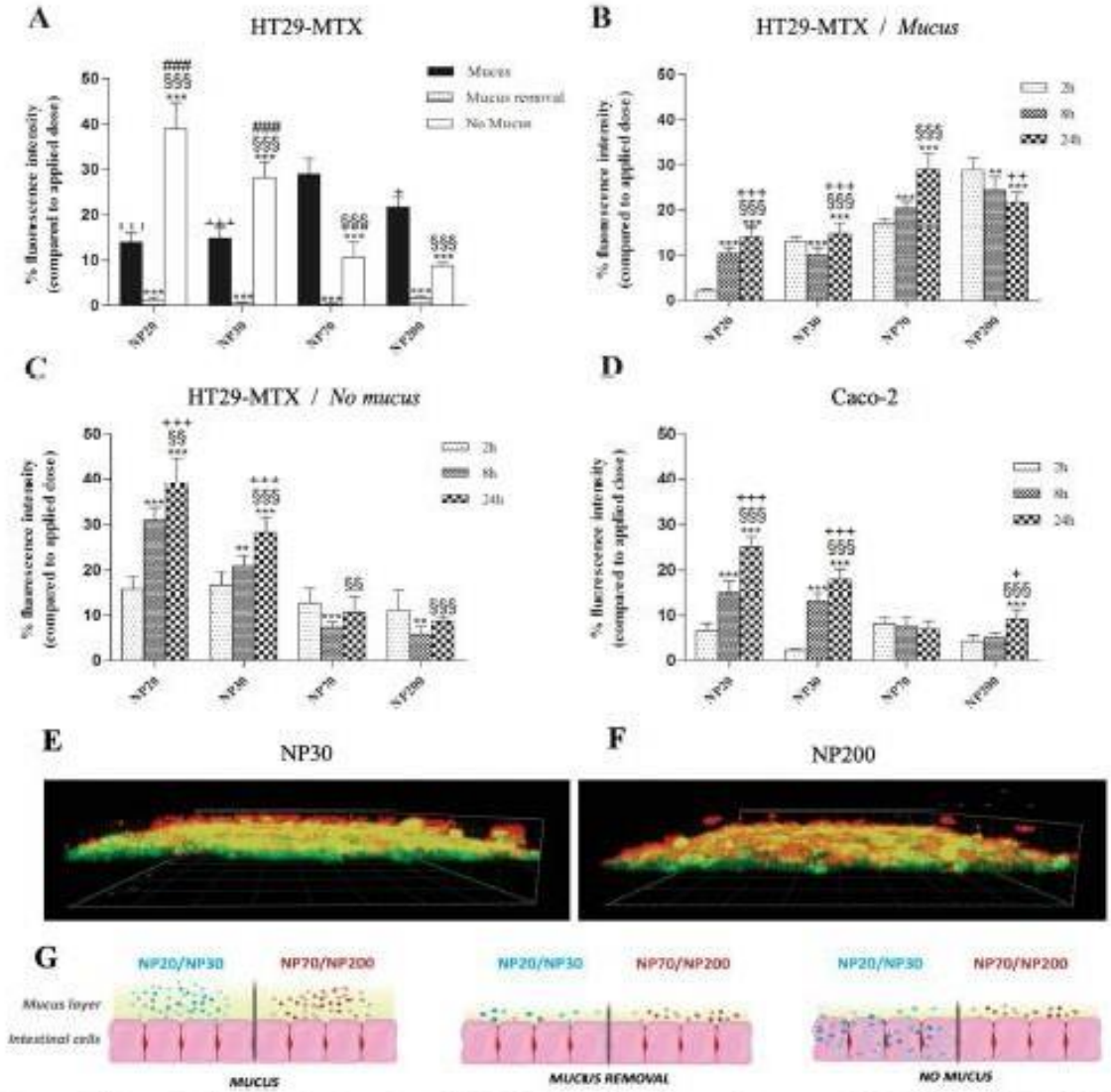


**Figure 4.** Accumulation of silica NPs in Caco-2 and HT29-MTX single cultures. Fluorescent NP20, NP30, NP70 & NP200 were exposed to intestinal cells at 1 mg.mL$^{-1}$. The percentage of fluorescence intensity was obtained after comparison with the applied dose. Some HT29-MTX cultures were washed with DPBS to remove the weakly adherent mucus layer before (no mucus) or after (mucus removal) the NP incubation. (A) Influence of the mucus layer and NP size on the fluorescence intensity percentage in HT29-MTX after 24 h exposure. *mucus compared to mucus removal and to no mucus; § mucus removal compared to no mucus; # NP70 compared to NP20, NP30 and NP200 in no mucus condition; + NP70 compared to NP20, NP30 & NP200 in mucus condition. (B and C) Fluorescence intensity percentage after 2 h, 8 h and 24 h of incubation in "mucus" and "no mucus" H29-MTX cultures respectively. (D) Fluorescence intensity percentage after 2 h, 8h and 24 h of incubation in Caco-2 single culture. *2 h compared to 8 and to 24 h; §8 h compared to 24 h; +NP70 compared to NP20, NP30 and NP200. Values were reported as mean ± standard deviation ($n = 3$). Statistical analysis was performed using one-way ANOVA followed by a Holm-Sidak test. Results were considered as statistically significant at $P < 0.001$ (***, §§§, ###, +++), $P < 0.01$ (**, §§, ##, ++), $P < 0.05$ (*, §, #, +). (E, F) Confocal microscopy images of HT29-MTX cells incubated with fluorescent NP30 and NP200 (in red), respectively. Muc5AC immunostaining was performed to visualize the mucus layer (in green). (G) Graphical representation of the accumulation of silica NPs in HT29-MTX single cultures for the different treatments.

interaction with mucins by hydrogen bonding but also to the dynamic properties of the mucus. The rapid intestinal mucus turnover could lead to the continuous elimination of embedded NPs before reaching the cells, especially when they slowly diffuse (Lehr et al. 1991; Liu et al. 2015). In Figures 4E and 4F, confocal microcopy images confirmed the co-localization of NP30 with the mucin 5AC similarly to NP200. The mucus effect on the accumulation of engineered silica NPs in the HT29-MTX single culture was summarized in Figure 4G. The size of 70 nm could be considered a threshold value for

cell uptake. These findings can be correlated to the viability assay and ROS quantification. Unlike NP70 and NP200, NP20 and NP30 induced cytotoxicity and ROS production for Caco-2 due to their internalization into the cells. By contrast, no toxicity was observed with mucus-covered HT29-MTX for all the silica engineered NPs. Their interaction with the cells, even for the smallest ones, was prevented by the mucus layer. The release of silicon in the culture medium could be reasonably assumed to explain the proliferative effect.

### *Interaction of engineered silica NPs with the actin cytoskeleton*

Some engineered NPs are also well known to interact with the actin cytoskeleton (Déciga-Alcaraz et al. 2020; Ispanixtlahuatl-Meráz et al. 2018). This can cause a disruption of actin filaments and then increase the epithelial permeability (Rodgers and Fanning 2011). The impact of silica NPs on the actin cytoskeleton was investigated by confocal microscopy (Figure 5). Cytochalasin was used as a positive control due to its impact on actin polymerization (Brown and Spudich 1979; MacLean-Fletcher and Pollard 1980). Large NPs including NP70, NP200 as well native and digested additives did not alter the actin cytoskeleton of Caco-2 and HT29-MTX. A time-dependent effect was reported with NP30. Disruption of the actin cytoskeleton was observed after 24 h exposure while the filaments were still intact at 2 h and 8 h. This result supports the internalization assay that demonstrated a significant cell-uptake increase over time. Besides, the MTS assay showed no cytotoxicity of NP30 after 24 h incubation with Caco-2 cells (data not shown). Thus, the actin disruption cannot be explained by cell death but rather by an interaction of internalized NPs with actin filaments (Ispanixtlahuatl-Meráz et al. 2018). Regarding the HT29-MTX, no disruption was observed, confirming the protective effect of the mucus layer even for small NPs.

### *Intestinal toxicity of silica nanoparticles in a co-culture model*

The human small intestine is composed of 80–90% of enterocytes and 8–10% of goblet cells (Gehart and Clevers 2019; Umar 2010). Paneth cells, enteroendocrine cells, M cells and stem cells are also located in the intestinal epithelium but in a smaller proportion (Barker et al. 2008). To mimic the human intestinal barrier, a co-culture of HT29-MTX and Caco-2 cell lines covered by a continuous mucus layer was established (Béduneau et al. 2014). The TEER values of the co-culture were close to 400 ohm.cm$^2$. They were in the same range as the values of the small intestine and the colon which are 50–100 and 300–400 ohm.cm$^2$, respectively (Srinivasan et al. 2015). After immunostaining, confocal microscopy images showed the uniform distribution of the tight junction protein *zonula occludens 1* in the co-culture (Figure 6A). This was consistent with the study of Gagnon et al. that demonstrated tight junction expression in both Caco-2 and HT29-MTX cells (Gagnon et al. 2013). Engineered silica NPs, as well as native and digested E551 additives, were incubated for 7 days. MTS assay was then performed (Figure 6B). Native and digestive additives did not affect the viability of the co-culture with values of 97 ± 11% and 99 ± 8%, respectively. Exposure to NP20 and NP30 reduced the viability at 53 ± 7% and 72 ± 4% while the values were 79 ± 6% and 97 ± 6% for NP70 and NP200. The results were in line with the measurements of the TEER. In Figure 6C, the percentages of the initial TEER were 96 ± 5% and 91 ± 8% with native and digested additives, respectively. A TEER drop of the co-culture started from 48 h exposure to small NPs in Figure 6D. After 7 days, the TEER level was equal to 50 ± 7% and 60 ± 12% of initial values with NP20 and NP30, respectively whereas it was at least 80% for NP70 and NP200. Accumulation of fluorescent NPs in the co-culture was reported in Figure 6E. No accumulation kinetic was observed for large NPs. The fluorescence values after NP70 exposure were 15 ± 6% and 17 ± 5% at 2 h and 24 h, respectively. These results demonstrate a rapid accumulation of NP70 and NP200 in the mucus layer. The behavior of NP20 and NP30 was tremendously different. The fluorescence intensities in the co-culture were 8 ± 0.4% and 11 ± 3% after 2 h incubation with NP20 and NP30, respectively. A significant fluorescence increase was noticed at 24 h with values close to 25% for both NPs. This accumulation profile correlated to the cytotoxicity and the TEER decrease suggests a time-dependent uptake of small NPs. Other toxicological

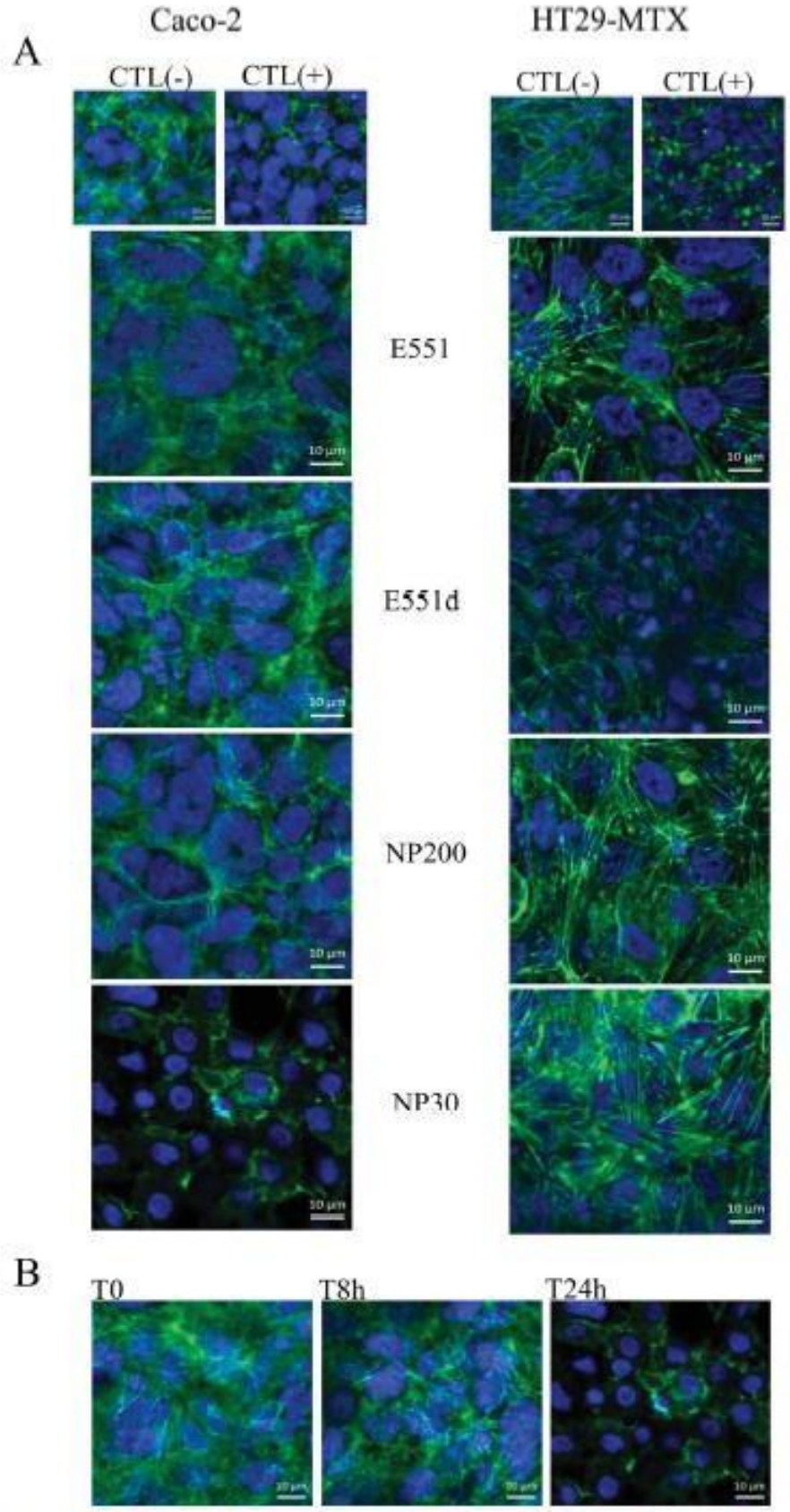


**Figure 5.** (A) Influence of native and digested E551 additive as well as NP30 and NP200 on the actin cytoskeleton of Caco-2 and HT29-MTX single cultures. Particles were incubated for 24 h at 1 mg.mL$^{-1}$. (B) Time-dependent disruption of the actin cytoskeleton in Caco-2 single culture after NP30 exposure at 1 mg.mL$^{-1}$.

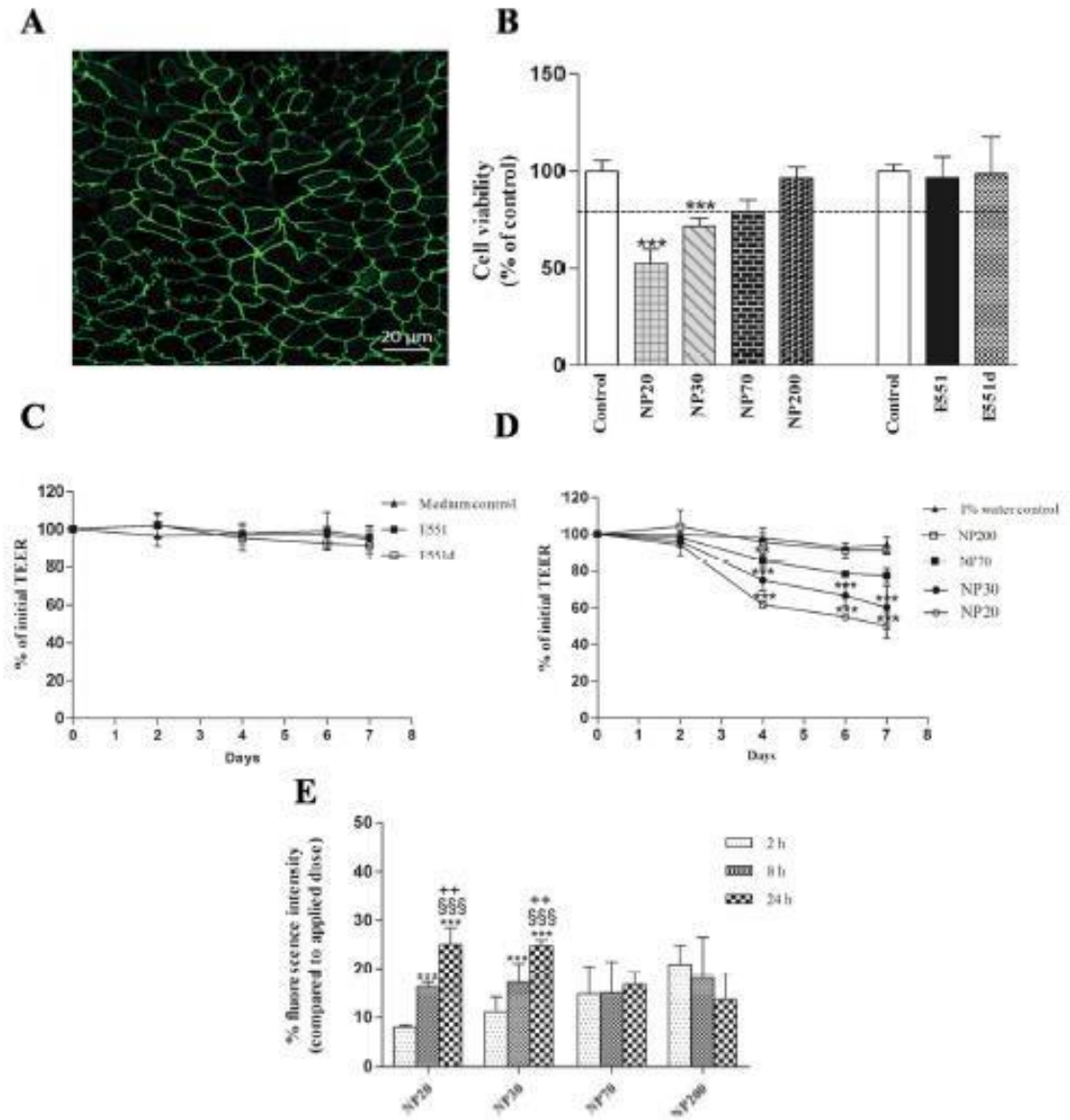


**Figure 6.** (A) ZO-1 immunostaining in the co-culture day 5 (B) Viability of the Caco-2/HT29-MTX co-culture after 7 day-incubation with E551 additives and engineered silica nanoparticles at 1 mg.mL$^{-1}$. Controls were performed in a culture medium. One percent water was added for silica NPs. (C and D) TEER monitoring of the Caco-2/HT29-MTX co-culture during 7 day-exposure to E551 additives and silica NPs, respectively. (E) Accumulation of fluorescent silica NPs in the co-culture. The percentage of fluorescence intensity was obtained after comparison with the applied dose. *2 h compared to 8 and 24 h; §8 h compared to 24 h; +NP70 compared to NP20, NP30 and NP200 after 24 h exposure. Values were reported as mean ± standard deviation ($n = 3$). Statistical analysis was performed using one-way ANOVA followed by a Holm-Sidak test. Results were considered as statistically significant at $P < 0.001$ (***, §§§, +++), $P < 0.01$ (**, §§, ++) and $P < 0.05$ (*, §, +).

endpoints such as ROS and IL-8 productions could be evaluated in a further study for a deeper characterization of the intestinal nanotoxicity. Unlike co-culture, previous results showed NP20 and NP30 were not internalized in the HT29-MTX single culture and did not induce any viability loss. This difference could be attributed to changes in the thickness, the mesh and the dynamic properties of the mucus layer considering the low ratio and the random distribution of HT29-MTX in the co-culture. Another hypothesis could be an alteration of the soluble mucus layer during the renewal of silica NP suspensions every 2 days. No mucus model has been standardized yet (Groo and Lagarce 2014). The origin of mucin is usually different according to the studies. Extraction methods and pretreatments including the drying process can affect the mucus structure. Finally, the thickness of reconstructed

mucus layers in the micrometer range is hard to control.

This study demonstrates the safety of native and digested Emprove® E551. In the light of results obtained with standardized engineered NPs, this could be explained by their mean size of close to 200 nm and their narrow size distribution. From a size of 70 nm, NPs did not cause any toxicity due to their inability to reach the intestinal cells. However, Emprove® E551 is not representative of all the food-grade silicon dioxides currently on the market. Their physicochemical properties are usually dependent on the manufacturing process. Nanosized silica detected in some E551 additives could change their toxicological profile (Barahona et al. 2016). As for NP20 and NP30, the presence of small silica aggregates would then induce a cytoskeleton disruption, altering the intestinal barrier function.

## Conclusion

The physicochemical properties of the Emprove® E551 additive including the surface area and the size were almost preserved after successive incubations in gastric and intestinal fluids. The viability and the integrity of a Caco-2/HT29-MTX co-culture mimicking the human intestinal barrier were not altered after 7 day-exposure to native and digested E551 additive. The safety of silica NPs was closely related to their hydrodynamic diameter. From a size of 70 nm, silica NPs were unable to be internalized in intestinal cells, including Caco-2 as well as HT29-MTX, even after mucus washout. A mucoadhesion process was identified for a great part of applied large NPs. By contrast, silica NPs characterized by a size of 20 and 30 nm induced a tremendous viability loss after exposure to a single culture of Caco-2 and a Caco-2/HT29-MTX co-culture. However, they did not cause cytotoxicity and ROS production after exposure to HT29-MTX. The mucus layer acted as an efficient protective barrier against silica NPs. Unlike the HT29-MTX model, the continuous mucus layer covering the co-culture did not hinder the diffusion of NP20 and NP30. The lower ratio of HT29-MTX related to the small intestine physiology and their random distribution in the co-culture could alter the properties of the mucus barrier. The question arises as to whether the gastrointestinal mucus layer in humans is closer to the co-culture model than the HT29-MTX single culture. However, in light of these results, the value of 70 nm should be considered as a lower size limit for the silica aggregates in the specifications of the E551 additive to limit the interaction with the intestinal cells.

## Acknowledgments

T. Zaiter was supported by a fellowship from the "Centre Islamique d'Orientation et de l'Enseignement Supérieur (CIOES)". The authors thank the cell imaging core facility, DImacell, for the confocal microscopy experiments (Plateforme DImaCell, Univ. Bourgogne Franche-Comté, F-25000 Besançon, France). NM and MH thank the European Union through the PO FEDER-FSE Bourgogne 2014/2020 programs and the EIPHI Graduate School (contract ANR-17-EURE-0002).

## Disclosure statement

There are no conflicts of interest to declare.

## References

Antoine, D., Y. Pellequer, C. Tempesta, S. Lorscheidt, B. Kettel, L. Tamaddon, V. Jannin, F. Demarne, A. Lamprecht, and A. Béduneau. 2015. "Biorelevant Media Resistant co-Culture Model Mimicking Permeability of Human Intestine." *International Journal of Pharmaceutics* 481 (1–2): 27–36. doi:10.1016/j.ijpharm.2015.01.028.

Athinarayanan, J., V. S. Periasamy, M. A. Alsaif, A. A. Al-Warthan, and A. A. Alshatwi. 2014. "Presence of Nanosilica (E551) in Commercial Food Products: TNF-Mediated Oxidative Stress and Altered Cell Cycle Progression in Human Lung Fibroblast Cells." *Cell Biology and Toxicology* 30 (2): 89–100. doi:10.1007/s10565-014-9271-8.

Atuma, C., V. Strugala, A. Allen, and L. Holm. 2001. "The Adherent Gastrointestinal Mucus Gel Layer: Thickness and Physical State in Vivo." *American Journal of Physiology. Gastrointestinal and Liver Physiology* 280 (5): G922–G929. doi:10.1152/ajpgi.2001.280.5.G922.

Bandi, S. P., Y. S. Kumbhar, and V. V. K. Venuganti. 2020. "Effect of Particle Size and Surface Charge of Nanoparticles in Penetration through Intestinal Mucus Barrier." *J. Nanoparticle Res* 22: 62. doi:10.1007/s11051-020-04785-y.

Barahona, F., I. Ojea-Jimenez, O. Geiss, D. Gilliland, and J. Barrero-Moreno. 2016. "Multimethod Approach for the Detection and Characterisation of Food-Grade Synthetic Amorphous Silica Nanoparticles." *Journal of Chromatography. A* 1432: 92–100. doi:10.1016/j.chroma.2015.12.058.

Barker, N., M. van de. Wetering, and H. Clevers. 2008. "The Intestinal Stem Cell." *Genes & Development* 22 (14): 1856–1864. doi:10.1101/gad.1674008.

Béduneau, A., C. Tempesta, S. Fimbel, Y. Pellequer, V. Jannin, F. Demarne, and A. Lamprecht. 2014. "A Tunable Caco-2/HT29-MTX co-Culture Model Mimicking Variable Permeabilities of the Human Intestine Obtained by an Original Seeding Procedure." *European Journal of Pharmaceutics and Biopharmaceutics* 87 (2): 290–298. doi:10.1016/j.ejpb.2014.03.017.

Behrens, I., P. Stenberg, P. Artursson, and T. Kissel. 2001. "Transport of Lipophilic Drug Molecules in a New Mucus-Secreting Cell Culture Model Based on HT29-MTX Cells." *Pharmaceutical Research* 18 (8): 1138–1145. doi:10.1023/A:1010974909998.

Brodkorb, A., L. Egger, M. Alminger, P. Alvito, R. Assunção, S. Ballance, T. Bohn, et al. 2019. "INFOGEST Static in Vitro Simulation of Gastrointestinal Food Digestion." *Nature Protocols* 14 (4): 991–1014. doi:10.1038/s41596-018-0119-1.

Brown, S. S., and J. A. Spudich. 1979. "Cytochalasin Inhibits the Rate of Elongation of Actin Filament Fragments." *The Journal of Cell Biology* 83 (3): 657–662. doi:10.1083/jcb.83.3.657.

Cone, R. A. 2009. "Barrier Properties of Mucus." *Advanced Drug Delivery Reviews* 61 (2): 75–85. doi:10.1016/j.addr.2008.09.008.

Cornu, R., C. Chrétien, Y. Pellequer, H. Martin, and A. Béduneau. 2020. "Small Silica Nanoparticles Transiently Modulate the Intestinal Permeability by Actin Cytoskeleton Disruption in Both Caco-2 and Caco-2/HT29-MTX Models." *Archives of Toxicology* 94 (4): 1191–1202. doi:10.1007/s00204-020-02694-6.

Déciga-Alcaraz, A., N. L. Delgado-Buenrostro, O. Ispanixtlahuatl-Meráz, V. Freyre-Fonseca, J. O. Flores-Flores, A. Ganem-Rondero, F. Vaca-Paniagua, et al. 2020. "Irreversible Disruption of the Cytoskeleton as Induced by Non-Cytotoxic Exposure to Titanium Dioxide Nanoparticles in Lung Epithelial Cells." *Chemico-Biological Interactions* 323: 109063. doi:10.1016/j.cbi.2020.109063.

Dekkers, S., P. Krystek, R. J. B. Peters, D. P. K. Lankveld, B. G. H. Bokkers, P. H. van Hoeven-Arentzen, H. Bouwmeester, and A. G. Oomen. 2011. "Presence and Risks of Nanosilica in Food Products." *Nanotoxicology* 5 (3): 393–405. doi:10.3109/17435390.2010.519836.

Diedrich, T., A. Dybowska, J. Schott, E. Valsami-Jones, and E. H. Oelkers. 2012. "The Dissolution Rates of SiO2 Nanoparticles as a Function of Particle Size." *Environmental Science & Technology* 46 (9): 4909–4915. doi:10.1021/es2045053.

Dong, X., Z. Wu, X. Li, L. Xiao, M. Yang, Y. Li, J. Duan, and Z. Sun. 2020. "The Size-Dependent Cytotoxicity of Amorphous Silica Nanoparticles: A Systematic Review of in Vitro Studies." *International Journal of Nanomedicine* 15: 9089–9113. doi:10.2147/IJN.S276105.

Fruijtier-Pölloth, C. 2016. "The Safety of Nanostructured Synthetic Amorphous Silica (SAS) as a Food Additive (E 551)." *Archives of Toxicology* 90 (12): 2885–2916. doi:10.1007/s00204-016-1850-4.

Gagnon, M., A. Zihler Berner, N. Chervet, C. Chassard, and C. Lacroix. 2013. "Comparison of the Caco-2, HT-29 and the Mucus-Secreting HT29-MTX Intestinal Cell Models to Investigate Salmonella Adhesion and Invasion." *Journal of Microbiological Methods* 94 (3): 274–279. doi:10.1016/j.mimet.2013.06.027.

Gehart, H., and H. Clevers. 2019. "Tales from the Crypt: New Insights into Intestinal Stem Cells." *Nature Reviews. Gastroenterology & Hepatology* 16 (1): 19–34. doi:10.1038/s41575-018-0081-y.

Gehrke, H., A. Frühmesser, J. Pelka, M. Esselen, L. L. Hecht, H. Blank, H. P. Schuchmann, et al. 2013. "In Vitro Toxicity of Amorphous Silica Nanoparticles in Human Colon Carcinoma Cells." *Nanotoxicology* 7 (3): 274–293. doi:10.3109/17435390.2011.652207.

Georgantzopoulou, A., T. Serchi, S. Cambier, C. C. Leclercq, J. Renaut, J. Shao, M. Kruszewski, et al. 2016. "Effects of Silver Nanoparticles and Ions on a co-Culture Model for the Gastrointestinal Epithelium." *Particle and Fibre Toxicology* 13: 9. 10.1186/s12989-016-0117-9.

Gerloff, K., C. Albrecht, A. W. Boots, I. Förster, and R. P. F. Schins. 2009. "Cytotoxicity and Oxidative DNA Damage by Nanoparticles in Human Intestinal Caco-2 Cells." *Nanotoxicology* 3 (4): 355–364. doi:10.3109/17435390903276933.

Gillois, K., C. Stoffels, M. Leveque, I. Fourquaux, J. Blesson, V. Mils, S. Cambier, et al. 2021. "Repeated Exposure of Caco-2 versus Caco-2/HT29-MTX Intestinal Cell Models to (Nano)Silver in Vitro: Comparison of Two Commercially Available Colloidal Silver Products." *The Science of the Total Environment* 754: 142324. doi:10.1016/j.scitotenv.2020.142324.

Gray, C. A., and H. Muranko. 2006. "Studies of Robustness of Industrial Aciniform Aggregates and Agglomerates—Carbon Black and Amorphous Silicas: A Review Amplified by New Data." *Journal of Occupational and Environmental Medicine* 48 (12): 1279–1290. 10.1097/01.jom.0000251477.40643.2a.

Groo, A.-C., and F. Lagarce. 2014. "Mucus Models to Evaluate Nanomedicines for Diffusion." *Drug Discovery Today* 19 (8): 1097–1108. doi:10.1016/j.drudis.2014.01.011.

Hempt, C., J.-P. Kaiser, O. Scholder, T. Buerki-Thurnherr, H. Hofmann, A. Rippl, T. B. Schuster, P. Wick, and C. Hirsch. 2020. "The Impact of Synthetic Amorphous Silica (E 551) on Differentiated Caco-2 Cells, a Model for the Human Intestinal Epithelium." *Toxicology in Vitro: An International Journal Published in Association with BIBRA* 67: 104903. doi:10.1016/j.tiv.2020.104903.

Hendriks, H. G., M. J. Kik, J. F. Koninkx, T. S van den. Ingh, and J. M. Mouwen. 1991. "Binding of Kidney Bean (Phaseolus vulgaris) Isolectins to Differentiated Human Colon Carcinoma Caco-2 Cells and Their Effect on Cellular Metabolism." *Gut* 32 (2): 196–201. doi:10.1136/gut.32.2.196.

Hilgendorf, C., H. Spahn-Langguth, C. G. Regårdh, E. Lipka, G. L. Amidon, and P. Langguth. 2000. "Caco-2 versus Caco-2/HT29-MTX co-Cultured Cell Lines: Permeabilities via Diffusion, Inside- and Outside-Directed Carrier-Mediated Transport." *Journal of Pharmaceutical Sciences*. 89 (1): 63–75. doi:10.1002/(SICI)1520-6017(200001)89:1<63::AID-JPS7>3.0.CO;2-6.

Ispanixtlahuatl-Meráz, O., R. P. F. Schins, and Y. I. Chirino. 2018. "Cell Type Specific Cytoskeleton Disruption Induced by Engineered Nanoparticles." *Environmental Science: Nano* 5 (2): 228–245. doi:10.1039/C7EN00704C.

Le Ferrec, E., C. Chesne, P. Artusson, D. Brayden, G. Fabre, P. Gires, F. Guillou, M. Rousset, W. Rubas, and M. L. Scarino. 2001. "In Vitro Models of the Intestinal Barrier. The Report and Recommendations of ECVAM Workshop 46. European Centre for the Validation of Alternative Methods." *Alternatives to Laboratory Animals* 29 (6): 649–668. doi:10.1177/026119290102900604.

Lehr, C.-M., F. G. J. Poelma, H. E. Junginger, and J. J. Tukker. 1991. "An Estimate of Turnover Time of Intestinal Mucus Gel Layer in the Rat in Situ Loop." *International Journal of Pharmaceutics*. 70 (3): 235–240. doi:10.1016/0378-5173(91)90287-X.

Lesuffleur, T., N. Porchet, J. P. Aubert, D. Swallow, J. R. Gum, Y. S. Kim, F. X. Real, and A. Zweibaum. 1993. "Differential Expression of the Human Mucin Genes MUC1 to MUC5 in Relation to Growth and Differentiation of Different Mucus-Secreting HT-29 Cell Subpopulations." *Journal of Cell Science* 106 (3): 771–783. doi:10.1242/jcs.106.3.771.

Liu, M., J. Zhang, W. Shan, and Y. Huang. 2015. "Developments of Mucus Penetrating Nanoparticles." *Asian Journal of Pharmaceutical Sciences*. 10 (4): 275–282. doi:10.1016/j.ajps.2014.12.007.

MacLean-Fletcher, S., and T. D. Pollard. 1980. "Mechanism of Action of Cytochalasin B on Actin." *Cell* 20 (2): 329–341. doi:10.1016/0092-8674(80)90619-4.

Mahler, G. J., M. L. Shuler, and R. P. Glahn. 2009. "Characterization of Caco-2 and HT29-MTX Cocultures in an in Vitro Digestion/Cell Culture Model Used to Predict Iron Bioavailability." *The Journal of Nutritional Biochemistry* 20 (7): 494–502. doi:10.1016/j.jnutbio.2008.05.006.

Mu, Q., N. S. Hondow, L. Krzemiński, A. P. Brown, L. J. C. Jeuken, and M. N. Routledge. 2012. "Mechanism of Cellular Uptake of Genotoxic Silica Nanoparticles." *Particle and Fibre Toxicology* 9: 29. doi:10.1186/1743-8977-9-29.

Mytych, J., M. Wnuk, and S. I. S. Rattan. 2016. "Low Doses of Nanodiamonds and Silica Nanoparticles Have Beneficial Hormetic Effects in Normal Human Skin Fibroblasts in Culture." *Chemosphere* 148: 307–315. doi:10.1016/j.chemosphere.2016.01.045.

Pearson, J. P., P. I. Chater, and M. D. Wilcox. 2016. "The Properties of the Mucus Barrier, a Unique Gel-How Can Nanoparticles Cross It??" *Therapeutic Delivery* 7 (4): 229–244. doi:10.4155/tde-2015-0002.

Peters, R., E. Kramer, A. G. Oomen, Z. E. Herrera Rivera, G. Oegema, P. C. Tromp, R. Fokkink, et al. 2012. "Presence of Nano-Sized Silica During *in Vitro* Digestion of Foods Containing Silica as a Food Additive." *ACS Nano* 6 (3): 2441–2451. doi:10.1021/nn204728k.

Rodgers, L. S., and A. S. Fanning. 2011. "Regulation of Epithelial Permeability by the Actin Cytoskeleton." *Cytoskeleton* 68 (12): 653–660. doi:10.1002/cm.20547.

Sakuma, S., R. Sudo, N. Suzuki, H. Kikuchi, M. Akashi, and M. Hayashi. 1999. "Mucoadhesion of Polystyrene Nanoparticles Having Surface Hydrophilic Polymeric Chains in the Gastrointestinal Tract." *International Journal of Pharmaceutics* 177 (2): 161–172. doi:10.1016/S0378-5173(98)00346-9.

Shie, M.-Y., S.-J. Ding, and H.-C. Chang. 2011. "The Role of Silicon in Cell Proliferation and Apoptosis." *Acta Biomaterialia*. 7 (6): 2604–2614. doi:10.1016/j.actbio.2011.02.023.

Srinivasan, B., A. R. Kolli, M. B. Esch, H. E. Abaci, M. L. Shuler, and J. J. Hickman. 2015. "TEER Measurement Techniques for in Vitro Barrier Model Systems." *Journal of Laboratory Automation* 20 (2): 107–126. doi:10.1177/2211068214561025.

Sydlik, U., K. Bierhals, M. Soufi, J. Abel, R. P. F. Schins, and K. Unfried. 2006. "Ultrafine Carbon Particles Induce Apoptosis and Proliferation in Rat Lung Epithelial Cells via Specific Signaling Pathways Both Using EGF-R." *American Journal of Physiology. Lung Cellular and Molecular Physiology* 291 (4): L725–L733. doi:10.1152/ajplung.00131.2006.

Tarantini, A., R. Lanceleur, A. Mourot, M.-T. Lavault, G. Casterou, G. Jarry, K. Hogeveen, and V. Fessard. 2015. "Toxicity, Genotoxicity and Proinflammatory Effects of Amorphous Nanosilica in the Human Intestinal Caco-2 Cell Line." *Toxicology in Vitro: An International Journal Published in Association with BIBRA* 29 (2): 398–407. doi:10.1016/j.tiv.2014.10.023.

Ude, V. C., D. M. Brown, K. Maciaszek, V. Stone, and H. J. Johnston. 2019a. "Comparing the Sensitivity of Different Intestinal Caco-2 in Vitro Monocultures and co-Cultures to Amorphous Silicon Dioxide Nanomaterials and the Clay Montmorillonite." *NanoImpact* 15: 100165. doi:10.1016/j.impact.2019.100165.

Ude, V. C., D. M. Brown, V. Stone, and H. J. Johnston. 2019b. "Using 3D Gastrointestinal Tract in Vitro Models with Microfold Cells and Mucus Secreting Ability to Assess the Hazard of Copper Oxide Nanomaterials." *Journal of Nanobiotechnology* 17 (1): 70. 10.1186/s12951-019-0503-1.

Umar, S. 2010. "Intestinal Stem Cells." *Current Gastroenterology Reports* 12 (5): 340–348. doi:10.1007/s11894-010-0130-3.

van Kesteren, P. C. E., F. Cubadda, H. Bouwmeester, J. C. H. van Eijkeren, S. Dekkers, W. H. de Jong, and A. G. Oomen. 2015. "Novel Insights into the Risk Assessment of the Nanomaterial Synthetic Amorphous Silica, Additive E551, in Food." *Nanotoxicology* 9 (4): 442–452. doi:10.3109/17435390.2014.940408.

Wikman-Larhed, A., and P. Artursson. 1995. "Co-Cultures of Human Intestinal Goblet (HT29-H) and Absorptive (Caco-2) Cells for Studies of Drug and Peptide Absorption." *European Journal of Pharmaceutical Sciences*. 3 (3): 171–183. doi:10.1016/0928-0987(95)00007-Z.

Yildiz, H. M., C. A. McKelvey, P. J. Marsac, and R. L. Carrier. 2015. "Size Selectivity of Intestinal Mucus to Diffusing Particulates is Dependent on Surface Chemistry and Exposure to Lipids." *Journal of Drug Targeting* 23 (7–8): 768–774. doi:10.3109/1061186X.2015.1086359.

Yoo, N.-K., Y.-R. Jeon, and S.-J. Choi. 2021. "Determination of Two Differently Manufactured Silicon Dioxide Nanoparticles by Cloud Point Extraction Approach in Intestinal Cells, Intestinal Barriers and Tissues." *International Journal of Molecular Sciences* 22 (13): 7035. doi:10.3390/ijms22137035.

Younes, M., P. Aggett, F. Aguilar, R. Crebelli, B. Dusemund, M. Filipič, M. J. Frutos, et al. 2018. "Re-Evaluation of Silicon Dioxide (E 551) as a Food Additive." *EFSA Journal.* 16 (1): 5088. doi:10.2903/j.efsa.2018.5088.

Zhuravlev, L. T. 2000. "The Surface Chemistry of Amorphous Silica. Zhuravlev Model." *Colloids and Surfaces A: Physicochemical and Engineering Aspects* 173 (1–3): 1–38. doi:10.1016/S0927-7757(00)00556-2.

# 2. LIPID NANOPARTICLES

## 2.1. Context and objectives

Lipid nanoparticles are composed of a solid (SLN) or liquid (NE) lipid core surrounded by an external corona of surfactants including phospholipids and PEGylated lipids. They exhibit numerous advantages as drug delivery systems. Hydrophobic drugs can be solubilized in the lipid core of NPs. The small size of droplets and the presence of surfactants improve the transport of drugs across the biological barriers. High and low energy methods can be used to produce nanoemulsions. High shearing rates are required to reduce the size of oil droplets in the nanometer scale. Another approach consists in the lowering of the tension at the oil/water interface using high quantities of surfactants and co-surfactants. A spontaneous nanoemulsification can then occur. Phase Inversion Temperature (PIT) is an alternative method based on the modification of the hydrophilic-lipophilic balance (HLB) of PEGylated surfactants with the temperature. A hydrophilic surfactant at low temperature becomes hydrophobic during the heating, leading to the inversion of the emulsion from O/W to W/O. This present work evaluates the critical parameters for the preparation of small and stable nanoemulsions containing medium and long chain triglycerides.

## 2.2. Methodology

In our study, the effect of the process temperature on the nanoemulsification of medium and long chain triglycerides (MCT & LCT) was investigated. The impact on the size and the stability of NE of the lipid composition, the molecular weight, and the viscosity of triglycerides as well as the surfactant-to-oil ratio was also studied.

## 2.3. Main Finding/Conclusions

This study showed that:

- A heating at 90°C was required to obtain nanodroplets of LCT while nanoemulsions of MCT were obtained at both 90°C and 37°C
- Due to a low molar volume, the NE of glyceryl trioctanoate (GT) were destabilized by Ostwald ripening unlike lipid mixtures of GT with glyceryl tridecanoate (Labrafac®) or LCT
- Mixtures of LCT and MCT allowed designing stable and fine NEs at 37°C.
- The surfactant-to-oil ratio influences the size of NEs.

## 2.4. Scientific article

Colloids and Surfaces B: Biointerfaces 197 (2021) 111432

Contents lists available at ScienceDirect

Colloids and Surfaces B: Biointerfaces

journal homepage: www.elsevier.com/locate/colsurfb

# Investigation of the spontaneous nanoemulsification process with medium- and long-chain triglycerides

Yasmine Jamoussi [a], Taghrid Zaiter [a], Catherine Desrumaux [b], Niyazi Acar [c], Yann Pellequer [a], Arnaud Béduneau [a,*]

[a] PEPITE EA4267, Labex LipSTIC, Univ. Bourgogne Franche-Comté, F-25000 Besançon, France
[b] Molecular Mechanisms in Neurodegenerative Dementia Laboratory (MMDN), INSERM, U1198, Environmental Impact in Alzheimer's Disease and Related Disorders (EiAlz) Team, 34095 Montpellier, France; University of Montpellier, 34095 Montpellier, France; EPHE, 75014 Paris, France
[c] Centre des Sciences du Goût et de l'Alimentation, AgroSup Dijon, CNRS, INRAE, Université Bourgogne Franche-Comté, Eye and Nutrition Research Group, Dijon, F-21000, France

ARTICLE INFO

*Keywords:*
Nanoemulsions
Triglycerides
Vegetable oils
Low-temperature process
Spontaneous emulsification
Ostwald ripening

ABSTRACT

Oil-in-water nanoemulsions are used in numerous biomedical applications as delivery systems. The droplet size in the nanometer range and their composition were extensively developed for carrying and enhancing the absorption of lipophilic drugs and lipids of interest. In the present study, critical parameters involved in the spontaneous nanoemulsification process such as the temperature, the oil type, the surfactant-to-oil and water-to-oil ratios were investigated. The aim was to design a solvent-free procedure for the spontaneous nanoemulsification at a low temperature of a large variety of triglycerides including vegetable oils. Nanoemulsification of medium-chain triglyceride (MCT) was not dependent on the temperature while nanodroplets of long-chain triglycerides (LCT) were only obtained by reaching the cloud point of ethoxylated surfactant Kolliphor® HS15. The molar volume of triglycerides was considered as a predictive parameter governing both, the spontaneous nanoemulsification at low temperature and the Ostwald ripening rate. The physical mixture of MCT and LCT was a promising strategy to prepare stable and fine nanoemulsions at 37 °C. They were characterized by a hydrodynamic diameter comprised between 20 and 30 nm and a narrow size distribution. These findings pave the way to new applications for the parenteral nutrition and the delivery of thermosensitive drugs and lipophilic molecules such as antioxidants.

## 1. Introduction

Water-in-oil nanoemulsions are colloidal lipid systems characterized with sizes below 200 nm [1]. Preparation processes are classified according to the energy required to reduce the size of oil droplets. High-energy methods including homogenizers and microfluidic devices generate high shear rates to expand the surface of oil droplets in water. Low-energy processes include phase inversion temperature methods (PIT) and spontaneous emulsification termed in some applications self-emulsifying methods. Then PIT method was first investigated by Shinoda et al. [2]. It consists in heating the preparation at temperatures above the PIT to convert an oil/water emulsion to a water/oil emulsion passing through a bicontinuous phase. A rapid dilution is then performed, leading to the formation of nanodroplets. The mechanism is based on the temperature-dependent solubility of ethoxylated surfactants in oil and water. The PIT corresponds to an equal solubility of surfactant for water and oil. The spontaneous emulsification or self-emulsifying methods is a low-energy method, allowing the rapid formation of oil droplets in the nanometer range. The organic phase is usually composed of oil, surfactant and water-miscible solvent termed co-solvent such as acetone and ethanol [3]. Various mechanisms were suggested to explain the nanoemulsion formation after mixing of two immiscible phases ; (a) organic phase diffusion in water [4]; (b) surfactant migration from the organic phase to the oil/water interface [5]; (c) water transfer in the organic phase leading to the surfactant solubilization and the fragmentation of the oil phase [6]. Besides the ease of preparation process, another advantage is the possibility to produce a nanoemulsion directly in the body after contact of the lipid phase with biologic fluids [7].

Nanoemulsions were widely used in biomedical applications. They

* Corresponding author.
*E-mail address:* arnaud.beduneau@univ-fcomte.fr (A. Béduneau).

https://doi.org/10.1016/j.colsurfb.2020.111432
Received 6 July 2020; Received in revised form 9 October 2020; Accepted 20 October 2020
Available online 27 October 2020

can deliver class II drugs according to the biopharmaceutical classification characterized by a poor water solubility. Class IV drugs were also loaded in nanoemulsions due to their ability to cross epithelia such as the intestinal barrier [8,9]. In addition to the size in the nanometer range, drug absorption is promoted by the presence of surfactants which can modulate the efflux transporters [10]. Antioxidant agents including curcumin, α-tocopherol, and polyunsaturated lipids were loaded in nanoemulsions [11]. Nanoemulsions composed of lipid mixtures were also developed for the parenteral nutrition. Within them, Lipidem® is composed of medium chain triglycerides (MCT), omega 3 polyunsaturated fatty acids and soybean triglycerides [12].

Despite the extensive studies dedicated to nanoemulsions, their development faced numerous problems. Firstly, high temperatures required for the PIT method [13] or resulting from the mechanical energy dissipation in high-energy processes can alter the chemical stability of drugs and lipophilic molecules such as antioxidants. Secondly, large quantities of co-solvents such as acetone and ethanol are often necessary to reduce the size of oil droplets in spontaneous emulsification methods [3]. They can be responsible for adverse effects, especially in *in situ* emulsification strategies such as oral lipid-based delivery systems where they cannot be removed [14]. In addition, co-solvent diffusion in water can trigger drug precipitation [7]. Third, the choice of excipients, and especially oils and surfactants, is often limited in low-energy processes [4], reducing the applications of nanoemulsions to lipid and drug delivery systems [15,16]. The last point concerns the long-term stability of nanoemulsions that represents a real challenge. The Ostwald ripening (OR) is the main mechanism responsible for the destabilization of nanoemulsions due to Laplace pressure differences between small and large droplets [1]. It consists in the migration of individual oil molecules from small to larger droplets by diffusion through the continuous aqueous phase. OR rate depends on the size distribution of droplets and the nature of the oil and can be affected by the presence of micelles in the continuous phase [17–19].

In the present study, the influence of the process temperature and of material attributes on the size and the stability of oil/water nanoemulsions was investigated. The aim was to design a low temperature nanoemulsification process without organic water-miscible solvent, allowing the delivery of a wide variety of triglycerides including MCT and long-chain triglycerides (LCT) as well as thermosensitive drugs and lipophilic molecules.

## 2. Materials and methods

### 2.1. Materials

Glyceryl trioleate (96 %) was provided by Santa Cruz Biotechnology (Heidelberg, Germany). Glyceryl trioctanoate (99 %), corn oil, olive oil and Kolliphor® HS15 (macrogol 15 hydroxystearate) were supplied by Sigma-Aldrich (Saint Quentin Fallavier, France). Labrafac WL 1349 was a gift of Gattefossé SAS (Saint Priest, France).

### 2.2. Nanoemulsion preparation

Lipid phase consisted of a mixture of Kolliphor® HS15 (Macrogol 15 hydroxystearate) with different oils including Labrafac WL 1349, vegetable oils, glyceryl trioctanoate or glyceryl trioleate (Table 1). Oils were composed mainly of triglycerides with different fatty chain lengths (Table 1). The surfactant-to-oil ratio (SOR) ranged from 1 to 6. Lipid phase and deionized water were separately heated under magnetic stirring in a water bath at equal temperatures comprised between 37 °C and 90 °C during 10 min. Water was then rapidly added in the lipid phase using a syringe at a water-to-oil ratio (WOR) ranging from 5 to 100. The two immiscible phases were magnetically stirred in the water bath at the target temperature for 5 min. The preparation was then removed from the water bath and stirred at room temperature for 15 min. Approximately 7.5 g of emulsion were prepared for each batch.

**Table 1**
Description of the oils used for the preparation of nanoemulsions.

| Oil | Composition | Density | Mw | Viscosity at 25°C (mPa.s) |
|---|---|---|---|---|
| Corn oil (CO) | C18:1 (29 %); C18:2 (56 %) | 0.9 | – | 54.0 ± 0.5 |
| Glyceryl trioctanoate (GT) | C8:0 (99 %) | 0.956 | 470.7 | 21.6 ± 0.0 |
| Glyceryl trioleate (GTOL) | C18:1 (96 %) | 0.915 | 885.4 | 65.6 ± 1.1 |
| Labrafac WL 1349 (Labrafac) | C8:0 (56 %); C10:0 (43 %) | 0.946 | 506.2 | 25.4 ± 0.2 |
| Olive oil (OO) | C18:1 (61 %); C18:0 (18 %) | 0.912 | – | 67.5 ± 0.1 |

### 2.3. Particle size measurements

The hydrodynamic and the polydispersity index (PDI) of emulsions were determined by dynamic light scattering using a Zetasizer Nano ZS 90, (Malvern Instruments, Orsay, France). The apparatus was equipped of a 4-mW HeNe laser at a wavelength of 632.8 nm. Light scattering was detected at an angle of 90°. The temperature was fixed at 25 °C. All measurements were performed in triplicate after a 1:10 dilution in deionized water.

### 2.4. Viscosity measurements

Viscosity of oils was measured using a Kinexus Pro rheometer in controlled shear mode (Malvern Instruments, Orsay, France). Measuring systems were composed of a cone with a 2° angle and a 50 mm diameter plate. Temperature was controlled using a Peltier system. A solvent trap device was used during the heating process. The apparent shear viscosity was measured at temperatures ranging from 25 °C to 90 °C using a steady state flow process at a shear rate of 100 $s^{-1}$. At least two independent measurements were performed for each type of oil.

## 3. Results and discussion

### 3.1. Influence of temperature

The nanoemulsification process was performed at 37 °C using MCT such as glyceryl trioctanoate, Labrafac WL 1349 and LCT including corn oil, olive oil and glyceryl trioleate. They were selected for their low melting point, allowing the synthesis of nanodroplets with a liquid lipid core. The surfactant-to-oil ratio (SOR) and the water-to-oil ratio (WOR) were first fixed at 3.5 and 22, respectively. In Fig. 1, only small nanodroplets were obtained with glyceryl trioctanoate and Labrafac WL 1349 with sizes below 25 nm and a polydispersity index (PDI) close to 0.1, demonstrating a monomodal distribution. This was consistent with the study of Lefevre et al. which demonstrated the spontaneous nanoemulsification of Labrafac at 30 °C and 50 °C [5]. For glyceryl trioleate, corn and olive oils, sizes and PDI were much larger than 100 nm and 0.1, respectively. These data demonstrate that the nanoemulsification process is clearly dependent on the type of oil, especially the hydrocarbon chain length. The glyceryl trioctanoate and the Labrafac are composed of fatty acids with a carbon chain length $\leq 10$ whereas LCT contain C18 fatty acids.

The emulsification mechanism could be affected by physicochemical properties of triglycerides such as the viscosity and the tension at the oil/water interface. However, literature showed interfacial tension of vegetable oils and MCT in water were within the same range, comprised between 23 and 25 $mN.m^{-1}$ [20]. Thus, the influence in this parameter was not investigated in the present study. Wooster et al. demonstrated that the oil viscosity plays a major role in the size of droplets. Heighty nm and 120 nm nanoemulsions were obtained with hexadecane and LCT, respectively [21]. Viscosities of triglycerides and lipid mixtures

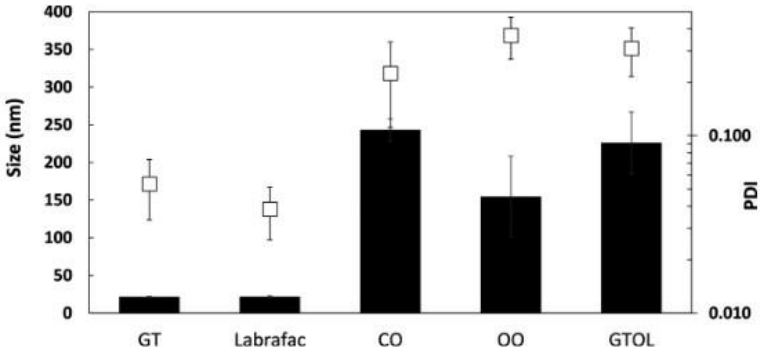


**Fig. 1.** Influence of the oil type on the size (black bars) and the PDI (open squares) of nanoemulsions prepared at 37 °C with a SOR and a WOR of 3.5 and 22, respectively. Formulations were prepared with glyceryl trioctanoate (GT), Labrafac WL 1349 (Labrafac), corn oil (CO), olive oil (OO) and glyceryl trioleate (GTOL). Results are expressed as mean values ± SD. Measurements were performed in triplicate from at least three independent experiments.

were measured at a shear rate of 100 $s^{-1}$. In Fig. 2, viscosity values of glyceryl trioctanoate and Labrafac at 37 °C were respectively of 13.2 and 15.8 mPa.s whereas the values were of 34.8 and 41.7 mPa.s for corn and olive oils, respectively. Heating process decreased drastically the viscosity of oils. At 70 °C, corn oil and olive oils reached values of 13 and 14.6 mPa.s, in the same range as glyceryl trioctanoate and Labrafac at 37 °C.

To investigate the role of viscosity, nanoemulsification of LCT was performed at temperatures higher than 37 °C such as 50 °C, 70 °C and 90 °C (Fig. 3). Nanodroplets with diameters of approximately 25 nm were only obtained at 90 °C for all the triglycerides. Between 37 °C and 70 °C, no clear evidence of a temperature-dependent effect was observed on the size of nanoemulsions. The polydispersity indexes were above 0.1, suggesting a heterogeneous size distribution. Despite the viscosity drop during the heating and values close to MCT at 70 °C, the heating did not significantly reduce the size of nanodroplets except at 90 °C. This result suggests the lack of relationship between the viscosity of oils and the size of nanoemulsions for the spontaneous nanoemulsification.

Besides the viscosity of triglycerides, temperature variations affect also the partition coefficient of ethoxylated surfactants in oil and water [22]. It was reported that temperature increase drastically reduces the aqueous solubility of nonionic surfactant [23]. The cloud point of macrogol 15 hydroxystearate in pure water was observed at a temperature of 85 °C [24]. By considering the correlation between the PIT and the cloud point demonstrated by Shinoda et al. [25], it could be reasonably assumed that the heating at 90 °C with LCT allowed reaching the PIT corresponding to an equal solubility of surfactant in oil and water and the formation of a bicontinuous system [26,27]. However, conductimetry measurements performed during the heating did not demonstrate a phase inversion likely due to the high water-to-oil ratio of 22:1.

In the case of MCT, the spontaneous emulsification did not require reaching the PIT. As discussed previously, the interfacial tension and the viscosity does not justify this difference. In presence of organic water-miscible solvent, spontaneous emulsification is usually reported as a diffusion driven process [28]. Due to the lack of co-solvent in our preparations, emulsification could be explained by the rapid diffusion of MCT in the aqueous phase. MCT are well known to be more soluble than LCT due shorter fatty acid chains [29]. Their solubility could be also improved by the presence of Kolliphor® HS15. Taylor et al. showed that the diffusion coefficient D of oil molecules including alkanes was calculated according to the following equation [30]:

$$D = 7.4 \times 10^{-12} \times \frac{(\Phi_s m_1)^{0.5} T}{\eta_1 V_2^{0.6}} \quad (1)$$

$m_1$ and $\eta_1$ are defined as the molar mass (g/mol) and the viscosity (mPa.s) of the solvent. $V_2$ is the molar volume of the diffusate ($cm^3$/mol) and is calculated by dividing the molar mass by the mass density. Φs is the association factor of the solvent allowing molecule interactions such as

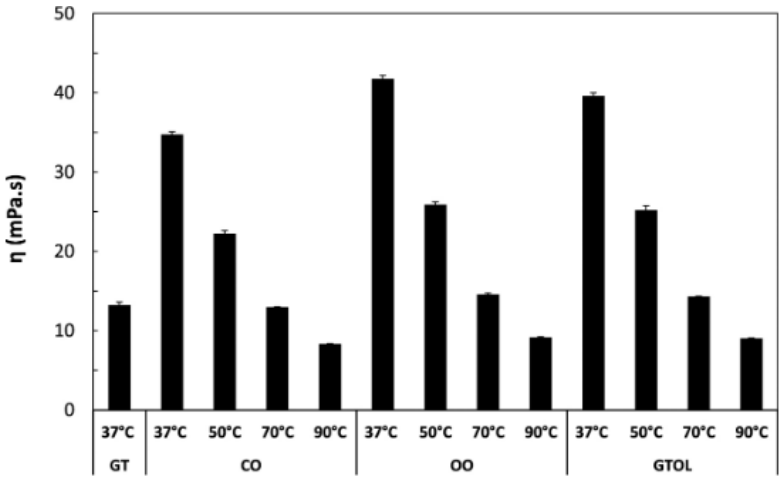


**Fig. 2.** Influence of the temperature on the viscosity of different oils including glyceryl trioctanoate (GT), corn oil (CO), olive oil (OO) and Glyceryl trioleate (GTOL) at a shear rate of 100 $s^{-1}$. Results are expressed as mean values ± SD. Measurements were performed in triplicate from at least two independent experiments.

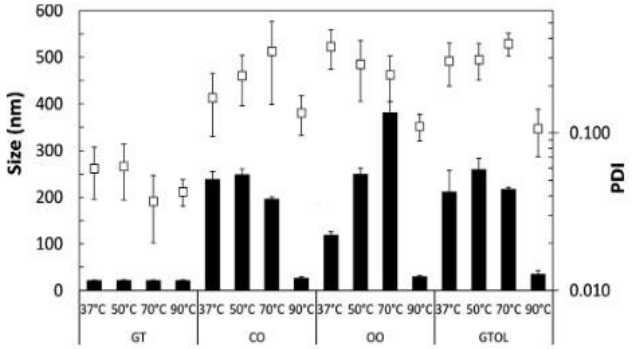


**Fig. 3.** Influence of the process temperature on the size (black bars) and the PDI (open squares) of nanoemulsions prepared with glyceryl trioctanoate (GT), corn oil (CO), olive oil (OO) and glyceryl trioleate (GTOL). Results are expressed as mean values ± SD. Measurements were performed in triplicate from at least two independent experiments.

hydrogen bonds. According to Eq. 1, the molar volume (Vm) would be the main intrinsic property of the oil phase which controls the diffusion coefficient in the water bulk phase. Considering the narrow density range of triglycerides (0.9–0.95), Vm could be also associated to the water solubility of MCT and LCT which depends of the length of fatty acids and consequently of the molecular weight [29]. This was in agreement with Wooster et al. who stated that the water solubility of an oil is inversely proportional to Vm [21]. By predicting both the aqueous solubility and the diffusion coefficient in water, the molar volume of triglycerides could be a critical parameter for the spontaneous nanoemulsification. This would explain the spontaneous nanoemulsification at 37 °C of glyceryl trioctanoate characterized a Vm of 492 $cm^3$/mol unlike glyceryl trioleate exhibiting a value of 968 $cm^3$/mol. Vm was not calculated for vegetable oils due to their complex composition. However, considering the high proportion of triglycerides in vegetable oils and by taking into account the preponderant C18 fatty acids, the value should be in the same range as that of glyceryl trioleate [31]. Thus, the higher water solubility and diffusion coefficient of MCT suggested by their low Vm compared to LCT could explain their spontaneous and rapid dispersion into nanodroplets at 37 °C.

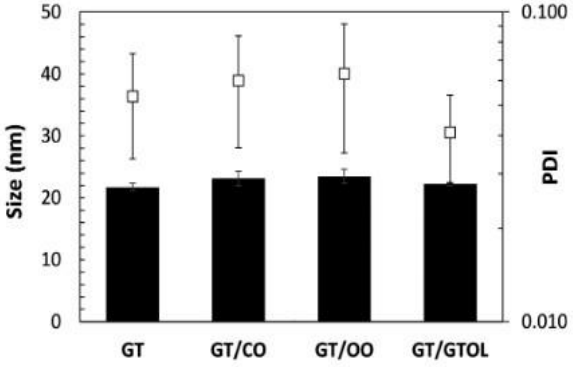


**Fig. 4.** Influence of the LCT/LGT mixture on the size (black bars) and PDI (open squares) of nanoemulsions prepared at 37 °C with a SOR of 3.5 and WOR of 22. Glyceryl trioctanoate was mixed at ratio 1:1 with corn oil (GT/CO), olive oil (GT/OO) and glyceryl trioleate (GT/GTOL). Results are expressed as mean values ± SD. Results were compared with pure glyceryl trioctanoate (GT). Measurements were performed in triplicate from at least three independent experiments.

### 3.2. Influence of the lipid composition

The high temperature required for the spontaneous nanoemulsification of long chain triglycerides could affect the chemical stability of lipids, and especially hat of unsaturated fatty acids. To facilitate the oil diffusion during the spontaneous emulsification at lower temperatures, water-miscible organic solvents termed as co-solvents such as acetone and ethanol are usually added in the lipid phase [3]. Our previous results demonstrated that MCT can diffuse easily in the external water phase and then could play the role of a co-solvent. To investigate their interest in the nanoemulsification process, glyceryl trioctanoate was added with LCT including glyceryl trioleate, olive and corn oils and at a ratio 1:1 (Fig. 4). SOR and WOR were first at 3.5 and approximately 22, respectively. Nanoemulsification process was performed at 37 °C. Interestingly, oil nanodroplets with a size below 25 nm were obtained for the 3 lipids mixtures. In addition, the polydispersity index was inferior to 0.1, suggesting the formation of a single population of nanodroplets.

### 3.3. Influence of SOR and WOR

To investigate the effect of the surfactant concentration on the size and the polydispersity of nanodroplets, nanoemulsions with different SOR comprised between 6 and 1 were prepared. Process temperature was 37 °C and WOR was fixed at 22. Nanoemulsions were prepared with different oil types including glyceryl trioctanoate, Labrafac, corn oils and a GT/CO mixture at a ratio 1:1. In Fig. 5A and B, nanoemulsions prepared at a SOR 6 were characterized by a size close to 20 nm for every oil type and a PDI close to 0.1. Interestingly, no heating was then necessary for the preparation of oil corn nanoemulsions at that SOR value. This could be due to the oil solubilization in Kolliphor® HS15 micelles. At a SOR 5, corn oil droplets reached a size of 173 nm and a PDI of 0.3. Regarding MCT and the mixture GT/CO, no significant size increase was observed for SOR comprised between 6 and 3. Hydrodynamic diameters was still below 30 nm and PDI close to 0.1. The size of the emulsion prepared with the lipid mixture increased drastically from a SOR of 2, reaching 70 nm. The PDI of 0.370 suggested a multimodal distribution. The same behavior was observed with MCT. Both size and PDI increases were observed between SOR 2 and 1. At SOR 1, sizes were approximately of 90 nm and the PDI above 0.3. This was consistent with the work of Lefebvre et al. showing a significant influence of SOR on the size and the polydispersity of nanoemulsions prepared with Labrafac [5]. Influence of WOR on the size of nanoemulsions prepared at 37 °C and composed of glyceryl trioctanoate alone or with corn oil were also investigated (Fig. 6). WOR comprised between 5 and 100 did not affect significantly the size of droplets with values close to 22 nm for MCT and between 24 nm and 22 nm for the triglyceride mixture. PDI was inferior to 0.1 except for the nanoemulsions prepared with the GT/CO mixture at a WOR 5. Nevertheless, the value was of 0.178, suggesting a narrow size distribution. In addition, the way to add together the two immiscible phases did not change the nanoemulsion properties. A size close to 20 nm and a monomodal size distribution were obtained after addition at

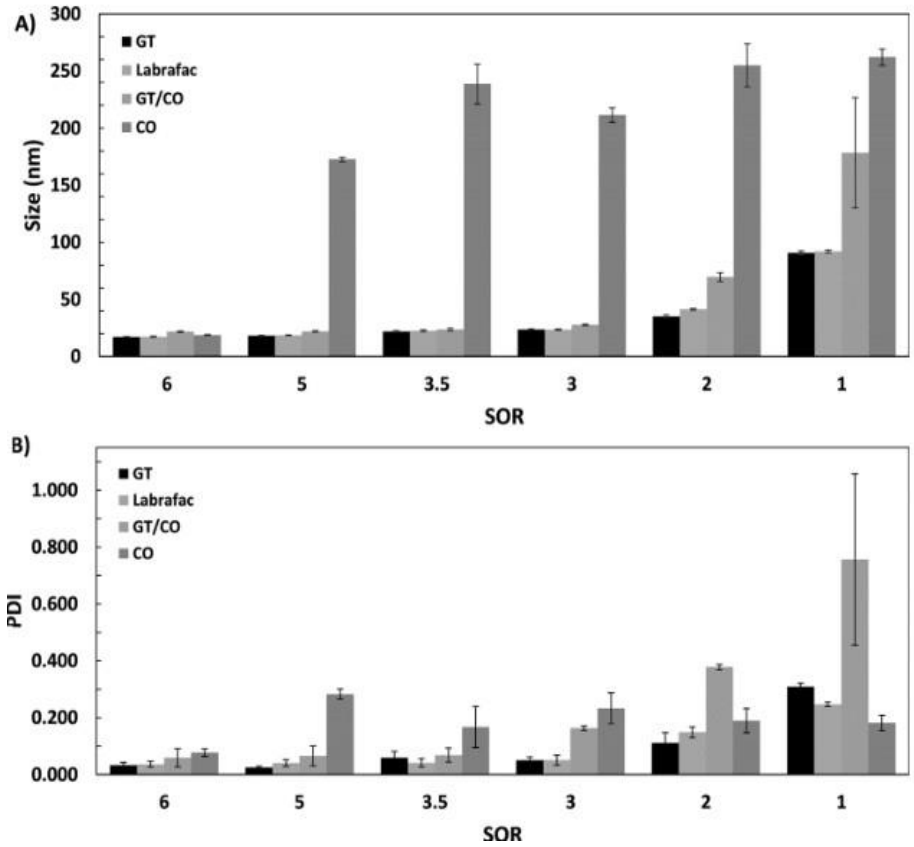


**Fig. 5.** Influence of surfactant-to-oil ratio on the nanoemulsification of glyceryl trioctanoate (GT), Labrafac WL 1349 (Labrafac) and 1:1 lipid mixtures composed of GT with corn oil (GT/CO) or olive oil (GT/OO). Preparations were performed at 37 °C and the water-to-oil ratio was fixed at 22. A: hydrodynamic diameters of oil droplets as a function of the SOR. B: PDI of nanoemulsions as a function of the SOR. Results are expressed as mean values ± SD. Measurements were performed in triplicate from at least two independent experiments.

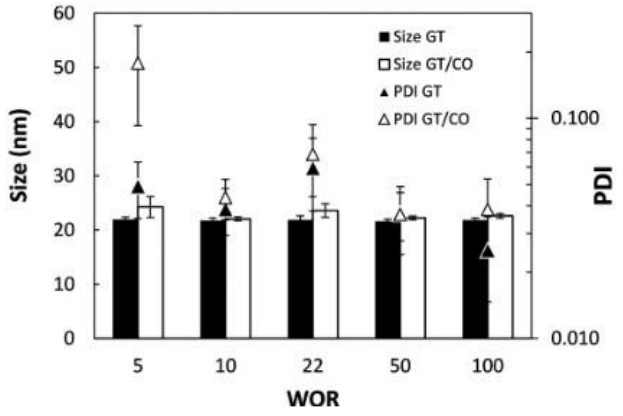


**Fig. 6.** Influence of water-to-oil ratio (WOR) on the size and the PDI of nanoemulsions prepared at 37 °C. SOR was fixed at 3.5. Lipid phase was composed of glyceryl trioctanoate (GT) or of a 1:1 mixture of GT and corn oil (GT/CO). Results are expressed as mean values ± SD. Measurements were performed in triplicate from at least two independent experiments.

37 °C of lipid phases composed of GT and a GT/CO mixture in water. This data appears as very interesting for the preparation of nanoemulsion after dilution in the biologic fluids.

### 3.4. Stability

The stability of nanoemulsions stored at 4 °C was evaluated over time (Fig. 7A-C). Except for pure glyceryl trioctanoate nanoemulsions, lipid mixtures, Labrafac and LCT were stable during 90 days. No significant size increase was observed and PDI stayed close to 0.1, suggesting a monomodal size distribution. Regarding GT nanoemulsions, no significant size increase was observed within the first days followed by a rapid growth of oil droplets. After the lag-phase, the cube of droplet radius increased linearly with time, suggesting a destabilization mechanism governed by the Ostwald ripening. This was confirmed by the PDI values, which increased at the beginning of the destabilization kinetic to finally drop to values inferior to 0.2, corresponding to the end of the droplet growth. Although it was reported that surfactant can increase the Ostwald ripening rate due to the oil solubilization in micelles [18], a retardation of the Ostwald ripening was also observed by Weiss et al. for high concentrations of non-ionic surfactants (above 10 %) [19]. This could be due to the high ability of micelles to solubilize large quantities of oil. Besides, according to the theory of Lifshitz, Slyozov and Wagner termed the LSW theory, the OR rate increases with the diffusion coefficient and the bulk solubility of the oil, and consequently could be also correlated to Vm [17,32]. It would explain the rapid destabilization of nanoemulsions containing the GT that is characterized by the lowest Vm among the studied triglycerides including MCT and LCT. This hypothesis was supported by a study showing that glyceryl trioctanoate and mygliol, a MCT composed of a mixture of C8 and C10 fatty acids chains were characterized by an OR rate of 0.345 and 0.0483 $nm^3/s$, respectively for Vm of 508 and 614 $cm^3/mol$ [21]. In the same article, no Ostwald ripening was observed over 3 months with peanut oils composed of long fatty acid chains (> C18). Unlike GT, stability of Labrafac nanoemulsions could be explained by the presence of 43 % of C10 fatty acids with 56 % of C8. Thus, the molar volume of Labrafac equal to 535 $cm^3/mol$ could be considered as a target value allowing both the spontaneous emulsification and the stability. Interestingly, the mixture of LCT with GT at a ratio 1/1 were still stable after 90 days. Higushi et al. demonstrated that the addition of insoluble oils enhances nanoemulsion stability by reducing the Ostwald ripening rate [33]. From a molar fraction of insoluble oil equal to 0.4, nanoemulsions composed of glyceryl trioctanoate and peanut oil were

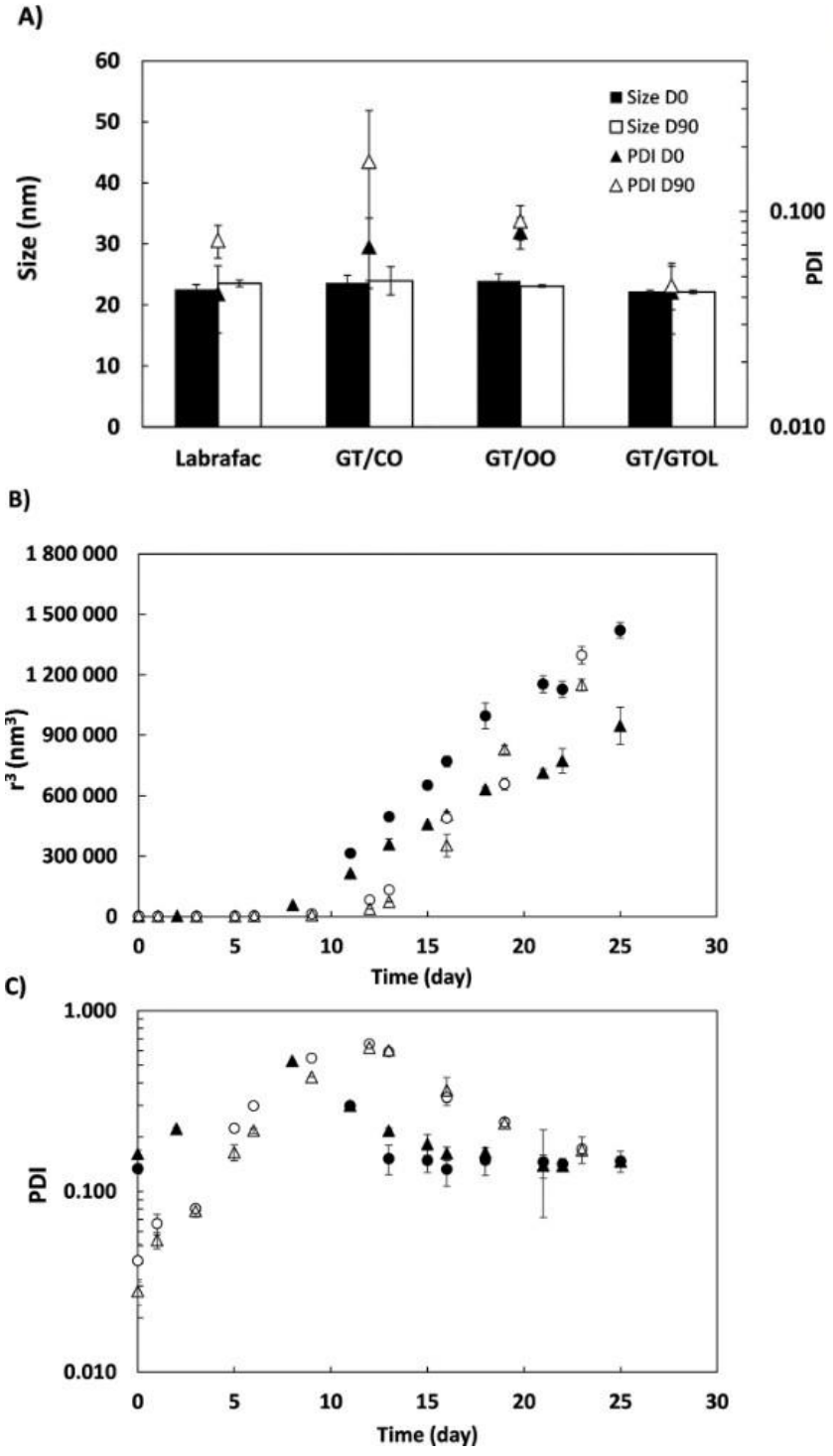


**Fig. 7.** Stability of nanoemulsions prepared at 37 °C with a SOR and a WOR of 3.5 and 22, respectively. A: Long-term stability of nanoemulsions composed of Labrafac and of 1:1 mixtures of glyceryl trioctanoate with corn oil (GT/CO), olive oil (GT/OO) and glyceryl trioctanoate (GT/GTOL). Size and PDI were measured immediately after preparation (D0) and after 90 days of storage at 4 °C (D90). Results are expressed as mean values ± SD. Measurements were performed in triplicate from at least two independent experiments. B: Cube of hydrodynamic radius of four batches of glyceryl trioctanoate nanoemulsion as a function of time. C: PDI of four batches of glyceryl trioctanoate nanoemulsion as a function of time. Results are expressed as mean values ± SD. Measurements were performed in triplicate.

stable over time [21]. This was explained by the entropy of mixing that dominates the Laplace pressure. This result demonstrates also that lipids droplets were composed of both MCT and LCT, since otherwise a destabilization would have been observed for droplet population composed of glyceryl trioctanoate. Thus, the LCT addition to glyceryl trioctanoate represents an interesting strategy to improve the physical stability of nanodroplets by limiting the Ostwald ripening rate.

## 4. Conclusion

This study emphasizes the major role of the oil type in the spontaneous nanoemulsification process. The molar volume of triglycerides represents a predictive factor for both the final size, the polydispersity and the stability of the emulsions prepared at a low temperature. Vm is correlated to the water solubility and the diffusion coefficient of oils molecules. Glyceryl trioctanoate characterized by a low Vm value facilitated both the spontaneous emulsification and the Ostwald

ripening. Nanoemulsification at 37 °C failed with vegetable oils due to long hydrocarbon chains (C18) which limits their diffusion in the continuous aqueous phase. Heating above the PIT was required to obtain LCT nanodroplets. Both stable and monodisperse nanoemulsions were obtained with Labrafac characterized by a Vm value of 535 $cm^3$/mol. Mixture of LCT with glyceryl trioctanoate allowed designing stable, fine and monodisperse nanoemulsions. This represents a promising approach to enlarge the variety of triglycerides in spontaneous emulsification processes at low temperature and without organic water-soluble solvent. This investigation paves the way to new strategies for the delivery of thermosensitive drugs and lipids such as polyunsaturated LCT.

## CRediT authorship contribution statement

**Yasmine Jamoussi:** Investigation, Formal analysis, Writing - original draft. **Taghrid Zaiter:** Investigation. **Catherine Desrumaux:** Funding acquisition, Writing - review & editing. **Niyazi Acar:** Funding acquisition, Writing - review & editing. **Yann Pellequer:** Resources, Writing - review & editing. **Arnaud Béduneau:** Supervision, Conceptualization, Methodology, Writing - original draft.

## Declaration of Competing Interest

The authors report no declarations of interest.

## Acknowledgments

This work was supported by grants from the Agence Nationale de la Recherche [ANR-11-LABEX-0021], the Conseil Régional Bourgogne, Franche-Comte (PARI grant), the FEDER (European Funding for Regional Economical Development) and the Fondation de France/Fondation de l'œil.

## References

[1] C. Solans, P. Izquierdo, J. Nolla, N. Azemar, M.J. Garcia-Celma, Nano-emulsions, Curr. Opin. Colloid Interface Sci. 10 (3) (2005) 102–110, https://doi.org/10.1016/j.cocis.2005.06.004.

[2] K. Shinoda, H. Saito, The effect of temperature on the phase equilibria and the types of dispersions of the ternary system composed of water, cyclohexane, and nonionic surfactant, J. Colloid Interface Sci. 26 (1) (1968) 70–74, https://doi.org/10.1016/0021-9797(68)90273-7.

[3] K. Bouchemal, S. Briançon, E. Perrier, H. Fessi, Nano-emulsion formulation using spontaneous emulsification: solvent, oil and surfactant optimisation, Int. J. Pharm. 280 (1–2) (2004) 241–251, https://doi.org/10.1016/j.ijpharm.2004.05.016.

[4] Y. Singh, et al., Nanoemulsion: concepts, development and applications in drug delivery, J. Control. Release Off. J. Control. Release Soc. 252 (2017) 28–49, https://doi.org/10.1016/j.jconrel.2017.03.008.

[5] G. Lefebvre, et al., Spontaneous nano-emulsification: process optimization and modeling for the prediction of the nanoemulsion's size and polydispersity, Int. J. Pharm. 534 (1–2) (2017) 220–228, https://doi.org/10.1016/j.ijpharm.2017.10.017.

[6] N. Anton, P. Saulnier, Adhesive water-in-oil nano-emulsions generated by the phase inversion temperature method, Soft Matter 9 (28) (2013) 6465–6474, https://doi.org/10.1039/C3SM51064F.

[7] C.W. Pouton, C.J.H. Porter, Formulation of lipid-based delivery systems for oral administration: materials, methods and strategies, Adv. Drug Deliv. Rev. 60 (6) (2008) 625–637, https://doi.org/10.1016/j.addr.2007.10.010.

[8] S. Peltier, J.-M. Oger, F. Lagarce, W. Couet, J.-P. Benoît, Enhanced oral paclitaxel bioavailability after administration of paclitaxel-loaded lipid nanocapsules, Pharm. Res. 23 (6) (2006) 1243–1250, https://doi.org/10.1007/s11095-006-0022-2.

[9] E. Roger, F. Lagarce, E. Garcion, J.-P. Benoit, Lipid nanocarriers improve paclitaxel transport throughout human intestinal epithelial cells by using vesicle-mediated transcytosis, J. Control. Release Off. J. Control. Release Soc. 140 (2) (2009) 174–181, https://doi.org/10.1016/j.jconrel.2009.08.010.

[10] R. Nieto Montesinos, A. Béduneau, Y. Pellequer, A. Lamprecht, Delivery of P-glycoprotein substrates using chemosensitizers and nanotechnology for selective and efficient therapeutic outcomes, J. Control. Release Off. J. Control. Release Soc. 161 (1) (2012) 50–61, https://doi.org/10.1016/j.jconrel.2012.04.034.

[11] D.H. Lohith Kumar, P. Sarkar, Encapsulation of bioactive compounds using nanoemulsions, Environ. Chem. Lett. 16 (1) (2018) 59–70, https://doi.org/10.1007/s10311-017-0663-x.

[12] S. Klek, et al., Home parenteral nutrition with an omega-3-fatty-acid-enriched MCT/LCT lipid emulsion in patients with chronic intestinal failure (the HOME study): study protocol for a randomized, controlled, multicenter, international clinical trial, Trials 20 (2019), https://doi.org/10.1186/s13063-019-3994-z.

[13] N. Anton, P. Gayet, J.-P. Benoit, P. Saulnier, Nano-emulsions and nanocapsules by the PIT method: an investigation on the role of the temperature cycling on the emulsion phase inversion, Int. J. Pharm. 344 (1) (2007) 44–52, https://doi.org/10.1016/j.ijpharm.2007.04.027.

[14] D.J. McClements, J. Rao, Food-grade nanoemulsions: formulation, fabrication, properties, performance, biological fate, and potential toxicity, Crit. Rev. Food Sci. Nutr. 51 (4) (2011) 285–330, https://doi.org/10.1080/10408398.2011.559558.

[15] J. Baloch, et al., Self-nanoemulsifying drug delivery system (SNEDDS) for improved oral bioavailability of chlorpromazine: in vitro and in vivo evaluation, Medicina (Mex.) 55 (5) (2019), https://doi.org/10.3390/medicina55050210.

[16] K. Hörmann, A. Zimmer, Drug delivery and drug targeting with parenteral lipid nanoemulsions - A review, J. Control. Release Off. J. Control. Release Soc. 223 (2016) 85–98, https://doi.org/10.1016/j.jconrel.2015.12.016.

[17] A.S. Kabalnov, K.N. Makarov, A.V. Pertzov, E.D. Shchukin, Ostwald ripening in emulsions: 2. Ostwald ripening in hydrocarbon emulsions: experimental verification of equation for absolute rates, J. Colloid Interface Sci. 138 (1) (1990) 98–104, https://doi.org/10.1016/0021-9797(90)90184-P.

[18] S. Ariyaprakai, S.R. Dungan, Influence of surfactant structure on the contribution of micelles to Ostwald ripening in oil-in-water emulsions, J. Colloid Interface Sci. 343 (1) (2010) 102–108, https://doi.org/10.1016/j.jcis.2009.11.034.

[19] J. Weiss, C. Canceliere, D.J. McClements, Mass transport phenomena in oil-in-Water emulsions containing surfactant micelles: ostwald ripening, Langmuir 16 (17) (2000) 6833–6838, https://doi.org/10.1021/la991477v.

[20] Interfacial Tensions of Commercial Vegetable Oils with water - FISHER - 1985 -, Journal of Food Science - Wiley Online Library (2020), https://doi.org/10.1111/j.1365-2621.1985.tb13052.x.

[21] T.J. Wooster, M. Golding, P. Sanguansri, Impact of oil type on nanoemulsion formation and Ostwald ripening stability, Langmuir ACS J. Surf. Colloids 24 (22) (2008) 12758–12765, https://doi.org/10.1021/la801685v.

[22] J.-L. Salager, N. Marquez, A. Graciaa, J. Lachaise, Partitioning of ethoxylated octylphenol surfactants in microemulsion–Oil–Water systems: influence of temperature and relation between partitioning coefficient and physicochemical formulation, Langmuir 16 (13) (2000) 5534–5539, https://doi.org/10.1021/la9905517.

[23] A.M. Al-Sabagh, N.M. Nasser, M.A. Migahed, N.G. Kandil, Effect of chemical structure on the cloud point of some new non-ionic surfactants based on bisphenol in relation to their surface active properties, Egypt. J. Pet. 20 (2) (2011) 59–66, https://doi.org/10.1016/j.ejpe.2011.06.006.

[24] N. Anton, T.F. Vandamme, The universality of low-energy nano-emulsification, Int. J. Pharm. 377 (1–2) (2009) 142–147, https://doi.org/10.1016/j.ijpharm.2009.05.014.

[25] K. Shinoda, H. Arai, The correlation between phase inversion temperature in emulsion and cloud point in solution of nonionic emulsifier, J. Phys. Chem. 68 (12) (1964) 3485–3490, https://doi.org/10.1021/j100794a007.

[26] D. Morales, J.M. Gutiérrez, M.J. García-Celma, Y.C. Solans, A study of the relation between bicontinuous microemulsions and Oil/Water nano-emulsion formation, Langmuir 19 (18) (2003) 7196–7200, https://doi.org/10.1021/la0300737.

[27] D. Morales, C. Solans, J.M. Gutiérrez, M.J. Garcia-Celma, U. Olsson, Oil/Water droplet formation by temperature change in the Water/C16E6/Mineral oil system, Langmuir 22 (7) (2006) 3014–3020, https://doi.org/10.1021/la052324c.

[28] C. Solans, D. Morales, M. Homs, Spontaneous emulsification, Curr. Opin. Colloid Interface Sci. 22 (2016) 88–93, https://doi.org/10.1016/j.cocis.2016.03.002.

[29] B. Marten, M. Pfeuffer, J. Schrezenmeir, Medium-chain triglycerides, Int. Dairy J. 16 (11) (2006) 1374–1382, https://doi.org/10.1016/j.idairyj.2006.06.015.

[30] P. Taylor, Ostwald ripening in emulsions: estimation of solution thermodynamics of the disperse phase, Adv. Colloid Interface Sci. 106 (1) (2003) 261–285, https://doi.org/10.1016/S0001-8686(03)00113-1.

[31] D. Boskou, Olive Oil: Chemistry and Technology, Elsevier, 2015.

[32] I.M. Lifshitz, V.V. Slyozov, The kinetics of precipitation from supersaturated solid solutions, J. Phys. Chem. Solids 19 (1) (1961) 35–50, https://doi.org/10.1016/0022-3697(61)90054-3.

[33] W.I. Higuchi, J. Misra, Physical degradation of emulsions via the molecular diffusion route and the possible prevention thereof, J. Pharm. Sci. 51 (5) (1962) 459–466, https://doi.org/10.1002/jps.2600510514.

## 2.5. Cytotoxicity of NE

### *2.5.1.* NE preparation

NEs were formulated by the PIT method. Non-ionic surfactant (Kolliphor® HS15) was provided by Sigma-Aldrich (Saint Quentin Fallavier, France). Labrafac® WL 1349, a mixture of glyceryl trioctanoate (56%) and glyceryl tridecanoate (43%), was obtained from Gattefossé (Saint Priest, France). Oil and Kolliphor® were added in a 20 ml vial. Approximately 15 ml of purified water were added into another 20ml vial. Both vials containing water and oil mixture were closed using a septum and heated in a water bath at 90°C for 15 minutes. After heating, 6.2 ml of water was transferred into the lipid phase and mixed under magnetic stirring for 5 minutes at 90°C. Formulation was then removed from the water bath and magnetically stirred at room temperature. Samples were sterilized by filtration across 0.22 µm membrane and transferred into 2ml sterile vials under a laminar flow hood. Vials were closed with an elastomer cap and crimp with an aluminium seal. Samples were stored at 4°C.

The quantities of Kolliphor® and Labrafac® were adjusted according to the desired size (**Table 1**).

***Table 1: The composition of blank nanoemulsions***

| Batch | Products | Theoretical amount | Surfactant to oil ratio (SOR) |
|---|---|---|---|
| **NE20** | Kolliphor® | 0.98g | 3.5 |
| | Labrafac® | 0.28g | |
| | Osmosed water | 6.24g | |
| **NE30** | Kolliphor® | 0.84g | 2 |
| | Labrafac® | 0.42g | |
| | Osmosed water | 6.24g | |
| **NE70** | Kolliphor® | 0.63g | 1 |
| | Labrafac® | 0.63g | |
| | Osmosed water | 6.24g | |
| **NE200** | Kolliphor® | 0.42g | 0.5 |
| | Labrafac® | 0.84g | |
| | Osmosed water | 6.24g | |

Hydrodynamic diameters, polydispersity index (PDI) and Zeta potentials of all the NEs were tested by Dynamic Light Scattering and laser doppler electrophoresis using the Zetasizer® Nano ZS90 (Malvern, UK). The stability of nanoemulsions during the incubation times with cells was

assessed by measuring the size during 2 hours at 37°C. Three independent measurements were performed for each time point. As demonstrated in the previous study, the surfactant-to-oil ratio (SOR) controls the final size of NEs (**Table 2**). Immediately after preparation, the hydrodynamic diameters were of 21.8 nm and 227.6 nm for SOR of 3.5 and 0.5, respectively. The polydispersity index was below 0.1 suggesting a monomodal distribution except for the NE200 with a value of 0.32. No size variation was observed during the 2h incubation at 37°C, demonstrating the stability of NEs.

***Table 2: Hydrodynamic diameter and Zeta potential of engineered blank NEs***

| | **NE20** | **NE30** | **NE70** | **NE200** |
|---|---|---|---|---|
| **Surfactant -to-oil ratio** | 3.5 | 2 | 1 | 0.5 |
| **Dynamic light scattering** | | | | |
| Hydrodynamic diameter (nm) | | | | |
| T0 | 21.8±0.9 | 31.8±0.2 | 76.5±0.6 | 227.6±2.4 |
| T2h | 21.4±0.1 | 32.4±0.6 | 75.8±1.5 | 213.4±3.6 |
| Polydispersity index | | | | |
| T0 | 0.04±0.01 | 0.057±0.05 | 0.049±0.03 | 0.32±0.03 |
| T2h | 0.04±0.02 | 0.039±0.03 | 0.075±0.03 | 0.23±0.03 |
| **Laser Doppler electrophoresis** | | | | |
| Zeta Potential (mV) | | | | |
| T0 | -6.7 | -1.9 | -3 | -3.1 |
| T2h | -4.2 | -3.3 | -2.7 | -3.2 |

### *2.5.2.* Cytotoxicity study of NE on intestinal cells

NE were incubated with Caco-2 and HT29-MTX at different concentrations for 2 hours. MTS assay was then performed to evaluate the viability of cells. The relationship between the cell viability and the Kolliphor® concentration was showed in **Figure 17** to consider the well-known intrinsic toxicity of surfactant. At 0.01 g kolliphor®/ml, the viability of Caco-2 cell-lines was of 76 % and 44% after exposure to NE20 and NE200, respectively (Figure 17A). This suggests that the cytotoxicity of NEs was not directly correlated to the concentration in Kolliphor®. The same finding was observed with HT29-MTX (Figure 17B). A viability drop was observed from a concentration in Kolliphor® of 0.086 and 0.025 g/ml for NE20 and NE200. For both cell-lines, at the same Kolliphor® concentration, NE200 seem much more cytotoxic than NE20.

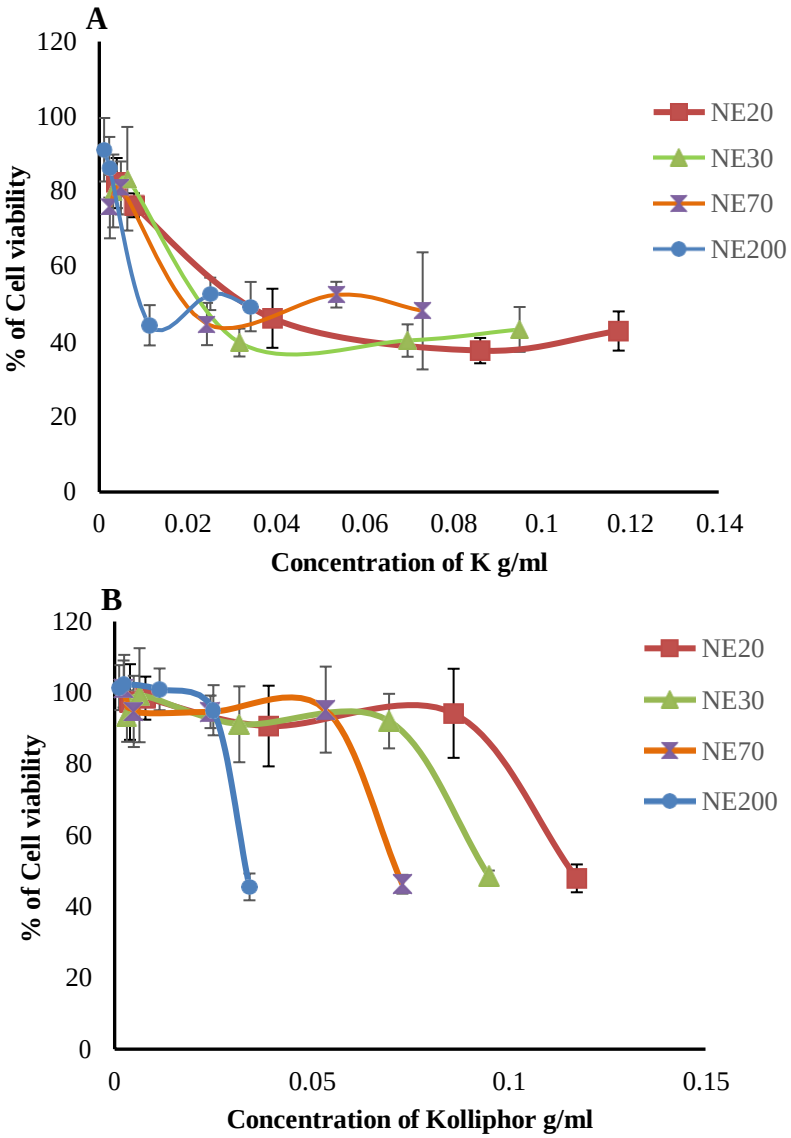


***Figure 17: Influence of the concentration in Kolliphor® on the viability of Caco-2 (A) and HT29-MTX (B).***

In **Figure 18**, the viability results were expressed as a function of the NE concentration (oil and Kolliphor®). For all the NEs, a viability drop was observed from a concentration of 0.05 and 0.11g/ml for Caco-2 and HT29-MTX, respectively. The HT29-MTX were less sensitive to NEs compared with Caco-2, likely due to the protective mucus barrier. Unlike previous results, no size influence was observed between the different NEs. Cytotoxicity was only dependent on the concentration in NE that includes the oil and the Kolliphor® amounts. NE200 were prepared with 2.3 fold less Kolliphor® compared with NE20. Thus, a high amount of NE200 was necessary to reach the same surfactant concentration as the small NE. This explains the differences observed between the different NEs in Figure 17. The lack of size influence could be due to the ability of

NEs to be internalized in intestinal cells at the same levels, even for the large ones. This suggests an internalization process different between NEs and silica NPs. Surprisingly, despite high concentrations in Kolliphor®, small NEs were not more toxic than the large ones. This could be explained by the adsorption of Kolliphor® at the surface of droplets, characterized by a large surface area.

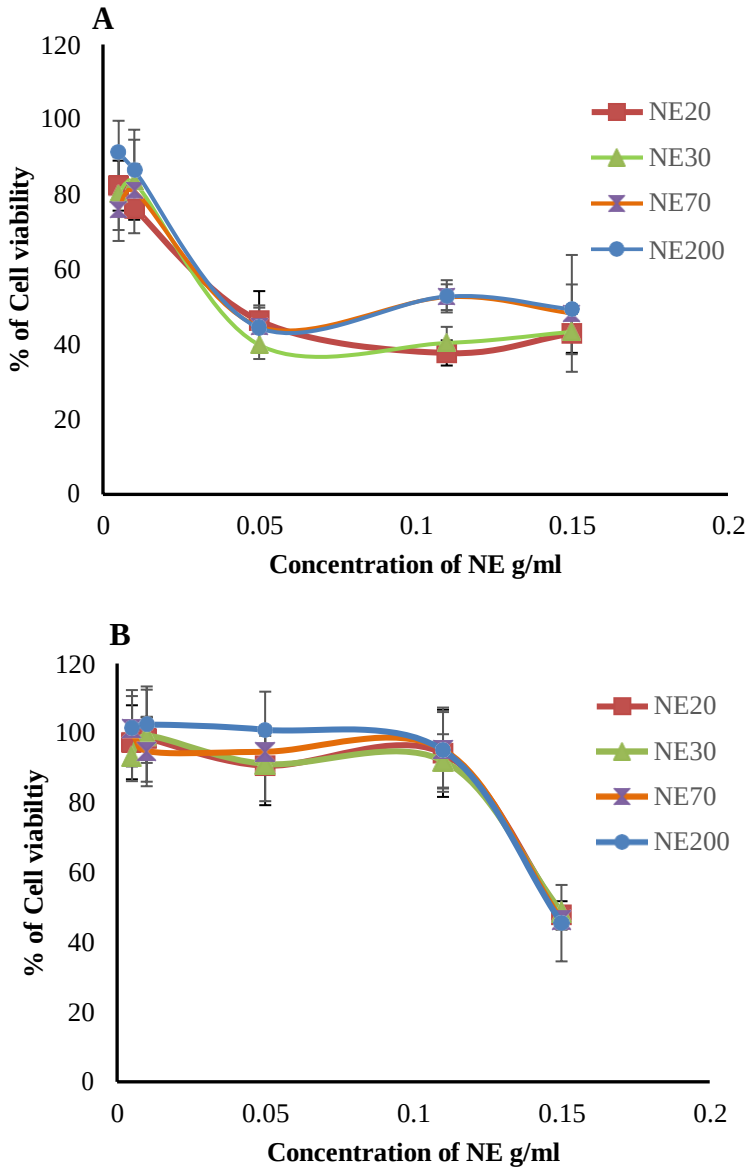


***Figure 18: Influence of the concentration in NEs on the viability of Caco-2 (A) and HT29-MTX (B).***

# CHAPTER IV: GENERAL DISCUSSION AND CONCLUSION

NM currently represent one of the most innovative compounds for many industries. For more than twenty years, many organizations and companies have taken part in multiple research and development projects to industrialize technologies and processes for synthesizing nanomaterials and to develop reliable tools for their characterization. NPs have unique physicochemical properties that make them very attractive. These properties offered by nanotechnology open a vast field of innovation but at the same time raise many uncertainties about their potential toxicity. Thus, the risks caused by these new systems must be identified. This thesis work combines classic cell biology approaches (cell viability test, permeability evaluation and ELISA assays), adapted cell-based models to investigate the toxicological profile of NPs. It also aims to identify the nanotoxicity factors and to understand the involved mechanisms. The work is divided into two main parts. The first one evaluates the interactions of the additive E551 and engineered silica NPs on the intestinal barrier. The second one is dedicated to the design and the intestinal toxicity evaluation of nanoemulsions used for the lipid supplementation and drug delivery.

Nanotechnology represents all sciences and techniques aimed for the producing and the using of objects at the nanometer scale and more precisely between 0.1 and 100 nm, for at least, one of their dimensions. The challenges for the researchers are to industrialize the manufacture of nano-objects to exploit their characteristics. The nanotechnology revolution has quickly resulted in the emergence of a very large number of nanoproducts with multiple applications on the market (1). Some of them so-called nanomedicines are used as drug delivery systems, to carry drugs until the action site. For example, a nanocapsule with optimized physicochemical properties were designed to cross both the mucus layer and the intestinal epithelium to finally reach the blood compartment (2). Biodegradable nano-objects such as NE, liposomes, polymeric micelles and nanoparticles were designed for the transport of anticancer agents (3). Inorganic NM are used as food additives in confectionery, pastry, and many culinary preparations such as the E171 additive. Colloidal silica particles contained in E551 additive prevent the agglomeration of food powders such as sugar and salt (4). However, their use in food and pharmaceutical products requests a deep investigation on their potential effect along the gastrointestinal tract, especially the intestinal barrier. It is also important to understand the mechanisms involved and to determine if these particles are able to cross biological barriers and then be disseminated in the body (5). The numerous applications of silica particles in food products (6) and the emergency of oral

lipid-based formulation such as nanoemulsions in therapy and nutrition request to fully characterize their effect on the intestinal barrier (7). This barrier is necessary for the absorption of vital nutrient and the protection of the organism against foreign bodies. Its alteration would be a source of several pathologies such as infection, local or systemic inflammation (8).

Technological advances over the 40 past years in the field of cell culture facilitated *in vitro* investigations on intestinal disorders and physiological mechanisms of the intestinal barrier, thus reducing the number of *in vivo* experiments. Despite properties very close to *in vivo*, the use of primary cell cultures is faced with availability issues and their short lifespan, limiting long-exposure treatments. Cell-lines represent a good alternative due to their homogeneity in terms of phenotype and genotype, their low cost and easy access (9). The first cell model of the intestinal barrier was the Caco-2 model. This model is defined as the gold standard for predictive studies of permeability and transport of molecules through the intestinal epithelium. This cell-line was isolated from human colorectal adenocarcinoma and established by *Fogh &Trempe* in 1975 (10). This lineage is well characterized as an enterocyte model regarding its morphological and functional characteristics expressed after differentiation. After reaching confluence, they spontaneously differentiate during approximately 21 days of culture. Once differentiated, they form a polarized cell monolayer, an intercellular junction complex, and a brush border with microvilli on the apical side (11). They express enzymes and membrane transporters (12). However, this cell line has some limitations, including the formation of a heterogeneous monolayer related to culture time and number of passages (13). However, Caco-2 model should be not considered as a relevant model for toxicity studies due to the lack of a mucus layer. Considering that the mucus could act as a protective barrier, an overestimation of the intestinal toxicity is usually observed. A model composed of mucus-secreting HT29-MTX cells associated with Caco-2 cells was developed to overcome this limitation. The HT-29 cell line is another intestinal cell-line established by *Fogh & Trempe*. It is derived from colon adenocarcinoma and has been used as an intestinal model for bioavailability and mechanistic studies (14). The HT-29 line is considered a pluripotent gut line because the changes in the culture medium can lead to different differentiation pathways. Unlike the Caco-2 cell line, HT-29 differentiation is not spontaneous but rather depends on nutritional and culture conditions (15). The major difference between HT-29 and Caco-2 cell lines is that under appropriate culture conditions, HT-29 differentiate into goblet cells and then produce mucus. They moderately express tight junction (16). The stable clone HT29-MTX is a sub-population of HT-29 cells resistant to high concentrations of methotrexate (MTX). This clone is thus capable of spontaneously

differentiating into mucus-producing cells (17). The mucus produced by HT29-MTX is a water-insoluble gel composed mainly of mucins such as MUC2 and MUC 5AC that form a protective layer in the intestine. The association of HT29-MTX with Caco-2 cell lines allows mimicking more accurately the human intestinal barrier by considering the mucus layer (18). In addition, the ratio between the number of Caco-2 and HT29-MTX cells can be adapted for a better correlation to the different segments of the intestine.

# 1. Oral toxicity of silica nanoparticles

## 1.1. Methodology

Regarding the first study, a re-evaluation of the E551 food additive was carried out according to the European Food Safety Authority (EFSA) recommendation. Structurally, this additive is composed of agglomerates and aggregates of primary NPs strongly bond between them. There are no available current specifications concerning their physical properties in terms of size distribution and polydispersity (19). To cover the full-size range of NPs potentially present in E551, four sizes of engineered silica NPs were evaluated in addition to the food additive. Besides, most *in vitro* tests using human cells do not consider the potential changes that NPs may undergo in physiological condition, for example after digestion. NPs can agglomerate, especially in acidic mediums, react with components of food bowl or digestive enzymes (20). The modification of physiochemical properties could then influence the interaction of silica particles with the gastrointestinal tract and therefore their toxicity (21). To consider the impact of digestion process, a digestion protocol was established according to the standardized INFOGEST protocol (22). Several studies have clearly shown the reproducibility of the standardized INFOGEST protocol (23). It was considered as an alternative method to the animal experiment to mimic the static *in vitro* digestion (21). The composition of gastric and intestinal fluids come from the US Pharmacopeia. After E551 digestion, single and coculture of Caco-2 and HT29-MTX were exposed to engineered silica NPs, native and digested E551 at $1mg.ml^{-1}$ for 7 days. The concentration choice agreed with the recommendations of the EFSA panel. The scientific committee noted that the highest exposure doses in the various available toxicity studies were always below no observed adverse effects (NOAEL). This explains why the panel could not guarantee the acceptable daily intake “not specified”. Thus, concentrations of silica NPs above

daily dietary intake, estimated between 0.3 and 0.8 mg/kg, were evaluated to identify a toxic concentration threshold. Besides, in the absence of a long-term study with nano-silicon dioxide, the scientific panel of EFSA could not extrapolate the toxic effects from the chronic available studies (24). For this reason, a long-term exposure in accordance with the lifespan of *in vitro* models (7 days) was performed.

## 1.2. Results

Transmission electron microscopy and BET specific surface area results confirmed the classification of E551 as nanomaterials. E551 is composed of primary aggregates particles strongly bonded between them, with a size of 14 nm (25). After successive digestions in simulated gastric and simulated intestinal fluids (SGF, SIF), the physicochemical characteristics of E551 did not change in a significant way. The size of the digested additive stayed around of 200 nm. Our results are in agreement with those of *Desai et al.*, where the transmission electronic microscopy images showed that the mesoporous silica NPs structure was intact after incubation with SGF and SIF at pH 1.2 and 6.8 respectively (26). However, studies reported in literature were not in accordance with our findings. *Sakai-Kato et al.* observed an agglomerated state of amorphous silica NPs after incubation with simulated intestinal fluids (27). *McCraken et al*, showed that the incubation of negatively charged silica NPs in SGF led to an agglomeration (28). This was explained by the modification of the surface charge at low pH and the presence of ions and enzymes in the simulated gastric fluid (29). Incubation in SIF by a pH of 6.8 could nevertheless reverse the agglomeration state of silica particles. Thermogravimetric analysis showed the absence of organic compounds at the surface of digested particles, likely due to washing steps after digestion. Besides, the isoelectric point was the same before and after the digestion process, indicating the lack of surface modification.

After full physicochemical characterization of native, digested E551 food additives and engineered silica NPs, single and coculture of Caco-2 and HT29-MTX were exposed to NPs. After 7 day-exposure, the cellular viability decreased in a size dependent manner in contact with Caco-2 single culture. 70 nm was identified as a cutoff size, from which viability of cells was preserved. Unlike large NPs, 20 nm and 30 nm nanoparticles induced a viability loss in Caco-2 single culture (30). This was in accordance with literature that showed the size-dependent cytotoxicity of silica NPs on different intestinal cell-lines. Small silica nanoparticles of 12 and

40 nm induced a viability decrease of Caco-2 (31), human hepatoma cell line (HepG2) (32), human colon cancer epithelial cell line (HCT116) (33,34).This result could be explained by an accumulation over the time of NP20 and NP30 in Caco-2 cell line. A time dependent disruption of actin filaments of Caco-2 was observed with NPs of 30 nm. Our findings were similar to those of *Cornu et al* where Caco-2 were exposed to 30 nm silica NPs during 2h and at a dose of 10 $mg.ml^{-1}$(35). The actin cytoskeleton remained intact with larger NPs and food additives, confirming the lack of cell uptake. The interactions of silica NPs with HT29-MTX exhibited a different pattern compared with Caco-2. The continuous mucus layer spread on HT29-MTX single culture prevented the cell internalization of silica NPs, even the smallest ones. No toxic effect including cytotoxicity, actin disruption, ROS production and inflammatory response was reported. Surprisingly, a proliferative effect of HT29-MTX cells was identified in presence of silica particles. Mucus layer secreted by HT29-MTX served as an effective barrier, preventing both small and large NPs to reach the cells. A rapid accumulation of engineered silica NPs in mucus layer was observed, due to the strong interaction of NPs with the mucus gel (36). In the lack of a mucus layer on HT29-MTX, a size-dependent cell uptake was noticed, similarly to Caco-2 cell line, proving the role of mucus Despite the mucus on the co-culture, a transepithelial electrical resistance drop was noticed with the 20 and 30 nm nanoparticles. The low ratio of HT29-MTX in the coculture model could change the mucus layer properties in comparison with the one spread on the HT29-MTX single culture. No damage of the co-culture was reported with E551 additive and engineered NPs of 70 and 200 nm. The safety of E551 food additives could be then guaranteed if it contains only silica NPs with a size of a least 70 nm.

## 1.3. Perspectives

It would be interesting to investigate the mechanism involved in the proliferative effect of silica NPs in contact with HT29-MTX single culture. Previous studies showed that silica NPs can stimulate the proliferation of human gastric carcinoma cell line GXF251L. The level of a nuclear proliferation marker Ki-67was enhanced in response to high concentrations of silica NPs. The author suggested the involvement of MAPK/EGFR pathway in the proliferation at different levels. Moreover, we could investigate more deeply the involved mechanism in the actin dependent disruption after Caco-2 exposure to NP30. Several mechanisms can be at the origin of the actin disruption. A direct physical interaction between NPs and actin filaments could be suggested. Cytoskeleton could be also affected in an indirect way due to the ROS or cytokine

productions (37). To understand the differences observed between the HT29-MTX single culture and the co-culture, mucus characterization could be performed. Biochemical composition, thickness and mesh could be studied. To assess the safety of E551 food additive in humans, it is necessary to confirm our results with *in vivo* models. It would be possible to evaluate the distribution, the excretion, and the toxic effects on the GIT but also in other organs such as the liver in the case of translocation. Long-term exposure could be also performed (38).

An assessment of nanomaterials impact on our health and the understanding of the involved toxicity mechanisms are recommended. This would help to define an appropriate regulatory and health framework for a safety use of NPs systems.

## 2. Oral toxicity of lipid nanoparticles

### 2.1. Methodology

A wide range of pharmaceutical nanoforms was developed as delivery systems of active substances. Among them, NEs have been designed for the administration of pharmaceutical active ingredients and lipid supplementation (39). Oil-in-water NEs allow the delivery of active ingredients with a poor-water solubility (40). The solubility of the active substance is a great challenge in biopharmaceuticals, especially for the drug adsorption. Thanks to the solubility improvement and protection against gastrointestinal enzymatic degradation, NEs increase the bioavailability of active substances orally administered (41). Due to their size in the nanometer range, NE can also facilitate the transport of drug though the intestinal epithelium by interacting with intestinal cells. However, this mechanism could also cause toxicity by altering the intestinal barrier integrity.

Methods such as high shear/pressure homogenization, ultrasonic or micro-fluidizer are used to generate nanoscale droplets. The desired size of NEs can be controlled by the amount of external energy applied. However, an excess applied energy can destabilize the NEs due to a local heating and affect the stability of the incorporated drug. 99% of the applied external energy is usually dissipated in heat. In contrast, the low-energy methods play on the tremendous reduction of the tension at the interface oil/water using surfactants and co-surfactants (42). Some of them require heating to shift the Hydrophilic Lipophilic Balance (HLB) of surfactants, inducing a phase

inversion of the emulsion (43). Unlike phase inversion temperature (PIT) method, the spontaneous emulsification does not require any intense heating. The process depends mainly on the interfacial tension, viscosity, structures and concentrations of surfactants and co-surfactants (44). Low-energy processes often require a high concentration in surfactant. Due to their amphiphilic properties, surfactants can insert into the cell membrane and reach the cytoplasmic compartment, affecting the viability and biological functions of cells. Thus, beside the nanometric size of droplets, the presence of a high amount of surfactant in NE preparations could cause an intestinal toxicity. In this second part, an evaluation of different critical parameters on the features of nanoemulsions was performed. This investigation aimed to prepare NE with different physicochemical properties and compositions to identify in a second step, the toxicity factors such as the size and the surfactant concentration. This was initiated through a viability assessment of Caco-2 and HT29-MTX exposed to different NEs.

## 2.2. Results

Nanoemulsification at 37°C of Medium Chain Triglycerides (MCT) led to the formation of 25 nm lipid droplets. This process temperature is slightly above the melting point of the Kolliphor® but does not lead to the phase inversion. Larger sizes, above 100 nm were obtained with Long Chain Triglycerides (LCT) at the same temperature. This agreed with Chang et al demonstrated that the oil phase composition has a major effect on the size of NEs. Only very fine nanoemulsions were obtained with LCT using the PIT method. The molar volume (MV) of triglycerides was considered as a critical factor for the spontaneous nanoemulsification. The MV of LCT could explain their limited diffusion in the aqueous phase (45). Addition of MCT with LCT at ratio 1:1 reduced the average MV of the oil mixture, allowing the spontaneous nanoemulsification at 37°C. The concentration in surfactant also played a major role in the nanoemulsification process by affecting the size and the polydispersity of droplets. High surfactant concentrations facilitated the production of fine NEs. At least two-fold more surfactants was requested to obtain droplets in the nanometer range. Despite the surfactant presence, NEs of glyceryl trioctanoate (GT) were not stable. Ostwald ripening was observed after a few days of storage. GT mixed with glyceryl tridecanoate (Labrafac®) and LCT oils such as glyceryl trioleate stabilized the nanoemulsions during at least 3 months. The mixture allowed increasing the VM value of the lipid core of NE, limiting the diffusion of oils in the water bulk

phase and then the Ostwald ripening. By predicting the water solubility of triglycerides, VM could be a very interesting indicator for both the spontaneous emulsification and the Oswald ripening-mediated destabilization.

### 2.2.1. *In vitro* study

NEs have been developed as promising nano-object for the administration of pharmaceutical active substances (39).The major interest in this field focuses on O/W NEs for the delivery of hydrophobic active ingredients with a poor water solubility and to increase their oral bioavailability (40, 41). In our study, we demonstrated that all NEs affected the viability of Caco-2 from a concentration of 0.05 g/ml without size influence. The same result was observed with HT29 MTX but at a higher concentration in NEs, 0.11 g/ml, suggesting a protective effect of mucus. Surprisingly, the Kolliphor® concentration that is inversely proportional to the size of NEs did not play a major role in the cytotoxicity of NEs. Despite high Kolliphor®concentrations in nanoemulsions of 20 nm and 30nm, no cytotoxicity difference was observed compared with larger NE. Majority of surfactant could be adsorbed at the surface of droplets characterized by a large surface area, limiting the interaction with cells. The lack of size influence could be explained by the ability of NEs to be internalized into the cells, even for lipid droplets of 200 nm. Thus, rather than the Kolliphor® concentration and the size, only the NE concentration affected the viability of intestinal cells. This finding suggests nanotoxicity factors depend on the nature of NPs. While the size governs the toxicity of silica NPs, only the exposed dose influenced the cytotoxicity of nanoemulsions.

## 2.3. Perspectives

This toxicity study needs to be completed by evaluating the influence of the digestion process on the physicochemical properties of NEs. The presence of lipase in the intestinal fluid could affect their structure. The potential release of surfactants from the surface of nanodroplets to gastrointestinal fluids could also exacerbate the toxicity of NEs. Free surfactants would interact then with the biological environment, especially the intestinal cells. Influence of NEs on the permeability of the intestinal barrier should be also investigated. Surfactants are well known to

interact with the multidrug resistance mechanism, especially the P-gp. An alteration of the P-gp would enhance the bioavailability of some xenobiotics and cause adverse effects, especially when NEs are used as drug delivery systems. Expression and functions of tight junctions such as ZO-1 and claudins could be also affected. The influence of NEs on the gut microbiota and the mucus layer needs also to be evaluated to identify a potential intestinal toxicity.

## 3. General conclusion

Despite the wide presence of nanomaterials in numerous manufactured products, their potential health hazard is still unclear due to the lack of available toxicological data and harmonized protocols. In addition, the exposure doses and times in the toxicity studies are not often correlated with the use conditions, especially for the daily products. In this present thesis work, we have demonstrated that the mucus needs to be considered in nanotoxicity studies due to its protective role. A size effect was identified in the toxicity mechanism of silica NPs. From a hydrodynamic diameter of 70 nm, silica particles were unable to be internalized in intestinal cells and to interact with the cytoskeleton. Our study also demonstrated that the exposure time is a critical parameter, especially for the lowly biodegradable particles. Small silica NPs accumulate into the cells, until reaching a toxic dose. The safety of the Emprove® E551 Food additive was demonstrated after subacute exposure to intestinal cells. This was explained by the large mean size of silica particles, close to 200 nm, even after the digestion process. Due to the lack of specifications on the dimensions of particles, nanosilicates could be nevertheless present in E551 additives provided by other manufacturers, affecting their toxicological profile. In contrast to silica NPs, no size effect was reported in the cytotoxicity of nanoemulsions. They provoked a cell viability drop in a concentration dependent manner for all the tested NE. This demonstrates that the mechanisms involved in the nanotoxicity is dependent on the composition of nanoparticles and consequently, toxicity factors cannot be extrapolated to all NPs.

# References


1. Bayda S, Adeel M, Tuccinardi T, Cordani M, Rizzolio F. The History of Nanoscience and Nanotechnology: From Chemical–Physical Applications to Nanomedicine. Molecules. 2019 Dec 27;25(1):112.

2. José Alonso M. Nanomedicines for overcoming biological barriers. Biomed Pharmacother. 2004 Apr 1;58(3):168–72.

3. Karlsson J, Vaughan H, Green J. Biodegradable Polymeric Nanoparticles for Therapeutic Cancer Treatments. Annu Rev Chem Biomol Eng. 2018 Jun 7;9.

4. Peters RJB, van Bemmel G, Herrera-Rivera Z, Helsper HPFG, Marvin HJP, Weigel S, et al. Characterization of titanium dioxide nanoparticles in food products: analytical methods to define nanoparticles. J Agric Food Chem. 2014 Jul 9;62(27):6285–93.

5. Warheit DB. Hazard and risk assessment strategies for nanoparticle exposures: how far have we come in the past 10 years? F1000Research. 2018 Mar 26;7:376.

6. Ogawa T, Okumura R, Nagano K, Minemura T, Izumi M, Motooka D, et al. Oral intake of silica nanoparticles exacerbates intestinal inflammation. Biochem Biophys Res Commun. 2021 Jan 1;534:540–6.

7. Chime SA, Kenechukwu FC, Attama AA. Nanoemulsions — Advances in Formulation, Characterization and Applications in Drug Delivery [Internet]. Application of Nanotechnology in Drug Delivery. IntechOpen; 2014 [cited 2022 Jun 13]. Available from: https://www.intechopen.com/chapters/undefined/state.item.id

8. Houdeau E. Nanoparticles and intestinal barrier : understanding the crossing mechanisms. Innov Agron. 2012 Jan 1;24:105–12.

9. Langerholc T, Maragkoudakis PA, Wollgast J, Gradisnik L, Cencic A. Novel and established intestinal cell line models - An indispensable tool in food science and nutrition. Trends Food Sci Technol. 2011 Nov;22:S11–20.

10. Fogh J, Trempe G. New Human Tumor Cell Lines | SpringerLink. 1975 [cited 2022 Sep 17]; Available from: https://link.springer.com/chapter/10.1007/978-1-4757-1647-4_5

11. Pinto M, Leon SR, M.D. Appay. Enterocyte-like differentiation and polarization of the human colon carcinoma cell line Caco-2 in culture. Biol Cell [Internet]. 1983 [cited 2022 Sep 18]; Available from: http://www.researchgate.net/publication/281082660_Enterocyte-like_differentiation_and_polarization_of_the_human_colon_carcinoma_cell_line_CACO-2_in_culture

12. Lea T. Caco-2 Cell Line. In: Verhoeckx K, Cotter P, López-Expósito I, Kleiveland C, Lea T, Mackie A, et al., editors. The Impact of Food Bioactives on Health: in vitro and ex vivo models [Internet]. Cham (CH): Springer; 2015 [cited 2022 Jun 13]. Available from: http://www.ncbi.nlm.nih.gov/books/NBK500149/

13. Artursson P, Palm K, Luthman K. Caco-2 monolayers in experimental and theoretical predictions of drug transport. Adv Drug Deliv Rev. 2001 Mar 1;46(1–3):27–43.

14. Andoh A, Kinoshita K, Rosenberg I, Podolsky DK. Intestinal trefoil factor induces decay-accelerating factor expression and enhances the protective activities against complement activation in intestinal epithelial cells. J Immunol Baltim Md 1950. 2001 Oct 1;167(7):3887–93.

15. Huet C, Sahuquillo-Merino C, Coudrier E, Louvard D. Absorptive and mucus-secreting subclones isolated from a multipotent intestinal cell line (HT-29) provide new models for cell polarity and terminal differentiation. J Cell Biol. 1987 Jul;105(1):345–57.

16. Zweibaum A, Pinto M, Chevalier G, Dussaulx E, Triadou N, Lacroix B, et al. Enterocytic differentiation of a subpopulation of the human colon tumor cell line HT-29 selected for growth in sugar-free medium and its inhibition by glucose. J Cell Physiol. 1985 Jan 1;122(1):21–9.

17. Lesuffleur T, Barbat A, Dussaulx E, Zweibaum A. Growth adaptation to methotrexate of HT-29 human colon carcinoma cells is associated with their ability to differentiate into columnar absorptive and mucus-secreting cells. Cancer Res. 1990 Oct 1;50(19):6334–43.

18. Béduneau A, Tempesta C, Fimbel S, Pellequer Y, Jannin V, Demarne F, et al. A tunable Caco-2/HT29-MTX co-culture model mimicking variable permeabilities of the human intestine obtained by an original seeding procedure. Eur J Pharm Biopharm Off J Arbeitsgemeinschaft Pharm Verfahrenstechnik EV. 2014 Jul;87(2):290–8.

19. Re-evaluation of silicon dioxide (E 551) as a food additive | EFSA [Internet]. [cited 2022 Jun 14]. Available from: https://www.efsa.europa.eu/en/efsajournal/pub/5088

20. Zhang Z, Zhang R, Xiao H, Bhattacharya K, Bitounis D, Demokritou P, et al. Development of a standardized food model for studying the impact of food matrix effects on the gastrointestinal fate and toxicity of ingested nanomaterials. NanoImpact. 2019 Jan 1;13:13–25.

21. DeLoid GM, Wang Y, Kapronezai K, Lorente LR, Zhang R, Pyrgiotakis G, et al. An integrated methodology for assessing the impact of food matrix and gastrointestinal effects on the biokinetics and cellular toxicity of ingested engineered nanomaterials. Part Fibre Toxicol. 2017 Oct 13;14(1):40.

22. Minekus M, Alminger M, Alvito P, Ballance S, Bohn T, Bourlieu-Lacanal C, et al. A standardised static in vitro digestion method suitable for food – an international consensus. Food Funct. 2014;5:1113–24.

23. Egger L, Ménard O, Delgado-Andrade C, Alvito P, Assunção R, Balance S, et al. The harmonized INFOGEST in vitro digestion method: From knowledge to action. Food Res Int. 2016;88:217–25.

24. EFSA Panel on Food Additives and Nutrient Sources added to Food (ANS), Younes M, Aggett P, Aguilar F, Crebelli R, Dusemund B, et al. Re-evaluation of silicon dioxide (E 551) as a food additive. EFSA J. 2018;16(1):e05088.

25. Fruijtier-Pölloth C. The safety of nanostructured synthetic amorphous silica (SAS) as a food additive (E 551). Arch Toxicol. 2016;90(12):2885–916.

26. Desai D, Prabhakar N, Mamaeva V, Sen Karaman D, Lähdeniemi I, Sahlgren C, et al. Targeted modulation of cell differentiation in distinct regions of the gastrointestinal tract via oral administration of differently PEG-PEI functionalized mesoporous silica nanoparticles. Int J Nanomedicine. 2016 Jan 22;11:299—313.

27. Sakai-Kato K, Hidaka M, Un K, Kawanishi T, Okuda H. Physicochemical properties and in vitro intestinal permeability properties and intestinal cell toxicity of silica particles, performed in simulated gastrointestinal fluids. Biochim Biophys Acta BBA - Gen Subj. 2014 Mar 1;1840(3):1171–80.

28. McCracken C, Zane A, Knight DA, Dutta PK, Waldman WJ. Minimal Intestinal Epithelial Cell Toxicity in Response to Short- and Long-Term Food-Relevant Inorganic Nanoparticle Exposure. Chem Res Toxicol. 2013 Oct 21;26(10):1514–25.

29. Powell JJ, Faria N, Thomas-McKay E, Pele LC. Origin and fate of dietary nanoparticles and microparticles in the gastrointestinal tract. J Autoimmun. 2010 May;34(3):J226-233.

30. Napierska D, Thomassen LCJ, Rabolli V, Lison D, Gonzalez L, Kirsch-Volders M, et al. Size-dependent cytotoxicity of monodisperse silica nanoparticles in human endothelial cells. Small Weinh Bergstr Ger. 2009 Apr;5(7):846–53.

31. Gehrke H, Frühmesser A, Pelka J, Esselen M, Hecht LL, Blank H, et al. In vitro toxicity of amorphous silica nanoparticles in human colon carcinoma cells. Nanotoxicology. 2013 May;7(3):274–93.

32. Li Y, Sun L, Jin M, Du Z, Liu X, Guo C, et al. Size-dependent cytotoxicity of amorphous silica nanoparticles in human hepatoma HepG2 cells. Toxicol Vitro Int J Publ Assoc BIBRA. 2011 Oct;25(7):1343–52.

33. Fritsch-Decker S, An Z, Yan J, Hansjosten I, Al-Rawi M, Peravali R, et al. Silica Nanoparticles Provoke Cell Death Independent of p53 and BAX in Human Colon Cancer Cells. Nanomater Basel Switz. 2019 Aug 16;9(8):E1172.

34. Dong X, Wu Z, Li X, Xiao L, Yang M, Li Y, et al. The Size-dependent Cytotoxicity of Amorphous Silica Nanoparticles: A Systematic Review of in vitro Studies. Int J Nanomedicine. 2020 Nov 18;15:9089–113.

35. Cornu R, Chrétien C, Pellequer Y, Martin H, Béduneau A. Small silica nanoparticles transiently modulate the intestinal permeability by actin cytoskeleton disruption in both Caco-2 and Caco-2/HT29-MTX models. Arch Toxicol. 2020 Apr;94(4):1191–202.

36. Pearson JP, Chater PI, Wilcox MD. The properties of the mucus barrier, a unique gel – how can nanoparticles cross it? Ther Deliv. 2016 Apr;7(4):229–44.

37. Dadras A, Riazi GH, Afrasiabi A, Naghshineh A, Ghalandari B, Mokhtari F. In vitro study on the alterations of brain tubulin structure and assembly affected by magnetite nanoparticles. J Biol Inorg Chem JBIC Publ Soc Biol Inorg Chem. 2013 Mar;18(3):357–69.

38. Fischer HC, Chan WCW. Nanotoxicity: the growing need for in vivo study. Curr Opin Biotechnol. 2007 Dec;18(6):565–71.

39. Shah P, Bhalodia D, Shelat P. Nanoemulsion: A pharmaceutical review. Syst Rev Pharm. 2010 Jan 1;1.

40. Gursoy RN, Benita S. Self-emulsifying drug delivery systems (SEDDS) for improved oral delivery of lipophilic drugs. Biomed Pharmacother Biomedecine Pharmacother. 2004 Apr;58(3):173–82.

41. Ganta S, Devalapally H, Amiji M. Curcumin enhances oral bioavailability and anti-tumor therapeutic efficacy of paclitaxel upon administration in nanoemulsion formulation. J Pharm Sci. 2010 Nov;99(11):4630–41.

42. McClements DJ. Nanoemulsions versus microemulsions: terminology, differences, and similarities. Soft Matter. 2012 Jan 18;8(6):1719–29.

43. Jaiswal M, Dudhe R, Sharma PK. Nanoemulsion: an advanced mode of drug delivery system. 3 Biotech. 2015 Apr;5(2):123–7.

44. López-Montilla JC, Herrera-Morales PE, Pandey S, Shah DO. Spontaneous Emulsification: Mechanisms, Physicochemical Aspects, Modeling, and Applications. J Dispers Sci Technol. 2002 Jan 1;23(1–3):219–68.

45. Wooster TJ, Golding M, Sanguansri P. Impact of oil type on nanoemulsion formation and Ostwald ripening stability. Langmuir ACS J Surf Colloids. 2008 Nov 18;24(22):12758–65.

# Annexes

## Size-dependent intestinal toxicity of silica particles in E551 food additive

Taghrid Zaiter[1], Raphaël Cornu[1], Nadine Millot[2], Mona Diab[3], Arnaud Béduneau[1]

*1 : PEPITE EA4267, Univ. Bourgogne Franche-Comté, F-25000 Besançon, France*

*2 : Laboratoire Interdisciplinaire Carnot de Bourgogne, UMR 6303, CNRS / Université Bourgogne Franche-Comté, BP 47870, 21078 Dijon, France.*

*3: EDST, Pharmacology and Cancerology Laboratory, Faculty of Sciences, Lebanese University, Beirut 1500, Lebanon*

### Introduction

E551 additive is commonly used as an anti-caking agent or thickener in numerous food products. It is composed of amorphous silica synthesized by thermal (fumed) and wet processes (precipitated). Particles in E551 are usually characterized by a mean diameter in the micrometer range. However, no size limit was mentioned in the specifications, while the dimensions of particles are often reported as a toxicity factor. A study showed the presence of silica nanoparticles (NPs) in food products with a diameter comprised between 10 and 50 nm (Athinarayanan et al. 2014). The European Food Safety Authority (EFSA) recommended a re-evaluation of the E551 toxicity including oral toxicity (Younes et al. 2018).Silica NPs in foods prepared with E551 additive were also present after intestinal digestion. Many *in vitro* studies were performed by incubation of NPs with intestinal cell lines, especially Caco-2 without considering the mucus layer (Hempt et al. 2020).The present study investigates the size-dependent intestinal toxicity of silica particles contained in E551 additive by considering the mucus layer.

### Physicochemical characterization of native and digested E551 food additive

| | E551 | E551d |
|---|---|---|
| **Dynamic light scattering** | | |
| **Hydrodynamic diameter (nm)** | | |
| **T0** | 232 ± 39 | 166 ± 17 |
| **T48h** | 245 ± 13 | 207 ± 16 |
| **Polydispersity index** | | |
| **T0** | 0.21 ± 0.01 | 0.17 ± 0.03 |
| **T48h** | 0.35 ± 0.06 | 0.19 ± 0.01 |
| **Laser doppler electrophoresis** | | |
| **Zeta potential (mv)** | -23 ± 1 | -23 ± 1 |
| **Isoelectric point** | 3.5 | 3.5 |
| **TEM Diameter (n =100, nm)** | 13.9 ± 2.1 | 13.7 ± 2.1 |
| **BET Surface area ($m^2.g^{-1}$)** | 208 | 181 |
| **ATG** | | |
| **Weight Loss (%)** | 0.32 | 2.96 |
| **Peak d(w)/d(T) (°C)** | 266 | 280 |

***Table 1:*** Physicochemical characteristics of E551 food additive.

- **The size, Zeta potential and IP were in the same range before and after digestion of E551 in gastro-intestinal simulated fluids.**
- **E551 additive is classified as nanomaterials due to the presence of primary nanoparticles (according to the European Commission definition).**
- **The size, Zeta potential of E551 were maintained after 48 h of incubation with intestinal cells (intestinal cells were incubated for 7 days, the treatment was renewed every 2 days).**

### Methodology

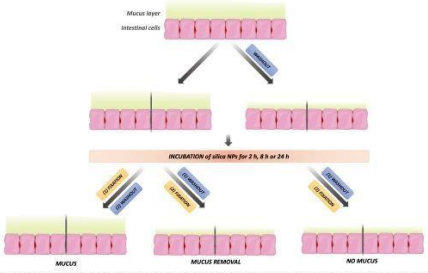


***Figure 1:*** Diagram describing the different washing steps of HT29-MTX before incubation with engineered silica NPs.

### Mucus effect on the cell uptake of engineered silica NPs

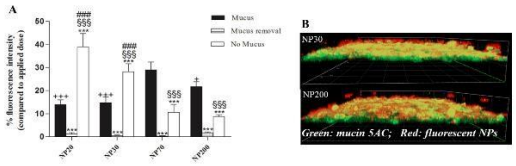


***Figure 2:*** Accumulation of silica NPs in HT29-MTX cultures. Fluorescent NP20, NP30, NP70 & NP200 were exposed to intestinal cells at 1 mg/ml. The percentage of fluorescence intensity was obtained after comparison with the applied dose. Some HT29-MTX cultures were washed with DPBS to remove the weakly adherent mucus layer before (no mucus) or after (mucus removal) the NP incubation (A). Confocal microscopy images of HT29-MTX cells incubated with fluorescent NP30 and NP200 (in red). Muc5AC immunostaining was performed to visualize the mucus layer (in green) (B).

- **All the silica NPs were mainly accumulated in the mucus layer of HT29-MTX cells.**
- **In the lack of mucus, only small silica NPs were able to reach the intestinal cells in a significant manner, suggesting a cytoadhesion or a cellular uptake.**

ICT2022
The XVI[TH] international Congress of Toxicology
MAASTRICH, THE NETHERLANDS
Septemnber 18-21, 2022

### Interaction of E551 and engineered silica NPs with the actin cytoskeleton

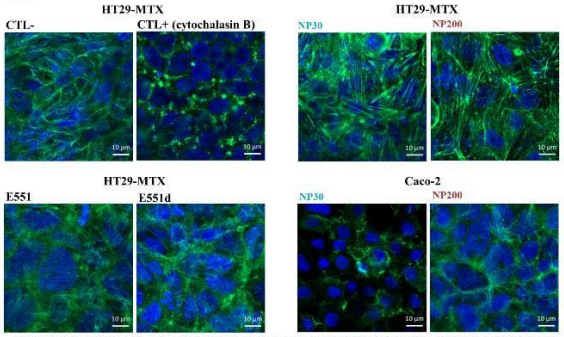


***Figure 3:*** (A) Influence of native and digested E551 as well as engineered silica NPs on the actin cytoskeleton of Caco-2 and HT29-MTX single cultures. Particles were incubated for 24 h at 1 mg/ml.

- **No effect of NP200 and E551 food additive on the the actin cytoskeleton**
- **Time-dependent disruption of actin cytoskeleton in Caco-2 after NP30 exposure**
- **No disruption of actin cytoskeleton in HT29-MTX, confirming the protective role of mucus layer**

### Effect of E551 and engineered silica NPs on coculture integrity

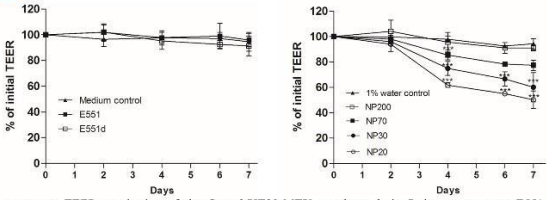


***Figure 4:*** TEER monitoring of the Caco-2/HT29-MTX coculture during7 day exposure to E551 additives and engineered silica NPs.

- **No effect of native and digestive E551 additives on the intestinal permeability after 7 day exposure**
- **The intestinal transcpithelial electrical resistance of the coculture was affected after exposure to engineered silica NPs except for NP200**

### Conclusion

- Digestion did not change the physicochemical properties of the E551 additive
- The size of silica nanoparticles is a critical factor, affecting the intestinal toxicity and permeability
- The mucus layer spread on the single culture HT29-MTX acted as an effective protective barrier against silica NPs
- The mucus layer of the co-culture did not prevent the small silica NPs to reach the intestinal cells.
- Native and digested E551food additive did not affect the actin cytoskeleton of both Cells Caco-2 and HT29-MTX.

**References:**

**ref 1**- Athinarayanan, J., V. S. Periasamy, M. A. Alsaif, A. A. Al-Warthan, and A. A. Alshatwi, 2014. "Presence of Nanosilica (E551) in Commercial Food Products: TNF Mediated Oxidative Stress and Altered Cell Cycle Progression in Human Lung Fibroblast Cells." *Cell Biology and Toxicology* 30 (3): 89–100. doi:https://doi.org/10.1007/s10565-014-9272-8. [Crossref], [PubMed], [Google Scholar]

**Ref 2**- Younes, M., P. Aggett, F. Aguilar, R. Crebelli, B. Dusemund, M. Filipič, M. J. Frutos, et al. 2018. "Re-Evaluation of Silicon Dioxide (E 551) as a Food Additive." *EFSA Journal* 16 (11): 5088. doi:https://doi.org/10.2903/j.efsa.2018.5088. [Google Scholar]

**ref 3**- Hempt, C., J. P. Kaiser, O. Schilder, T. Jhoeki Hirsbrunner, H. Hofmann, A. Rippl, I. B. Schuster, P. Wick, and U. Hirsch, 2020. "The Impact of Synthetic Amorphous Silica (E 551) on Differentiated Caco-2 Cells, a Model for the Human Intestinal Epithelium." *Toxicology in Vitro: An International Journal Published in Association with BIBRA* 67: 104903. doi:https://doi.org/10.1016/j.tiv.2020.104903. [Crossref], [PubMed], [Google Scholar]

ÉCOLE DOCTORALE
Environnements - Santé
Bourgogne | Franche-Comté

## Evaluation *in vitro* du profil toxicologique des nanoparticules de silice et nanoémulsions

**Mots clés :** nanoparticules de silice, nanoémulsions, toxicité, barrière intestinale, mucus

**Résumé :** La quantité de nanoparticules manufacturées sur le marché est en constante augmentation du fait de leurs propriétés uniques. Elles sont utilisées comme excipients en cosmétique, additifs alimentaires, et systèmes de délivrance de médicaments. Leur taille nanométrique est responsable de leur forte interaction avec l'environnement biologique. Ce travail a pour but d'évaluer la toxicité intestinale de deux types de nanoparticules (NPs) : des nanoparticules de silice potentiellement présentes dans l'additif E551 et des nanoémulsions utilisées pour la délivrance de lipides et substances actives. L'évaluation toxicologique a été réalisée à partir de modèles in vitro, à savoir des monocultures et une co-culture de cellules intestinales (Caco-2 et HT29-MTX). Avant l'incubation, l'additif a été digéré en présence de fluides gastriques et intestinaux simulés afin de mimer fidèlement les conditions in vivo. Les plus petites NPs de silice caractérisées par des diamètres de 20 et 30 nm ont altéré la viabilité des entérocytes et induit la production de ROS après 7 jours d'exposition. Cependant, ces dernières n'ont pas causé de cytotoxicité sur la monoculture de cellules caliciformes en raison du rôle protecteur du mucus. Les NPs de silice avec une taille supérieure à 70 nm et l'additif E551 n'ont présenté aucune toxicité, même en l'absence de mucus. Contrairement aux NP20 et NP30, elles n'ont pas modulé significativement la résistance électrique transépithéliale de la co-culture. Concernant les nanoémulsions, une cytotoxicité dose-dépendante a été observée dans les cultures de Caco-2 et HT29-MTX, sans influence de la taille. La composition en lipides ainsi que la présence de tensioactif pourraient faciliter l'internalisation cellulaire des gouttelettes, même les plus grossières. Cette étude démontre que les facteurs de nanotoxicité varient selon la composition des NPs. Contrairement aux nanoémulsions, le profil toxicologique des particules de silice est fortement dépendant du diamètre hydrodynamique. Le mucus doit également être pris en compte dans les études de toxicité pour une meilleure prédiction.

## *In vitro* investigation of the toxicological profi e of silicate nanoparticles and nanoemulsions

**Keywords:** silica nanoparticles, nanoemulsions, toxicity, intestinal barrier, mucus

**Abstract :** The quantity of manufactured nanoparticles (NPs) on the market is constantly increasing due to their unique properties. They are used as cosmetic ingredients, food additives and as drug delivery systems. Their size in the manometer range confers them a strong ability to interact with the biological environment. This work aims to evaluate the intestinal toxicity of two types of nanoparticles (NPs): silica NPs potentially present in E551 food additive and nanoemulsions used as drug/lipid delivery system. The toxicological evaluation was carried out using in vitro models consisting in single cultures and co-culture of intestinal cells (Caco-2 and HT29-MTX). Prior to the incubations, E551 additive was digested with gastric and intestinal simulated fluids, to accurately mimic the in vivo conditions. The smallest silica NPs characterized by hydrodynamic diameters of 20 and 30 nm, altered the viability of enterocytes and induced ROS production after 7-day exposure. However, the single culture of goblet cells was not affected due to the protective barrier of mucus. Silica NPs with a size of at least 70 nm and additive E551 were not toxic, even in the lack of mucus. Unlike NP20 and NP30, they did not significantly modulate the transepithelial electrical resistance of the co-culture. Regarding nanoemulsions, a cytotoxicity in a dose-dependent manner was observed in Caco-2 and HT29-MTX cultures, without any size effect. The lipid composition and the presence of surfactant could facilitate the cell internalization of droplets, even the largest ones. This study demonstrates that the nanotoxicity factors vary according to the composition of NPs. Unlike nanoemulsions, the toxicological profile of silica particles is strongly dependent on the hydrodynamic diameter. Mucus also needs to be considered in toxicity studies for a better prediction.

UBFC UNIVERSITE BOURGOGNE FRANCHE-COMTE
Université Bourgogne Franche-Comté
32, avenue de l'Observatoire
25000 Besançon